RESISTANCE TO FLOW IN OPEN CHANNELS

A thesis submitted in fulfilment of the requirements for the Degree of Doctor of Philosophy in the Faculty of Engineering of the University of London.

by

Haji Mahmood Memon

Department of Civil Engineering,
Imperial College of Science and Technology,
LONDON S.W.7.

December 1967

SYNOPSIS

This thesis on resistance to flow in open channels includes an experimental investigation of some of the basic actions and details of the steady and of the unsteady parts of the motion. The experiments were done in a glass walled channel using clear water and with smooth as well as rough beds of non-mobile material though one bed was of ripple mark type having been generated hydraulically and subsequently consolidated.

Certain analytical expressions for the friction coefficient for laminar flow in wide rectangular section are verified experimentally and the lower value of the critical Reynolds number for this section is established.

To find the effect of the air water interface on the turbulence, measurements are made in two-dimensional fully developed turbulent flows using a photographic technique and the results are compared with those previously obtained in pipes. Also the effect of roughness on turbulence is investigated and the results with different roughnesses are correlated.

In an attempt to detect the secondary currents in straight channels, a photographic technique is developed to visualize and record the motion across the main flow. From the photographs some patterns of the secondary currents are mapped out.

The problem of resistance to flow is finally considered. Smooth channel results are compared with those of smooth pipes and the effect of depth-width ratio on the resistance is disclosed. For the channel with various forms of bed roughness and smooth side walls, the surface roughness in terms of equivalent sand roughness is evaluated from velocity distributions and from the friction coefficient results. It is shown that for such cases the method, proposed by Einstein and Johnson, commonly used to eliminate the effect of side walls for evaluating the bed roughness gives misleading results.

ACKNOWLEDGEMENTS

This work was carried out under the supervision of Professor (Emeritus) C.M. White, D.Sc(Eng)., Ph.D., Department of Civil Engineering, Imperial College of Science and Technology, University of London. The author is greatly indebted to him for his help, encouragement and continuous guidance throughout the course of the work. He also wishes to thank Professor J.R.D. Francis, B.Sc(Eng)., M.I.C.E., for his encouragement and interest in the work.

The author expresses his appreciation to the members of staff and colleagues in the Hydraulics section for their fullest cooperation. Also it is a pleasure to thank Mr. R. Brannon and the staff of the Hydraulics Laboratory for their assistance in photographic and other laboratory work.

The assistance of the University of Sind, Hyderabad (Pakistan) is gratefully acknowledged for granting leave of absence and recommending for the Central Government Scholarship.

CONTENTS

	page
Synopsis	ii - iii
Acknowledgements	iv
Contents	v - vi
Notations	vii - ix
Chapter I General Introduction	1 - 6
Chapter II. Experimental set-up and photographic techniques.	
II.1. General set-up	7 - 9
II.2. Bed Forms	9 - 15
II.3. Experimental procedure	15
II.4. Photographic techniques	
II.4.1. Introduction	15 - 17
II.4.2. Photographs to measure turbulence and local velocity	17 - 22
II.4.3. Visualization and photographs of motion in a plane normal to the main flow.	22 - 28
Chapter III. The onset of turbulence in rectangular channels.	29 - 35
Chapter IV. Turbulence measurements.	
IV.1. Introduction	36 - 39
IV.2. Measurement of turbulence	39 - 50
IV.3. The turbulent quantities measured in the present experiments.	50 - 51
IV.4. Experimental results.	
IV.4.1. Results obtained on smooth bed.	52 - 68
IV.4.2. Results obtained on rippled bed.	69 - 76
IV.4.3. Results obtained on rippled bed when the troughs were filled with gravel.	76 - 82
IV.4.4. Results obtained on fully gravelled bed.	82 - 88
IV.5. Turbulence and the several beds.	88 - 94

Chapter V. Secondary currents in straight channels.

V.1. Introduction. 95 - 100

V.2. Analytical considerations. 101 - 105

V.3. Results from photo-method. 105 - 119

Chapter VI. Friction coefficient in open channels.

VI.1. Introduction. 120 - 131

VI.2. Application of logarithmic laws to flow in open channels. 131 - 140

VI.3. Experimental results on smooth rectangular channel.

VI.3.1. Velocity measurements. 140 - 145

VI.3.2. Friction coefficient 145 - 151

VI.4. Experimental results on rectangular channel with rough bed and smooth side walls.

VI.4.1. Determination of datum plane for measurement of depth when the bed is rough. 151 - 154

VI.4.2. Surface roughness measurement. 154 - 156

VI.4.2.1. From velocity measurements. 156 - 160

VI.4.2.2. From friction coefficient neglecting side wall. 160 - 169

VI.4.2.3. Applying Einstein - Johnson method for side wall effect. 169 - 170

VI.4.3. Discussion of results. 170 - 177

The main findings. 178 - 179

References 180 - 186

Appendix I. Optics of photographic arrangement to record motion across main flow.

I.A. Design calculations. 187

I.B. Apparent outward drift due to optical parallax. 188

Appendix II. Experimental data

II.A. Friction coefficient results. 190 - 200

II.B. Velocity distribution and turbulence measurements. 201 - 210

Appendix III. Data of u,v and u'v' obtained from photographs. 211 - 228

NOTATIONS

Symbol	Meaning
A	Area of cross-section
B	Width of flume
C	Chezy's coefficient, in $V = C\sqrt{RS}$.
D	Diameter of pipe
d	Depth of flow or half distance between parallel plates.
f	Friction factor, in $h = \frac{4fLV^2}{2gD}$
g	Acceleration due to gravity.
h	Head loss
K	Linear measurement of roughness.
Ks	Nikuradse equivalent sand roughness.
ℓ	Prandtl's Mixing length.
P	Wetted perimeter
Q	Discharge
R	Hydraulic radius, $\frac{A}{P}$
Rb	Bed hydraulic radius.
Rw	Wall hydraulic radius

r	Radius of pipe
S	Hydraulic gradient or slope of channel for uniform flow.
u	Local instantaneous velocity in direction of main flow.
$\bar{u}$	Local mean velocity in direction of main flow.
u',v',w'	Turbulent velocity components in x, y and z axes respectively.
$\sqrt{\overline{u'^2}}$, $\sqrt{\overline{v'^2}}$, $\sqrt{\overline{w'^2}}$	Root-mean-square values of u', v' and w'.
V	Average velocity of flow, Q/A.
Vxo	Shear velocity at the bed, in central plane for two-dimensional flow. $\sqrt{\frac{\tau o}{\rho}} = \sqrt{dgs}$
Vx	Average shear velocity over the wetted perimeter, $\sqrt{\frac{\tau}{\rho}} = \sqrt{Rgs}$
Vxb	Average bed shear velocity, $\sqrt{\frac{\tau b}{\rho}} = \sqrt{Rbgs}$.
y	Distance from bed.
X,Y,Z	Coordinate axes.
α	Universal turbulent constant.
γ	Specific weight of water.
ρ	Mass density of water.
μ	Dynamic viscosity.

ν	Kinematic viscosity, $\frac{\mu}{\rho}$
τo	Shear stress at the bed, for two-dimensional flow, ρgds.
τ	Average shear stress over the perimeter, ρgRs.
τb	Average bed shear stress, $\rho gRbS$.
ϕ	A Coefficient, $\frac{V}{\overline{V}x}$
Ψ	Coefficient of correlation, $\frac{\overline{u'v'}}{\sqrt{\overline{u'^2}}\sqrt{\overline{v'^2}}}$ Also used as stream function in Chapter V.
ξ, η, ζ	Vorticity components in x,y and z axes respectively.

CHAPTER I

GENERAL INTRODUCTION

The hydraulic aspects of flow in canals and rivers, such as the resistance they offer to the discharge of flood water and their capacity to bring clear water for agriculture and town supply, are problems difficult to investigate in the field where even the simplest basic actions may become obscured by natural irregularities beyond control.

In the laboratory, however, it is possible to simplify and to restrict the variables and treat the problem as one of steady uniform flow in a channel in which the depth of the stream and the velocity of flow remain constant with time and distance. These are ideal conditions seldom occuring in the irregular channels of natural water courses, nor are they often found in artificial channels of uniform cross section since these are usually obstructed by various weirs or other structures across them. Yet it is clear that such simplifications are essential in a search for a sound knowledge of the subject.

An attempt to derive a formula for predicting the velocity in open channels was made by De Chezy in 1775. In the well known Chezy's formula the coefficient, known as Chezy's coefficient C, being dimensional was later expressed in a non-dimensional form and since then many expressions have been put forward to evaluate its value, by

many workers in this field, the majority relying mainly upon an empirical approach.

A new trend, however, started at the end of the Nineteenth Century with the work of Osborne Reynolds who investigated the mechanism and stability of the two types of fluid motion - laminar and turbulent.

In laminar flow, where fluid particles move in parallel layers, certain forces, tending to equalise the speed of the different layers, come into play in the form of shear stresses due to the cohesion and molecular momentum exchange between fluid layers. These effects are represented by the viscosity of the fluid, defined by μ in the expression, $\tau = \mu \frac{du}{dy}$, and are fully included in the Navier-Stokes equations. For steady motion, these equations have been solved for various boundary shapes and the derived friction coefficients agree with those measured experimentally.

In turbulent flow, the mean values of velocity and pressure have ~~are~~ superimposed on them ~~with~~ turbulent fluctuations and the motion of the fluids is steady only in so far as the mean values are concerned. Reynolds, in his theoretical analysis, demonstrated that the superposition of fluctuations on the mean motion gives rise to additional stresses, and that the Navier-Stokes equations are satisfied by the mean values of the turbulent flow if the viscous stresses are increased by the additional turbulent stresses - now also known as Reynolds

stresses. In two dimensions the resulting expression for the shear stress reduces to:

$$\tau = \mu \frac{d\bar{u}}{dy} - \rho \overline{u'v'},$$

in which the second term representing the turbulent shear stress is the temporal mean of the product of the turbulent fluctuations u' and v', multiplied by ρ. It is observed from experiments that when the Reynolds number is large, the term $\mu \frac{d\bar{u}}{dy}$ is usually very small compared to $-\rho\overline{u'v'}$ and therefore is usually neglected. However this is not so very close to a wall where the viscous forces usually tend to dominate the flow.

Although the Reynolds equations suitably represent the turbulent flow, in practice they are not sufficient to determine the unknowns which are of practical interest e.g., the velocity distribution or the friction coefficient.

With the development of Prandtl's mixing length theory, a new approach started to represent the mechanism of turbulent flow. This resulted in Universal logarithmic velocity distribution for two-dimensional flows.

The friction coefficient laws for flow in circular pipes and between parallel plates can be derived by an integration of the logarithmic velocity distribution to obtain the average velocity of flow in the section. An open wide rectangular channel can be compared with that of flow between parallel plates if it is assumed that the free

surface does not affect the motion. A complication arises when the rectangular channel is deep in relation to its width. Under these conditions the position of maximum velocity is usually displaced downwards some distance below the free surface, and this is the result of a secondary current in the form of a spiral motion, in a direction normal to the main flow.

The present study was concerned with the resistance and some of the basic factors which influence the flow and was made on a rectangular flume with smooth glass side walls. The bed conditions were changed to various forms of roughness including one with a smooth glass bed. The general set up of the flume with measuring devices and different bed forms is described in Chapter II.

In the preliminary investigations on the flume with smooth bed, some measurements of the friction coefficient under laminar flow conditions were made to investigate the onset of turbulence; some of the previous work on rectangular pipes and open rectangular channels is included together with the description of the present results in Chapter III.

Chapter IV deals with turbulence measurements. There have been many previous measurements of turbulent quantities in pipes and closed rectangular channels and mainly air has been the working medium and the hot-wire anemometer the instrument. Also some attempts have been made to measure these quantities in free surface flows but the

results have been unreliable because of lack of suitable instruments for use in water. However a photographic technique, described in (II.4.2), reveals some of the basic information needed to understand turbulence in two dimensional surroundings with a free surface. The measurements were made along axes X and Y, in the direction of main flow and normal to the bed respectively. Previous results, mainly concerning pipes and closed channels are summarized and brought together in a dimensionless form. The present results include some with a smooth bed and these are compared with the previous results on pipes and closed channels, and the effect of the free surface in modifying the turbulence is established. Also the effect of roughness in relation to the intensity of turbulence is investigated and correlated with beds of different roughness.

Chapter V deals with the study of secondary currents in straight channels. For nearly a century, the well known depression of the position of maximum velocity has drawn the attention of many engineers and the cause of it is attributed to a kind of spiral motion with components in the plane normal to the main flow. Such a motion is found to exist in most conduits except those of circular cross section. Theoretical considerations show that the phenomenon is associated with the three-dimensional structure of turbulence in conjunction with changes in the direction of the boundary. Various patterns of this motion have been suggested based on experimental findings and hypotheses.

Recently, with further development of hot-wire anemometry, the motion near the corners of rectangular conduits has been investigated to find the magnitude and direction of this motion but no direct observation has previously been made on open channels. A photographic technique, described in (II.4.3.), was developed to visualize and record the motion of illuminated particles moving in a direction normal to the main flow. With the aid of the photographs, an attempt is made to map the patterns of the secondary currents.

Finally, in Chapter VI, a general study of the friction coefficient is made in analogy with the laws of friction in pipes. Some of the previous work is reviewed in comparison with the present experiments. In the case of a channel with rough bed and smooth side walls, the value of the equivalent sand roughness is obtained from velocity profiles derived from the local instantaneous values measured from the photographs. The corresponding friction coefficients were obtained by two different methods, one by neglecting the effect of side walls for small depths of flow and the other by using Einstein - Johnson's method to eliminate the effect of side walls. The results are compared with those obtained from the velocity profiles.

CHAPTER II

EXPERIMENTAL SET-UP AND PHOTOGRAPHIC TECHNIQUES

II.1. GENERAL SET-UP

The experiments were carried out in a 40 ft long glass walled tilting flume, with average width of 1.005 ft. Water surface levels were read by a point gauge mounted on a carriage which moved on rails fixed on top of the flume. Photograph, Fig. (II.1), showing a part of the flume near its inlet gives some details. The rails were adjusted until within ± 0.005" of a plane parallel to the still water surface when the flume was horizontal. The deviations at the measuring stations were then recorded and subsequently applied as corrections to all later gauge readings. The various bed forms studied are described later in the next section.

The water was supplied from an overhead tank, by piping connections, to the inlet of the flume and the rate of flow was controlled by a valve. To dissipate the energy of water, some baffles and screens were introduced in the inlet tank. A tail-gate provided in the outlet tank was used to control depth of flow. Two butterfly valves, fixed in the bottom of the outlet tank and connected to two different pipes, discharged water either into the sump or into the measuring tank. The pipe carrying water to the measuring tank was taken sufficiently down to remain always submerged, so reducing the disturbances in the tank.

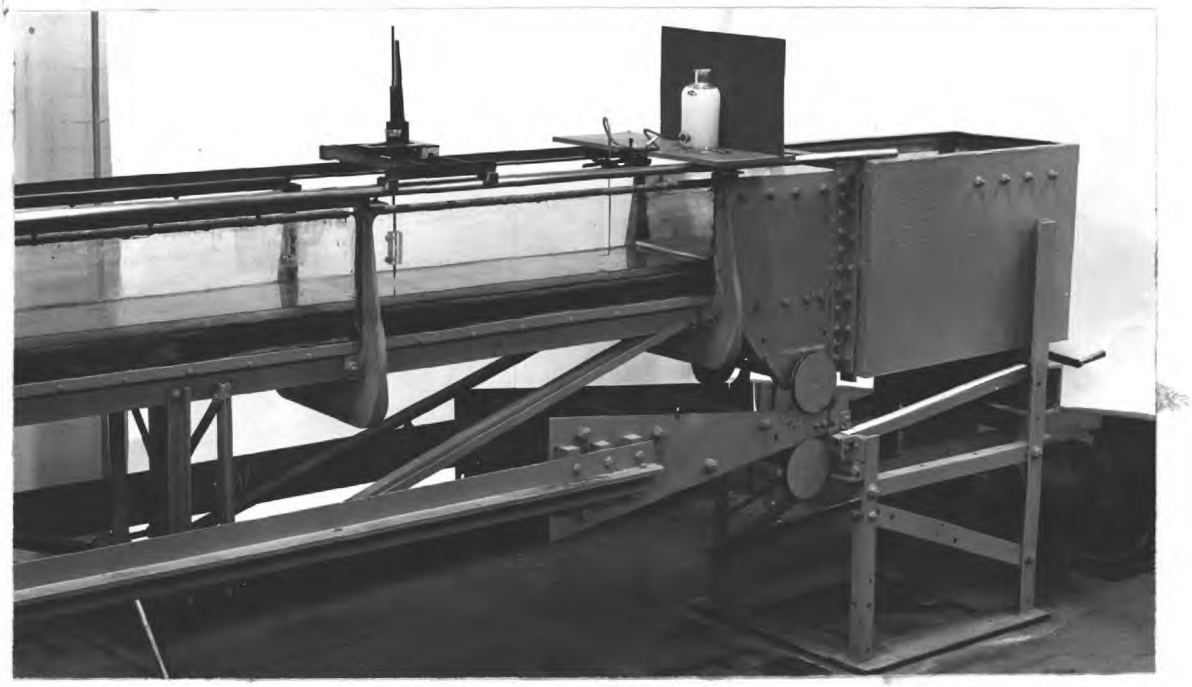


FIG.II.1. EXPERIMENTAL FLUME NEAR INLET .

The measuring tank had a plan area of 117.5 sq.ft. and an effective depth of 3 ft., so giving a total volume of about 350 cu.ft available for measurement. A point gauge, connected to a magic eye, was installed in a stilling well for measurement of depths in the tank. The tank was also calibrated by weighing but no difference was found from that obtained by linear measurements. The measuring tank, which was a part of one large underground tank, was connected to its other part by a valve and a pump was installed there to drain the water into the sump.

The pump, supplying water to the over head tank, was kept running while the experiments were performed to get a constant head. The sump water was constantly recirculating through a Filter Plant, installed in the laboratory.

II.2. BED FORMS

The first part of the investigation concerned the resistance of an already prepared stabilized sand rippled bed. To find the average ripple height and its length, three longitudinal profiles of the bed, one at the centre and two at 3 inches from the side walls, were taken. The depths were measured with point gauge and the readings were recorded to an accuracy of $\pm$ 0.010". More than 50 ripples were covered in each profile and the mean values obtained are given in the table below :

Table II.1.

Profile	Average Ripple height (inches)	Standard deviation (inches)	Average Ripple length (inches)	Standard deviation (inches)	Av. Ripple height / Av. Ripple length
At 3" from L.H.S. wall	0.310	0.060	3.855	0.430	0.081
At centre of flume	0.320	0.060	3.860	0.400	0.083
At 3" from R.H.S. wall	0.320	0.060	3.870	0.500	0.083

From the table above it is seen that the average values for the three places do not differ much and are within the accuracy of the measurements. To describe the form of these ripples, a small length of these profiles is shown in Fig. (II.2). Also to show how the bed varied across the flume, full contours of the bed, except within an inch of the two side walls, are shown in Fig. (II.3), over a length of few ripples.

The second bed investigated was formed by filling up the troughs of the ripples with gravel just up to their crest levels. A photograph of the resulting bed is shown in Fig. (II.4).

The third bed investigated was formed by adding gravel until the crests of the ripples were fully covered. This bed was made as plane as possible with a spirit level and point gauge readings taken on a plate, kept above the bed. The bed form is shown by a photo-

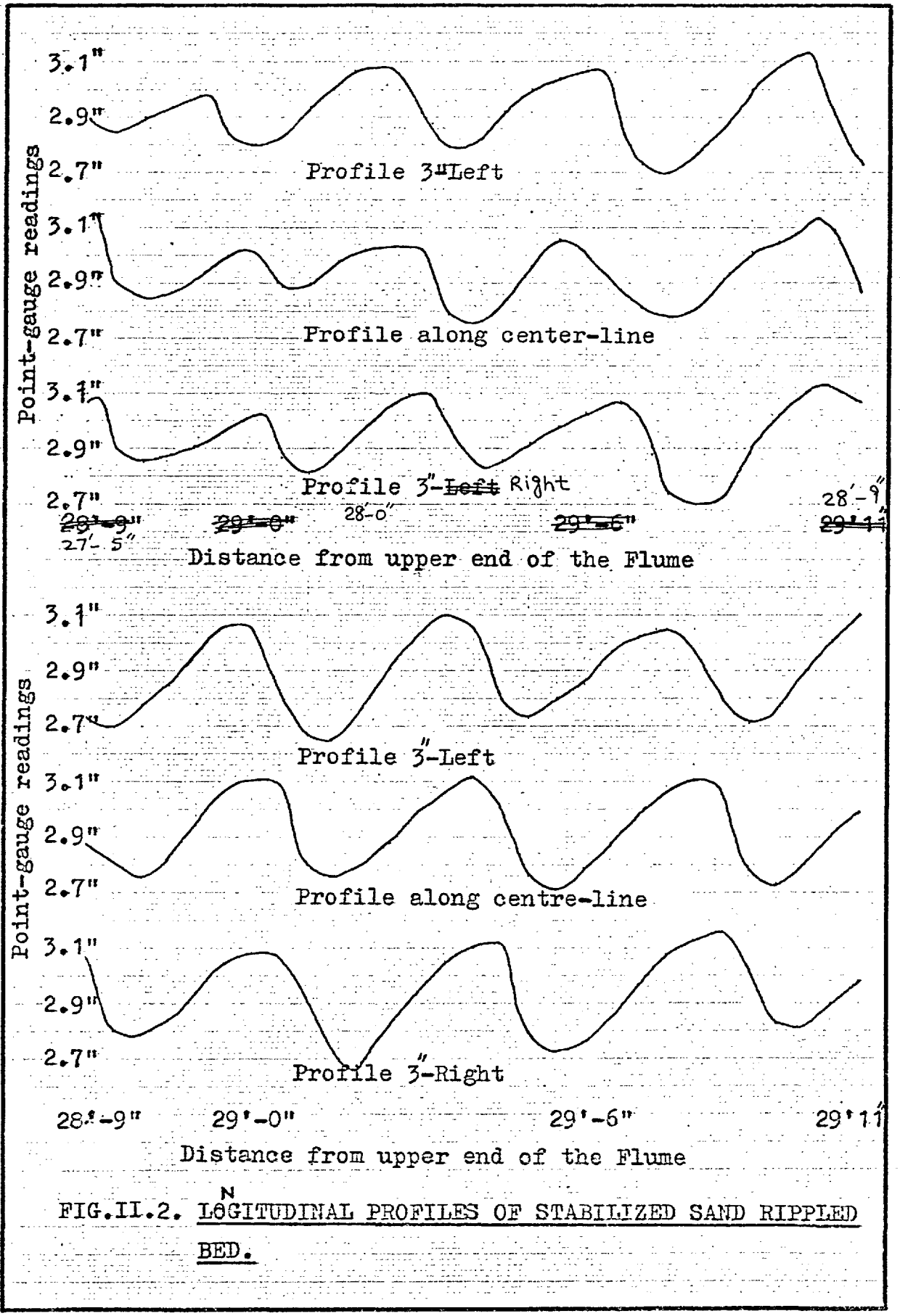


FIG.II.2. LONGITUDINAL PROFILES OF STABILIZED SAND RIPPLED BED.

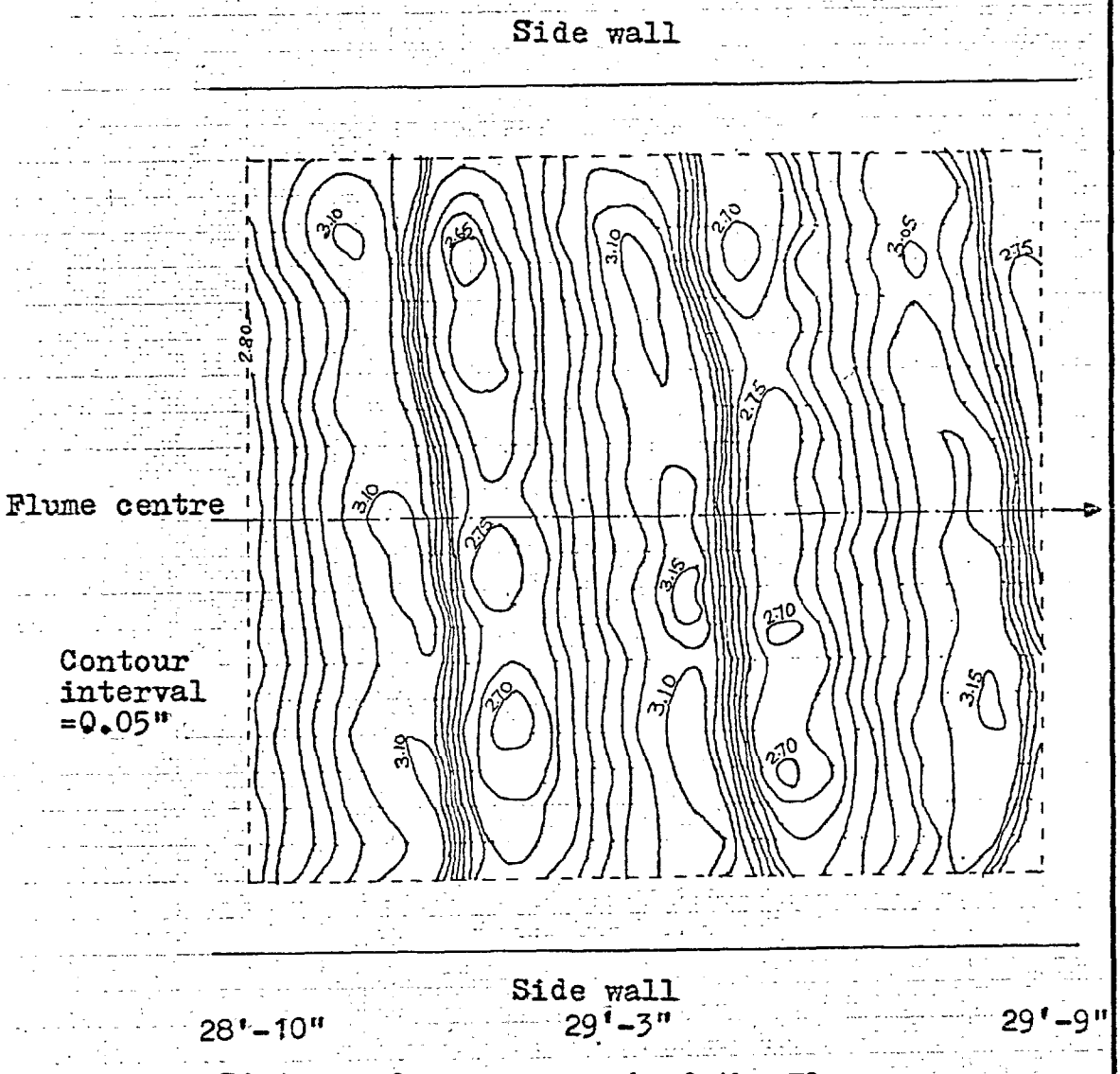


FIG.II.3. TYPICAL CONTOURS OF THE RIPPLED BED.

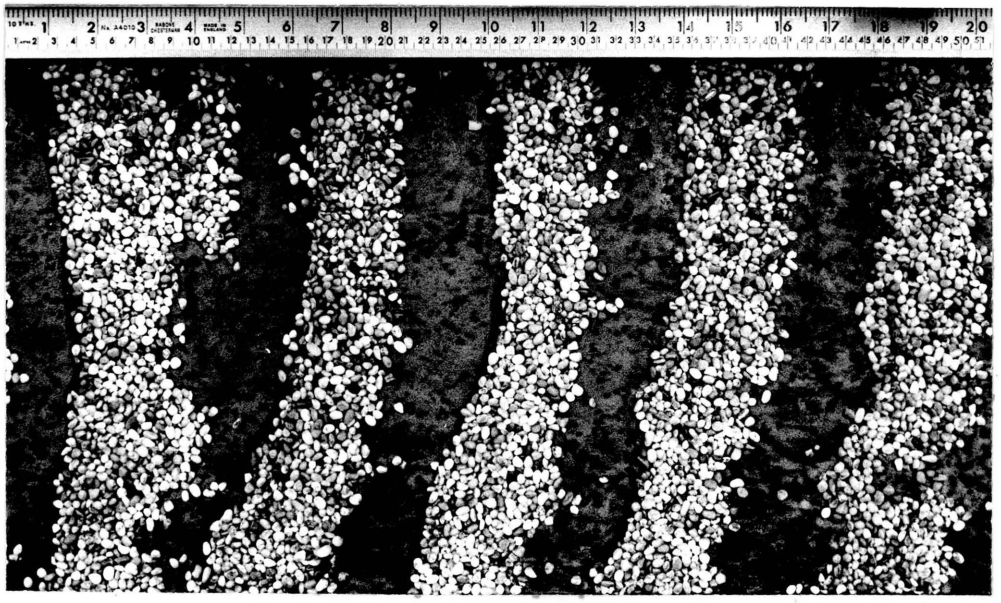


FIG.II.4. TOP VIEW OF RIPPLED BED WITH GRAVEL FILLED IN TROUGHS OF THE RIPPLES .

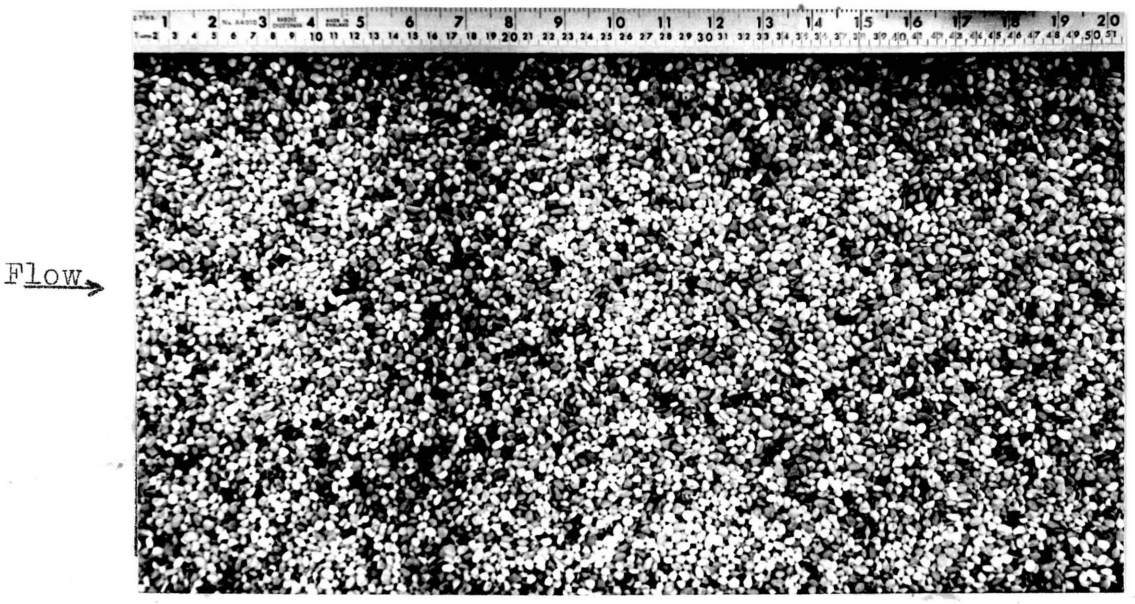


FIG.II.5. TOP VIEW OF FULLY GRAVELLED BED .

graphs in Fig. (II.5).

The gravel for the above two beds, was fine gravel (size 2 m.m to 6 m.m). A plane rough bed could be obtained with this gravel and, moreover, it did not start moving in the range of shear velocities investigated. For example, taking the median diameter of the grains as 3.6 m.m, the shear velocity at which they could move, according to Shields' diagram, would be 4.0 cm/sec. This value of shear velocity would correspond to a depth of flow about 10 cm., for the slope of the flume 0.0015.

The last bed investigated had a smooth glass bottom, about 36 ft long. The glass for the bed was supported on sand. Machined cross-pieces of aluminium 2" wide, $\frac{1}{4}$" thick and in lengths slightly less than the width of the flume, were placed on a prepared plane sand bed at distances of 3' - $7\frac{1}{2}$" where the flume had braces to hold the side glass walls. More sand was filled inbetween the cross-pieces to make a plane level bed. The glass plates, $\frac{1}{4}$" thick, $11\frac{3}{4}$" wide and in lengths of 7' - 3", were laid on the sand bed with ends over the cross-pieces. About one ft length of a glass plate where the photographs had to be taken was painted black from the bottom. All the joints were filled with a putty (Arbostrap) and carefully smoothed. The two ends of the bed were sealed and a transition in the entrance was provided by a ramped wooden board. Before any experiments were made, levels were taken with point gauge on the

glass bottom and the bed adjusted accordingly. The greatest deviation of the glass bottom from a perfect plane was about ± 0.005".

II.3. EXPERIMENTAL PROCEDURE

In order to determine the friction coefficient, the usual measurements of depth, discharge and slope would be required. Discharge and slope were treated as independent variables and depth as dependent variable. For every slope of the flume the inlet valve was adjusted to give various discharges; uniform flow was established by regulating the tail gate until the same depth was obtained throughout the measuring zone. The depths for this were measured by point gauge at 5 ft intervals in a 15 ft length of measuring zone, starting from 15 ft after the entrance. When the free surface was smooth, water levels could be measured within ± 0.001"; however when waves appeared, the depths were taken to be average values over crests and troughs of the waves and the accuracy of measurement then might be up to ± 0.010". The flow was sub-critical throughout with Froude number much less than unity. A thermometer was installed in the inlet tank to read the water temperature within ± 0.1°C.

II.4. PHOTOGRAPHIC TECHNIQUES

II.4.1. INTRODUCTION

Since the early days many photographic and other methods for

visualizing fluid motion have been developed. Recently Clayton and Massey (1967) have summarised the methods particularly suitable for water and given an extensive bibliography.

Outstanding among these techniques for use with water is one in which highly reflective tracer particles are held in suspension, and strongly illuminated by a thin sheet of intense light, so appearing as bright points when viewed from a direction perpendicular to the light. The motion of the particles in the illuminated plane can be photographed to provide a record in the form of streaks whose lengths vary according to the velocity of flow and the duration of exposure.

The tracer particles may be gas bubbles, droplets of immiscible liquids, or solid particles of some suitable substance giving high optical contrast with the surrounding fluid. The paths of the tracer particles are likely to be identical with the flow paths of the fluid particles only when their size is very small and their density is the same as that of the fluid.

If the duration of the photographic exposure be known, the velocity in any region in the illuminated plane can be obtained from a photograph of the paths traced by the illuminated particles. However, when the flow is turbulent, the tracer particles may be lost because they completely cross the thin sheet of light in the transverse direction. The loss depends on the width of slit and on the

intensity of the turbulence,as well as upon the duration of the exposure. One way of overcoming this difficulty is by putting a rotating disc, with slots, either in front of the illuminating system or in front of the camera. Then the paths of the illuminated particles are obtained as a series of dashed streaks, from which the particle velocity may be computed. The installation of such an optical chopper can be avoided by using an electric discharge lamp which has the advantage over a continuous light source that it provides virtually continuous but interrupted illumination with a pulse from the ordinary A.C. supply.

II.4.2. PHOTOGRAPHS TO MEASURE TURBULENCE AND LOCAL VELOCITY

As mentioned before, the local velocities can be computed from the total lengths of the streaks recorded on the photographs.

To obtain local instantaneous velocity along X axis, in the direction of main flow, and turbulent component along y axis, normal to the bed, the photographs were taken in plane XY at the centre of the flume where the main flow was substantially two dimensional. To be free from anomalies from upstream, the photographic section was selected to be at 30 ft, from the flume entrance. The general arrangement of the photographic equipment, showing the position of lamp and camera, is shown in photograph Fig. (II.6.a) and diagram Fig. (II.6.b).

The tracer particles used were a plastic powder, with trade name



FIG.II.6.a. PHOTOGRAPHIC ARRANGEMENT TO RECORD MOTION OF PARTICLES IN CENTRAL PLANE OF FLUME .

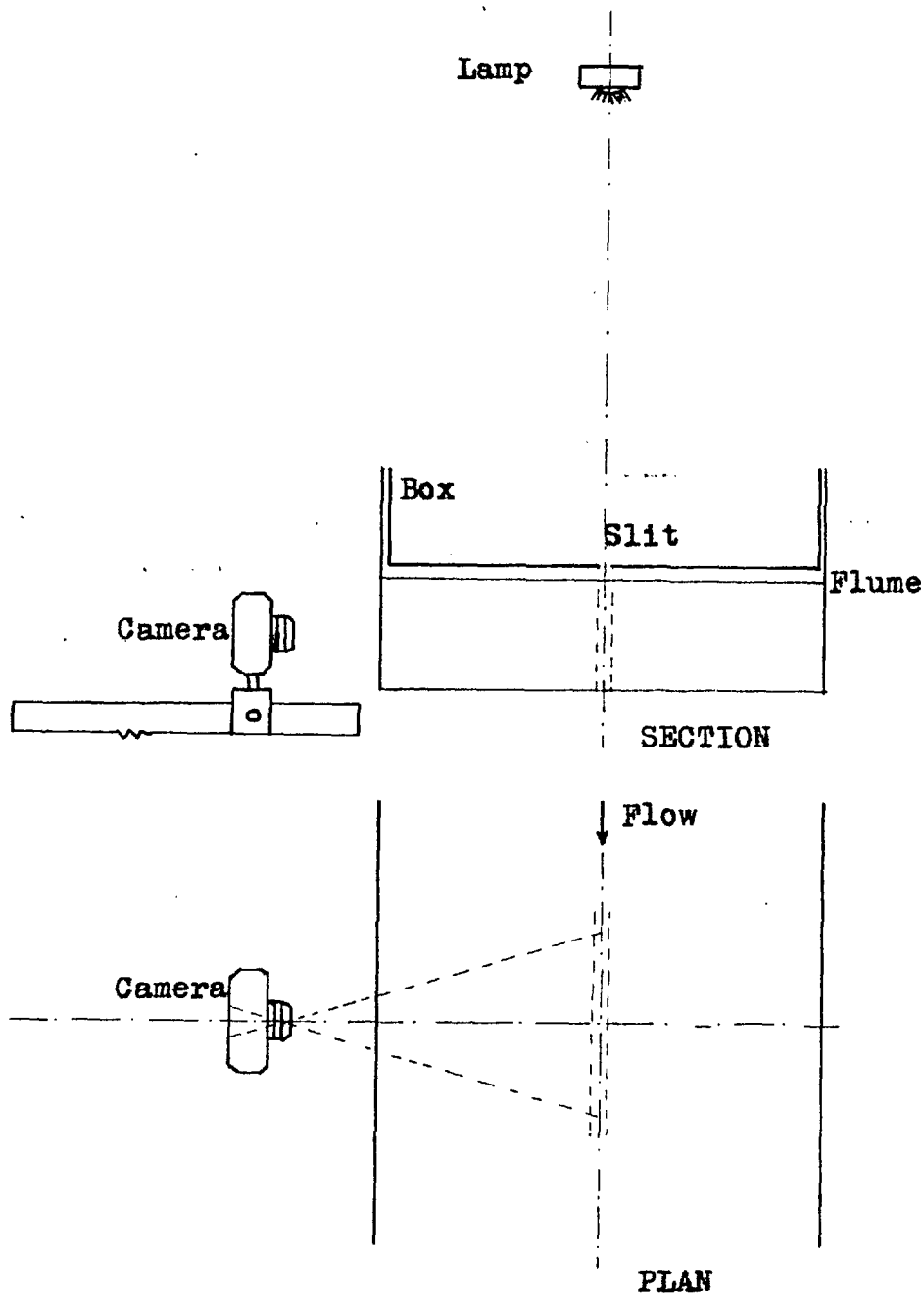


FIG.II.6.4. PHOTOGRAPHIC ARRANGEMENT TO RECORD MOTION OF PARTICLES IN CENTRAL PLANE OF FLUME.

TELCON, white in colour and with good reflection property. The specific gravity of the powder was about 0.95 which is about 0.05 less than that of water. This difference in specific gravity is sufficient to create discrepancies in particle velocity relative to that of water; but for this difference of specific gravity the rising velocity of 0.1 mm diameter particles is no more than 0.3 mm/sec and such particles will follow the fluid motion more faithfully than larger ones. But unfortunately, better photographs can be obtained with larger particles since these would reflect more light. In view of this, particles of various sizes were tried and it was found that with the illuminating system available, the suitable minimum size was 0.10 mm to give photographs bright enough to be analysed without much difficulty. Therefore particles which passed through B.S seive 100 and were retained on seive 150 were used. The suspension of the particles in water was made by adding a little "Teepol" and the lighter particles which floated very quickly were skimmed out. The suspension was fed into the flowing water at a place about 15 ft upstream from the photographic section, through a fine tube, (Photograph Fig. (II.1)).

The lamp used was a water cooled Mercury vapour lamp of 500W connected through a ballast to the A.C. supply with frequency 50 C/S. Thus the light flashed 100 times a second which served as the fundamental timing device in measuring the velocity of the tracer particles. This lamp was mounted on an optical bench, supported on two stands,

about 3 ft above the flume. It was adjusted to be exactly above a slit to give a thin vertical sheet of light at the flume centre. The slit, provided in the bottom of a box, was kept near the water surface. Its width was 0.25", the minimum possible, to avoid excessive lateral loss of particles due to turbulence. No light, other than that coming through the slit, was allowed and the photographs were taken with dark back and fore ground by covering the whole system with a black cloth.

The camera, mounted on an optical bench, was set parallel to the glass side wall of the flume. For exact focussing, a scale was introduced into the water at the flume centre below the illuminated plane of light and a photograph of the same scale gave the magnification ratio. Altogether a length of about 5 inches, along the x axis was explored, thus the photographs covered about one ripple length; and this length was kept the same for the other beds also.

A Praktica VF reflex camera, for 24 x 36 mm pictures, with interchangeable lens was used. A Merritar lens, focal length 50 mm and f/2.9, with small extension to take close photographs was attached to the camera. The photographs were takem with aperture ratio of f/2.9 and the exposure time of 1/6th second so giving about 16 dashes in each streak. Tri - x pan Kodak film was used for all the photographs.

Sufficient exposures (about 20 to 30) were taken to record altogether 200 or 300 streaks for each depth of flow. The film was

projected through an enlarger onto a sheet of squared paper to read ± 0.5 mm. It was magnified five times the original size and hence an accuracy of measurements ± 0.1 mm or 0.004" was obtained. In each streak 10 or 15 dashes for a time of $\frac{10}{100}$ or $\frac{15}{100}$ seconds were measured to estimate values of local instantaneous velocity components in the X and Y directions. Some of the paths traced by particles during any exposure, perhaps 1 in 10, were curved in which case a small number of dashes in straight portions were measured.

II. 4.3. VISUALIZATION AND PHOTOGRAPHS OF MOTION IN A PLANE NORMAL TO THE MAIN FLOW

Certain puzzling features about secondary currents in straight channels ~~laid~~ led to the development of the photographic technique described below. The aim was to visualize the motion of the fluid in a plane normal to its main flow and to record it photographically. The method is based on the principle that if the motion of the fluid is made visible by brightly illuminated tracer particles and is observed axially such that the main flow is directly towards the observer, then, on average, only the secondary currents would be seen.

In certain preliminary investigations, for flow visualization in a cross-section, a 12" wide mirror was installed, in the outlet tank, facing the main flow and at 45° to the flume cross section. At about 10 ft upstream from the outlet tank, the cross section of the flume

was illuminated by passing a beam of light through the glass side wall. A Cathetometer telescope was installed on the outlet tank, above the mirror, and it could slide horizontally across the width to observe the motion of tracer particles coming from upstream. These got illuminated when they passed through the lighted cross section. The remaining portion of the flume was covered with black cloth to give a dark back and fore ground. When the telescope was sharply focussed, the illuminated tracer particles appeared as bright points and some of their path lines in the plane normal to the main flow could be observed.

To record this motion, the telescope was replaced by a suitable photographic equipment installed over the outlet tank. It consisted of a telephoto lens screwed on to the bottom of a vertical aluminium tube, painted black inside, and on the top of which was mounted the camera complete with bellows extension. An Aero-camera f/5 lens of focal length 500 mm was used. The design calaulations for the photographic equipment are given in Appendix (I). As the mirror was of an inferior quality, good photographs could not be obtained with it, and hence was replaced by an old $4\frac{1}{2}$" Wray prism,. the largest available. The prism was attached to the lower end of the tube, below the lens, by brass strips, slotted for small adjustments. In front of the prism a water-filled perspex box was attached to avoid distortion due to surface waves. The photograph Fig. (II.7a) and diagram Fig. (II.7b) show the various units. The whole arrangement was mounted on a levelled

horizontal steel frame, clamped to the top of the outlet tank, such that the tube and its mountings could be slid across the width and indeed moved in any direction. The lighting arrangement consisted of the 500 W water cooled Mercury vapour lamp, a condenser, slit and a field lens mounted on an optical bench, shown in photograph Fig. (II.8). The glass side wall was blackened except for a slit, one inch wide and about four inches deep, through which a nearly parallel beam of light passed across the darkened channel. Again, for correct focussing a scale was photographed in the illuminated cross section. The prism and the tube, holding the lens and the camera, were adjusted to be in correct position so that the rays reflected by the prism were vertical and along the axis of the tube until the sharp pictures were obtained.

It was necessary to identify the direction of motion of each particle, traced on the photograph for knowing the direction of the secondary motion. To do this, one-half of the width of the slit on the glass side wall was covered with a small strip of unexposed developed film to allow less amount of light through this than the other half. As the particles travelled from dim light to bright light, such difference of illumination was observed on the streaks traced on the photographs, each streak showing also the direction in which the particle was going.

As about 5" width of the flume could be photographed each time, an attempt was made to cover the full width of 12" by taking over-

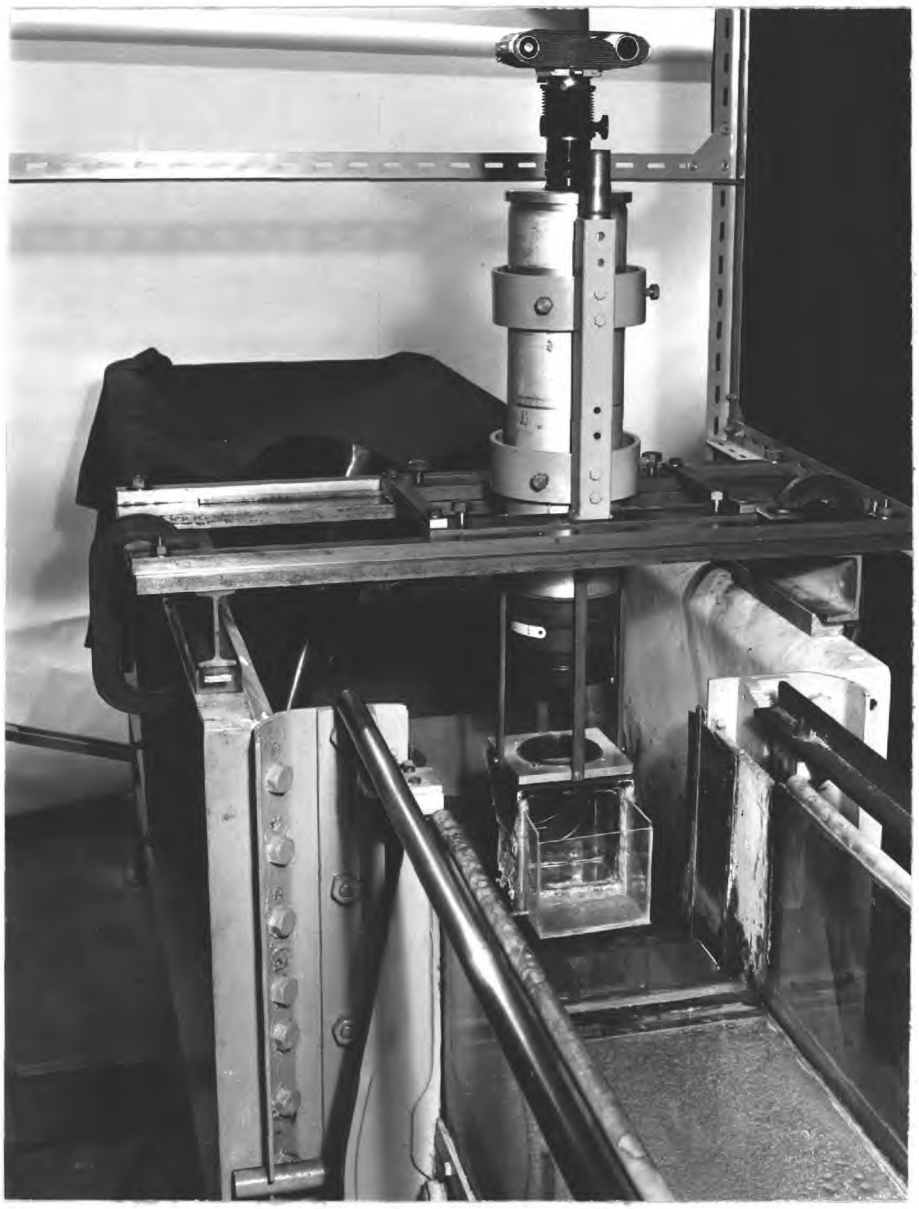


FIG.II.7.a. PHOTOGRAPHIC ARRANGEMENT TO VISUALIZE AND RECORD MOTION OF PARTICLES ACROSS MAIN FLOW .

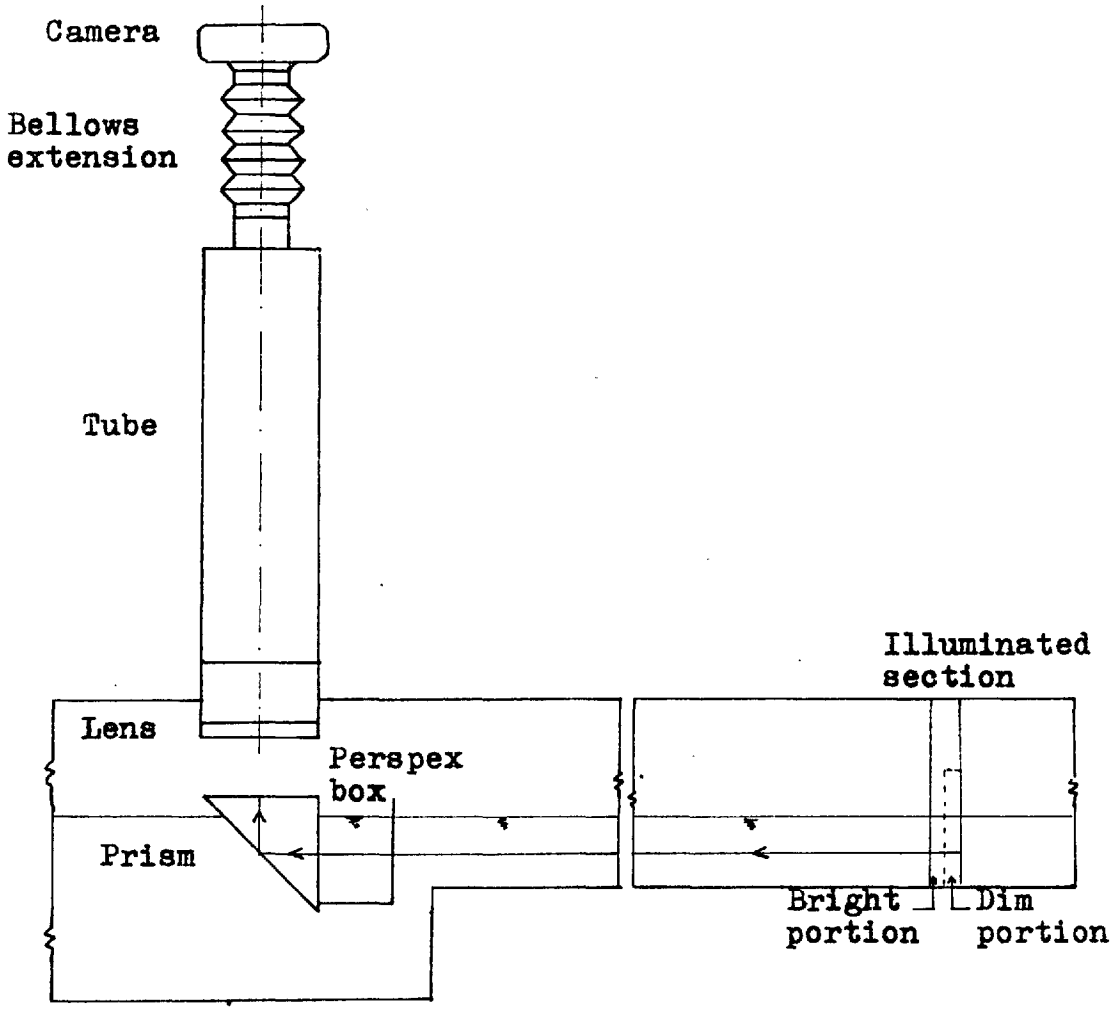


FIG.II.7.b. PHOTOGRAPHIC ARRANGEMENT TO VISUALIZE AND RECORD MOTION OF PARTICLES ACROSS MAIN FLOW.

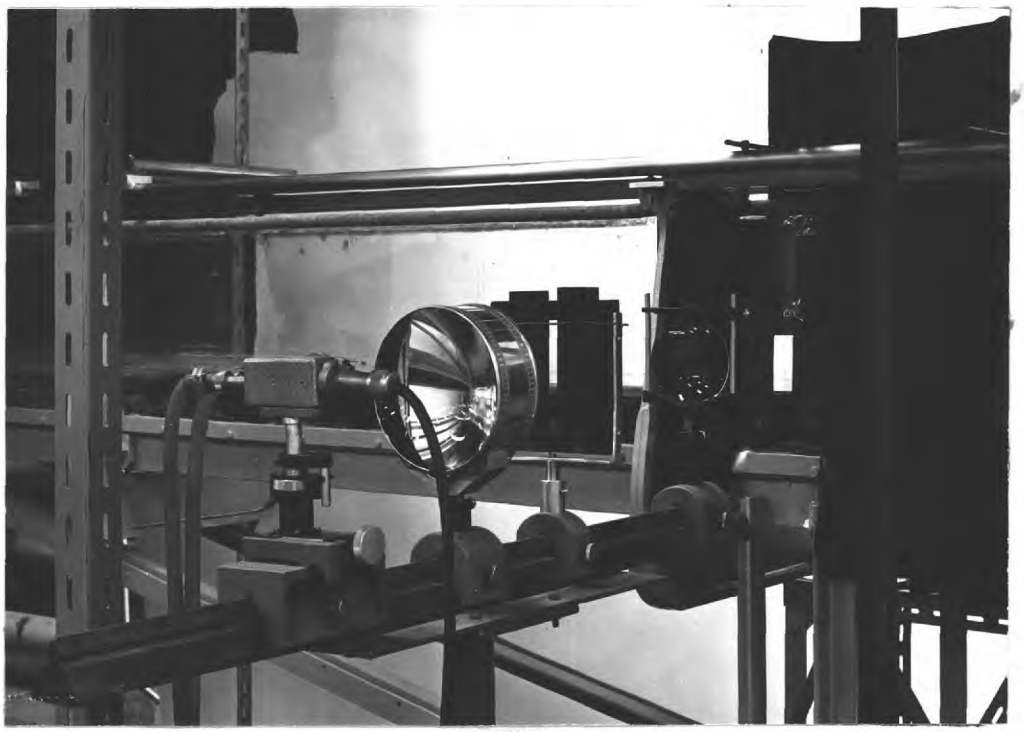


FIG.II.8. LIGHTING ARRANGEMENT FOR FIG II.7.

lapping photographs in three stages. Unfortunately the intensity of light decreased as it passed through the water and hence good photographs could not be obtained close to the side wall away from the light source. Hence the photographs were taken only in two stages and therefore covered about one-half of the flume width. Different aperture ratios and exposure times were tried and it was found that with aperture ratio f/8 or f/11 and exposure time $\frac{1}{4}$ sec, good sharp pictures with enough traces were obtained.

Enough photographs were taken to get statistical mean values, so eliminating turbulence and disclosing the residual patterns of the secondary currents.

A maximum depth of flow of about 2.50" could be investigated with this arrangement.

CHAPTER III

THE ONSET OF TURBULENCE IN RECTANGULAR CHANNELS

In a fluid of kinematic viscosity ν and density ρ flowing between parallel walls, the critical value of the pressure gradient, dp/dx, which will generate a flow in which turbulence is just self-sustaining, can be defined by a Reynolds number $\frac{RV}{\nu}$, or $\frac{RVx}{\nu}$, where V is the velocity defined as discharge divided by the cross sectional area, R is the hydraulic radius being the cross sectional area divided by the wetted perimeter, ν is the kinematic viscosity, $Vx = \sqrt{\frac{\tau}{\rho}}$, $\tau = R\frac{\partial p}{\partial x}$, and when there is a free surface with gradient S, $Vx = \sqrt{RgS}$. As Osborne Reynolds (1883) explained, the criterian as to whether or not the motion will be turbulent can be stated in a number of ways. For example, there is a "lower critical velocity" below which all disturbances are so damped that they decay as they are carried along by the fluid and, far downstream, the motion ultimately becomes steady. Also for each particular disturbance, or set of disturbances, there is a "higher critical velocity" below which decay always occurs, and above which disturbances rapidly grow to become what is known as fully developed turbulence, which is a self supporting random set of disturbances moving along with the particular volume of fluid in which it originates. The manner in which such disturbances are diffused laterally and longitudinally remains a topic of considerable interest. Possibly the following experimental observations are relevant.

Schiller (1921) established that in pipes of circular section the lower critical velocity is very nearly given by $\frac{RV}{\nu}$ equal to 550, and he went to considerable pains to establish that disturbances of all strength did really decay when the pipe was sufficiently long and the Reynolds number $\frac{RV}{\nu}$ below 550. Since this concerns stability one would hardly expect the critical Reynolds number to be the same for all shapes of the cross section. Later, Schiller (1923), studying the friction in various pipes, obtained the value of the lower critical Reynolds number $\frac{RV}{\nu}$ equal to 570 for a pipe of square cross section, with an entrance length of 220 R. However, Davies and White (1928) experimenting with wide retangular pipes, whose width ranged from 170 times the depth to 40 times the depth, found that the very large disturbances caused by a sharp corner at the entrance to the pipe had completely decayed in a length of 54 to 80 times the depth when $\frac{RV}{\nu}$ was less than 700, but they still persisted when $\frac{RV}{\nu}$ exceeded 720. Davies and White also distinguished a much lower critical value, which, they considered was due to the first sign of the shedding of disturbances from the entry. But, as Taylor pointed out, and White (1929) later confirmed, this could have concerned the persistence of helical motions of the kind found in curved flows. Cornish (1928) in an investigation of flow through a rectangular pipe (with sides 1 : 2.92) found that the entrance disturbances persisted up to a distance of 400 R and the lower critical Reynolds number obtained was 525.

An interesting variation occurs with the experiments of Allen (1934) who worked on an open channel where the width-depth ratios were in the range 2.81 to 0.525. At first sight a rectangular channel may seem like one-half of a closed rectangular pipe with the free surface corresponding to the mid plane of the pipe and both being planes of zero shear stress. However, concerning stability the difference in dissipation in the plane of the free surface would be quite different, and Allen's type of experiments are seen to be of great importance. The value of the lower critical Reynolds number $\frac{RV}{\nu}$ for smooth channel, with obstructions in the entrance, he obtained was 1400. This value is about twice the value Davies and White obtained in wide rectangular pipes and about 2.6 times the value obtained by Cornish in a narrow rectangular pipe. He attributed this to the free surface which "favours stability".

Since then Horton (1934), Straub (1939), Owen (1954), Straub, Silberman and Nelson (1958), Allen and Ullah (1967) and many others have worked on open channels of various sections. These works have been summarised by Allen and Ullah (1967). Various values of the critical Reynolds number, even for same cross sectional shapes, have been reported and it is difficult to know as to how far the varying entry conditions influenced their results.

In the present experiments, the entrance was initially designed for minimum disturbances. The discharge and the slope were varied and the width-depth ratio was in the range of 60:1 to 30:1. With this

entrance, the critical value of $\frac{RVx}{\nu}$ was about 61 (or $\frac{RV}{\nu}$ equal to 1250). The results are shown in Fig. (III.1) and are seen to follow the two theoretical curves, for flow between parallel plates, for laminar and turbulent regions. The curve on the left for laminar flow is $\frac{V}{Vx} = \frac{1}{3} \frac{RVx}{\nu}$ and that on the right for turbulent flow is $\frac{V}{Vx} = 5.75 \log_{10} \frac{RVx}{\nu} + 3.0$. When the flow was in the critical range, eddies could be seen coming in series from the entrance and were clearly marked on the water surface. Two distinct depths occurred for the same discharge; one : when the eddies were passing the gauge point, this depth being greater; and, the other : when the eddies had passed off, this depth being smaller. These points are marked by crosses in Fig: (III.1). This critical value of $\frac{RV}{\nu}$ namely 1250 is less than the lowest value obtained by Allen although this entrance was smoother than his.

However, in a new series of experiments, the entrance of the present channel was partly obstructed by some course angular gravel varying from 1" to 2" in size to see what effect this would have on the critical Reynolds number. The results shown in Fig. (III.2.) are in good agreement with the curve for laminar flow up to $\frac{RVx}{\nu}$ equal to 44.5 (or $\frac{RV}{\nu}$ equal to 670). At $\frac{RVx}{\nu}$ equal to 48.5 (or $\frac{RV}{\nu}$ equal to 735), there is a deviation from the theoretical curve showing a drop in the value of $\frac{V}{Vx}$ of about 6 per cent.

It may be mentioned that the eddies created by the obstructions in the entrance travelled progressively larger distances down stream

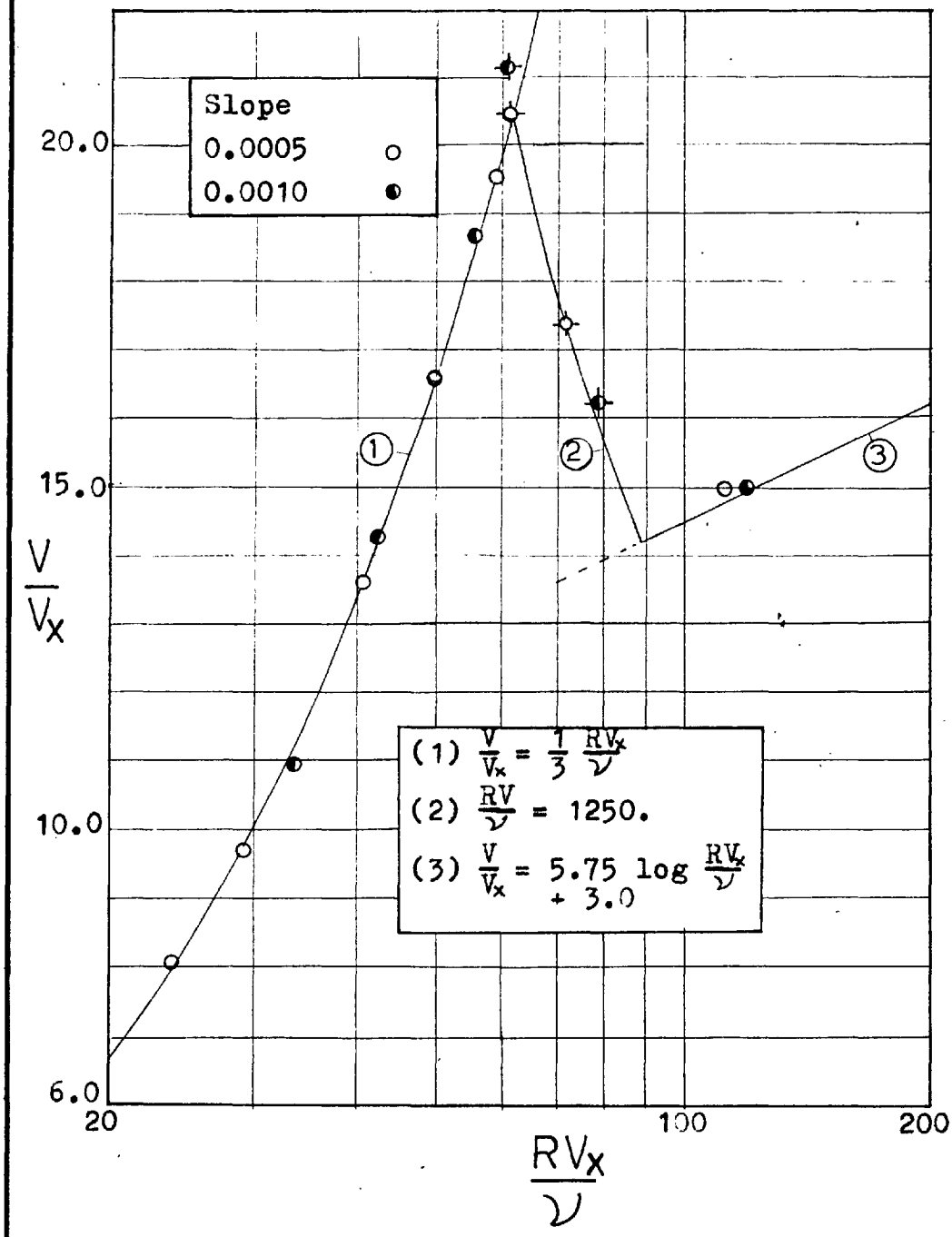


FIG.III.1. LAMINAR FLOW RESULTS WITH ENTRANCE FOR MINIMUM DISTURBANCES.

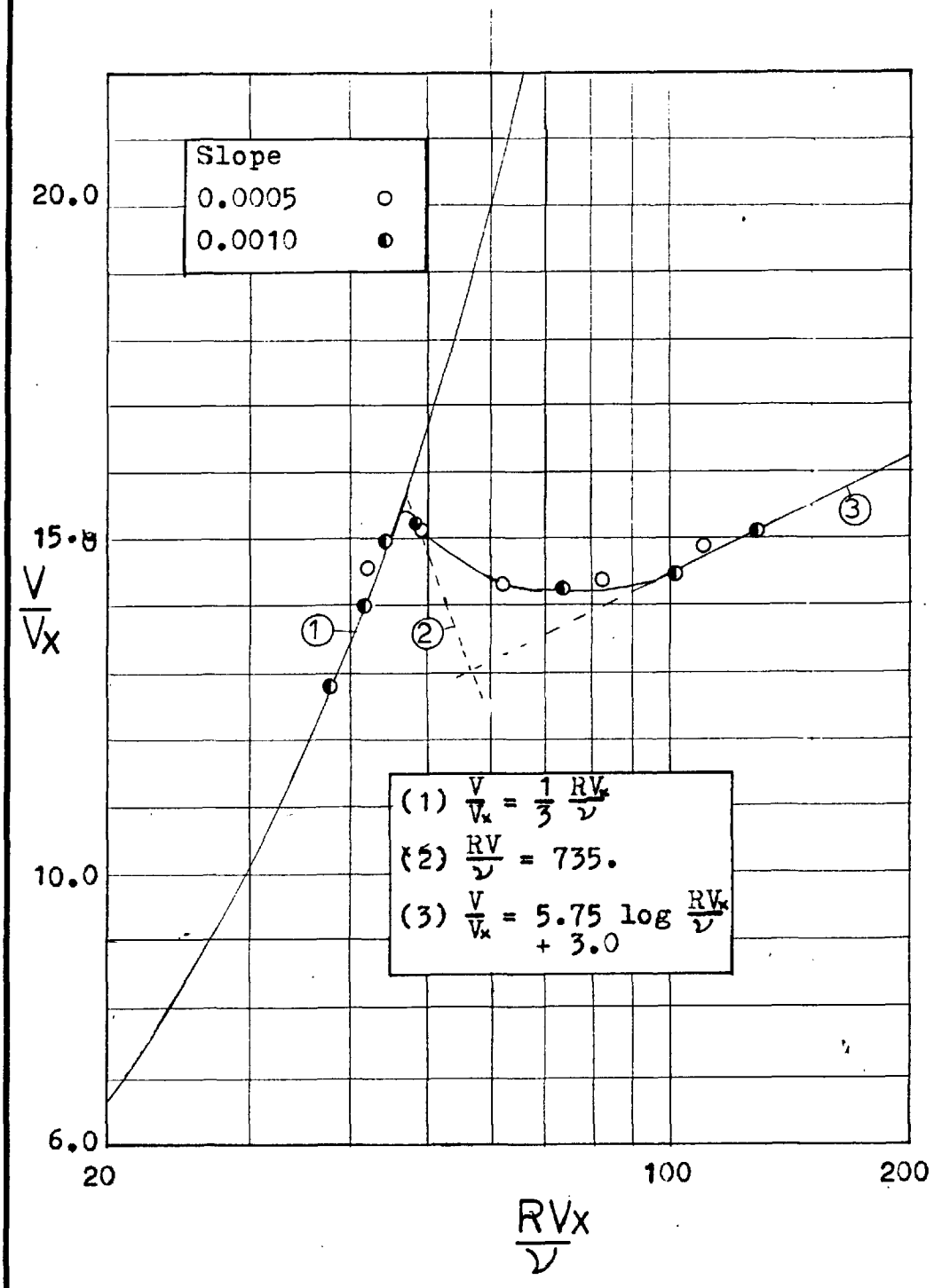


FIG.III.2. LAMINAR FLOW RESULTS WITH OBSTRUCTIONS IN THE ENTRANCE.

both when the water depth was increased and also when $\frac{RVx}{\nu}$ was increased independently. At $\frac{RVx}{\nu}$ equal to 44.5 (or $\frac{RV}{\nu}$ equal to 670), the eddies completely died out within 4 to 5 ft. from the entrance, giving L/R equal to 200 to 250. The eddies thus did not reach the test length which was at 15 ft.($\frac{L}{R}$ = 750 approx) from the entrance. At $\frac{RVx}{\nu}$ equal to 48.5 (or $\frac{RV}{\nu}$ equal to 735), the eddies did not die out completely and some continued throughout the length of the channel. As $\frac{RVx}{\nu}$ was further increased, the value of $\frac{V}{Vx}$ decreased; but the sudden drop, like the one observed in Fig. (III.1), did not occur when the entrance was obstructed, Fig. (III.2). In Fig. (III.2.) the transition from the laminar to the turbulent region is via a more rounded curve than in Fig. (III.1). In both Figures, fully developed turbulent flow starts more or less at the same value of $\frac{RVx}{\nu}$, namely 100.

Taken as a whole, the present results show that the lower critical value of $\frac{RV}{\nu}$ (as defined above) for wide rectangular channels is approximately 700. This seems to be valid for free surface flow as well as for closed rectangular pipe flow.

CHAPTER IV

TURBULENCE MEASUREMENTS

IV.1. INTRODUCTION

In turbulent flow, the velocity and pressure with which one is concerned fluctuate irregularly in time and space over their temperal mean values. Although these mean values give a complete piecture of the motion, yet to get a deeper understanding of the mechanism of the turbulent flow, particularly of the forces concerned, one requires information regarding the magnitudes and the variations of the turbulent fluctuations.

The simplest type of turbulence, idealised theoretically, is the isotropic turbulence, the statistical features of which have no preference for any particular direction. Next is the homogeneous turbulence which has the same structure throughout the flow field. However, the type of turbulence which occurs most frequently in nature, namely the shear flow turbulence, differs greatly from these ideal types primarily because it includes a gradient of the mean velocity and a gradient of the average shear stress. Two frequently occuring types, i.e. the "wall turbulence" generated by friction forces at the wall, and the "free turbulence" generated by the flow of fluid layers with varying velocities, passing over one-another in the absence of the walls, also come

into this non-isotropic class. The present investigation is concerned solely with such a non-isotropic shear flow and wall turbulence, generated at the bed of a channel by friction forces due to the flow of water.

In a flow consisting of a parallel mean motion in the direction of the x axis, where the local mean velocity, $\bar{u}$, is a function of distance normal to the wall, y, only, the shear stress is mainly due to the velocity fluctuations which transfer the momentum from layer to layer. The magnitude of this shear stress is given by $-\rho\,\overline{u'v'}$, where u' and v' are the velocity fluctuations superimposed on the mean values in the direction of flow and normal to the wall respectively. The mean value of the product of u' and v', $\overline{u'v'}$, is zero, when both the components are randomly distributed as in the case of isotropic turbulence.

The main characteristics of the turbulent flow at a certain point are conveniently defined by the magnitude of the velocity fluctuations, u', v' and w', in the directions of the X, Y and Z axes respectively, and the correlations between them. If the local instantaneous value of the velocity is written as $u = \bar{u} + u'$ (where the overscore denotes the average value and the prime its turbulent fluctuation) then, by definition, $\overline{u'} = 0$. It is not possible, therefore, to take the average value of the fluctuations as a measure of the turbulence. However, the average of the

absolute values of the fluctuations, i.e., $\overline{|u'|}$, or the maxima of the fluctuation, $|u'|_{max}$, may be taken as a measure of the turbulence. But the magnitudes of the turbulent fluctuations are usually represented by their root mean square values, i.e. $\sqrt{\overline{u'^2}}$ etc., which is a particular measure of the average required in connection with stresses. The magnitude of the turbulence, presented in this form is designated as the intensity of turbulence. The relative intensity of the turbulence is expressed by the ratio of the intensity to some mean value of the velocity. This mean value may either be the local mean velocity, $\bar{u}$, or the average velocity of flow in the section, V, or, sometimes, the maximum local mean velocity, $(\bar{u})_{max}$., or alternatively the mean shear velocity at the bed, v_{xo}.

One aspect of the correlation between two velocity fluctuations is given by the mean value of their product as shown above. Often, a correlation coefficient (Weatherburn 1946) is used to define a particular relationship between the fluctuating components. Such a correlation coefficient between u' and v', measured at a point, is expressed as $\overline{u'v'} / \sqrt{\overline{u'^2}}\ \sqrt{\overline{v'^2}}$. This correlation coefficient can have any value between -1.0 and +1.0. It is zero if the fluctuating components are randomly distributed, and is equal to unity if they are proportional to each other. It is negative if one component has a positive value and the other has a negative value.

In the present work, the average values of the turbulent quantities were determined in approximate ways. When measurements are taken at a fixed point in space over a long period of time then their time average is a true measure. Alternatively, when the motion is homogeneous, the average with respect to space at a fixed time is a satisfactory measure. However, the experimental conditions were such that, neither the time-mean nor the space-mean at any point could be ascertained; and this being so, a nearest convenient substitute was evaluated, by averaging the local instantaneous values, as described later in (IV.3.).

IV.2. MEASUREMENT OF TURBULENCE

A field engineer interested in the measurement of velocities in a river, using a sensitive current meter equipped with an electrical registering device, is likely to detect certain departures from the mean values on his record. Similarly, a research worker in the laboratory, using a pitot tube in a pipe or a channel, indeed, finds the same type of fluctuations in the readings of his instrument. The engineers, seeking mean values, sometimes take measures to dampen these fluctuations. However, recently the fluctuations themselves have been the object of the measurement and it is interesting to review some of the main results.

Fage and Townend (1932) were probably the first to use an ultra-microscope with a moving objective to measure the turbulence.

In a pipe, the minute particles usually present in water were made visible by intense light and examined by an ultra-microscope against a dark background. They measured the "maximum values" of the turbulent components u', v' and w'. At the centre of a pipe, they found the three components to be approximately equal in magnitude approaching isotropic conditions. Near the wall, the magnitude of v' relative to the mean velocity in the pipe decreased to zero while u' and w' increased. They examined the flow very near the wall in a square pipe, right down to a distance of $\frac{1}{40,000}$ inch from the wall, and observed that owing to the tendency of the component v' to vanish at the wall, the flow tended to the laminar type, although the motions of particles in the laminae were sinuous. Fage (1936) extended further this work on circular pipe and found that the turbulent components relative to the shear velocity V_{xo} have their maximum values at a distance of $\frac{22.4\nu}{V_{xo}}$ from the wall. Fage (1933) also examined, the flow in a square pipe with the sides artificially roughened in pyramidal form and compared these results with those of a smooth pipe for approximately the same value of Reynolds number, $\frac{RV}{\nu}$. The turbulent components when related to both the local mean velocity and the average velocity in the pipe were found to be greater in the rough pipe than in the smooth pipe.

Other investigators have successfully used the hot-wire anemometer to measure the various components of the turbulence.

This method is particularly suitable for air-flows. Interesting results have been obtained in pipes, closed channels and in the boundary layers on flat plates.

Wattendorf and Kuethe (1934) carried out such measurements in the central section of a closed channel, 5 cm. wide and 90 cm. deep. They measured only the intensity of the u' component. From their results (for one value of Reynolds number) plotted as $\frac{\overline{u'^2}}{(\bar{u})_{max}^2}$ against the distance from the centre, they concluded that a straight line could be drawn through all the points except those close to the wall or very near the channel centre. Moreover, the relative intensity, $\frac{\sqrt{\overline{u'^2}}}{(\bar{u})_{max}}$, taken at the channel centre for fully developed turbulent flow, decreased with the increasing velocity which showed that $\overline{u'^2}$ was related to τ_o, the shear stress at the wall.

Taylor (1936) has described the measurements, obtained by Simmons, in a pipe $2\frac{7}{8}$ inches diameter, of $\sqrt{\overline{u'^2}}$ at points along the radius of the pipe. The maximum air velocity in the pipe was 9.50 ft/sec. The curve plotted as $\sqrt{\overline{u'^2}}$ against the distance from the centre of the pipe rises towards the wall and then suddenly drops to zero at the wall.

Hall (1938) measured $\sqrt{\overline{u'^2}}$ in a pipe of 3" diameter for two values of Reynolds number, corresponding to maximum velocities of 8.4. ft/sec and 18.4 ft/sec. He concluded that the shape of the curve relating $\frac{\sqrt{\overline{u'^2}}}{\bar{u}}$ and $\frac{y}{r}$, where y = distance from the wall and

r_0 = radius of the pipe, depends on the Reynolds number only, except in the region near the wall. Furthermore, he compared his results with those obtained by Simmons for the same Reynolds number and the agreement was good.

Reichardt (1938) succeeded in measuring $\sqrt{\overline{u'^2}}$ as well as $\sqrt{\overline{v'^2}}$. He used a closed channel 100 cm. wide and 24.4 cm. deep (aspect ratio 4 : 1). The measurements were made at the central section, with a maximum velocity of 100 cm/sec. He plotted his results as $\sqrt{\overline{u'^2}}$ and $\sqrt{\overline{v'^2}}$ against the dimensionless distance from the wall. The maximum intensities were found to be near the wall and both components diminished to zero at the wall. He found that the magnitude of $\sqrt{\overline{v'^2}}$ did not vary considerably over the section, with its average value about $0.04\ (\bar{u})_{max}$, whereas $\sqrt{\overline{u'^2}}$ varied greatly with a maximum value of $0.13\ (\bar{u})_{max}$ very close to the wall. Reichardt also measured the values of $-\overline{u'v'}$. It was confirmed that its value is zero at the channel centre, with a maximum value near the wall outside the region affected by viscous forces. He also obtained the value of the coefficient of correlation between the turbulent fluctuations, u' and v', and its maximum value, -0.45, occurred in the region away from both the wall and the channel centre.

Detailed and rather complete measurements of the turbulent fluctuations, u', v' and w', were taken by Laufer (1951), in two channels 60 inches wide, and 1 inch and 5 inches deep respectively.

He used one value of Reynolds number in his 1 inch channel and three values of Reynolds number in his 5 inch channel. The distribution of $\sqrt{\overline{u'^2}}$ shows the same general trend as that obtained by Reichardt. The magnitudes of $\sqrt{\overline{v'^2}}$ and $\sqrt{\overline{w'^2}}$ for the same flow conditions are equal at the channel centre but $\sqrt{\overline{w'^2}}$ increases rapidly towards the wall. This is in accordance with the results obtained by Fage and Townend for the maximas. The measurements of $\sqrt{\overline{u'^2}}$ were taken very close to the wall and revealed that $\sqrt{\overline{u'^2}}$ relative to local mean velocity increases very rapidly near the wall and reaches a maximum value where $\frac{y\, v_{xo}}{\nu} \approx 17$, then drops and tends towards a constant value of $\frac{\sqrt{\overline{u'^2}}}{\bar{u}} \approx 0.18$ at the wall. This supports the observations reported by Fage and Townend, who examined the flow very close to the wall with ultramicroscope and found that, although v' is suppressed at the wall, the motion remains sinuous in the direction of flow. Laufer could not obtain the measurements for v' and w' very near the wall. The intensities of $\sqrt{\overline{u'^2}}$, $\sqrt{\overline{v'^2}}$ and $\sqrt{\overline{w'^2}}$ compared either with the local mean velocity, $\bar{u}$, or with the maximum mean velocity $(\bar{u})_{max}$, when plotted against the dimensionless distance from the wall are seen to decrease as the Reynolds number increases. This confirms the results obtained by Wattendorf and Kuethe, who measured only $\sqrt{\overline{u'^2}}$ at the channel centre, for various values of the Reynolds number. The results of $-\overline{u'v'}$ agree well with the shear stresses as calculated from the pressure gradient. Also the magnitude of $-\overline{u'v'}$ decreased to zero

near the wall, where the viscous forces dominate the flow. The values of the correlation coefficient obtained in the two channels for different values of Reynolds number varied slightly. These results are discussed later.

Laufer (1954) also carried out turbulence measurements at two very high Reynolds numbers in a 10 inches diameter pipe. The corresponding maximum mean velocities were 10 ft/sec and 100 ft/sec. He represented his results as $\frac{\sqrt{u'^2}}{V_{xo}}$, $\frac{\sqrt{v'^2}}{V_{xo}}$ and $\frac{\sqrt{w'^2}}{V_{xo}}$ against $\frac{y}{r}$. There is no significant influence of the Reynolds number on the relative intensities when plotted in this way.

Similarly, turbulence in various boundary layers has been investigated experimentally in many laboratories. The results show the same trend as those in pipes and channels and are summarised by Hinze (1959). He has compared the results obtained in the boundary layers on smooth and rough surfaces and concluded that the ratio between the relative turbulence intensities, for the rough wall boundary layer and those for the smooth wall boundary layer, is roughly equal to the ratio between the corresponding wall shear stresses.

The hot-wire anemometer has not been successful in water due to various difficulties such as the collection of the air bubbles and other foreign materials on the wire. Kalinske (1940), in Iowa, used a photographic technique to measure the turbulence intensities in a 3" conduit. Droplets, 1 m.m. to 2 m.m. in size,

made from a mixture of carbon-tetrachloride and benzene having specific gravity equal to that of water were used and illuminated by a narrow plane of light. Photographs of these droplets flowing in water were taken on a motion picture film. Sufficient data were obtained to calculate $\sqrt{\overline{u'^2}}$ and $\sqrt{\overline{v'^2}}$. Assuming that the droplets of such a size can follow the motion truly, the technique seems attractive although sometimes the motion picture cameras are apt to be inconvenient.

Elsewhere, several other techniques are being developed for use in water particularly with free surface flows. Ippen and Raichlen (1957), at the Massachusetts Institute of Technology (U.S.A.) used a combination of a total head tube and a rapidly responding pressure transducer to measure the values of $\sqrt{\overline{u'^2}}$ in a free surface flow. Grossman, Li and Einstein (1957), in Berkeley (U.S.A.), developed a method based on electromagnetic induction and carried out their experiments on water flowing in a 2 inch diameter pipe. Chuang and Cermark (1965), in Colorado (U.S.A.) used electrokinetic transducers for the measurement of turbulence in open channels; the turbulent velocity nearly instantaneously causes fluctuations of the electrokinetic potential, which can be detected by electrodes on the transducer. Schuyf (1966) in Delft, used a propeller type current meter 1.50 cm diameter to investigate the extent to which turbulence can be measured in water with this instrument. Raichlen (1967), in California (U.S.A.) with a hot-film anemometer, obtained some limited

indication of the turbulent fluctuations in the longitudinal axis in a rectangular open channel. Because of the technical limitations, none of these instruments has revealed the motion in the vicinity of the free surface of an open channel. Moreover, all are still in a preliminary stage needing further developments before their readings in water can be relied upon.

From hot-wire anemometry, on air flow inpipes and channels, it is known that in general the intensity of turbulence relative to both the local mean velocity and the maximum velocity of the flow, decreases with increase in the Reynolds number. However, Laufer's measurements in a pipe show that when the turbulent intensities are related to the shear velocity, the distributions tend to remain the same for all values of the Reynolds number. To examine this hypothesis, the results of several investigators are brought together and plotted in Figures (IV.1., IV.2. and IV.3.) as $\frac{\sqrt{u'^2}}{v_{xo}}$, $\frac{\sqrt{v'^2}}{v_{xo}}$ and $\frac{\sqrt{w'^2}}{v_{xo}}$ against the dimensionless distance from the wall. The values of the Reynolds number, the shape of the section and the aspect ratio are given for each flow condition. There is a wide range of the Reynolds number and although there is some deviation of the points from the general trend, it is not very systematic: all the points lie in a strip of small width. Such a deviation may be due to the different kinds of instruments used by the various experimenters, to the different calibrations, or to some other factors not obvious at this stage. However, on the average, the

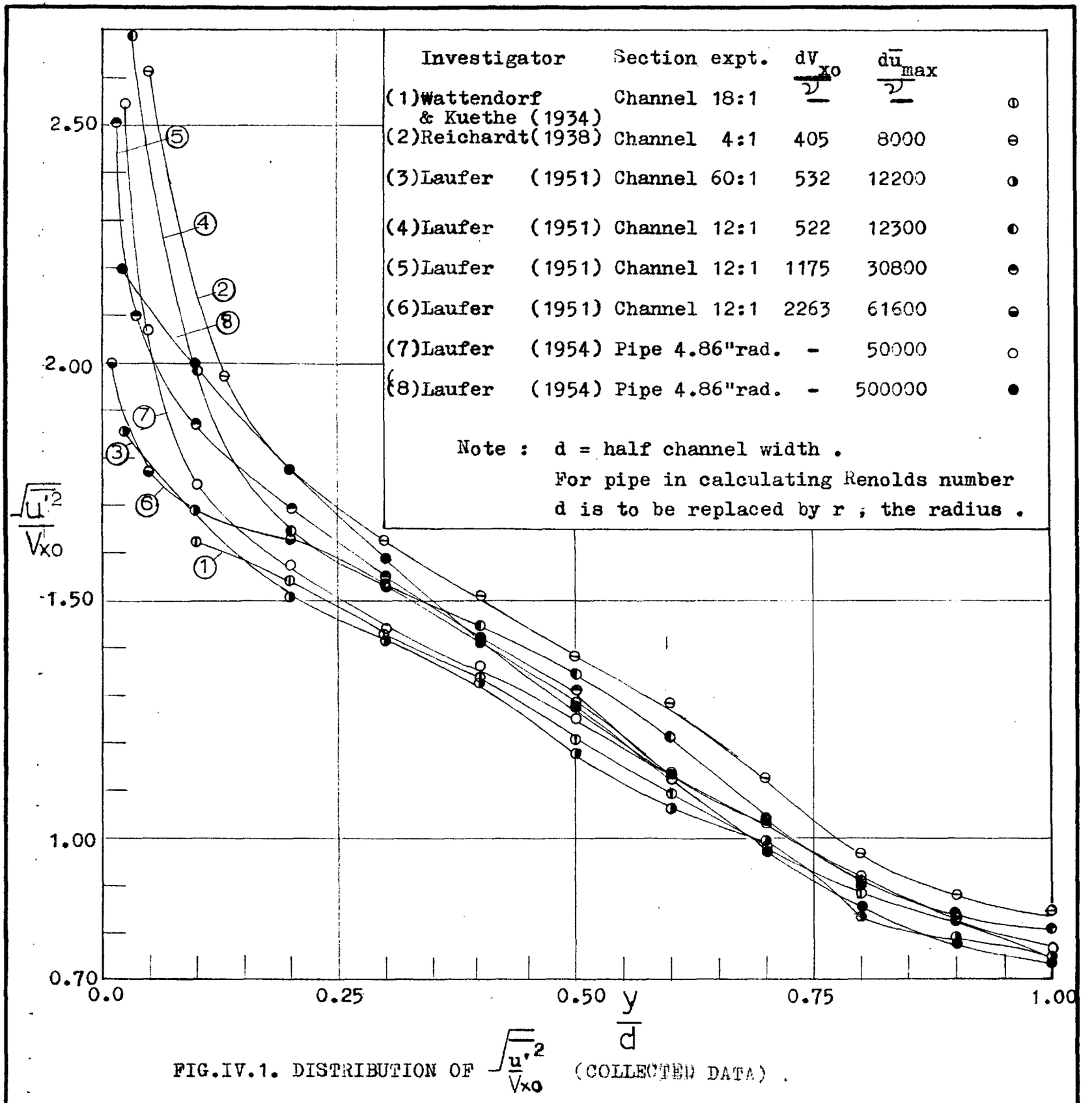


FIG.IV.1. DISTRIBUTION OF $\frac{\sqrt{\overline{u'^2}}}{V_{xo}}$ (COLLECTED DATA) .

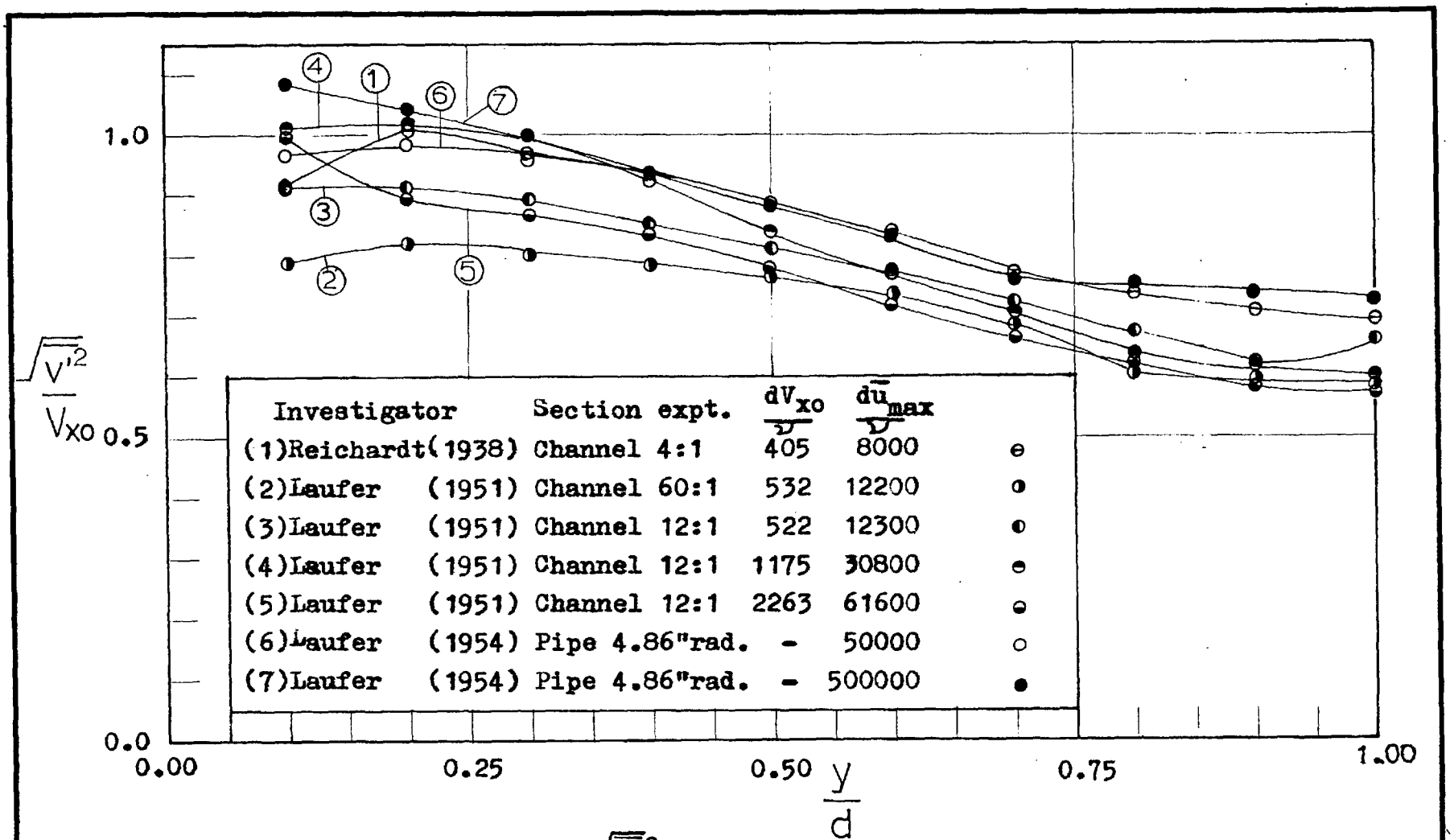


FIG.IV.2. DISTRIBUTION OF $\sqrt{\overline{v'^2}}/V_{xo}$ (COLLECTED DATA) .

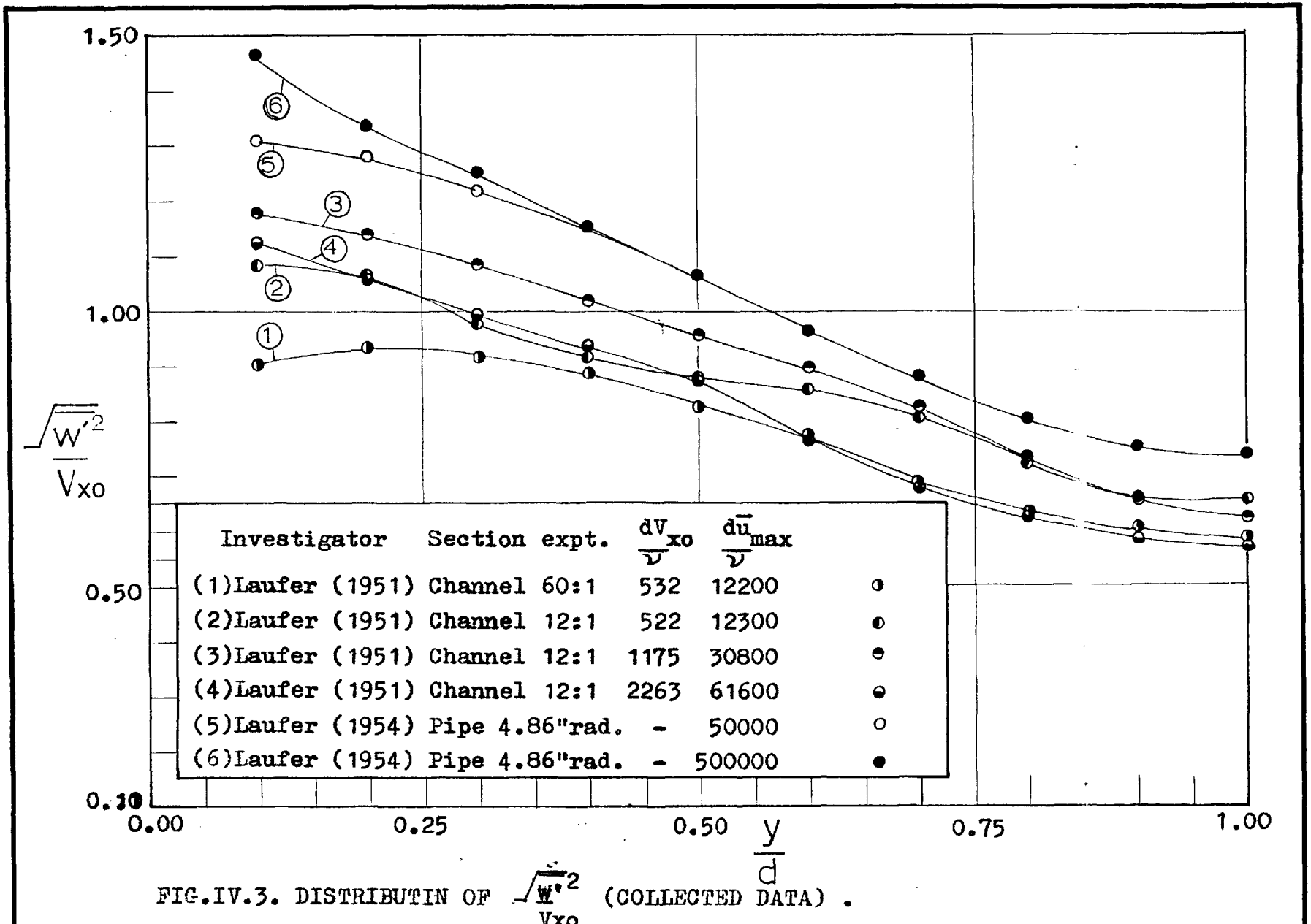


FIG.IV.3. DISTRIBUTIN OF $\frac{\sqrt{\overline{w'^2}}}{V_{xo}}$ (COLLECTED DATA) .

value of $\frac{\sqrt{\overline{u'^2}}}{v_{xo}}$ varies from 0.80 at the centre to about 2.50 near the wall, the value of $\frac{\sqrt{\overline{v'^2}}}{v_{xo}}$ varies from 0.65 at the centre to about 0.95 near the wall and the value of $\frac{\sqrt{\overline{w'^2}}}{v_{xo}}$ varies from about 0.65 at the centre to about 1.20 outside the wall region.

IV.3. THE TURBULENT QUANTITIES MEASURED IN THE PRESENT EXPERIMENTS

To investigate just how the free surface of an open channel may influence the turbulence, the photographic technique already described in (II.4.2.) was used particularly to determine the turbulence components in the direction of X and Y axes, where the X axis is parallel to the bed and in the direction of the main flow and the y axis is normal to the bed. Photographs of white particles dispersed in the water were taken at the centre line of the channel in in the xy plane. Each streak recorded on the film gave two components of the velocity at the particular place. The resulting component in the x axis was assumed to be the local instantaneous velocity, u, and likewise, the component in the y axis to be the turbulent fluctuation v'. The local mean velocities in the direction of flow were obtained by averaging the local instantaneous velocities and the turbulent fluctuations u' were obtained from the difference of the instantaneous and local mean values. The product of the turbulent fluctuations u' and v' gives the local instantaneous value

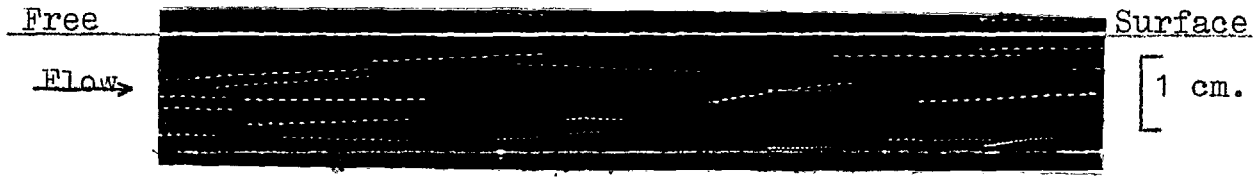
of the Reynolds shear stress. The values of u, v' and u'v', so obtained at various heights, were plotted on graphs with each point representing the streak measured at its particular depth. It is obvious that the result obtained from these streaks approaches the true value only when the number of streaks approaches infinity. To be practical, and to economise time in analysing the photographs and making the calculations, a compromise was made between the number of streaks measured and the accuracy of the results obtained. 200 to 300 streaks were measured for each depth; more streaks were measured for larger depths than the smaller depths of the flow. To obtain the mean values of the velocities at various heights above the bed a number of strips of small width were taken and the instantaneous values in each strip were averaged. The width of strip in the case of the channel with the rough bed was made equal to 4 m.m. so that there were 20 or 30 points in each strip to be averaged. But in the case of the smooth bed, the width of the strips varied from 1 m.m. near the bed to 4 m.m. near the water surface. Very close to the bed, where the turbulence was weak, a single streak could often be relied upon to represent the velocity at a particular point. $\overline{u'v'}$, $\sqrt{\overline{u'^2}}$ and $\sqrt{\overline{v'^2}}$ were evaluated in the same manner. The correlation coefficient $\overline{u'v'}/\sqrt{\overline{u'^2}}\sqrt{\overline{v'^2}}$, was eventually computed from the above quantities.

IV.4. EXPERIMENTAL RESULTS

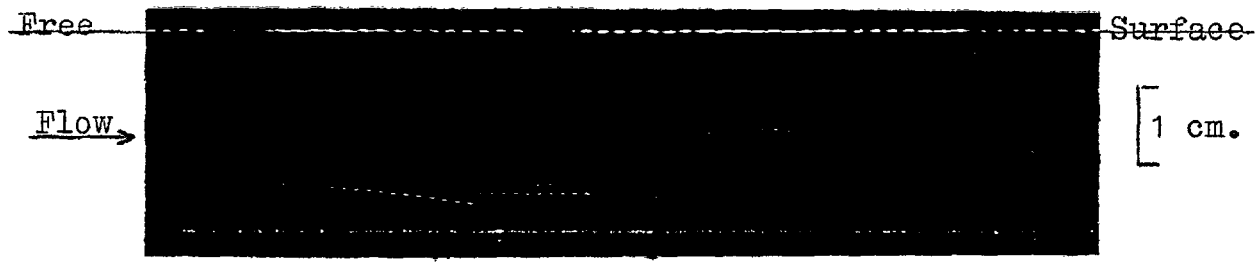
IV.4.1. RESULTS OBTAINED ON SMOOTH BED

By varying the depth and slope, four different values of the Reynolds number were included in the experiments with the smooth bed, with depths 1.55 c.m. and 2.58 c.m. for the slope of the channel 1 in 2000 and 2.555 c.m. and 5.085 c.m. for the slope 1 in 1000. The values of the shear Reynolds number $\frac{d\, V_{xo}}{\nu}$ were 132.2, 283.0, 394.0 and 1115.0 respectively. The first two depths for the slope of 1 in 2000 were so chosen as to have fully developed turbulent flow together with such low values of the velocity, that informative measurements could be taken near the wall. For the slope 1 in 1000, the depth 5.095 c.m. was the deepest consistent with two-dimensional conditions, i.e. nearly free from side effects at the centre of the channel and was also the shallowest consistent with absence of surface waves. Photographs for few depths, to represent the flow on this bed, are attached in Figure (IV.4.). The local instantaneous values of u, v' and u'v' obtained from such photographs for different depths are shown on graphs, given in Appendix (III), with each point representing the streak measured. The values of different turbulent quantities calculated from these graphs are given in Appendix (II.B.), Tables (1 to 4).

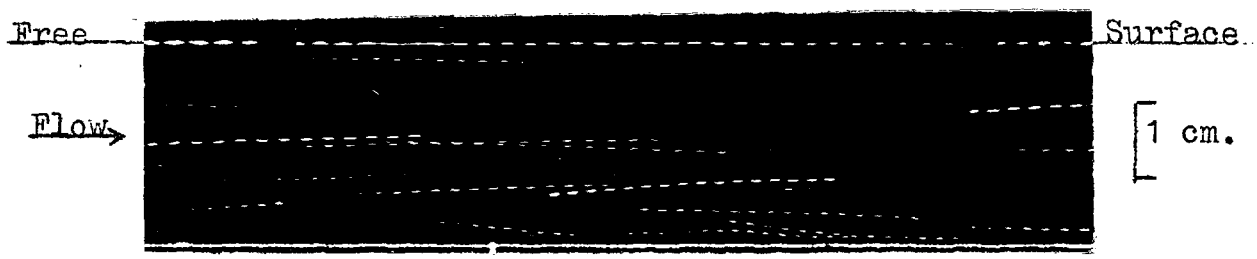
The values of $\sqrt{u'^2}$ related to the shear velocity, V_{xo}, are plotted against the distance from the wall made dimensionless



Depth = 1.55 cm. ; Slope = 0.0005 .



Depth = 2.58 cm. ; Slope = 0.0005 .



Depth = 2.555 cm. ; Slope = 0.0010

FIG.IV.4. SAMPLE PHOTOGRAPHS IN CENTRAL PLANE OF FLUME ON SMOOTH BED .

with the depth of flow. Figure (IV.5.a.) shows such results for the flow with depth 1.55 c.m. and slope 1 in 2000 and the Figure (IV.5.b.) shows the results for the other three flows. Although the distribution of $\frac{\sqrt{u'^2}}{v_{xo}}$ has the same tendency in the two diagrams, with certain value at the water surface and increasing towards the bed, the mean curve drawn through the points of Figure (IV.5.a) lies higher than the mean curve in Figure (IV.5.b). This may be explained as follows.

Near the wall, the curve in Figure (IV.5.b.), splits into three different curves, one for each flow. Also this figure demonstrates clearly that the relative intensity $\frac{\sqrt{u'^2}}{v_{xo}}$ increases rapidly near the wall in the transition zone where turbulent as well as viscous stresses influence the flow. The maximum value of $\frac{\sqrt{u'^2}}{v_{xo}}$ occurs near the wall, at that place where the turbulent stresses begin to diminish and then rapidly drops to zero at the wall. This is in accordance with the motion in pipes or closed channels as known from investigations with hot-wire anemometers. Moreover from Figure (IV.5.b) it is clear that the position of the maximum value of $\frac{\sqrt{u'^2}}{v_{xo}}$ depends on the value of v_{xo}, being closer to the wall when v_{xo} is large. The depth and also the shear stress v_{xo} for the flow in Figure (IV.5.a) are very small and so the wall region occupies a large enough part of the depth of flow. In the wall region where the magnitude of the relative turbulence intensity $\frac{\sqrt{u'^2}}{v_{xo}}$ is very high, the curve for this smallest flow generally lies higher than for the other flows.

Very close to the wall, Laufer, from his measurements, showed that according to wall proximity law of Prandtl, the relative intensities are functions of $\frac{yV_{xo}}{\nu}$. His results are shown in Figure (IV.6.). The points for $\frac{\sqrt{\overline{u'^2}}}{V_{xo}}$ lie on a single curve up to $\frac{yV_{xo}}{\nu} \approx 60$, for all values of the Reynolds number, both for the pipe and the channel flows, except for the two values of high velocity channel flow for which there is no obvious reason. The results obtained in the present experiments close to the wall are plotted similarly in Figure (IV.7.). Although there is an insufficient number of points, the mean curves for $\frac{\sqrt{\overline{u'^2}}}{V_{xo}}$ and $\frac{\sqrt{\overline{v'^2}}}{V_{xo}}$ show the same general trend as obtained by Laufer. The maximum value of $\frac{\sqrt{\overline{u'^2}}}{V_{xo}}$ occurs at $\frac{yV_{xo}}{\nu} \approx 13$, whereas the maximum value of $\frac{\sqrt{\overline{v'^2}}}{V_{xo}}$ occurs at $\frac{yV_{xo}}{\nu} \approx 40$.

The value of $\frac{\sqrt{\overline{u'^2}}}{V_{xo}}$ from Figures (IV.5.a, b) at the free surface is about 0.80, whereas near the wall it varies from about 2.10 to 2.40. The values of $\frac{\sqrt{\overline{u'^2}}}{V_{xo}}$ for pipes and closed channels at their centres and near the wall obtained from Figure (IV.1.) are in the range 0.75 to 0.85 and 2.0 to 2.70 respectively. Thus, despite the free surface, the distribution of $\frac{\sqrt{\overline{u'^2}}}{V_{xo}}$ remains the same in an open channel as it is in a pipe or in a closed channel.

The relative turbulence intensity $\frac{\sqrt{\overline{v'^2}}}{V_{xo}}$ is similarly plotted against $\frac{y}{d}$ in Figures (IV.8.a) and (IV.8.b). Figure (IV.8.a.) gives the results for two depths 1.55 c.m. and 2.58 c.m., taken with

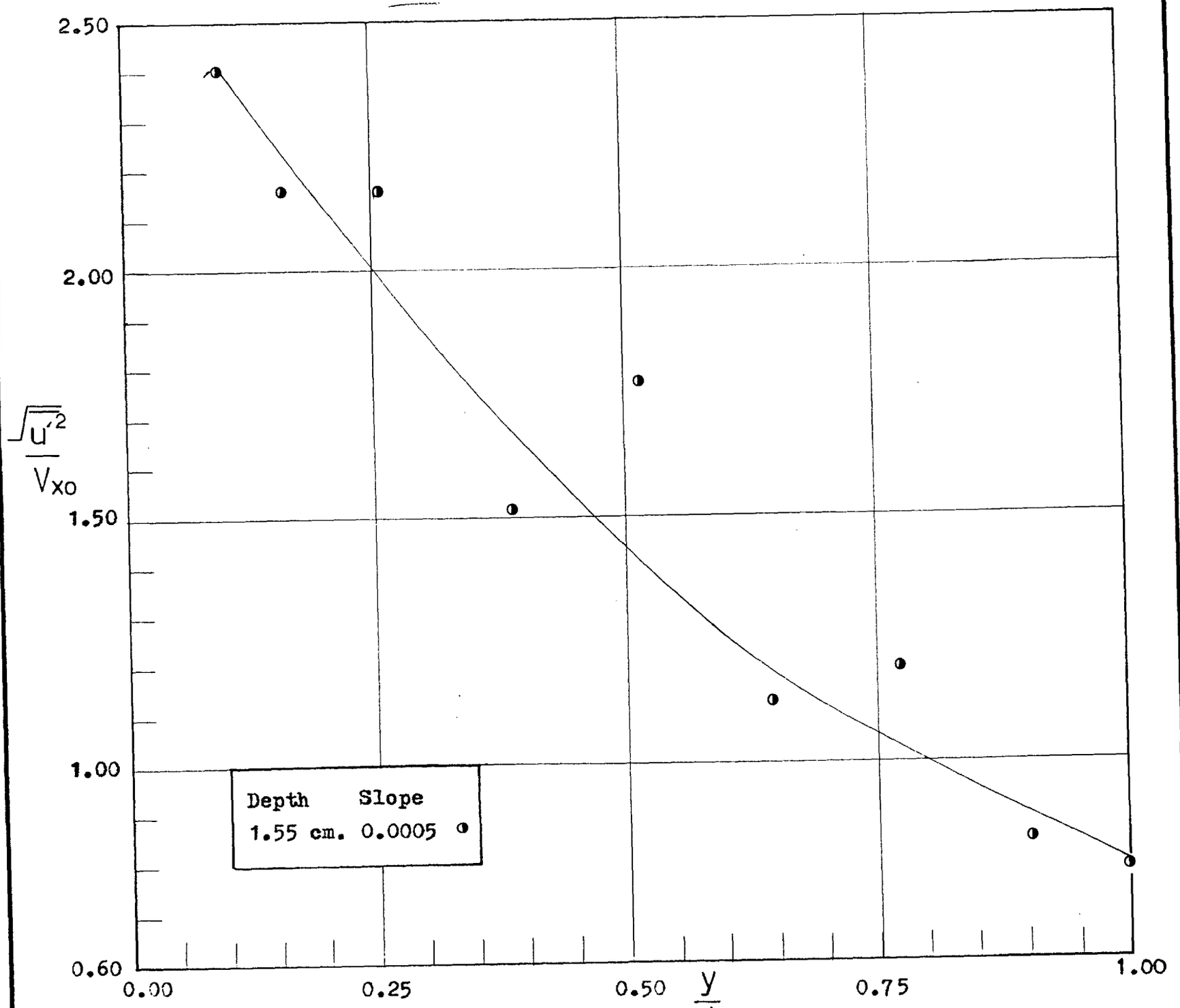


FIG.IV.5.a. DISTRIBUTION OF $\frac{\sqrt{\overline{u'^2}}}{V_{xo}}$ (SMOOTH BED) .

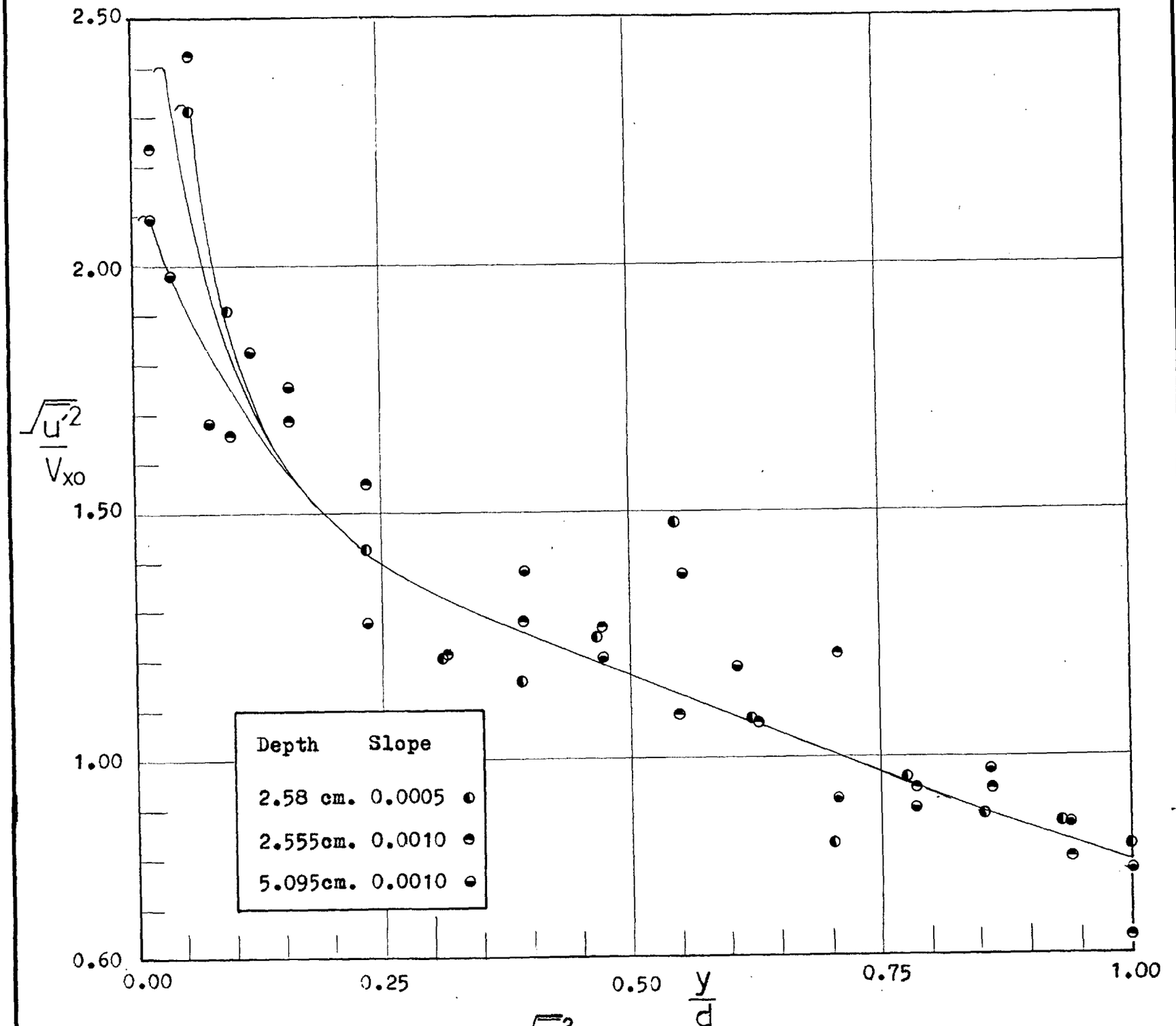


FIG.IV.5.b. DISTRIBUTION OF $\frac{\sqrt{\overline{u'^2}}}{V_{xo}}$ (SMOOTH BED) .

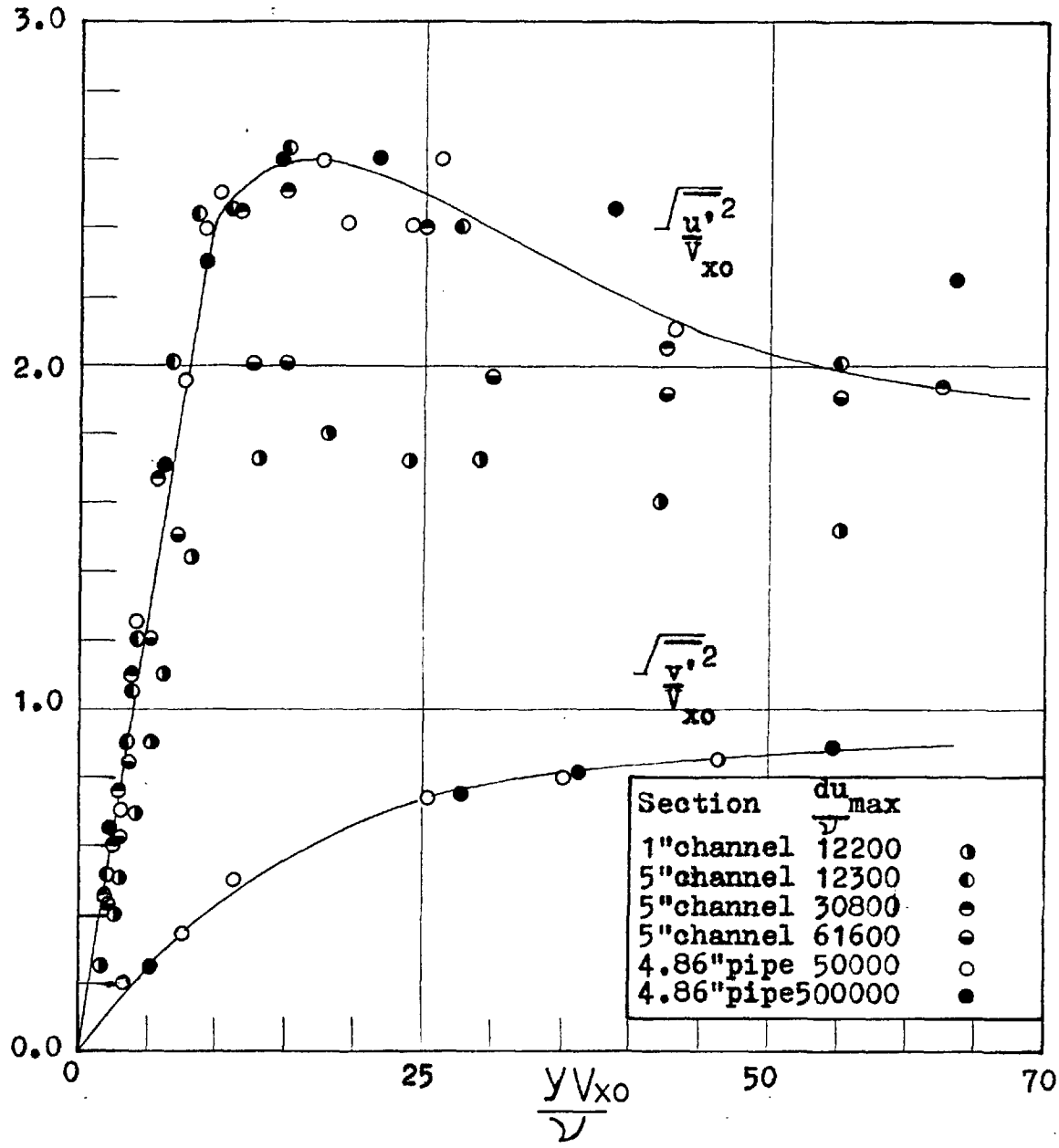


FIG.IV.6. DISTRIBUTION OF $\sqrt{\frac{\overline{u'^2}}{V_{xo}}}$ AND $\sqrt{\frac{\overline{v'^2}}{V_{xo}}}$ NEAR THE WALL (LAUFER'S DATA) .

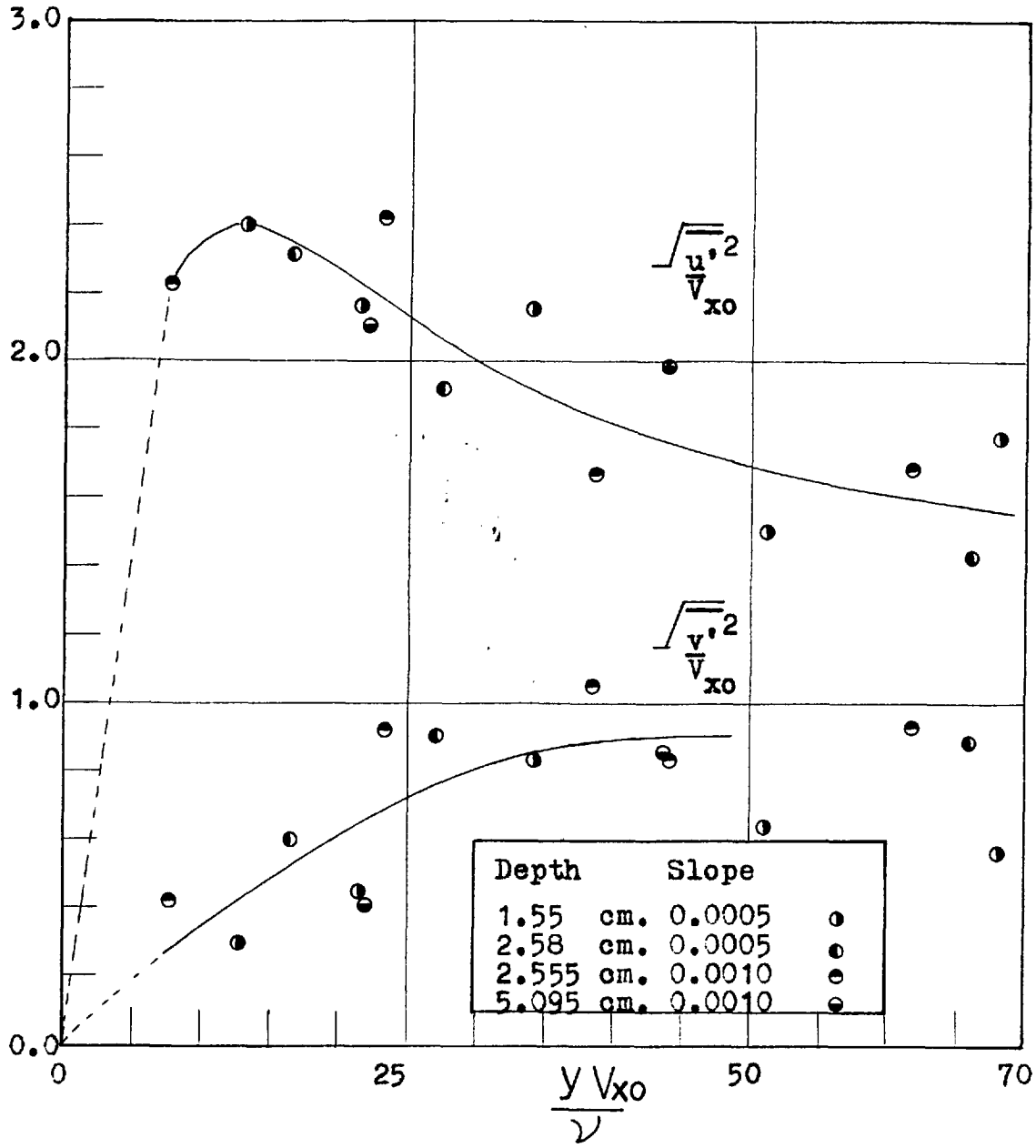


FIG.IV.7. DISTRIBUTION OF $\sqrt{\overline{\frac{u'^2}{V_{xo}}}}$ AND $\sqrt{\overline{\frac{v'^2}{V_{xo}}}}$ NEAR THE BED (SMOOTH).

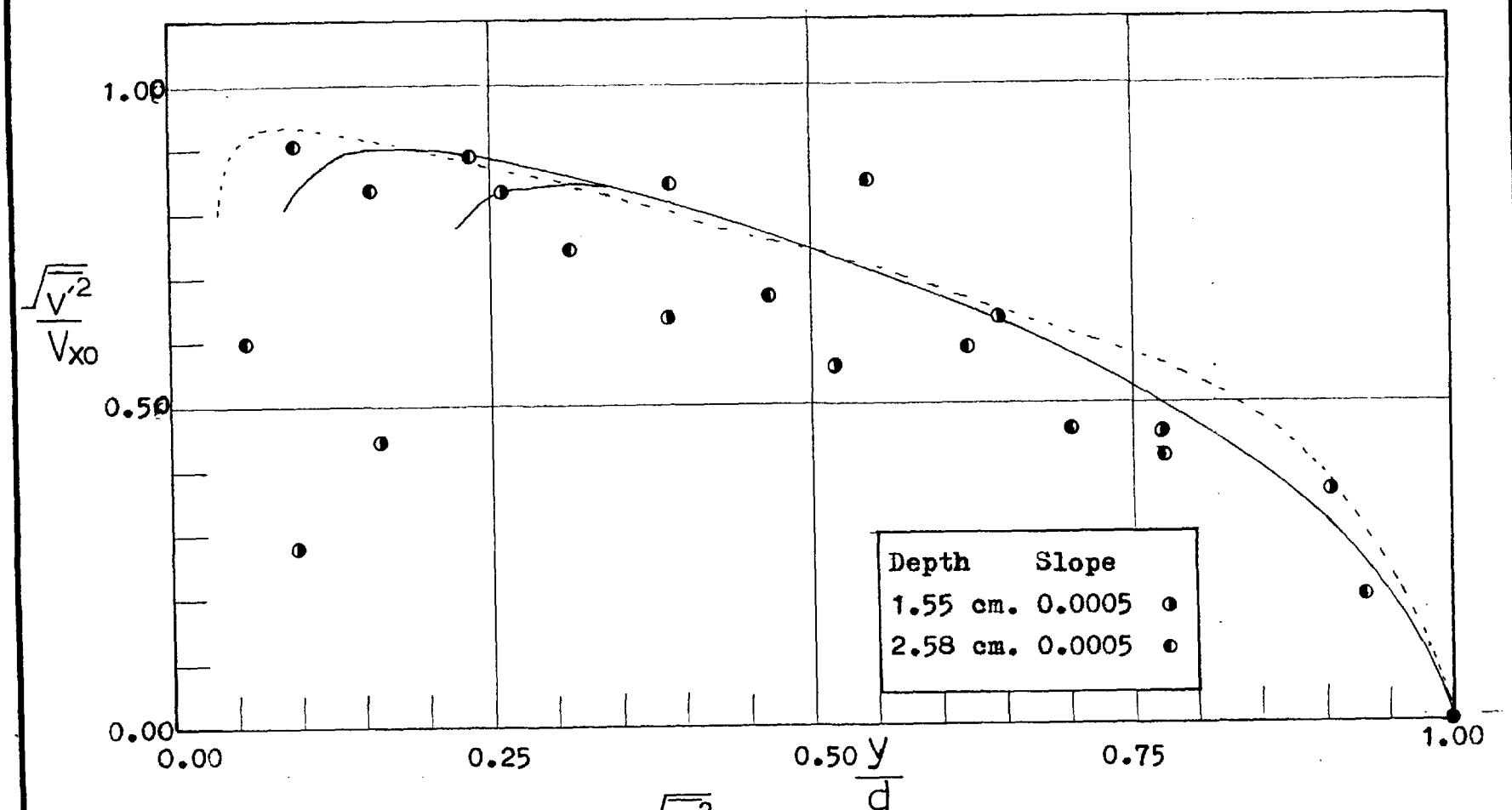


FIG.IV.8.a. DISTRIBUTION OF $\frac{\sqrt{\overline{v'^2}}}{V_{xo}}$ (SMOOTH BED) .

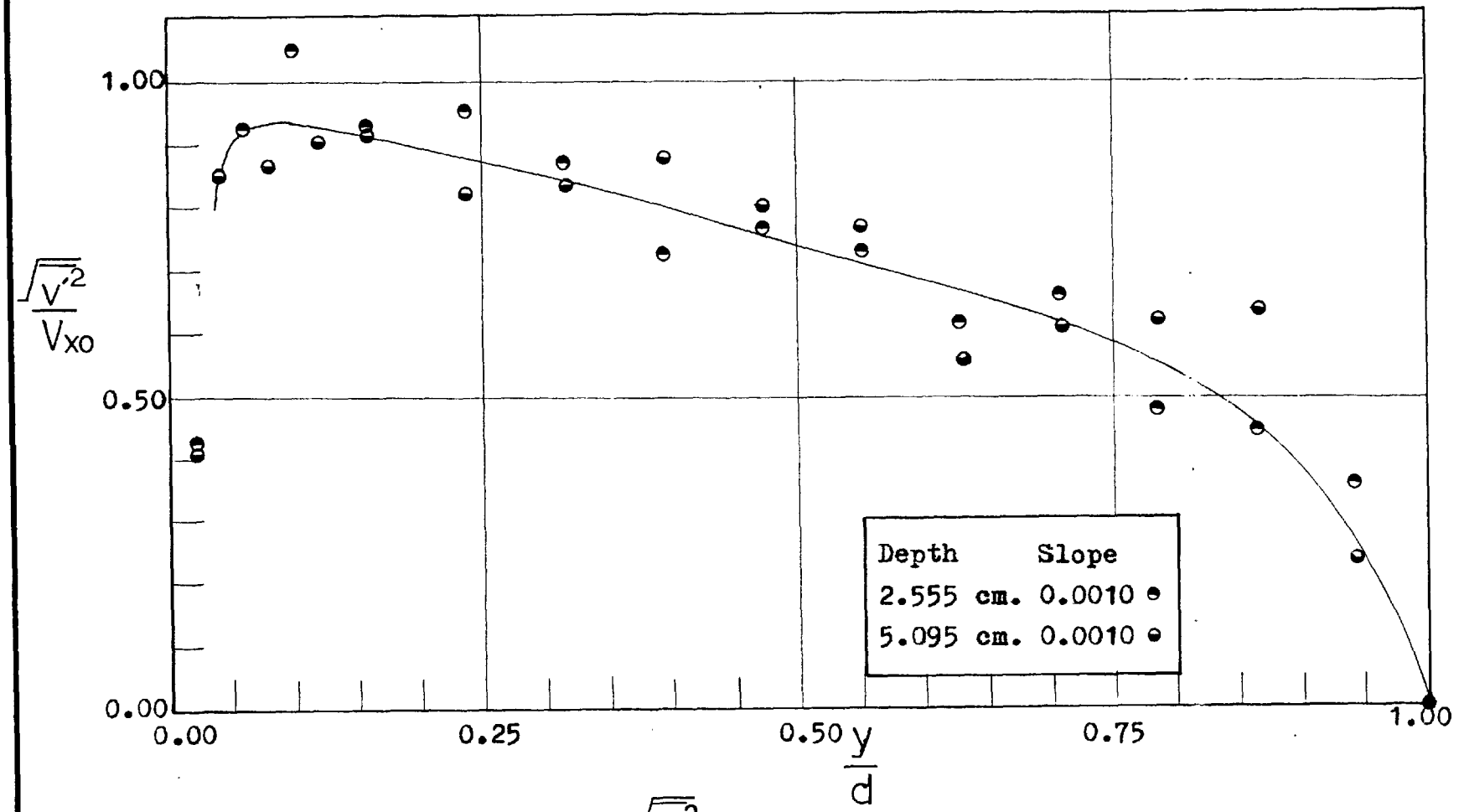


FIG.IV.8.b. DISTRIBUTION OF $\frac{\sqrt{\overline{v'^2}}}{V_{xo}}$ (SMOOTH BED) .

slope 1 in 2000, where the slow motion near the wall could be measured down to $\bar{u} = 3v_{xo}$. Figure (IV.8.b) gives the results for the other two depths. Mean curves are drawn through the points in these two figures and the curve of Figure (b) is superimposed on Figure (a), shown dotted. Except near the wall, the two curves are nearly the same. The relative intensity $\frac{\sqrt{\overline{v'^2}}}{v_{xo}}$ is zero at the free surface and increases towards the wall. Its maximum value occurs near the wall, in the region where $\frac{yv_{xo}}{\nu} \approx 40$ (Figure IV.7.), where the turbulent stresses completely dominate the flow. In the transition zone, e.g. when $\frac{yv_{xo}}{\nu} < 40$, where the viscous forces influence the flow, the fluctuations normal to the bed are reduced. Therefore the magnitude of $\frac{\sqrt{\overline{v'^2}}}{v_{xo}}$ decreases in this region, with its zero value occurring at the wall. In Figure (IV.8.a), the curve near the wall splits into two, deviating from the main curve, in the region where viscous forces start influencing the flow. In this region, the relative intensity is function of $\frac{yv_{xo}}{\nu}$, as shown earlier in Figure (IV.7.). The maximum value of $\frac{\sqrt{\overline{v'^2}}}{v_{xo}}$ for the two flows in Figure (IV.8.b) is about 0.95. The results obtained on pipes and closed channels represented in Figure (IV.2.) give this value in the range 0.8 to 1.10, their mean being 0.95. The present results are in good agreement with the previous ones in the region $0 < \frac{y}{d} < 0.60$ beyond which they deviate. In the case of an open channel $\frac{\sqrt{\overline{v'^2}}}{v_{xo}}$

approaches zero at the free surface, whereas at the centre of a pipe or a closed channel it has a finite value; the shear stress in both cases is zero at these planes. At the central plane of a pipe or closed channel, the turbulent fluctuations can occur at right angles to this plane and pass masses of fluid from one side to the other, but they contribute nothing to the mean shear stress since the correlation between u' and v' is zero there. In an open channel, the masses of fluid do not usually come out of the free surface, and usually the turbulent fluctuations at right angles to this plane are completely suppressed. There being no v' component, although the u' component still exists, the shear stress is zero. From the present results it seems that the influence of the free surface on the v' component of turbulent fluctuations occurs significantly within a distance of 0.40 times the depth from the water surface.

It is interesting to note that near the wall the magnitude of $\frac{\sqrt{u'^2}}{v_{xo}}$ increases rapidly in the transition zone reaching its maximum well inside the viscous region; whereas the magnitude of $\frac{\sqrt{v'^2}}{v_{xo}}$ decreases in the transition zone with its maximum definitely beyond the limit of viscous influence at the place, $\frac{y v^*_{xo}}{\nu} \approx 40$, where the turbulent stresses completely dominate the flow. This is what Fage and Townend (1932) obtained by observing maximas of the turbulent fluctuations with their ultra-microscope. Also Laufer (1954) obtained the same results in pipe flow. But Fage

and Townend who examined the flow very close to the wall, at $\frac{1}{40,000}$ inch, observed that although the turbulent fluctuations at right angles to the wall seemed damped completely and flow tended to the laminar type, yet the motions of the particles parallel to the wall were sinuous. This may pass unnoticed by ordinary instruments and particularly with the present photographic technique where foreign particles of about 0.005" size were introduced to study the motion.

The total shear stress at any point in turbulent flow is given by the relation $\tau = \mu \frac{d\bar{u}}{dy} - \rho \overline{u'v'}$. Very near the wall in the viscous region where the turbulent fluctuations tend to zero value, the total shear stress is determined by the term $\mu \frac{d\bar{u}}{dy}$. In the transition region, both terms play their part; whereas in the fully turbulent region, the viscous term contributes very little and the total shear stress is given by $-\rho \overline{u'v'}$.

The values of $-\overline{u'v'}$, made dimensionless with $\frac{\tau_o}{\rho}$, where $\tau_o = \rho g d s$, are plotted in Figure (IV.9.) against the dimensionless distance from the wall. For all the four values of Reynolds number, the points lie around the theoretical straight line except near the wall. As the wall is approached, they start deviating from the straight line, the position of the deviation depending on the value of the Reynolds number. This effect is clearly shown in Figure (IV.10.) by plotting the dimensionless

turbulent shear stress against the wall shear Reynolds number. In the wall region $\frac{\overline{u'v'}}{\tau_{o/\rho}}$ seems to be a function of $\frac{y\, V_{xo}}{\nu} \approx 40$, when $\frac{\overline{u'v'}}{\tau_{o/\rho}}$ reaches its maximum value.

Figure (IV.11.) gives the values of the correlation coefficient, $\Psi = \frac{\overline{u'v'}}{\sqrt{\overline{u'^2}}\sqrt{\overline{v'^2}}}$. A mean curve drawn through the points remains horizontal in the central portion, approaching zero at the bed and at the free surface. The mean value of the correlation coefficient in the central region is about - 0.53. The values of the correlation coefficient obtained by previous workers for different flow conditions are given in the table below.

TABLE IV.1.

Experimenter	Aspect ratio of channel section	$\frac{d\, V_{xo}}{\nu}$	$\frac{d\, U_{max}}{\nu}$	Ψ
Reichardt (1938)	4 : 1	405.0	8,000	-0.45
Laufer (1951)	60 : 1	531.8	12,200	-0.63
Laufer (1951)	12 : 1	521.8	12,300	-0.50
Laufer (1951)	12 : 1	1175.6	30,800	-0.45
Laufer (1951)	12 : 1	2263.3	61,600	-0.40

In the above table there seems to be no regular variation of the correlation coefficient with the Reynolds number, the flow being substantially two dimensional in all cases. The average value seems to be nearly equal to -0.50.

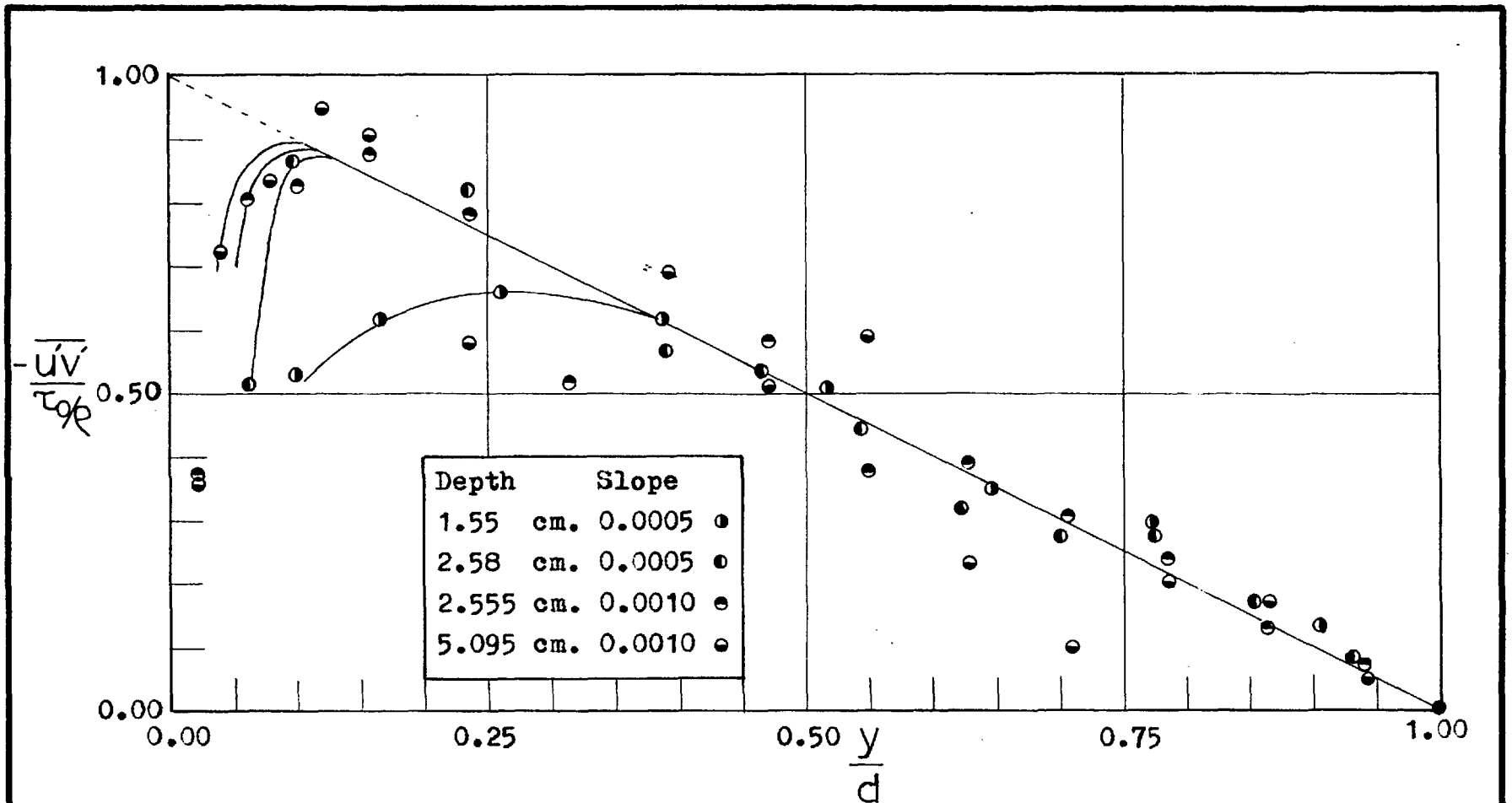


FIG.IV.9. DISTRIBUTION OF TURBULENT SHEAR STRESS (SMOOTH BED) .

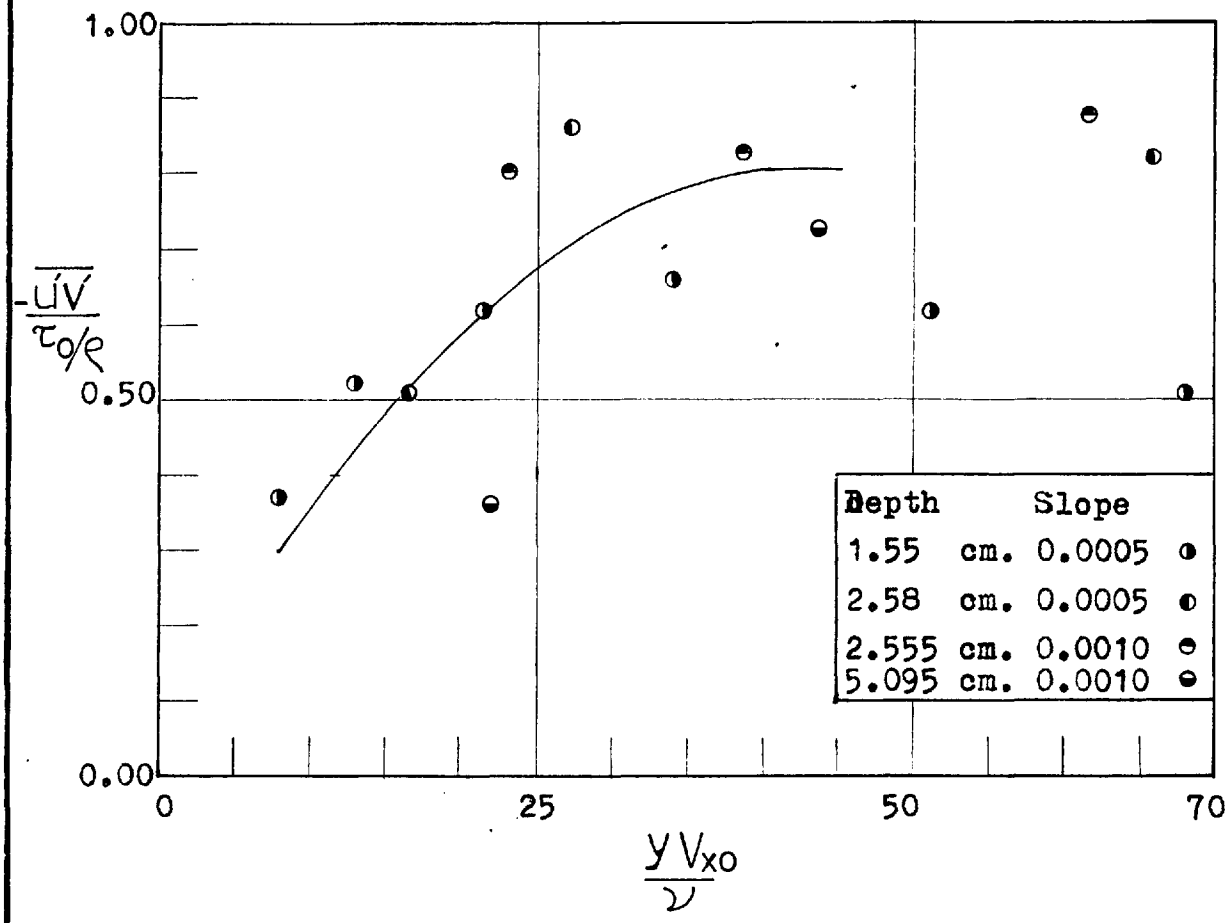


FIG.IV.10. DISTRIBUTION OF TURBULENT SHEAR STRESS NEAR THE BED (SMOOTH) .

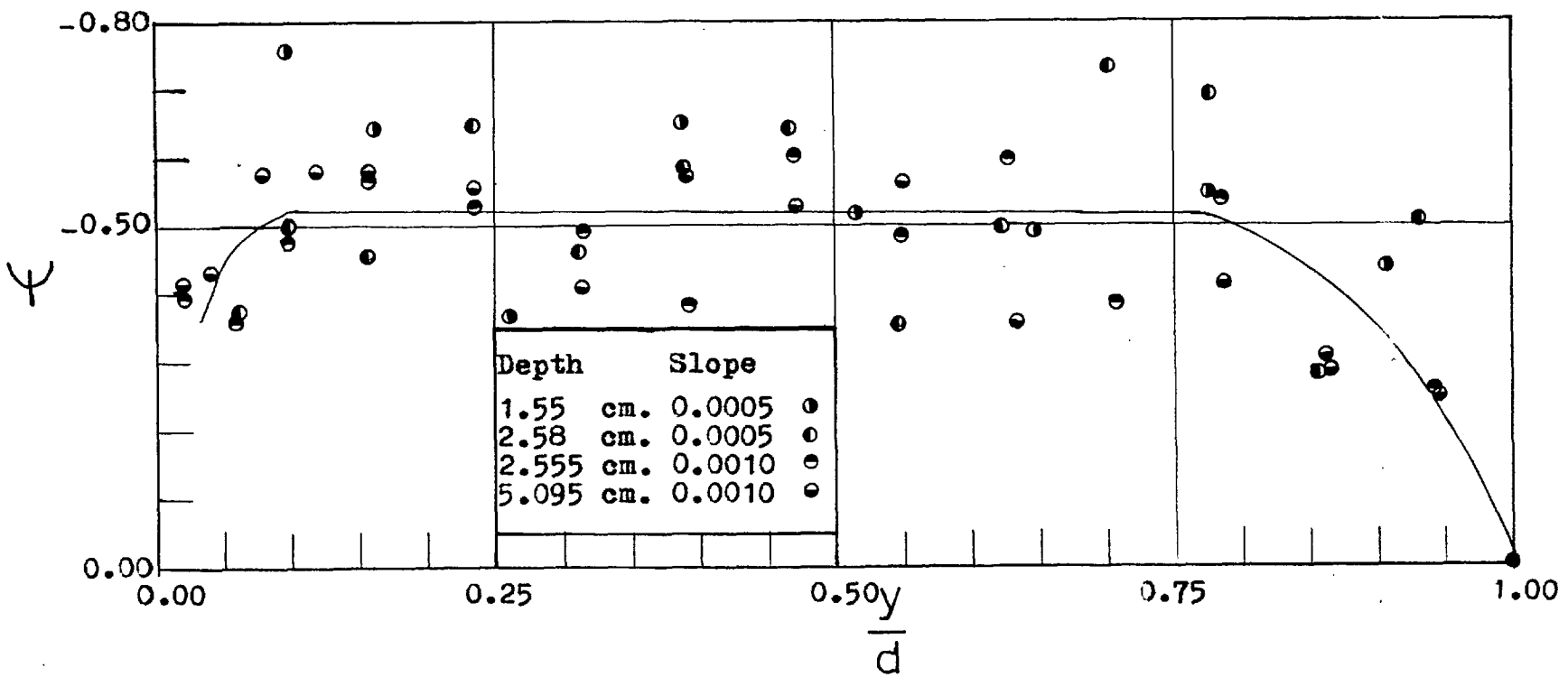


FIG.IV.11. DISTRIBUTION OF COEFFICIENT OF CORRELATION (SMOOTH BED) .

IV.4.2 RESULTS OBTAINED ON RIPPLED BED

As the ripples were about 1 c.m. high, the depth of flow was made deeper for this bed than on the smooth bed, but not so deep that the side walls could be likely to distort the flow in the central plane. A total of five depths with two different slopes of 1 in 2000 and 1 in 1000 were used; the width-depth ratio varied from 8 : 1 to 5 : 1. Two photographs for about the same depth but different slope are attached in Figure (IV.12) to represent the flow on this bed. The local instantaneous values of u, v' and u'v' obtained from such photographs, for various depths, are plotted on graphs in Appendix (III). The turbulent quantities calculated from the local instantaneous values for different depths of the flow are given in Appendix (II.B.), Tables (5 to 9).

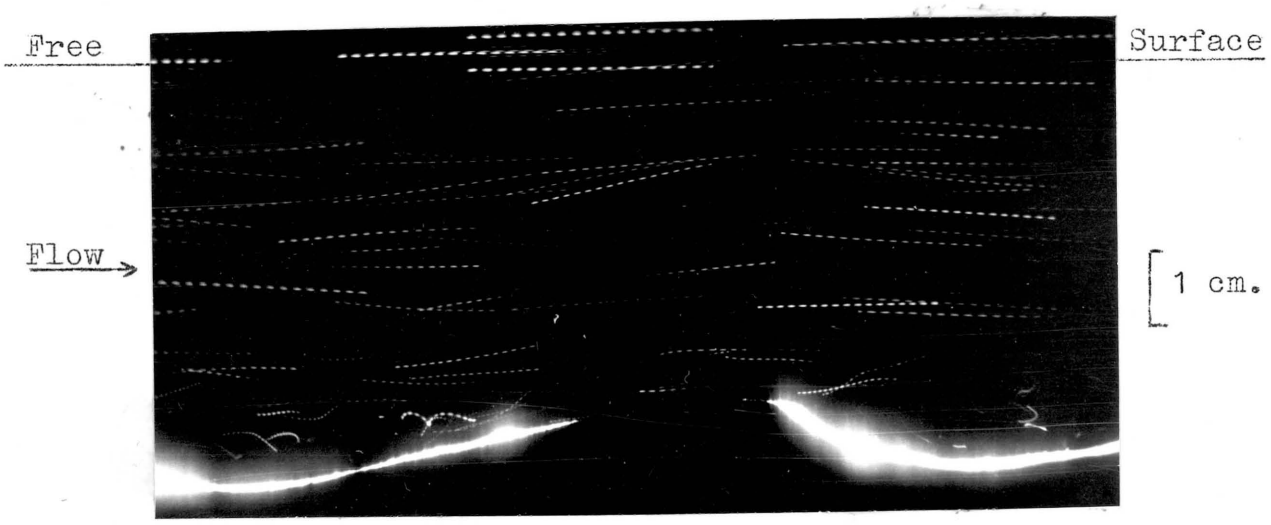
The turbulent intensities $\sqrt{\overline{u'^2}}$ and $\sqrt{\overline{v'^2}}$, related to the shear velocity, are plotted in Figures (IV.13.) and IV.14.) respectively for all the flows. There is much scatter of the points particularly in Figure (IV.13.) for $\sqrt{\overline{u'^2}}$, because the depths taken were large and the number of streaks measured was limited. Moreover some liability to error was unavoidable since the local mean velocities, which were obtained by averaging instantaneous values, may not represent the true values. However, the average values obtained from a number of flows concern a

larger sample and are probably reliable. Mean curves through the points in the Figures (IV.13.) and (IV.14.) are drawn only so far as the ripple crests, as there are insufficient points for reliable results inside the troughs.

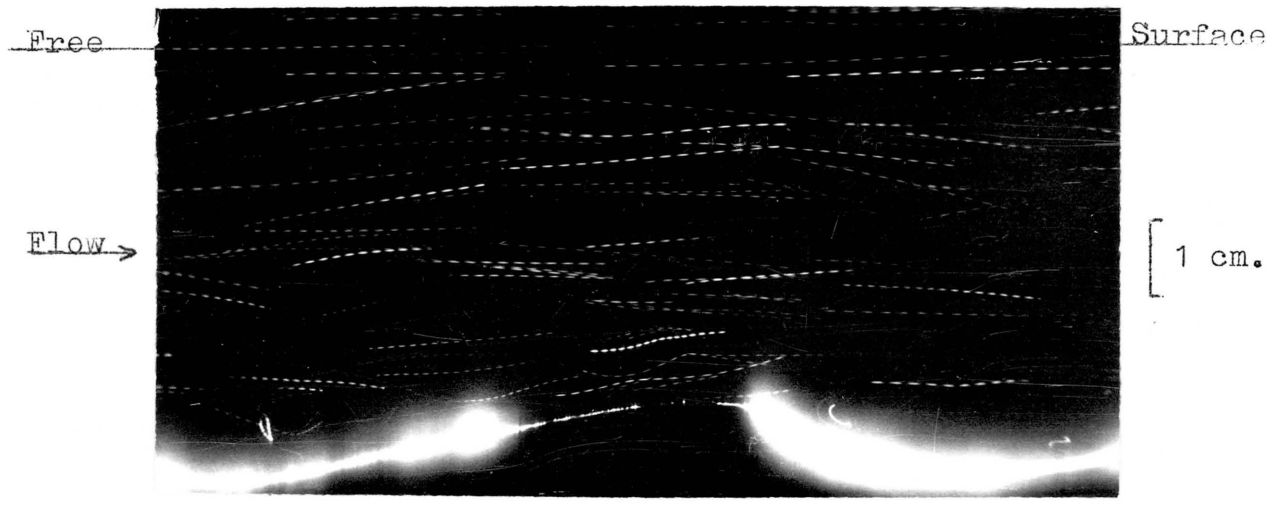
The curve of $\frac{\sqrt{\overline{u'^2}}}{V_{xo}}$ in Figure (IV.13.) has a value about 0.85 at the free surface and towards the wall rises to a value of about 1.35 at y = 0.18d. Then it has a tendency to fall again giving the indication that the ripples tend to restrict the turbulent component in the direction of flow, which is in marked contrast to the smooth bed where the corresponding fluctuations increased rapidly until quite near the bed.

The mean curve for $\frac{\sqrt{\overline{v'^2}}}{V_{xo}}$, in Figure (IV.14.), with its zero value at the free surface rises towards the rippled bed as observed in case of the smooth bed, but near the bed, it increases rapidly instead of diminishing, giving a value of $\frac{\sqrt{\overline{v'^2}}}{V_{xo}}$ as great as 1.35 at y/d = 0.10. In the region of the ripples, the eddies no doubt rapidly pass the crests of the roughness so increasing the intensity of the turbulent fluctuations at right angle to the wall, while at the bed the main stream lines tend to follow most of the bed profile.

The values of the turbulent shear stress are plotted in Figure (IV.15.). Although there is much scatter of the results, the points lie around the correct straight line calculated from



Depth = 5.08 cm. ; Slope = 0.0005 .



Depth = 5.18 cm. ; Slope = 0.0010 .

FIG.IV.12. SAMPLE PHOTOGRAPHS IN CENTRAL PLANE OF FLUME ON RIPPLED BED .

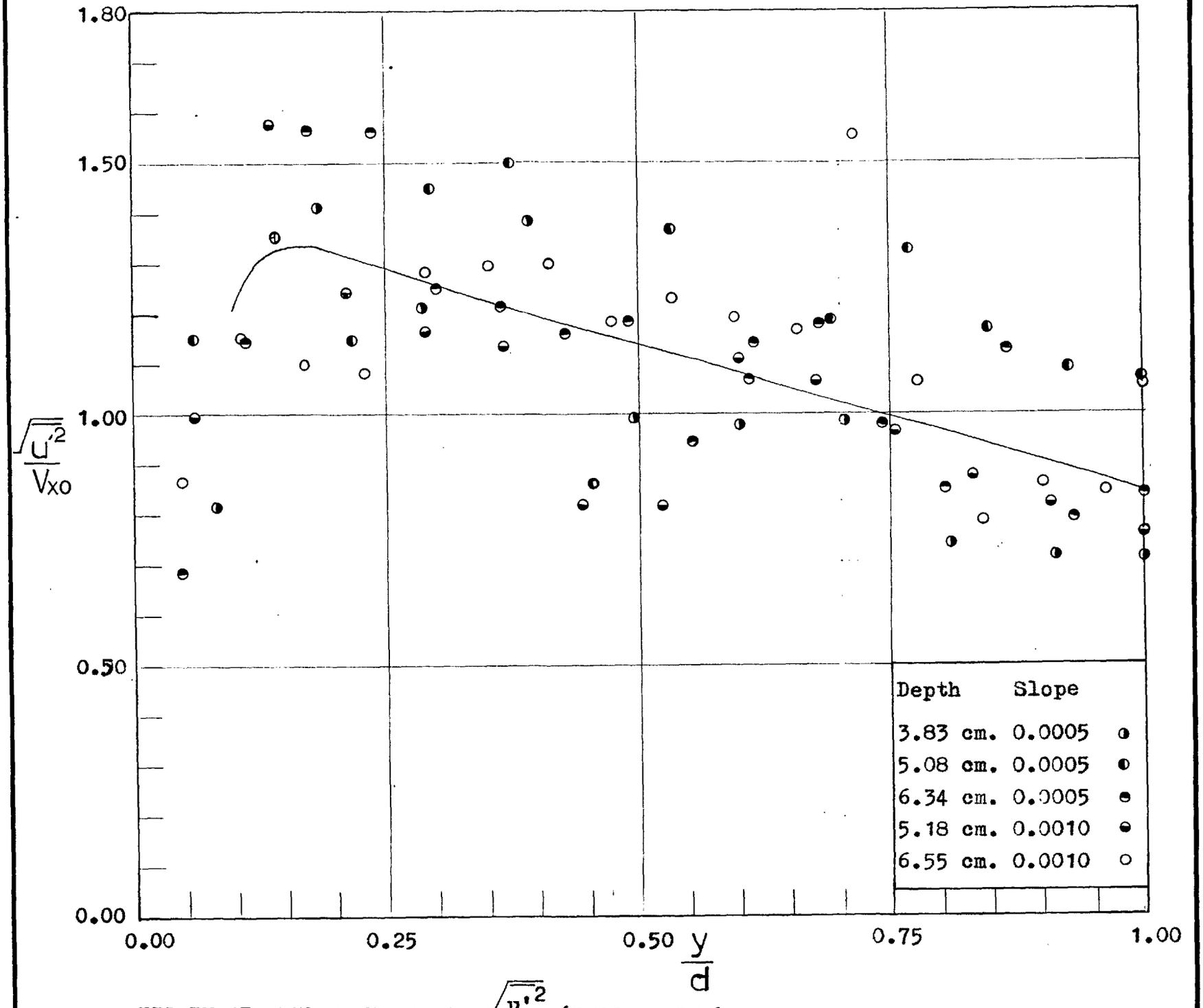


FIG.IV.13. DISTRIBUTION OF $\frac{\sqrt{\overline{u'^2}}}{V_{xo}}$ (RIPPLED BED) .

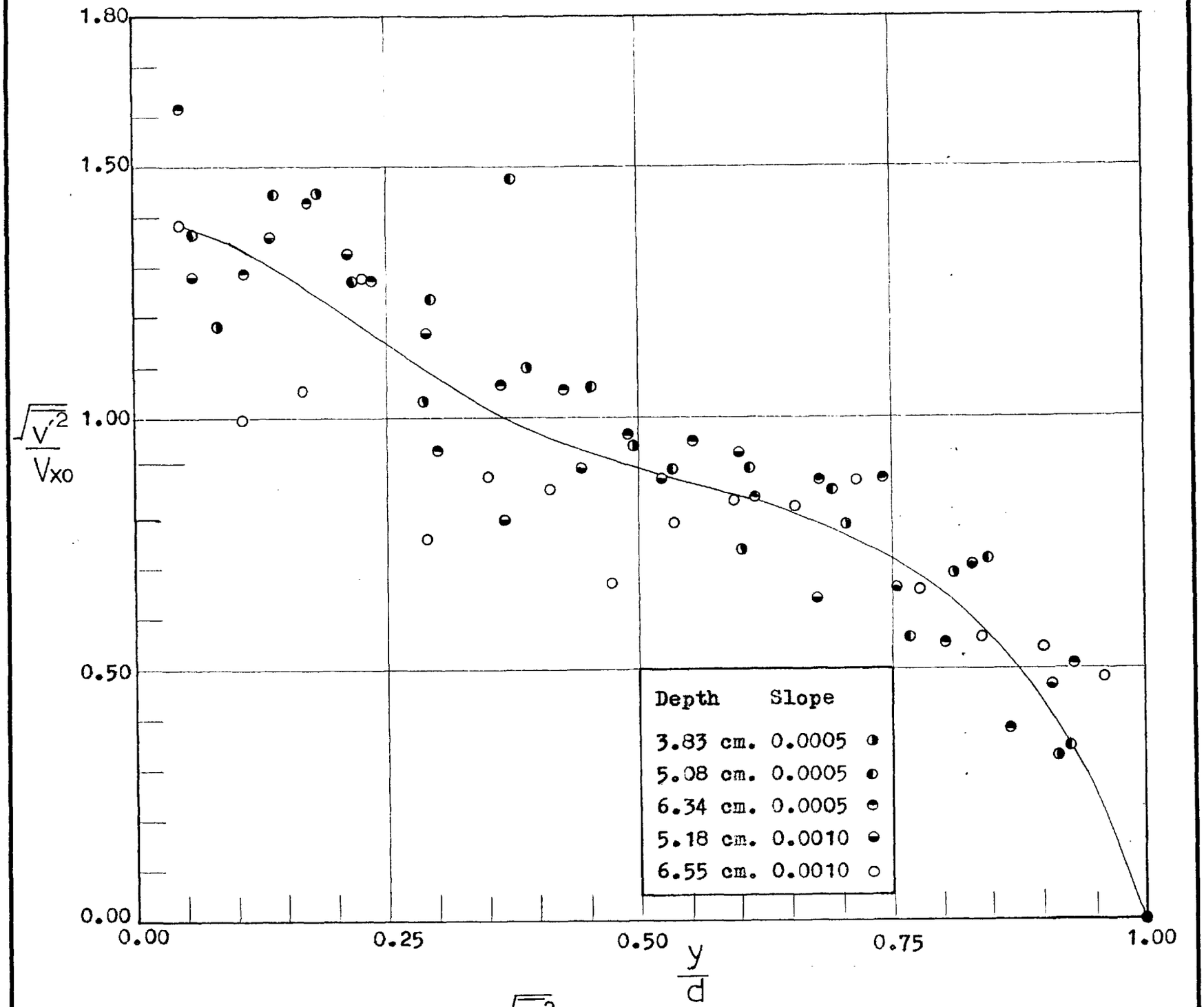


FIG.IV.14. DISTRIBUTION OF $\frac{\sqrt{\overline{v'^2}}}{V_{xo}}$ (RIPPLED BED) .

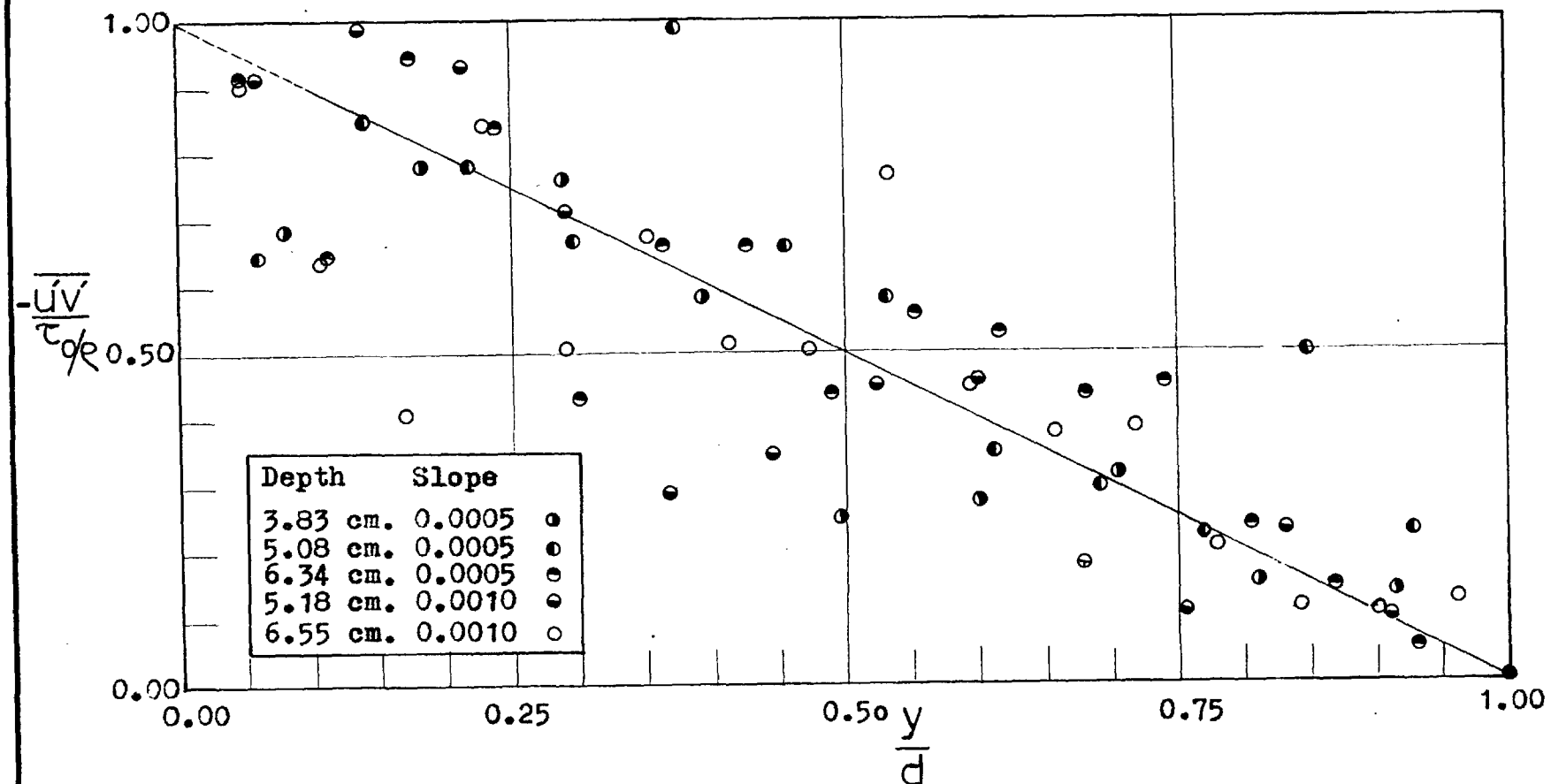


FIG.IV.15. DISTRIBUTION OF TURBULENT SHEAR STRESS (RIPPLED BED) .

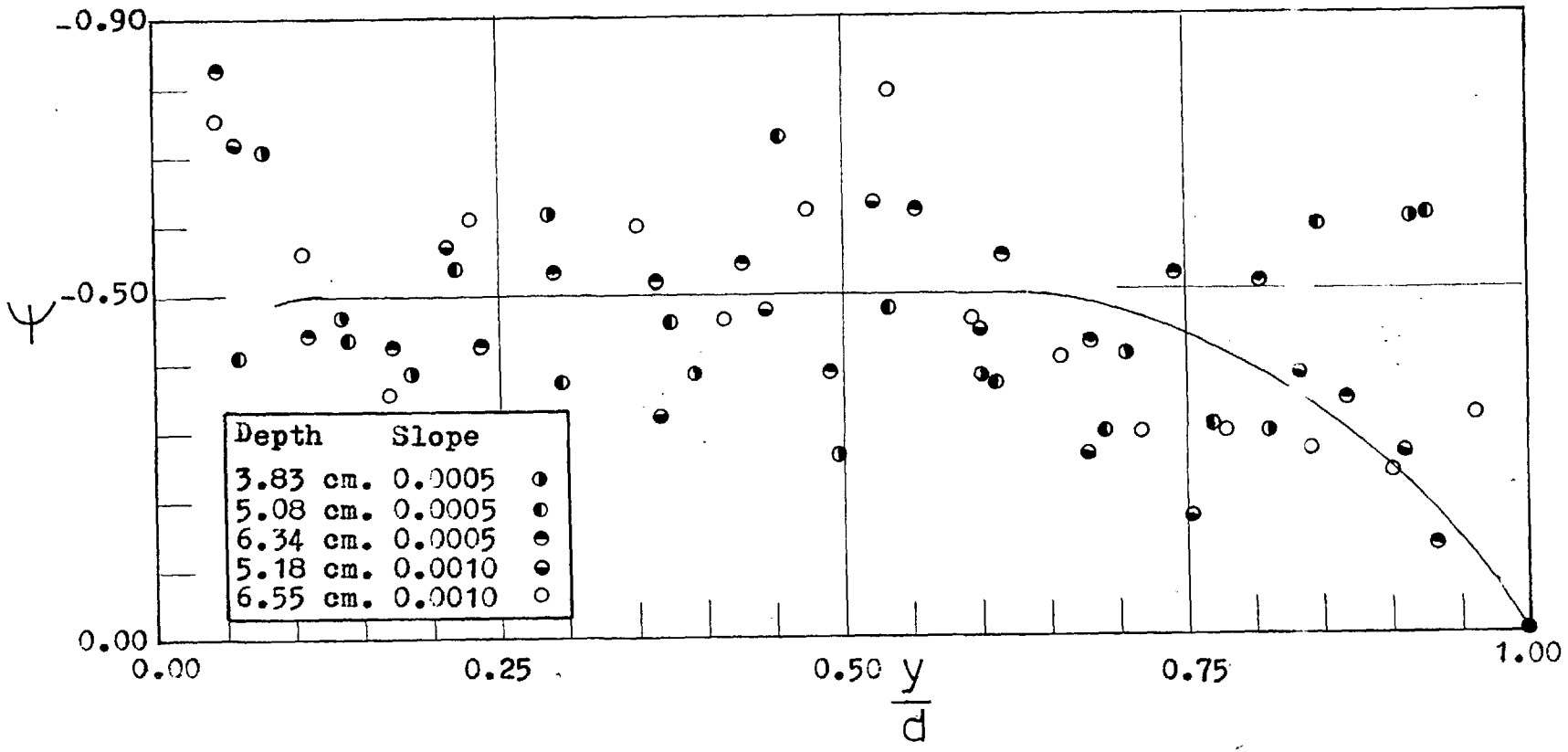


FIG.IV.16. DISTRIBUTION OF COEFFICIENT OF CORRELATION (RIPPLED BED).

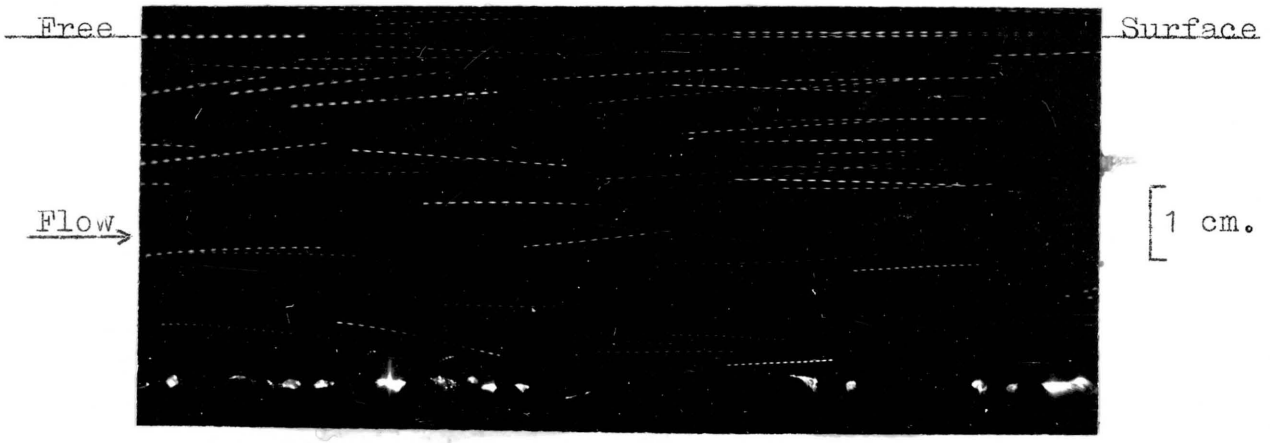
slope and depth, and therefore completely account for the external forces.

The values of the correlation coefficient $\frac{\overline{u'v'}}{\sqrt{\overline{u'^2}}\sqrt{\overline{v'^2}}}$ are plotted in Figure (IV.16.). The mean value of the coefficient in the central region, away from the wall and the free surface, again is about -0.50.

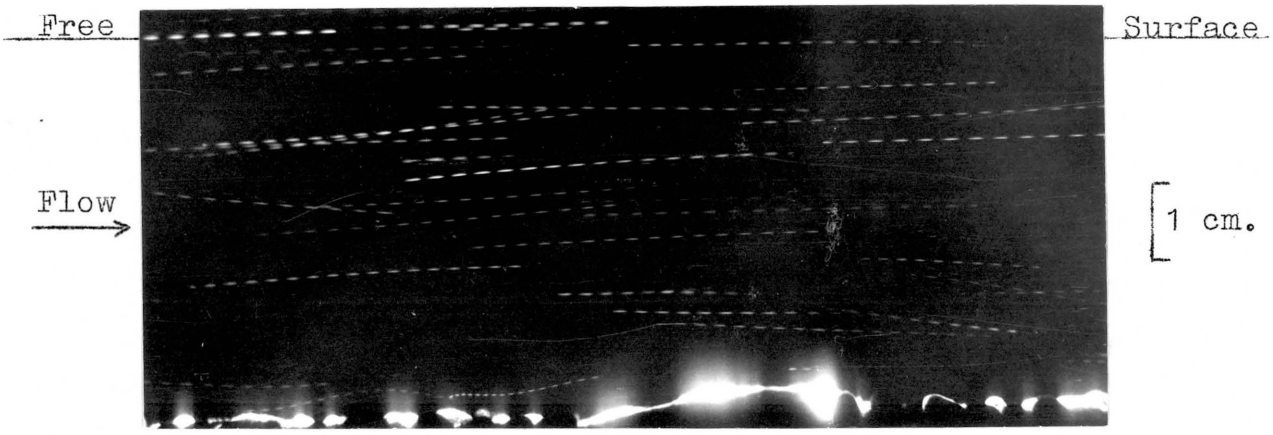
IV.4.3 RESULTS OBTAINED IN RIPPLED BED WHEN THE TROUGHS WERE FILLED WITH GRAVEL

A total of five depths, with the width-depth ratios from 8 : 1 to 4.5 : 1, for two slopes, 1 in 2000 and 1 in 1000, were investigated. The value of $\frac{d\,V_{xo}}{\nu}$ varied from 600 to 1400. Two photographs at nearly the same depth, for the two slopes, are attached in Figure (IV.17.) to represent flow on this bed. The local instantaneous values of u, v' and u'v' for various depths are plotted on graphs in Appendix (III). The turbulent quantities calculated from the local instantaneous values are given in the Appendix (II.B.), Tables (10 to 14).

The relative turbulence intensities $\frac{\sqrt{\overline{u'^2}}}{V_{xo}}$ are plotted in Figure (IV.18.) and a mean curve is drawn through the points. The value of $\frac{\sqrt{\overline{u'^2}}}{V_{xo}}$ obtained at the free surface is again equal to 0.85 and increases towards the bed reaching 1.40 at $\frac{Y}{d} = 0.10$.



Depth = 4.60 cm. ; Slope = 0.0005 .



Depth = 5.11 cm. ; Slope = 0.0010 .

FIG.IV.17. SAMPLE PHOTOGRAPHS IN CENTRAL PLANE OF FLUME ON RIPPLED BED WITH GRAVEL FILLED IN THE TROUGHS .

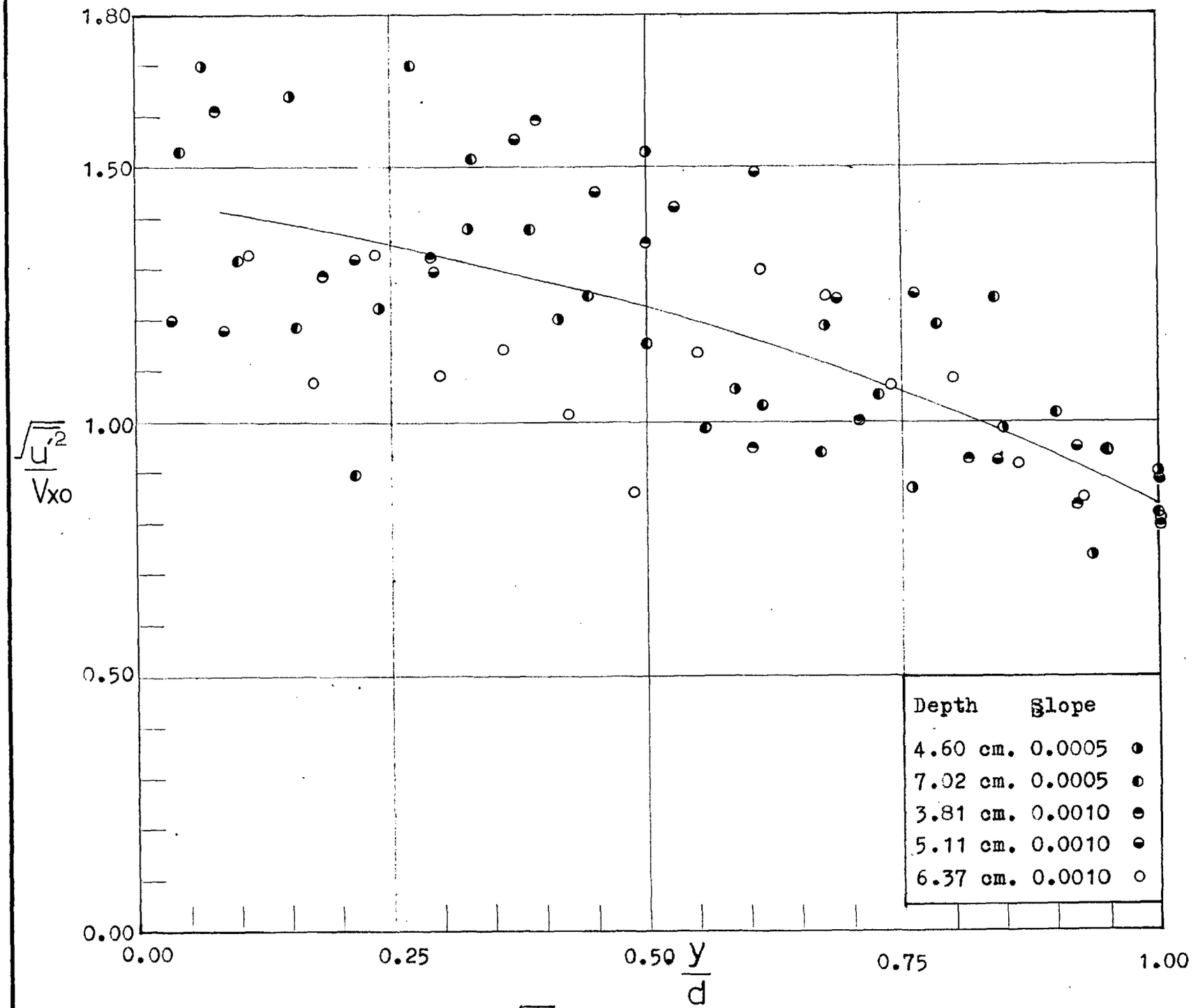


FIG.IV.18. DISTRIBUTION OF $\frac{\sqrt{\overline{u'^2}}}{V_{xo}}$ (GRAVEL FILLED IN TROUGHS OF RIPPLED BED) .

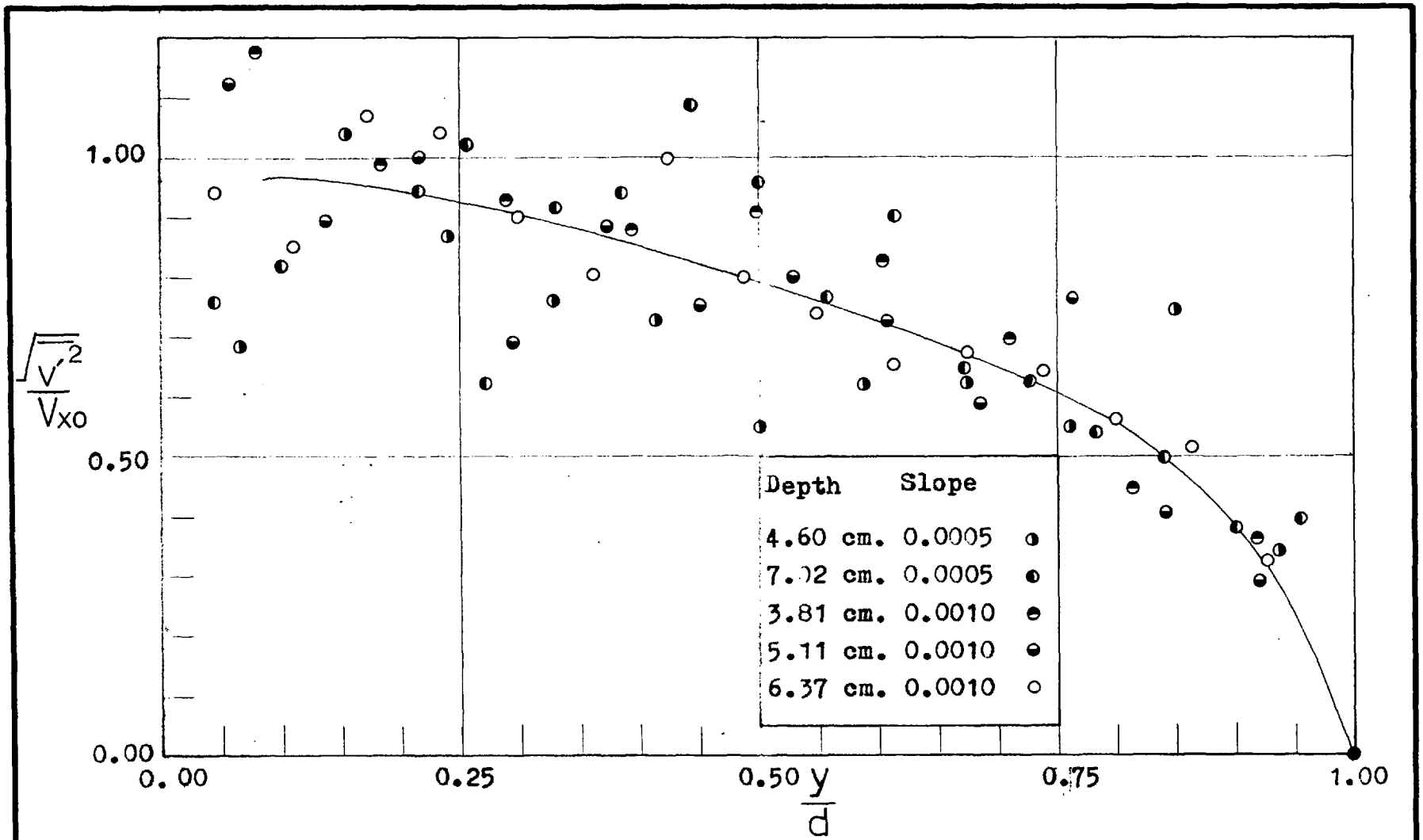


FIG.IV.19. DISTRIBUTION OF $\frac{\sqrt{\overline{v'^2}}}{V_{xo}}$ (GRAVEL FILLED IN TROUGHS OF RIPPLED BED).

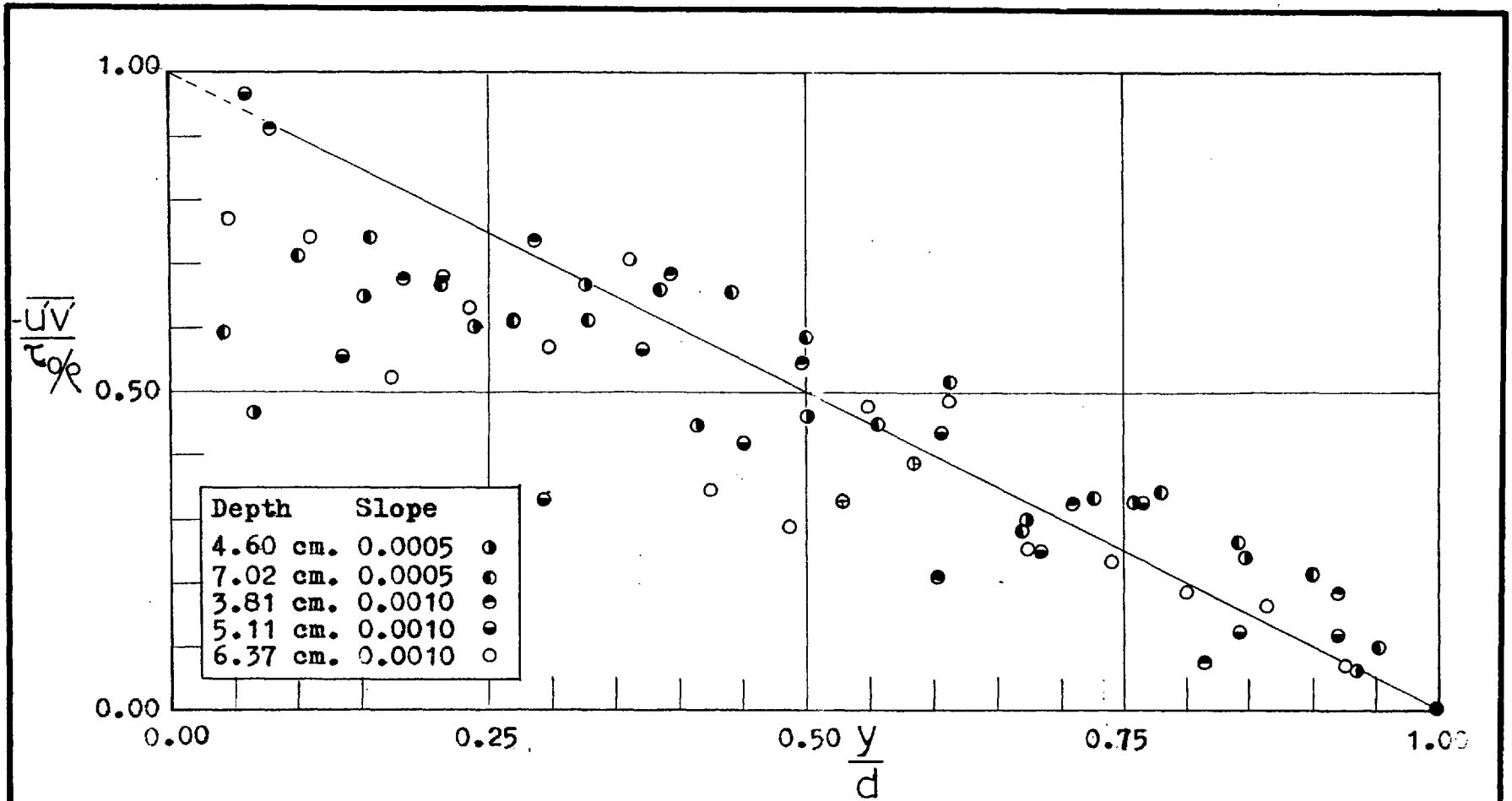


FIG.IV.20. DISTRIBUTION OF TURBULENT SHEAR STRESS (GRAVEL FILLED IN TROUGHS OF RIPPLED BED).

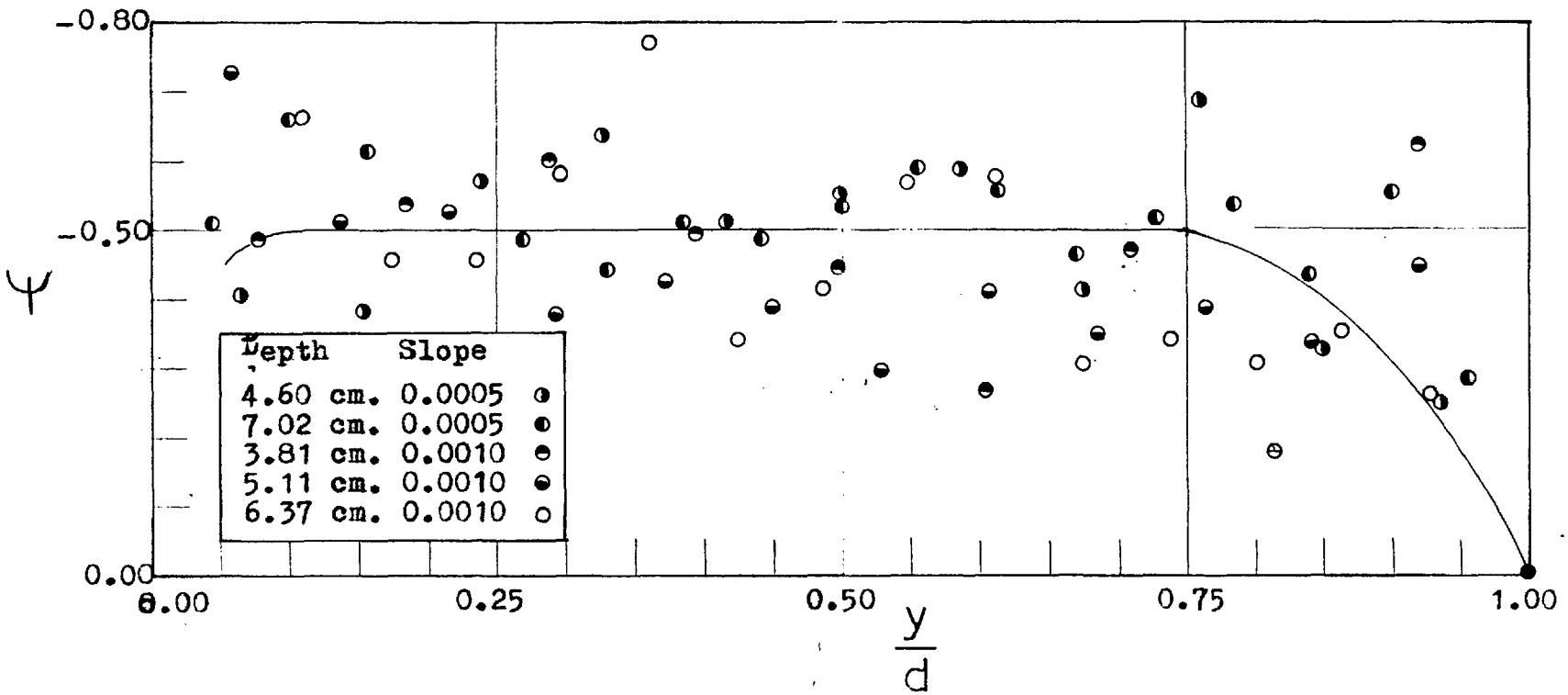


FIG.IV.21. DISTRIBUTION OF COEFFICIENT OF CORRELATION (GRAVEL FILLED IN TROUGHS OF RIPPLED BED).

The values of $\frac{\sqrt{\overline{v'^2}}}{V_{xo}}$ are plotted in Figure (IV.19.). The mean curve drawn through the points, with zero value at the free surface, rises towards the bed giving the value of $\frac{\sqrt{\overline{v'^2}}}{V_{xo}}$ equal to about 1.0 at $\frac{y}{d} = 0.10$.

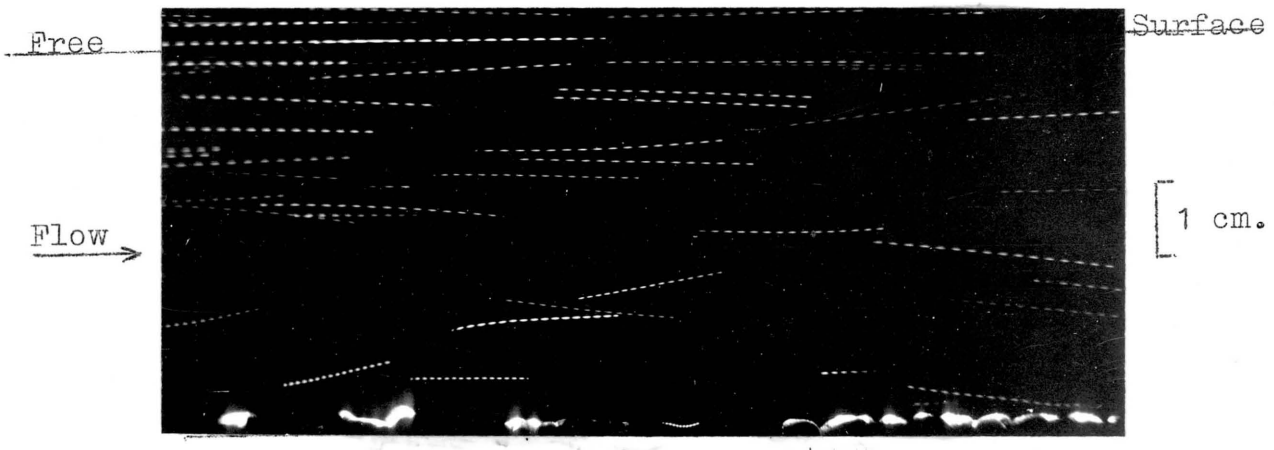
The values of $\frac{-\overline{u'v'}}{\tau_o/\rho}$ are plotted in Figure (IV.20.) and are seen again to agree well with the theoretical line except close to the bed.

The values of the correlation coefficient $\frac{\overline{u'v'}}{\sqrt{\overline{u'^2}}\sqrt{\overline{v'^2}}}$, are plotted in Figure (IV.21.). The mean value of the coefficient in the central region is again about -0.50.

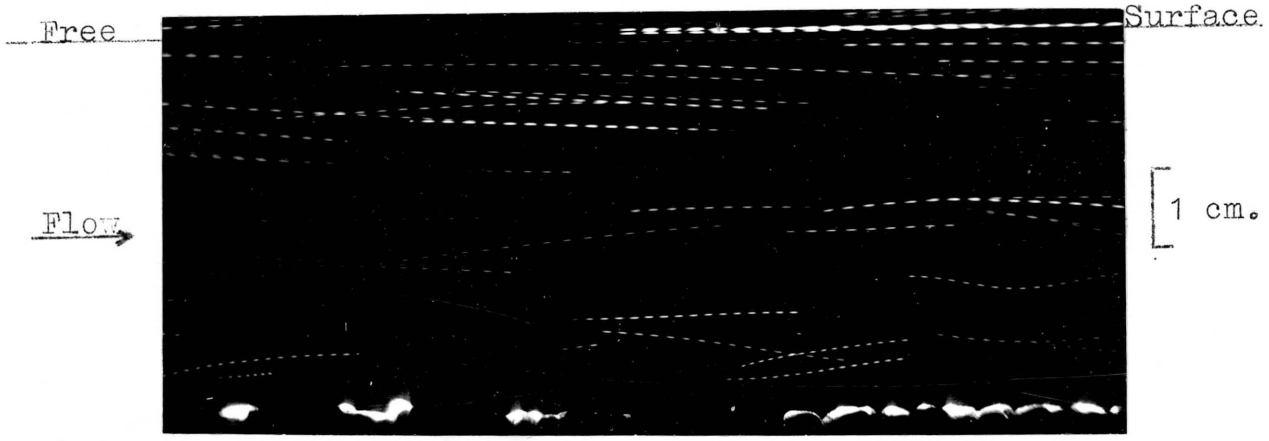
IV.4.4. RESULTS OBTAINED ON FULLY GRAVELLED BED

Two depths of about 5.0 c.m. and 6.25 c.m. were taken for each of the slopes of 1 in 2000 and 1 in 1000. The value of $\frac{d\,V_{xo}}{\nu}$ varied from 750 to 1500. Two photographs for depth 5.0 c.m., one for each slope, are attached in Figure (IV.22.) to represent the flow on this bed. The local instantaneous values of u, v' and u'v' obtained for various flows, are plotted on graphs in Appendix (III). The turbulent quantities calculated are given in Appendix (II.B.), Tables (15 to 18).

The values of $\frac{\sqrt{\overline{u'^2}}}{V_{xo}}$ are plotted in Figure (IV.23.) and a mean curve is drawn through the points. The mean value at the free surface is 0.65 and increases towards the bed giving the value



Depth = 5.00 cm. ; Slope = 0.0005 .



Depth = 4.98 cm. ; Slope = 0.0010 .

FIG.IV.22. SAMPLE PHOTOGRAPHS IN CENTRAL PLANE OF FLUME ON FULLY GRAVELLED BED .

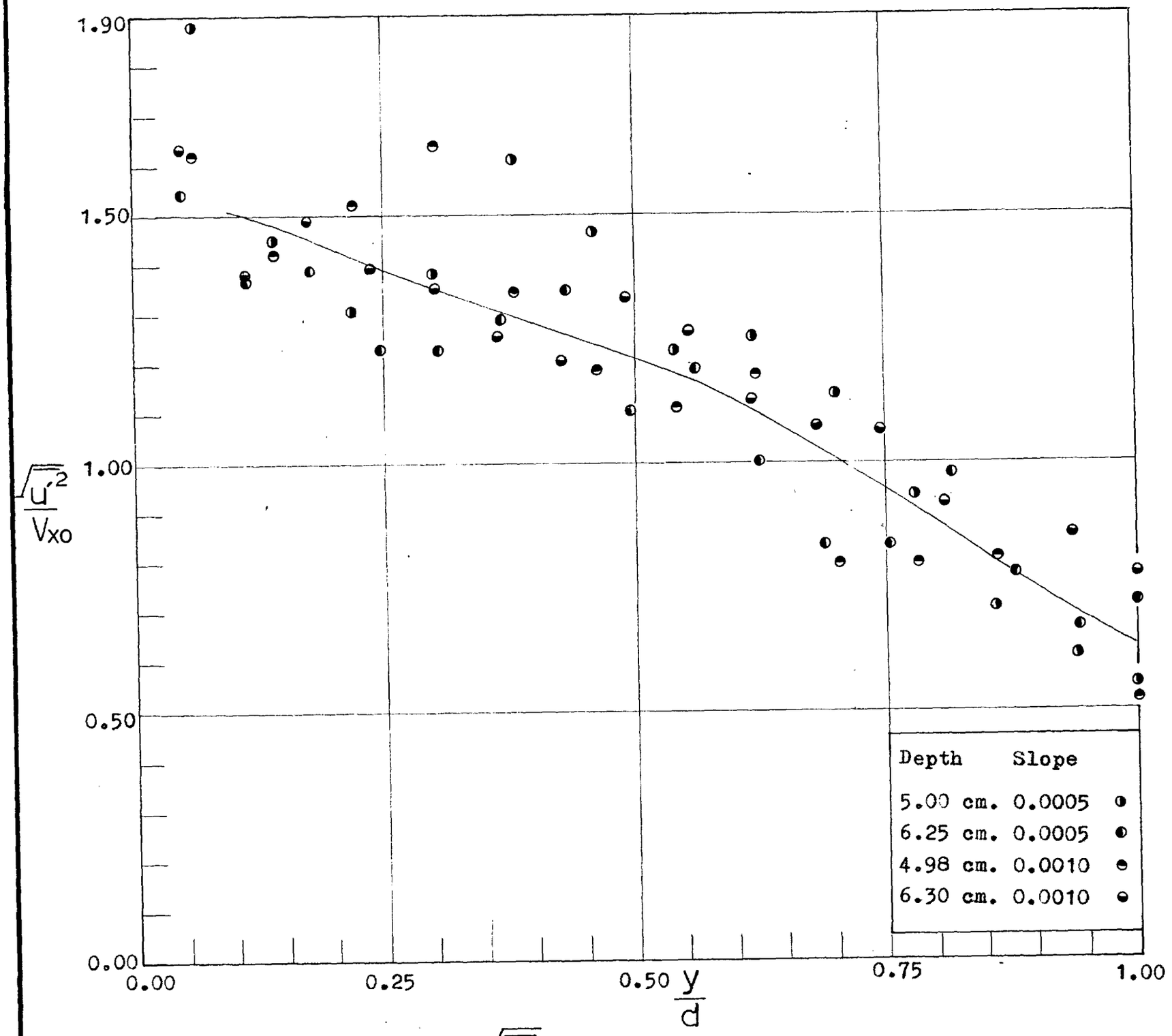


FIG.IV.23. DISTRIBUTION OF $\frac{\sqrt{\overline{u'^2}}}{V_{xo}}$ (FULLY GRAVELLED BED) .

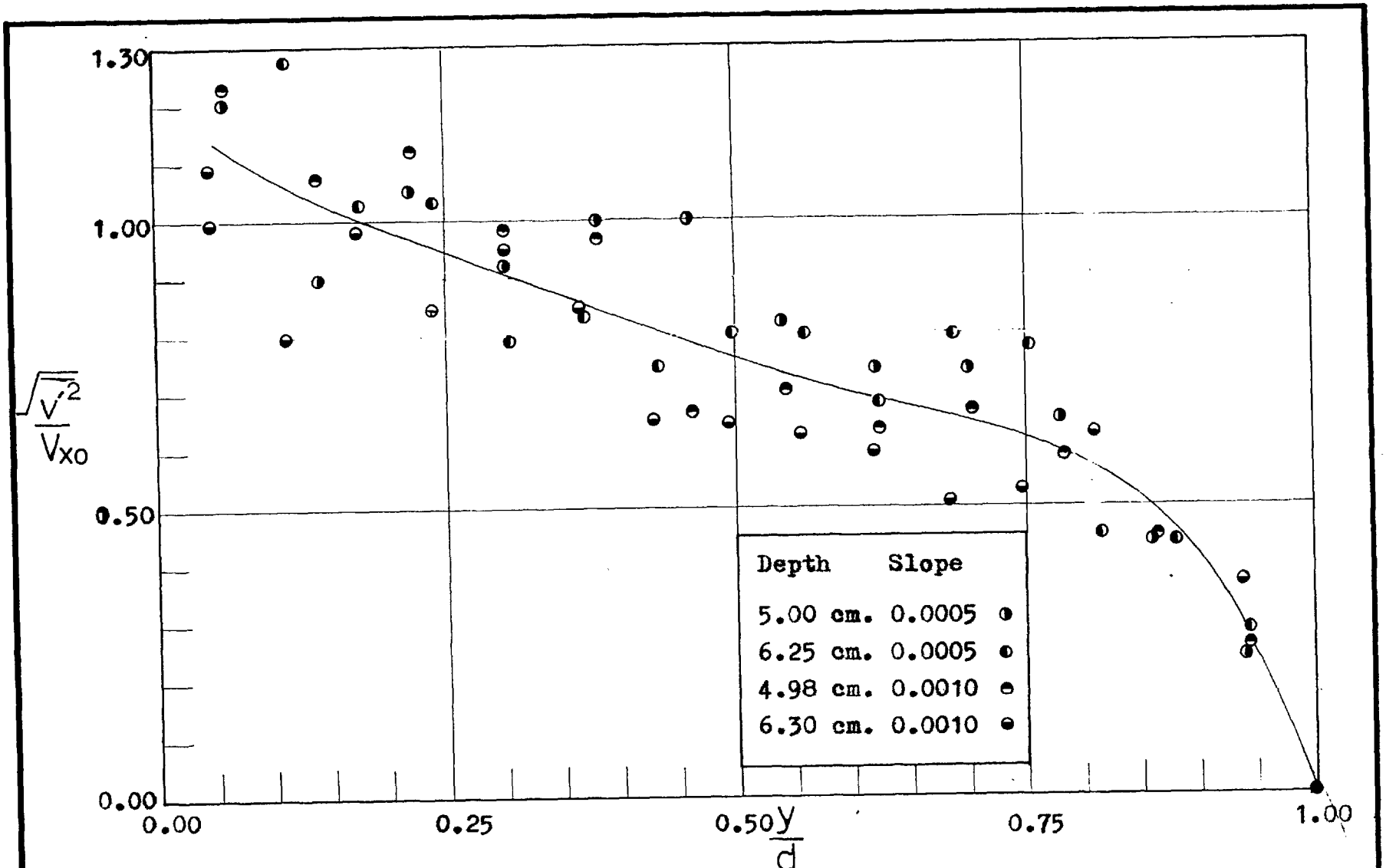


FIG.IV.24. DISTRIBUTION OF $\frac{\sqrt{\overline{v'^2}}}{V_{xo}}$ (FULLY GRAVELLED BED) .

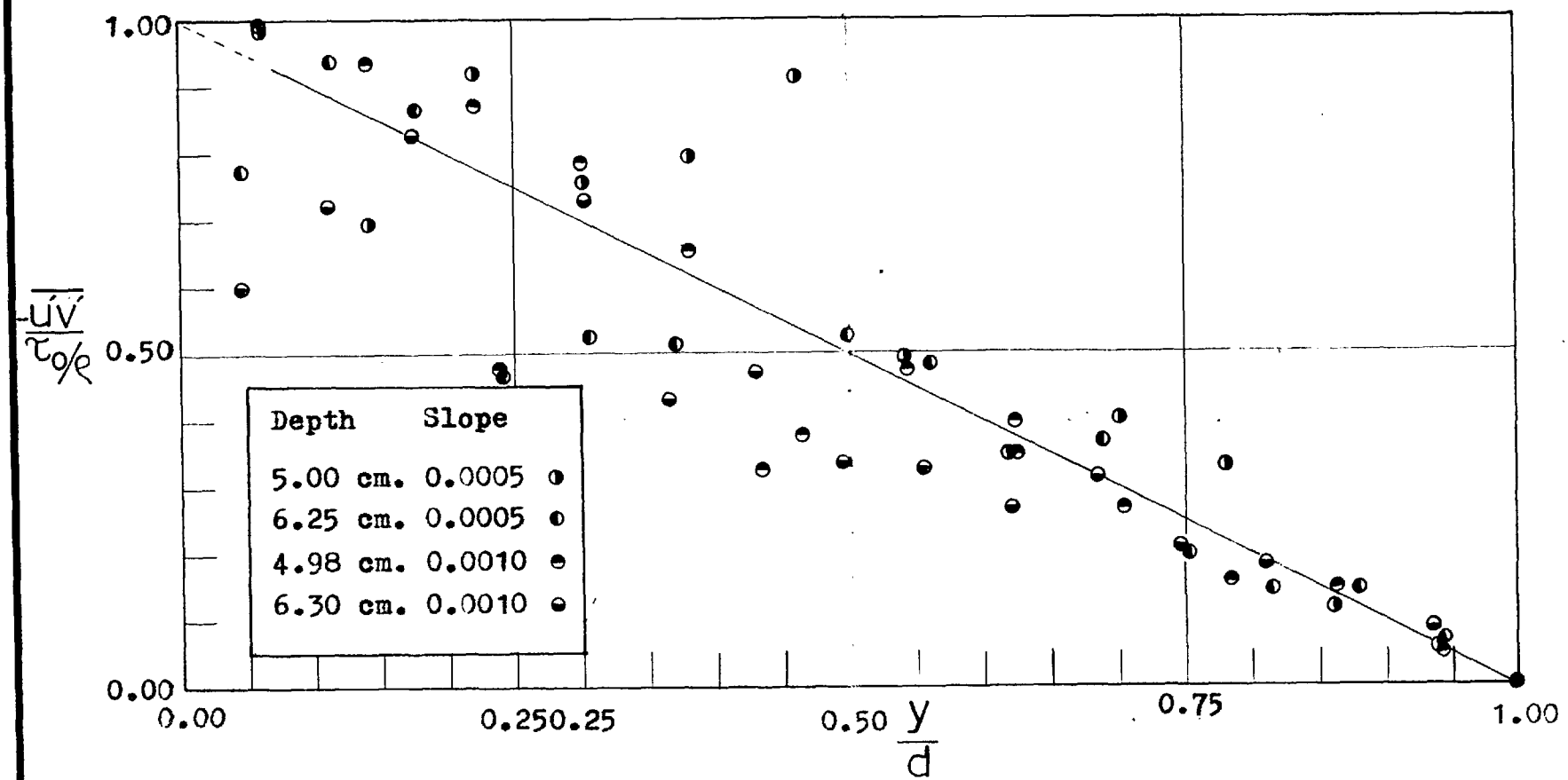


FIG.IV.25. DISTRIBUTION OF TURBULENT SHEAR STRESS (FULLY GRAVELLED BED) .

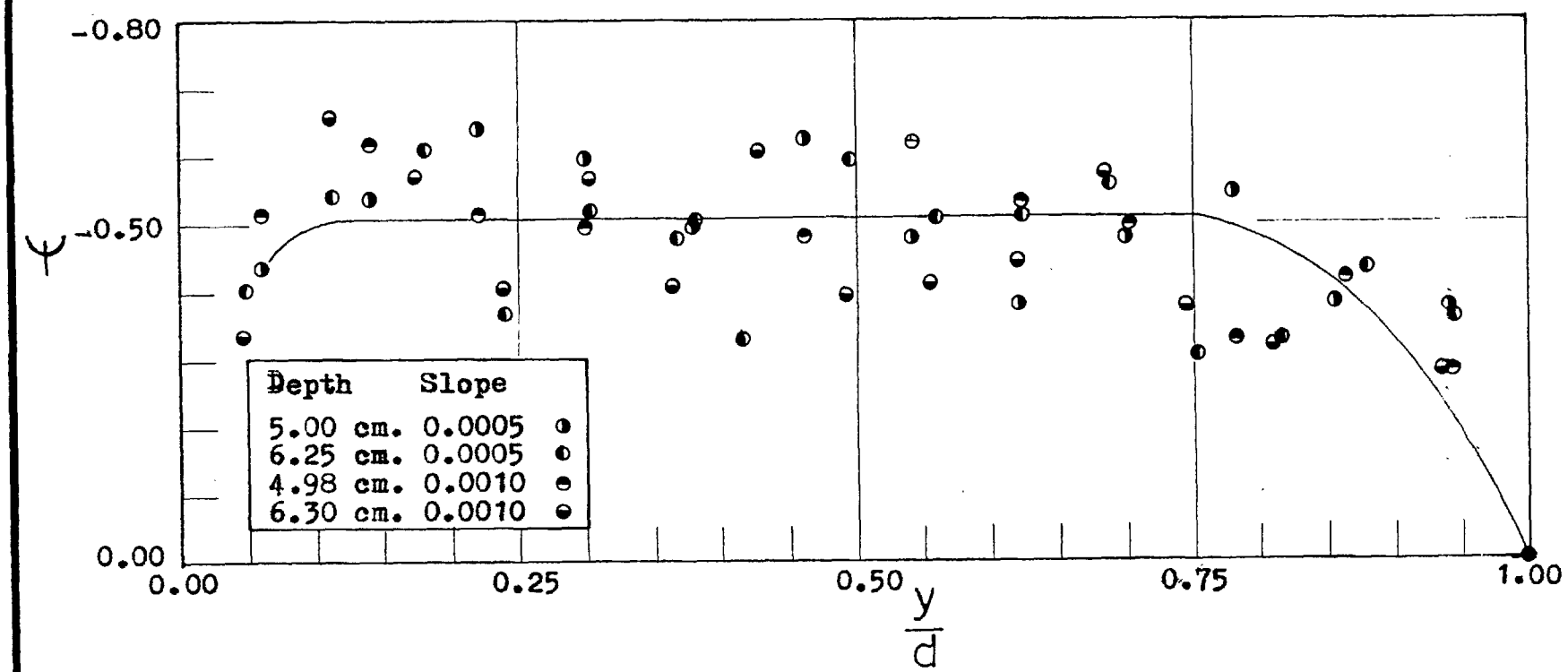


FIG.IV.26. DISTRIBUTION OF COEFFICIENT OF CORRELATION (FULLY GRAVELLED BED).

of 1.50 at y/d = 0.10. The value 0.65 at the free surface is much lower than the values obtained in the three previous cases. There seems no obvious reason for this. Perhaps the discrepancy could be statistical, in that the streaks measured may on average have had instantaneous velocities nearer to the mean velocities, though the odds against this could be quite great.

The values of $\frac{\sqrt{\overline{v'^2}}}{v_{xo}}$ are plotted in Figure (IV.24.). The mean curve, having zero value at the free surface, rises towards the wall reaching a value of about 1.10 at $\frac{y}{d}$ = 0.10.

The values of $-\overline{u'v'}$ are plotted, as before, in Figure (IV.25). The points lie around the theoretical straight line.

The values of the correlation coefficient are plotted in Figure (IV.26.). The mean values of the coefficient in the central region is again about - 0.51.

IV.5. TURBULENCE AND THE SEVERAL BEDS

The previous investigations on pipes and closed channel sections with smooth surfaces, revealed that the intensity of turbulent fluctuations depends only on the shear velocity at the bed. Assuming this to be valid for rough surfaces, the present results relating to the various beds have been plotted accordingly giving a set of mean curves each for a different bed. It is interesting to see to what extent these curves for the various bed conditions can be correlated.

The curves of $\frac{\sqrt{\overline{u'^2}}}{v_{xo}}$ obtained on different bed surfaces, excluding the wall region, are represented in Figure (IV.27.). In the upper region, all the curves except the one for the fully gravelled bed, which shows some discrepancy near the free surface, lie within a narrow strip. Near the bed, and for a distance of 0.25 times the depth from the bed, the relative turbulent intensity $\frac{\sqrt{\overline{u'^2}}}{v_{xo}}$ is evidently affected by the bed conditions, since its highest value occurs for the smooth bed and its lowest value for the rippled bed. In this figure, curve (5) represents the mean of all the curves, for various bed surfaces.

Similarly, Figure (IV.28.) represents the mean curves of $\frac{\sqrt{\overline{v'^2}}}{v_{xo}}$ with various beds. Again, in the region well away from the bed, most of the curves lie in a narrow strip. However, the curve for the rippled bed is clearly different, and reveals a distinctly more intense turbulence extending throughout the stream. Possibly, compared with the size of ripples which were about 1 c.m. high, the range of depths investigated (none exceeded 6.5 c.m.) was too shallow in which $\frac{\sqrt{\overline{v'^2}}}{v_{xo}}$ could not be independent of the bed roughness; and so the eddies generated by the bed ripples influenced the whole of the flow giving higher values of the v' component even near the free surface. Also the points for the rippled bed have their maximum, $\frac{\sqrt{\overline{v'^2}}}{v_{xo}}$, near the bed, whereas those for the smooth bed have their maximum little away from the bed. In view of these differences, the points for the rippled bed were ignored

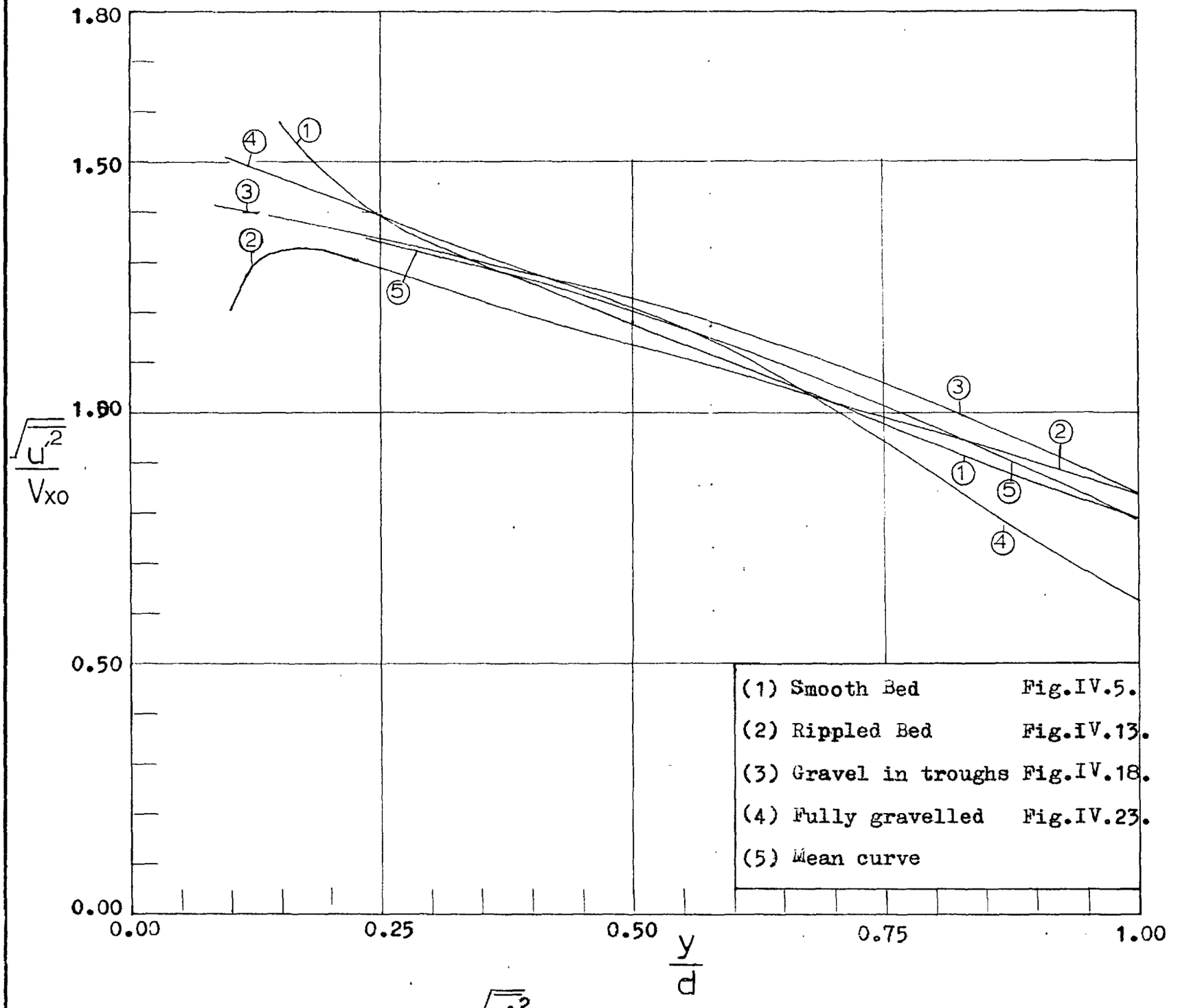


FIG.IV.27. DISTRIBUTION OF $\frac{\sqrt{\overline{u'^2}}}{V_{xo}}$ ON VARIOUS BEDS.

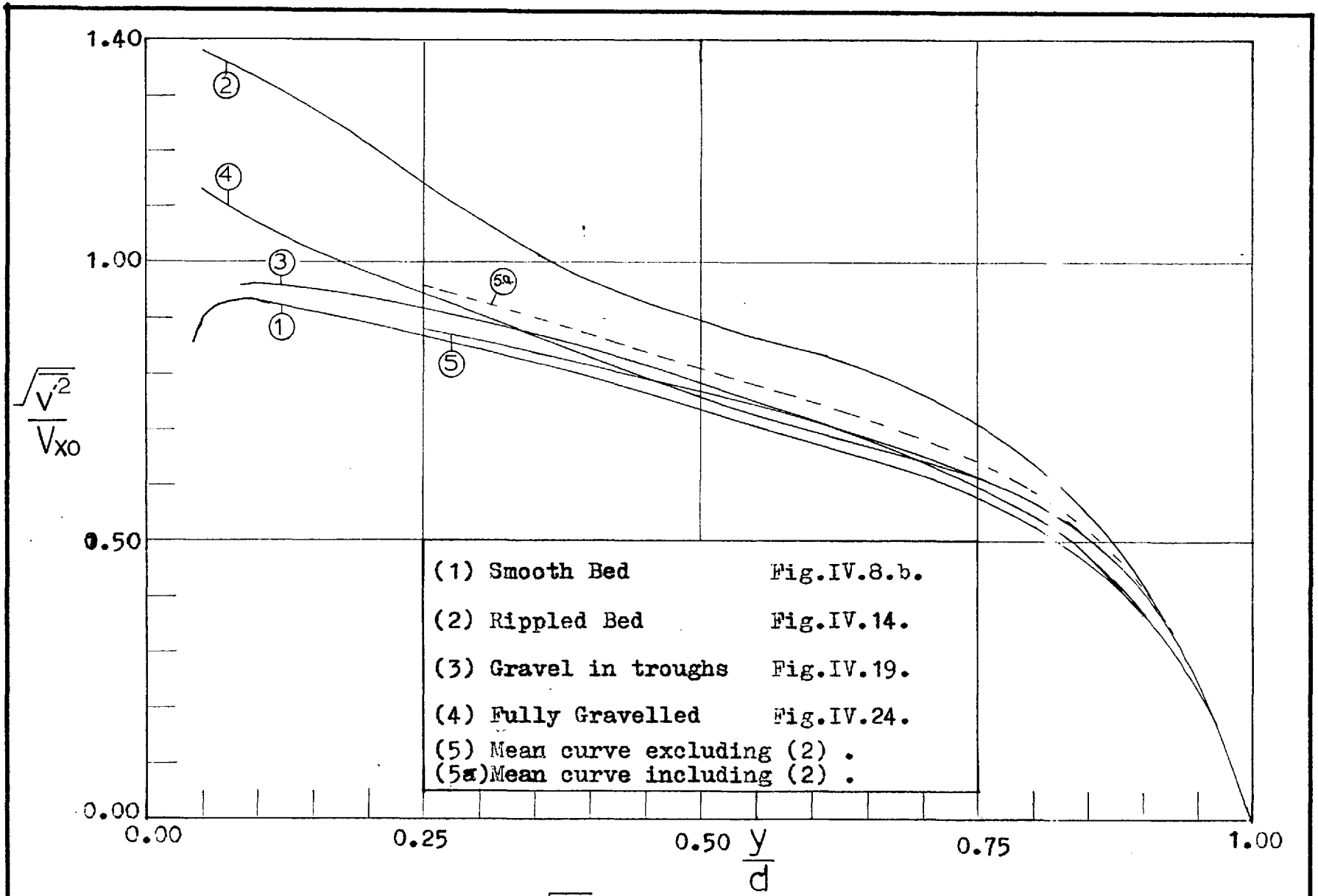


FIG.IV.28. DISTRIBUTION OF $\frac{\sqrt{\overline{v'^2}}}{V_{xo}}$ ON VARIOUS BEDS .

when drawing the mean curve in Figure (IV.28.), otherwise the dotted curve would have been the mean.

Hence, except very close to the wall, there is substantial support for the view that the turbulence at any point depends on the position of the point and on the shear stress at the wall, and on these two variables alone; it is independent of the nature of the wall or of other variables such as Reynolds number or Froude number. Therefore, the mean curves drawn in Figures (IV.27.) and (IV.28.) for u' and v' can be taken generally to represent the two dimensional flow in wide open channels.

Near the wall, particularly for the two extreme cases, the smooth and the very rough beds, it is evident that when the turbulent intensity of one velocity component becomes great then the intensity of the other component becomes small. For example $\frac{\sqrt{\overline{u'^2}}}{v_{xo}}$ near the smooth wall, in the transition zone, increases whereas $\frac{\sqrt{\overline{v'^2}}}{v_{xo}}$ decreases, but for the rippled bed near the wall $\frac{\sqrt{\overline{v'^2}}}{v_{xo}}$ increases and $\frac{\sqrt{\overline{u'^2}}}{v_{xo}}$ decreases. Such a relationship would be expected if u' and v' happened to obey the same statistical distributions and if they were completely in phase, since their product determines the Reynolds stress.

When the intensities of the turbulent fluctuations in this open channel are compared with those in pipes, the value of $\frac{\sqrt{\overline{u'^2}}}{v_{xo}}$ is found to be the same, though the value of $\frac{\sqrt{\overline{v'^2}}}{v_{xo}}$ is characteristically different: since, in the open channel v' is zero at the

free surface whereas it always has some definite value at the centre of a pipe. Regarding v', this influence of the free surface is clearly seen to extend to a distance as far as 0.40 d from the free surface.

Although the relative intensities of the turbulence were not actually calculated in terms of the local mean velocities or in terms of the maximum velocity of the flow, it is obvious that, expressed in these terms, they are greater for the rough surface than for the smooth surface: since, for equal v_{xo}, the velocities are higher with the smooth surface than with the rough surface. Such values can be obtained readily from the foregoing results, since the necessary values of the local mean or maximum velocities can be estimated from v_{xo}. The relevant data can be found in the same Tables in Appendix (II.B).

The value of the correlation coefficient in the central region, away from the bed and the free surface, seems to be constant, for the various bed surfaces. Its value obtained for the rippled bed and the bed with gravel filled in the troughs of the ripples is -0.50 but for the fully gravelled bed and for the smooth bed its value is -0.51 and -0.53 respectively. Previous workers give the mean value equal to -0.50 for smooth pipes and closed channels at all Reynolds numbers. It seems that the correlation coefficient has a constant value, irrespective of the nature of the

wall, and the average can be taken as -0.50. In mixing length theories one of the assumptions made is that $u' \sim v'$; also the correlation between them is assumed to be constant. These assumptions seem to be justified.

In conclusion, it may be said, that the present investigations give some idea about the variation of the two fluctuating velocity components u' and v' on various bed surfaces, and particularly in the region of the free surface of open channel flow. At present, not much can be said about the third component w', except that we have the work by Fage and Townend (1932), who obtained the maximas in square and circular pipes, and the complete work by Laufer, (1951, 1954) for closed channel and circular pipe; but its magnitude in open channel flow particularly near the free surface is a question which remains unexplored.

CHAPTER V

SECONDARY CURRENTS IN STRAIGHT CHANNELS

V.1. Introduction

Secondary currents in open channels or closed conduits may be described as regular and systematic motions occuring in the plane of the cross-section; and complete in themselves so that they may be regarded as separate circulations superimposed on the main flow and transforming it into helicoidal type of flow. Secondary currents occur most typically in bends of pipes and channels of every cross-sectional shape and are associated with the pressure gradients due to centrifugal action. The type of secondary motion with which the present study is concerned, occurs in turbulent flow only in straight channels with a free surface or in straight non-circular pipes.

These secondaries have long been a topic of discussion and, from time to time, a number of different patterns, based partly on experimental findings and partly on a variety of reasonings, have been suggested. The existence of these motions were recognised about a century ago, when the search started to find the cause for the maximum velocity occurring below the free surface in rivers. Darcy and Bazin (Bazin 1865) considered the problem of maximum velocity by working on channels of different cross-sections. For rectangular channels, they found that, with large width-depth ratio, the maximum velocity occurred at the free surface; but, with this ratio less than

five, the maximum velocity was below the free surface. Similarly, in semi-circular channels, as the depth increased, the isovels were distorted so that the maximum velocity occurred below the free surface; but in 90°- triangular channels the maximum velocity always occurred below the free surface. No clear reason was given for these observations but it was suggested that the cause of these irregularities in the upper regions was perhaps due to some interior fluid movements.

Francis (1878), confident that always the maximum velocity in open channels occurs below the free surface even when the wind is in the same direction as the current, suggested the cause to be slow water masses rising from the bottom, finding their way to the surface. He demonstrated the possibility of such an action by discharging white wash through a pipe near the bed in the middle of the channel and the white wash eventually appeared at the surface not very far down stream.

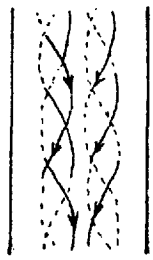
Wood (1879), considering the demonstration by Francis, argued that a downward flow of water must occur to replace the water rising from the bottom.

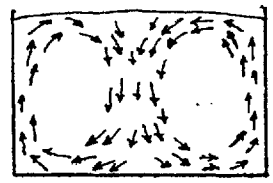
While working with floats for velocity measurements, although Cunningham (1882) attributed the depression of maximum velocity to the resistance caused by air, he drew attention to some possible kind of transverse flow.

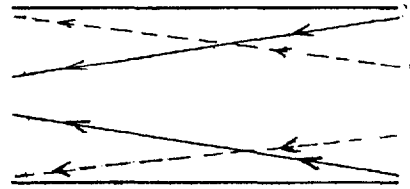
Stearns (1883), Moller (1883) and Gibson (1909) categorically

suggested the existence of secondary currents. Even though the three investigators had been working independently and gave different reasons, yet all three suggested the same flow pattern - two symmetrical cells, their movement being directed towards the centre of the channel at the surface and outwards along the bottom as sketched in Fig.(V.1.)

Nikuradse (1926) carried out velocity measurements for turbulent flow in a smooth rectangular pipe and an equilateral triangular pipe. The isovels, instead of having rounded shape near the corners, as known to occur in laminar flow, showed marked indentations and the values of the velocities in the corners were high. Prandtl (1927) attributed this to the secondary movements occurring in conduits of non-circular cross section. He explained the existence of the secondary currents in straight conduits based on the assumption that the turbulence fluctuations along the isovels are of a greater magnitude than those perpendicular to them. Based on this hypothesis and from momentum distribution he deduced resultant forces pointing towards the convex side of the isovel, with their greatest magnitude at places where the isovels have their greatest curvature. While his hypothesis regarding the turbulent fluctuations of this particular type may be open to question, the secondaries predicted by him were satisfactorily confirmed by Nikuradse (1930) in an equilateral triangular pipe by taking photographs of skimmed milk injected at the various points over the section.





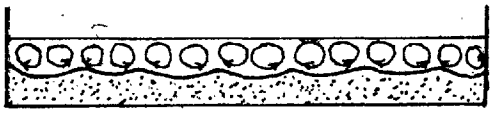


Gibson (1909)



Moller (1883)

Original observations .

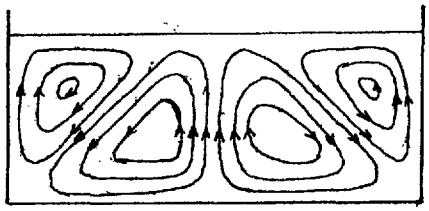


Casey (1935)

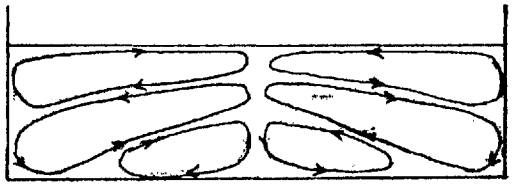


Vanoni (1946)

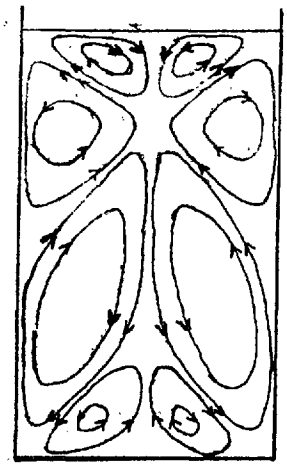
Observations from sediment tests .



Powell (1946)



Nemenyi (1946)



Nemenyi (1946)

Patterns based on Prandtl's hypothesis .

FIG.V.1. SECONDARY CURRENTS ACCORDING TO VARIOUS INVESTIGATORS .

Casey (1935), working on a broad channel with mobile bed and turbulent flow, observed some hollows and ridges on the bed. The patterns of the secondary currents assumed by him are reproduced in Fig (V.1), which shows that the material is shifted from certain places and deposited at others by these secondary currents. As seven hollows occurred in his channel, seven pairs of circulation were suggested.

Vanoni (1946) also noticed this kind of motion while working on transportation of suspended sediment. He observed bands of sand parallel to the flow on the channel bottom and suggested four pairs of circulation in the cross-section, shown in Fig (V.1.).

If the pattern suggested by Vanoni is compared with that given by Casey, it is noticed the motion is downward where the bands of the sand were observed in Vanoni's experiments whereas it is upward on the ridges of the mobile bed in Casey's expereiments. This gives motion in opposite directions in the two cases, one with suspended sediments and the other with mobile bed. Also the number of pairs of the circulation is less in Vanoni's case, which might have been controlled by the width-depth ratio of the channel. From his paper, Vanoni seems to be of the opinion that the secondary currents are due to the non-uniform distribution of sediments across the flow. But the difficulty remains that these have been observed even with clear water flows.

While discussing Vanoni's paper, Powell and Nemenyi suggested certain other patterns based on Prandtl's hypothesis. These are re-

produced in Fig (V.1).

The lack of agreement in the patterns suggested by various writers (Fig (V.1).) is because no direct observations were taken.

In so far as flows in closed conduits is concerned, the hot-wire anemometer has been successfully used to measure the secondary currents. Investigations on secondary currents, using hot-wire anemometers have been made on rectangular and square sections by Brundrett and Baines (1964), Gessner and Jones (1965) and Tracy (1965). The measurements on rectangular sections were restricted to the corner regions only. The pattern of the secondary currents disclosed by them, confirmed that predicted by Prandtl. The magnitude of the velocities of the secondary currents were found to be much smaller than the root-mean-square values of the turbulent fluctuations, and their maximum was perhaps 0.38 Vxo (Brundrett and Baines 1964).

However, flow with a free surface concerns liquids and no such instrument, as hot-wire anemometer, exists for them except possibly the hot-film anemometer. Liggett, Chiu and Miao (1965) investigated certain parts of the secondary currents in a 90°-triangular channel, using this instrument. Their measurements, because of the limitations and the tedious calibration of the instrument, were restricted to the corner region only. The results obtained show definite motion towards the corner and then along the side walls.

V.2. ANALYTICAL CONSIDERATIONS

For a secondary current to exist it must, by definition, be in the form of a loop and this pre-supposes the existence of angular velocity or vorticity about an axis parallel to the main flow direction. It is interesting to consider the conditions which occur in a field possessing vorticity.

Lamb (1932) showed the three Navier-stokes equations for lateral equilibrium could be converted into a form concerning rotational equilibrium thus :

$$\frac{\partial \xi}{\partial t} + u\frac{\partial \xi}{\partial x} + v\frac{\partial \xi}{\partial y} + w\frac{\partial \xi}{\partial z} = \xi\frac{\partial u}{\partial x} + \eta\frac{\partial u}{\partial y} + \zeta\frac{\partial u}{\partial z} + \nu\left(\frac{\partial^2 \xi}{\partial x^2} + \frac{\partial^2 \xi}{\partial y^2} + \frac{\partial^2 \xi}{\partial z^2}\right) \qquad \ldots\ldots(1)$$

where u, v and w are the velocity components and ξ, η and ζ are the vorticity components, along x, y and z directions respectively; ν is the kinematic viscosity of the fluid.

The three components of vorticity are defined as :

$$\xi = \frac{\partial w}{\partial y} - \frac{\partial v}{\partial z}$$

$$\eta = \frac{\partial u}{\partial z} - \frac{\partial w}{\partial x}$$

$$\zeta = \frac{\partial v}{\partial x} - \frac{\partial u}{\partial y}$$

The equation of continuity is -

$$\frac{\partial u}{\partial x} + \frac{\partial v}{\partial y} + \frac{\partial w}{\partial z} = 0 \qquad \ldots\ldots(2)$$

and there exists a corresponding equation for continuity of vorticity, given by Einstein and Li (1958), as :

$$\frac{\partial \xi}{\partial x} + \frac{\partial \eta}{\partial y} + \frac{\partial \zeta}{\partial z} = 0 \qquad \text{.....(3)}$$

For turbulent flow all the velocity and the vorticity components can be separated into their mean and fluctuating components, designated by overscore and prime respectively, such as $u = \bar{u} + u'$, $\xi = \bar{\xi} + \xi'$.

For uniform flow, with mean flow in the direction of x axis, if Eq. (1) is transformed in such a way and averaged with respect to time, the following relation is obtained after using Eqs. (2) and (3) to eliminate some of the terms.

$$\frac{\partial \bar{\xi}}{\partial t} + \bar{v}\frac{\partial \bar{\xi}}{\partial y} + \bar{w}\frac{\partial \bar{\xi}}{\partial z} = \frac{\partial^2}{\partial y \partial z}(\overline{v'^2} - \overline{w'^2}) + \frac{\partial^2}{\partial z^2}(\overline{v'w'}) - \frac{\partial^2}{\partial y^2}(\overline{v'w'}) + \nu\left(\frac{\partial^2 \bar{\xi}}{\partial y^2} + \frac{\partial^2 \bar{\xi}}{\partial z^2}\right) \qquad \text{.....} \quad (4)$$

Einstein and Li (1958), examining the case in which ξ is zero everywhere at any instant, obtained the corresponding relation for the rate of growth of vorticity as :

$$\frac{\partial \bar{\xi}}{\partial t} = \frac{\partial^2}{\partial y \partial z}(\overline{v'^2} - \overline{w'^2}) + \frac{\partial^2}{\partial z^2}(\overline{v'w'}) - \frac{\partial^2}{\partial y^2}(\overline{v'w'}) \qquad \text{.....} \quad (5)$$

From Eq. (5) they concluded that secondary currents can not exist with uniform laminar flow in straight conduits; and that, in turbulent flow, secondary currents can develop only when the terms on the right hand side of Eq. (5) have values different from zero, which they expected to occur chiefly in the region of frictional boundary

particularly where the lines of constant velocity are not parallel.

For steady flow $\frac{\partial \bar{\xi}}{\partial t}$ is equal to zero and Eq. (4) is written as;

$$\bar{v}\frac{\partial \bar{\xi}}{\partial y} + \bar{w}\frac{\partial \bar{\xi}}{\partial z} = \frac{\partial^2}{\partial y \partial z}(\overline{v'^2} - \overline{w'^2}) + \frac{\partial^2}{\partial z^2}(\overline{v'w'}) - \frac{\partial^2}{\partial y^2}(\overline{v'w'}) + \nu\left(\frac{\partial^2 \bar{\xi}}{\partial y^2} + \frac{\partial^2 \bar{\xi}}{\partial z^2}\right) \quad \ldots\ldots(6)$$

In the above equation, the various terms can be given physical interpretation. The terms on the left represent the convection of vorticity by secondary flow. The first three terms on the right can be regarded as representing the production process and the last term representing the dissipation of vorticity by viscosity (Brundrett and Baines 1964).

For isotropic turbulence $\overline{v'^2} = \overline{w'^2}$ and $\overline{v'w'} = 0$ and for homogeneous turbulence, the derivatives of these quantities with respect to any space coordinate have zero values. Hence the conditions favouring the growth of secondary currents are that the turbulence must be anisotropic and non-homogeneous.

For two-dimensional flow between parallel plates or in a circular pipe, $\overline{v'w'}$ is zero every where. At the centre of the section, measurements show that $\overline{v'^2} = \overline{w'^2}$, whereas near the wall and away from the centre $\overline{v'^2} - \overline{w'^2}$ is not zero and the contours of equal $\overline{v'^2} - \overline{w'^2}$ are parallel to the boundaries. Also the value of $\frac{\partial}{\partial y}(\overline{v'^2} - \overline{w'^2})$ is different from zero but $\frac{\partial^2}{\partial y \partial z}(\overline{v'^2} - \overline{w'^2})$ (or its counterpart for circular pipe in cylindrical coordinates) is zero. Hence the secondary

currents can not develop in these two cases also. The term $\frac{\partial^2}{\partial y \partial z}$ $(\overline{v'^2} - \overline{w'^2})$ cannot be different from zero unless the contours of equal $\overline{v'^2} - \overline{w'^2}$ are not parallel in the YZ plane. This can be expected to occur, in rectangular or other polygonal sections, near the corners where the boundary changes direction.

Such corners have been investigated by hot-wire anemometry (described earlier) and it has been shown that $\frac{\partial^2}{\partial y \partial z}$ $(\overline{v'^2} - \overline{w'^2})$ is different from zero there. Although the production terms establish a reason for the existence of the secondary currents, they do little to predict their pattern which is revealed only by measuring the three velocity components throughout the section.

Such considerations can be applied to flow near a free surface. It has been shown in chapter IV that for two-dimensional flow the structure of turbulence near a wall is the same for a free surface as for flow under pressure. But in an open channel as the free surface is approached the magnitude of $\overline{v'^2}$ diminishes to zero, and in the present experiments the effect of this was observed to extend as far as 0.40 times the depth from the water surface.

How important a role the free surface plays may be seen by considering a wide rectangular channel with large width-depth ratio. At the free surface near the side wall the value of $\frac{\partial^2}{\partial y \partial z}$ $(\overline{v'^2} - \overline{w'^2})$ can be expected to be different from the corresponding value obtained for flow in a channel under pressure. This statement is based on the

reasoning that $\overline{v'^2}$ is zero at the free surface, whereas $\overline{w'^2}$ may have the same or different value from that in closed channel. Hence strong secondary currents can be expected in an open channel and, if the width-depth ratio permits, they may extend to the central plane, depressing the filament of maximum velocity. The isovels obtained in semi-circular channels, by Bazin (1864) and recently by Sharp (1966) and Replogle and Chow (1966), show that these are not parallel to the channel boundary; and as the depth in the channel approaches half the diameter, the maximum velocity occurs below the free surface. Thus some secondary currents exist in semi-circular channels also although there is no change in the profile of the boundary except at the free-surface. If this conclusion is correct, the production terms are sustained at the free surface near the wall and in result the secondary currents are generated.

V.3. RESULTS FROM PHOTO-METHOD

Using the photographic technique, described in (II.4.3), the motion in the plane of the cross-section was revealed. Through the view finder of the camera, the picture at first appeared as a confused mass of starry lights moving irregularly like motes in a sunbeam, and the picture seemed devoid of pattern except very close to the side wall where the motes appeared to be shooting at great speed.

Individual photographs such as Figs.(V.2),(V.3) and (V.4), may not



FIG.V.2. SAMPLE PHOTOGRAPH ACROSS MAIN FLOW ON RIPPLED BED (d = 2.54", S = 0.0005).

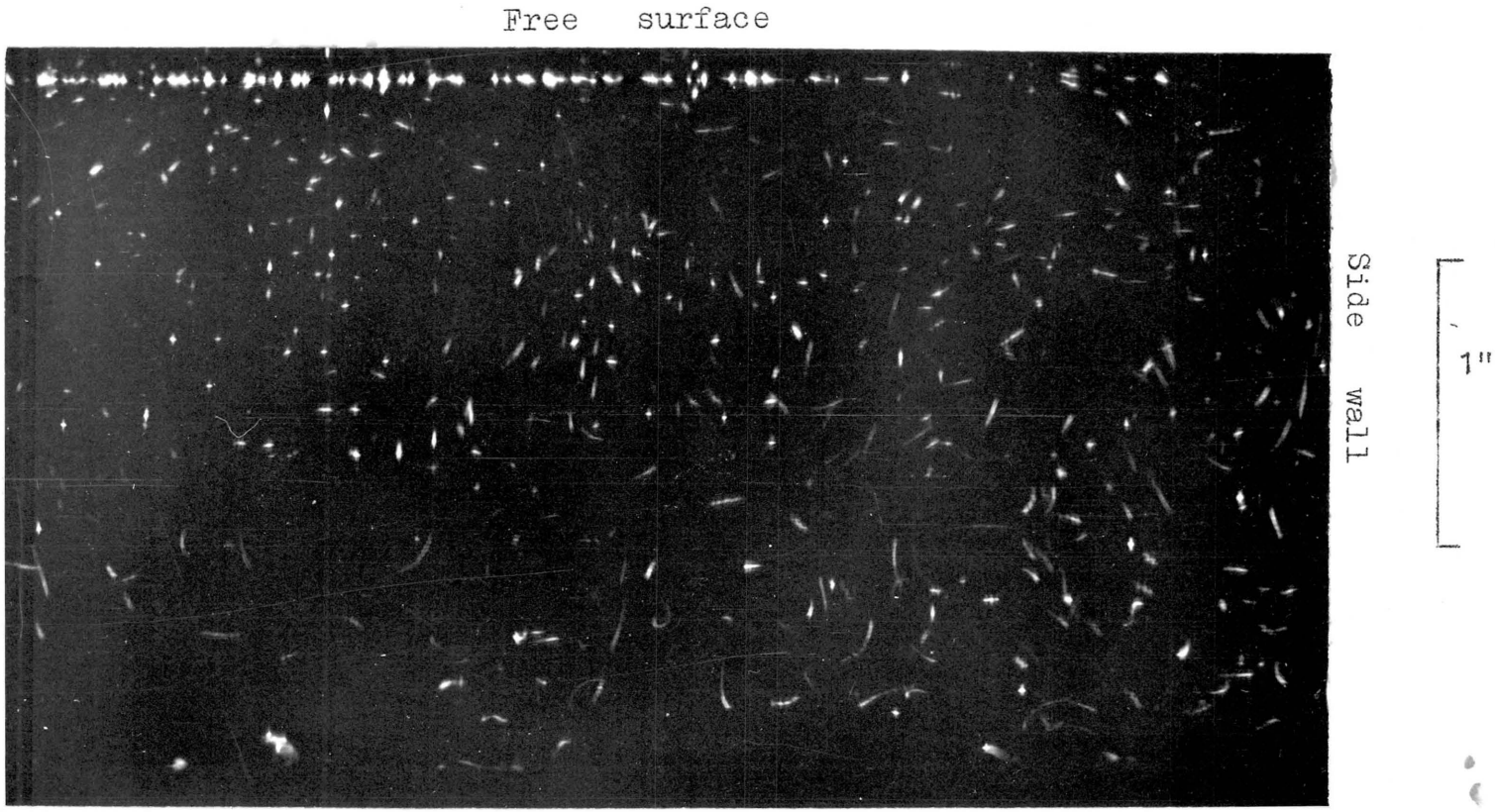


FIG.V.3. SAMPLE PHOTORAPH ACROSS MAIN FLOW ON FULLY GRAVELLED BED (d = 2.37", S = 0.0005) .

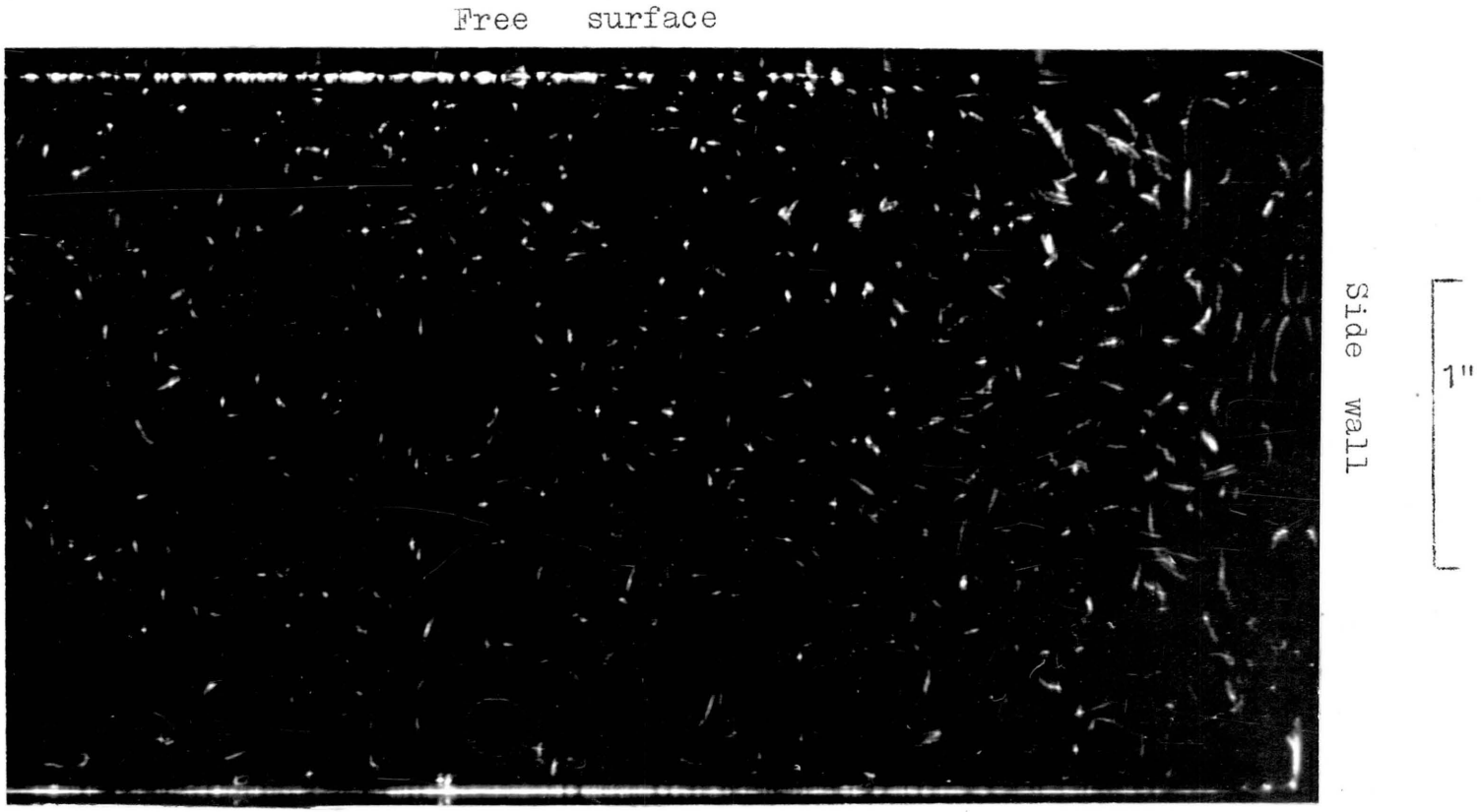


FIG.V.4. SAMPLE PHOTOGRAPH ACROSS MAIN FLOW ON SMOOTH BED (d = 2.47" , S = 0.0005).

show any pattern and to a glance, they may even fail to disclose any upward flow near the wall, though this upward stream seemed very strong when seen in motion. However, certain features of the secondary motion emerge when such photographs are analysed numerically.

This may be done by combining many photographs, since the sum of turbulent displacements tends to average to zero, while displacements due to steady currents, remaining always of the same direction, tend to reveal the secondary flow. Similarly in the equation of continuity, the flow being uniform, the axial space-derivative of the motion, when averaged for a long period of time, becomes zero.

Thus, with velocities suitably time-averaged, the equation of continuity is :

$$\frac{\partial \bar{u}}{\partial x} + \frac{\partial \bar{v}}{\partial y} + \frac{\partial \bar{w}}{\partial z} = 0$$

and with no change in $\bar{u}$, along the channel in the x direction, the two components $\bar{v}$ and $\bar{w}$ across the channel are related by :

$$\frac{\partial \bar{v}}{\partial y} + \frac{\partial \bar{w}}{\partial z} = 0$$

which is satisfied by a stream function such that

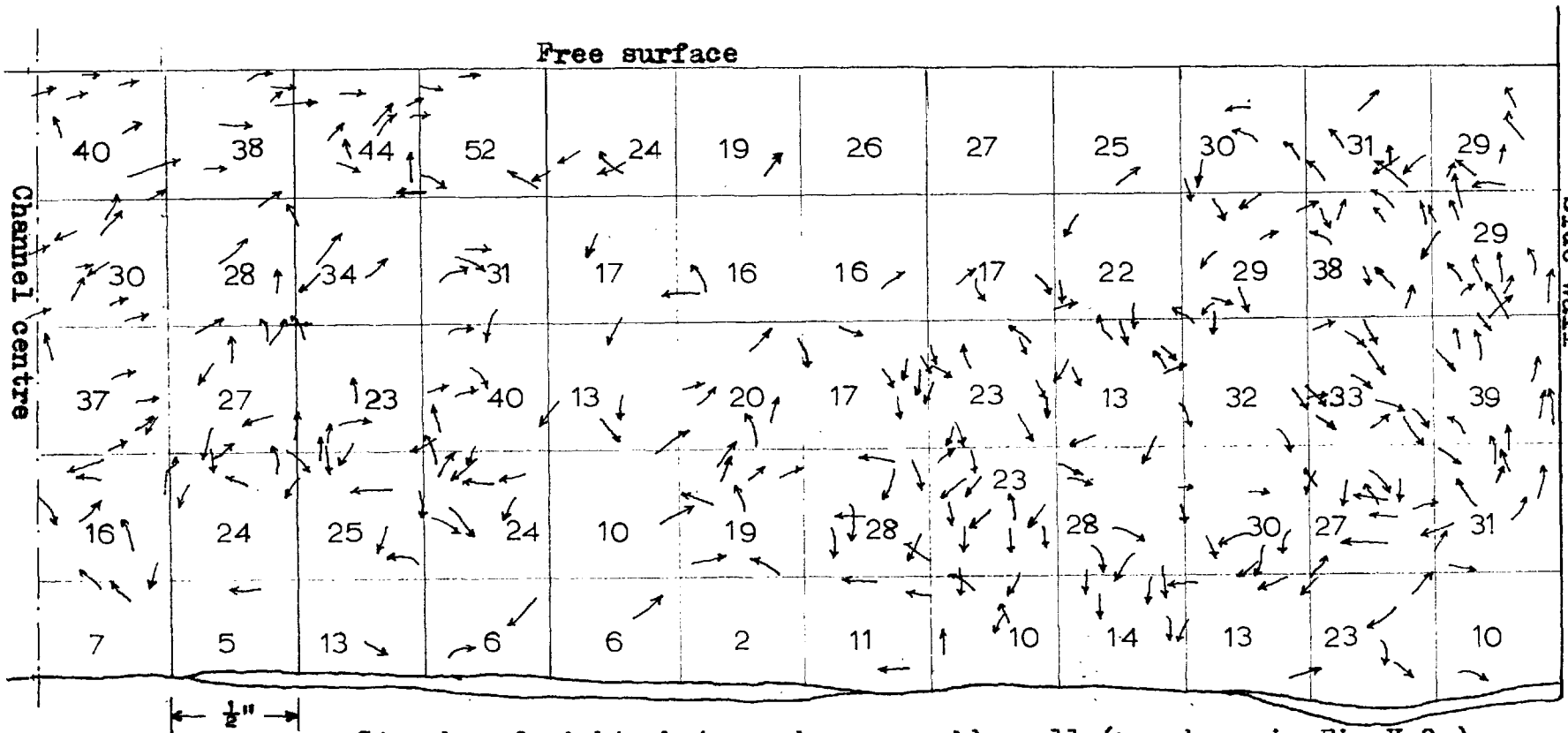
$$\bar{v} = - \frac{\partial \Psi}{\partial z} \text{ and } w = + \frac{\partial \Psi}{\partial y},$$

and contours of Ψ = constant are stream-lines in the plane of the cross-section. These contours describe the motion whose direction at every point is given by the time-average of the streaks photographed.

Thus from the combined record of many photographs (Figs.(V.5), (V.6) and (V.7)), conveniently subdivided into a number of small squares each containing a score or more of streaks, the total lateral and vertical displacements in each square were summed up, and the sum was divided by the number of streaks (including stationary stars) so giving the components of the displacement of a typical particle in each square of the cross-section.

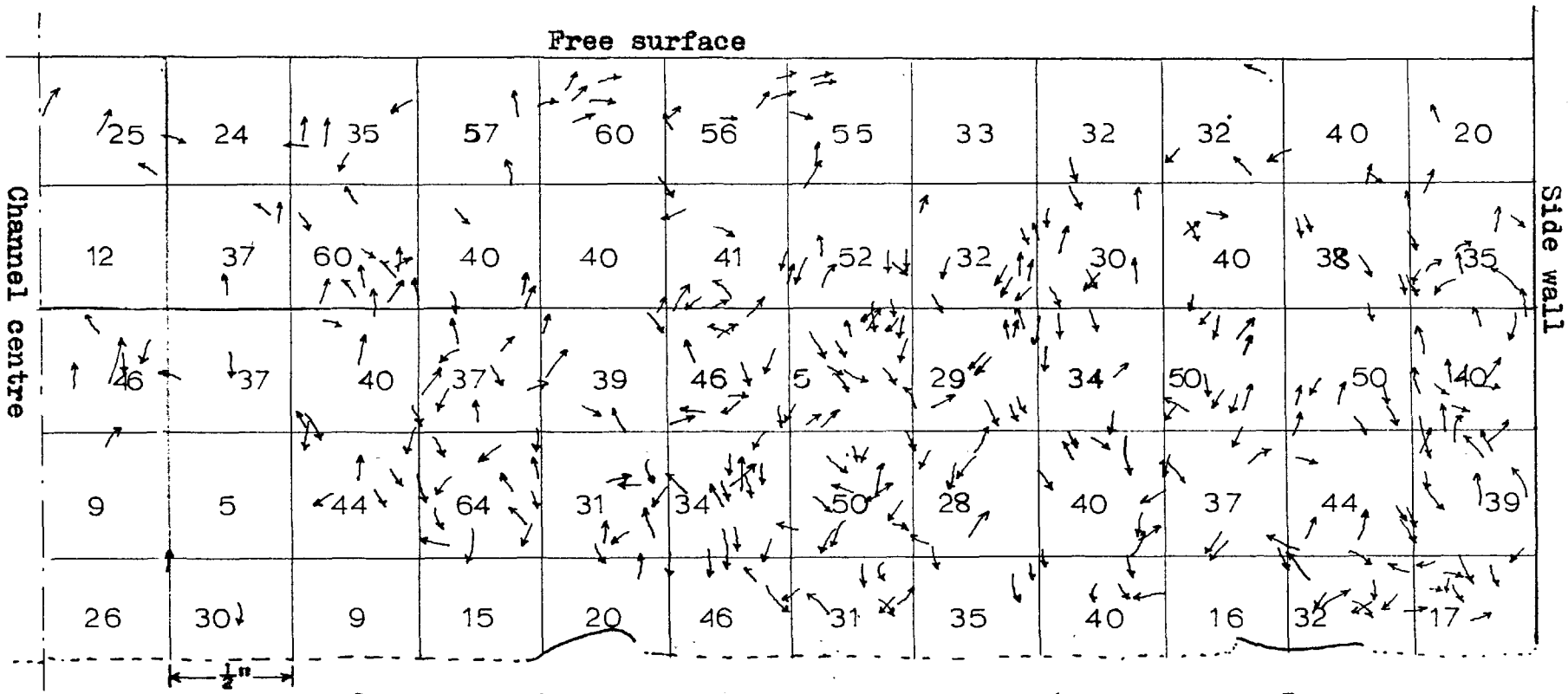
Because the same streaks were concerned, the total time for the horizontal displacements was identical with that for the vertical displacements, and consequently in each square, the vector sum of the many streaks lies truly along a stream line of the secondary in the square in question, and does so independently of the timing of the shutter of the camera, and independently of the width of the illuminated gap, and of the speed of flow across it.

However certain difficulties occur with this method, and chief among them is an apparent lateral displacement due to optical parallax as particles move across the lighted gap in their movement towards the camera. All particles other than those exactly in the optical axis appear to be moving radially away from it. The illuminated gap was 25 m.m, the distance to the camera 2.400m, and the depth of the stream 60 m.m. With such dimensions the parallax sometimes exceeded the displacement to be measured.



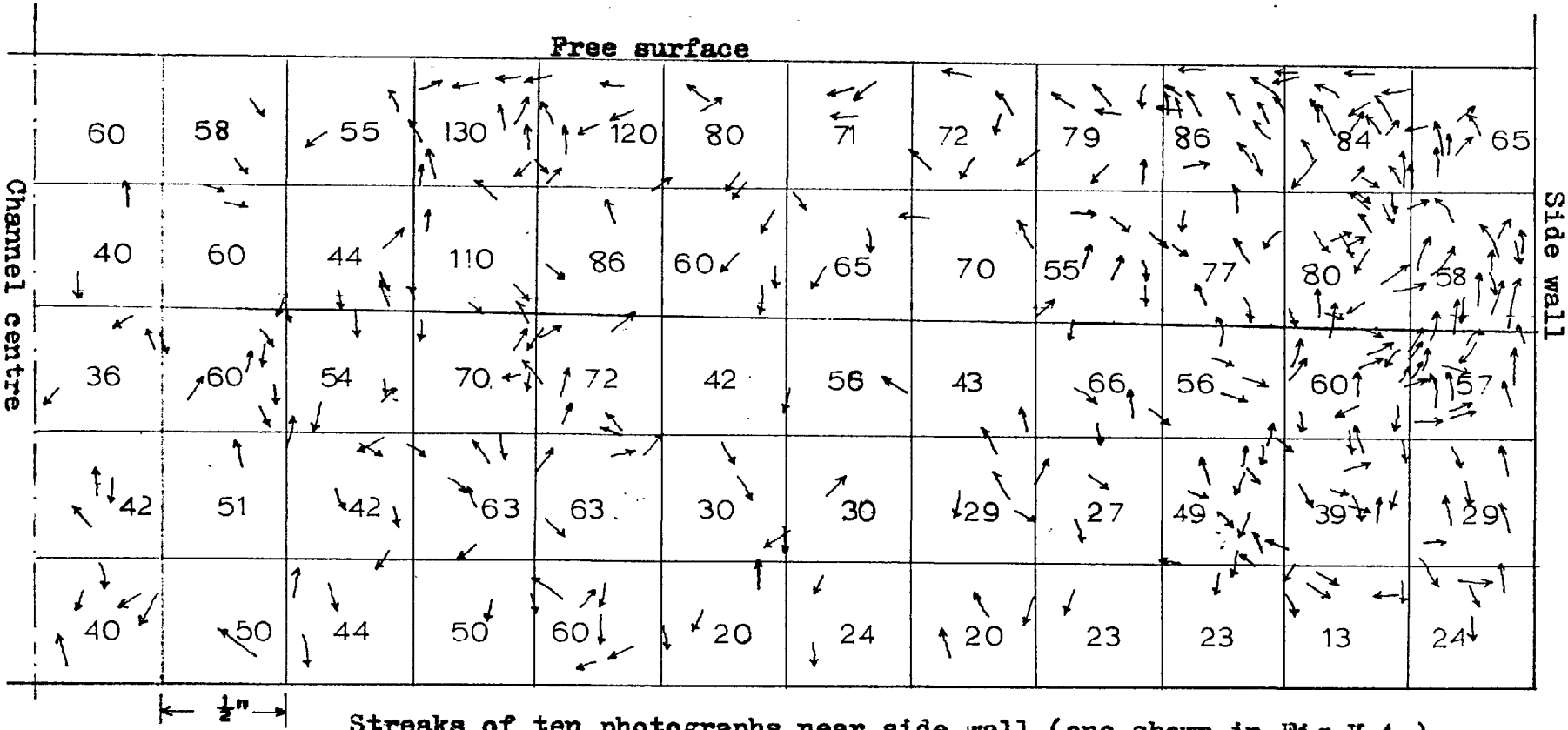
Streaks of eight photographs near side wall (One shown in Fig.V.2.) and of eight photographs in centre are traced.
Numericals give number of streaks including stationary stars in each selected square.

FIG.V.5. COMBINED RECORD OF PHOTOGRAPHS IN CROSS-SECTION (RIPPLED BED) .



Streaks of ten photographs near side wall (one shown in Fig.V.3.) and of ten photographs in centre are traced .
Numericals give number of streaks including stationary stars in each selected square .

FIG.V.6.COMBINED RECORD OF PHOTOGRAPHS IN CROSS-SECTION (FULLY GRAVELLED BED) .



Streaks of ten photographs near side wall (one shown in Fig.V.4.) and of ten photographs in centre are traced .
Numericals give number of streaks including stationary stars in each square selected .

FIG.V.7. COMBINED RECORD OF PHOTOGRAPHS IN CROSS-SECTION (SMOOTH BED) .

However, the geometry of the parallax is simple (Appendix I) and each displacement was appropriately corrected.

Another error was more difficult to eliminate. The sample of particles was insufficient and the effect of individual excursions due to turbulence often obscured the steady displacement . At each place, 25 streaks or more were averaged; yet the average of the turbulence may sometimes have deviated from zero as much as one-fifth of a streak.

The camera shutter remained open much longer than the time taken for a particle to pass through the gap and therefore many of the streaks, perhaps more than one-half of them, continued completely across the illuminated gap. The displacements due to such streaks therefore occurred in times inversely proportional to the local velocity $\bar{u}$ which varied appreciably from place to place. Thus different times should have been used when calculating the displacements depending on their position. Also the number of the stars needed correction as some of them appeared stationary, because they were caught by the shutter of the camera either as they were going out while the shutter of the camera was opening or coming in when the shutter was closing. This correction also depended on the local velocity. However the two corrections tended to cancel each other, and for convenience of calculation, the time for all streaks was assumed equal. Had time permitted, the errors due to these known inequalities of time could no doubt have been eliminated, though the pattern of the streamlines

would not have been modified very much.

Such errors, when present, tend to disclose themselves by deviations from the requirements of continuity. In the ideal case when the shutter of the camera is open for only a brief time compared with the time particles take to cross the gap, then all displacements in different parts of the photograph represent velocities all to the same scale. Thus the vertical and horizontal components of such displacements represent $\bar{v}$ and $\bar{w}$ to a scale depending on the exposure time. If correct, these components should therefore satisfy the continuity requirement:

$$\int_o^{B/2} \bar{v}\, dz = o \qquad \int_o^{d} \bar{w} dy = o$$

and should do so because the same stream line bounds top and bottom, $y = d$, $y = o$, as bounds side and centre, $z = \frac{B}{2}$, $z = o$. In applying this test the interpretation was replaced by the simple finite summations:

$$\sum_1^{12} \bar{V}n = o, \quad \sum_1^{5} \bar{W}n = 0$$

thus making use of the fact that all the heights and widths of the squares were equal. In short, the observed vertical displacements in each row of squares should sum to zero, and the horizontal displacements in each column should also sum to zero. Thus with 5 rows and 12 columns, a total of 17 tests were possible. Perhaps about one third of these summed satisfactorily to zero or nearly so. Errors when found were distributed.

The resultant displacements for the three sets, Figs (V.5,6,7), appropriately corrected for the optical parallax and continuity requirements, are given in Figs. (V.8.a,b,c).

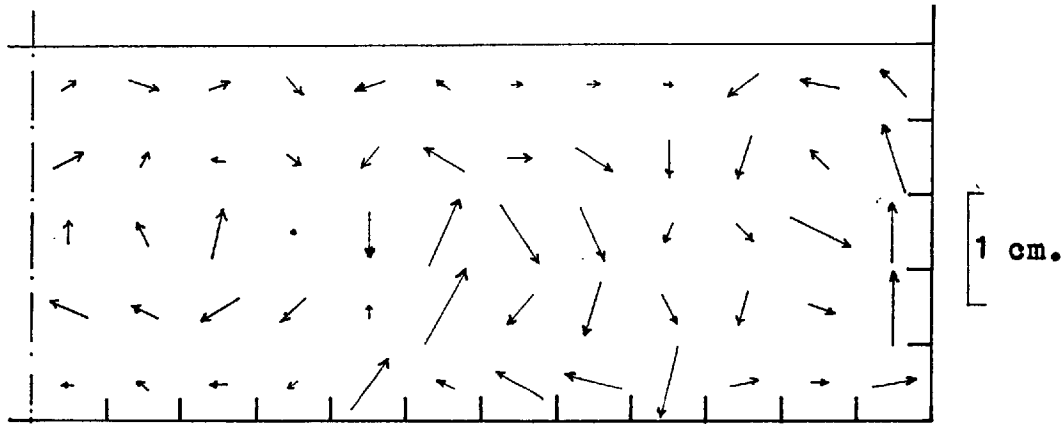
When integrated in the usual way, the two components of each displacement or velocity gives rise to two values of stream function Ψ, according to whether $\bar{w}$ or $\bar{v}$ is used, thus:

$$\Psi a = \Psi o + \int_o^z \bar{v} dz \; ; \; \Psi b = \Psi o + \int_o^y \bar{w} dy.$$

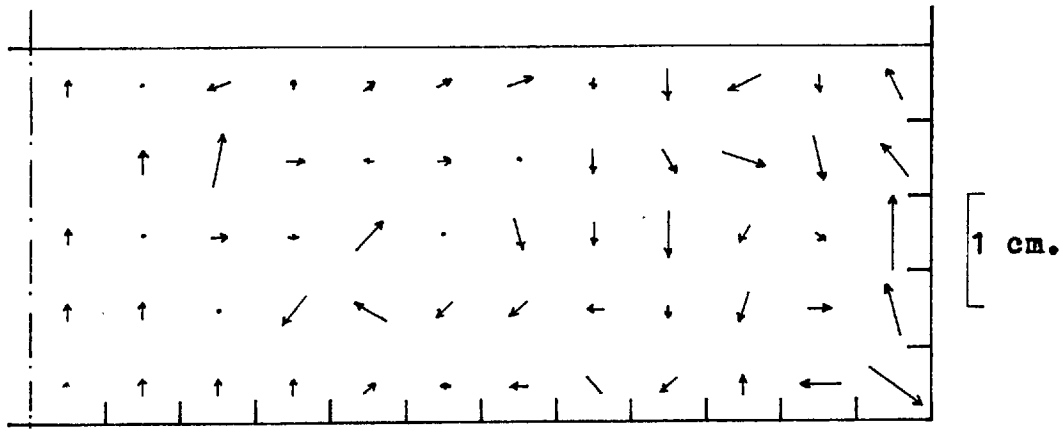
Taking a convenient value of Ψo, equal to 20, the values for Ψa and Ψb, corresponding to each displacement are given in Figs. (V.9.a,b,c) for the three sets. The resulting stream lines are consistent with all Ψ values, within $\pm$ 1, except these marked with crosses over.

Regarding the patterns of these secondary flows, perhaps the chief difference to be seen between the three cases is that for the rippled bed the secondary motion is seen to be divided into four distinct cells (Fig.V.9.a) whereas for fully gravelled and smooth beds (Fig.V.9.b & c) a clear pattern is found only near the side wall where the motion is seen to be towards the corner. The upward motion along the side walls, from bed towards the free surface, is common to all the three cases.

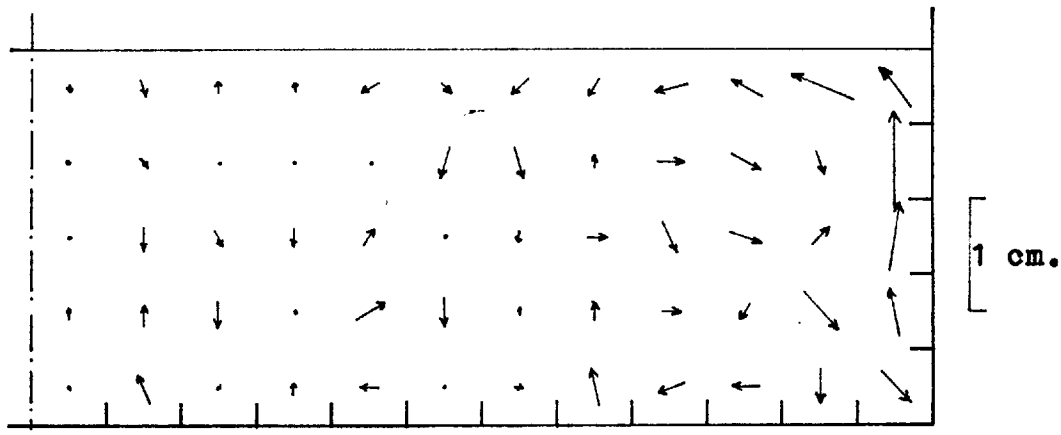
With plane beds (rough or smooth) the patterns seem to satisfy Prandtl's hypothesis. Two cells are obtained but the one near the



(a) Resultant displacements on rippled bed scaled for 10 particles in each square .

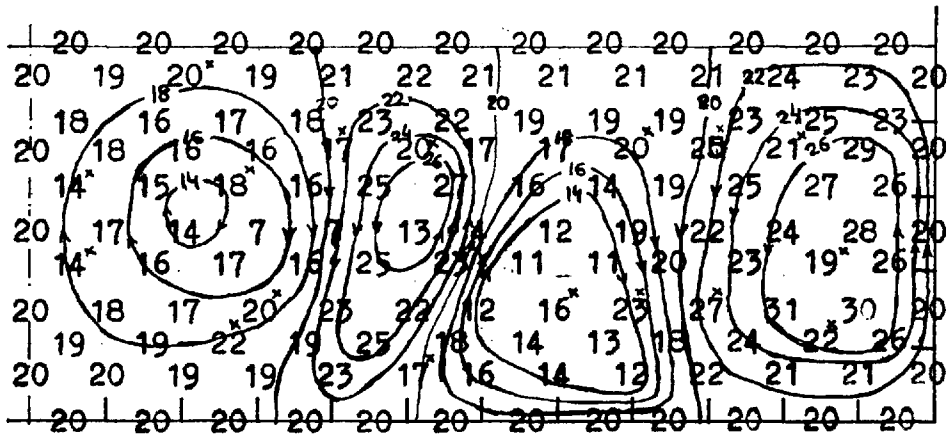


(b) Resultant displacements on fully gravelled bed scaled for 20 particles in each square .

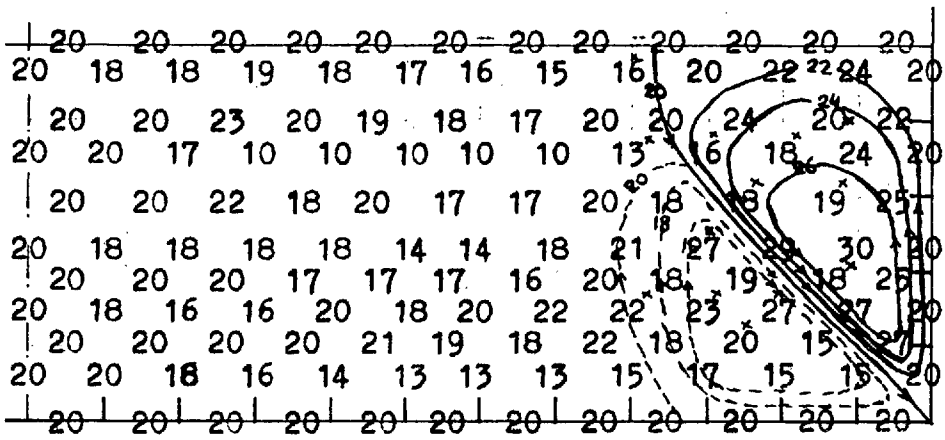


(c) Resultant displacements on smooth bed scaled for 20 particles .

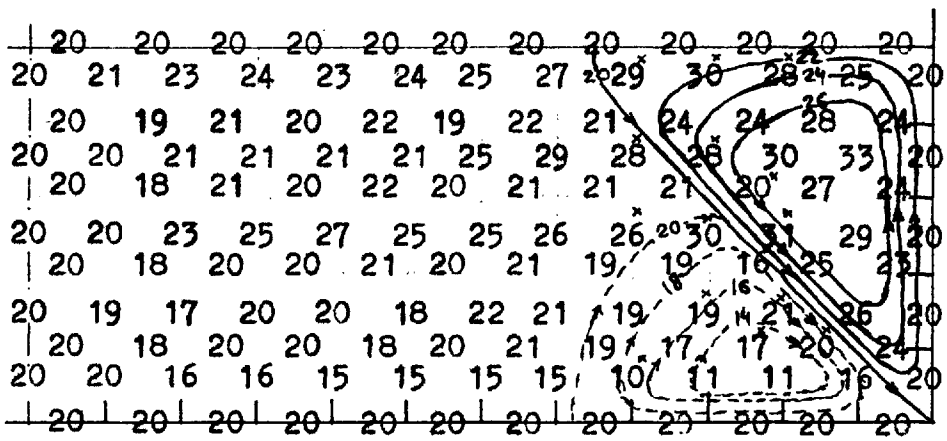
FIG.V.8. RESULTANT DISPLACEMENTS IN CROSS-SECTION .



(a) Rippled bed .



(b) Fully gravelled bed .



(c) Smooth bed .

FIG.V.9. STREAM FUNCTION VALUES AND RESULTING STREAMLINES .
(Values with crosses above are omitted)

side wall seems more definite than the other and hence the second one is shown by dotted line.

For the rippled bed the most striking feature is that the stagnation point, previously in the corner, has now moved well away into the bed and the flow is now, outwards towards the side wall. Perhaps the ripples dominate the flow patterns. The patterns obtained here confirm those suggested by Casey (Fig.V.1) in explanation of the ridges and the hollows which developed on a mobile bed, but in the present case there are fewer cells.

CHAPTER VI

FRICTION COEFFICIENT IN OPEN CHANNELS

VI. 1. INTRODUCTION

The formulae in use today mainly stem from the work of Antoine de Chezy, a French engineer, who, in 1775, derived his classic formula relating the speed of flow in open channels to their size and slope. He reasoned that the resistance to flow would vary with the wetted perimeter and with the square of the velocity; and that the force balancing this resistance would vary with the area of the cross-section and with the slope of the channel bed. Chezy's formula is expressed as:

$$V = C\sqrt{RS} \qquad \ldots.(1)$$

where V is the velocity defined as discharge divided by the cross sectional area, R is the hydraulic radius being the cross-sectional area divided by the wetted perimeter, S is the slope and C is known as Chezy's coefficient. This C at that time was regarded as a constant for each particular channel. The dimensions of the two sides of Eq: (1) do not balance unless C includes length and time; and this difficulty was not resolved until early in the last century, when Weisbach developed an almost identical formula, intended originally for flow through pipes, and usually written in the form

$$h = \frac{4 f L}{D} \frac{V^2}{2g} \quad \text{or} \quad S = \frac{f V^2}{2 g R} \qquad \ldots(2)$$

in which f is known as the friction coefficient whose magnitude depends on the roughness of the walls, and D is the diameter in the case of a pipe. When Eq: (2) is written as

$$V = \sqrt{\frac{2\ g\ R\ S}{f}} \qquad \ldots(2a)$$

it becomes identical with the Chezy's formula. C is then inversely proportional to f related by the identity

$$C = \sqrt{\frac{2g}{f}} \quad \text{or} \quad \frac{C}{\sqrt{g}} = \sqrt{\frac{2}{f}} \qquad \ldots(3)$$

However, since 1930 the work of Prandtl and of Nikuradse, has led to a simpler form in which Eq: (1) could be expressed as

$$V = \phi\ Vx \qquad \ldots(4)$$

where $Vx = \sqrt{g\ R\ S}$, and is a coefficient replacing C or f. Thus the ratio $\frac{V}{Vx}$ i.e., ϕ, embraces the whole mechanism of the dissipation of energy in a moving fluid. That the coefficient C was not a constant was demonstrated by many earlier investigators also.

For instance, Darcy and Bazin (Bazin 1865) working on channels of various shapes and with various wall surfaces, demonstrated very clearly that these coefficients (C and f) were not constant but varied with surface roughness and other variables. Subsequently, other investigators developed numerous empirical formulae seeking to predict Chezy's coefficient C for various

kinds of pipes and channels. Most of them had introduced different coefficients for each particular kind of surface. Such formulae are summarised in the Progress Report of Task Force (1963) on "Friction Factors in Open Channels".

Two outstanding contributions to the subject were due to Osborne Reynolds; in 1883 he showed that $\frac{DV}{\nu}$ was the criterion determining whether a motion would be laminar or turbulent; and later, in 1894, while attempting a numerical prediction of the critical value of $\frac{DV}{\nu}$, he showed that the mean intensity of the forces due to turbulence was no more than the mean value of $\rho u'v'$ where u' and v' are the fluctuations of the instantaneous velocity components. These two contributions provided the essential basis for the later evolution of the logarithmic velocity formula developed in Göttingen around 1930 and now widely used.

Perhaps the full implication of Reynolds' earlier work remained obscure until Stanton, in 1911, successfully correlated the distribution of velocity ~~with~~ $\frac{DV}{\nu}$ across the diameter of a number of pipes of different sizes with $\frac{DV}{\nu}$. $\frac{V}{V_x}$ or any of its equivalents ($\frac{C}{\sqrt{g}}$, $\sqrt{\frac{2}{f}}$) is expressible as a function of $\frac{DV}{\nu}$. Such an inevitable sequel was indeed achieved by Blasius (1913) in Germany followed independently by Stanton and Pannel (1914) in England. Blasius, using the results of earlier investigators,

showed that all experiments on flow through smooth pipes conformed to the formula

$$f = 0.3164 \,/\, \left(\frac{DV}{\nu}\right)^{\frac{1}{4}}$$

or

$$\left(\frac{Vx}{V}\right)^2 = 0.0395 \,/\, \left(\frac{DV}{\nu}\right)^{\frac{1}{4}} , \qquad \ldots(5)$$

which is valid in the range $3000 < \frac{DV}{\nu} < 80{,}000$. Stanton and Pannel had already started experimenting with the flow of oil, water and air through several pipes of different diameters. The mass of information thus obtained plotted with $\left(\frac{Vx}{V}\right)^2$ against $\frac{DV}{\nu}$ gave a single curve in the range $5000 < \frac{DV}{\nu} < 200{,}000$. For nearly twenty years the curve remained the standard source of information on flow through smooth pipes.

In the early twenties, the problem of hydraulic roughness was investigated by Hopf (1923). He showed that the resistance is affected not only by the size of the roughness irregularities but also by their form. He distinguished between the two extreme cases of granular wall roughness and wall waviness. In the former, the friction coefficient, while nearly independent of Reynolds number, is mainly dependent on the relative roughness; and, in the latter, it depends on Reynolds number yielding, however, higher values than for the smooth pipe case. This was confirmed by Fromm (1923) by his experiments on flow between parallel plates of different surface roughnesses.

Hopf's attempts to solve the resistance problem for wall waviness have so far proved unsuccessful although the granular case was resolved successfully by Nikuradse, in 1933, on the basis of a far reaching assumption suggested by Prandtl for turbulent shear stress $\rho\overline{u'v'}$. Having proved that the relation between the turbulent shear stress and the velocity was impossible to predict, Prandtl considered the following very crude model in which the turbulence was represented by an eddy created by difference of velocity. He considered that u' and v' would simply depend on the average size of an eddy, l, and on the difference of the mean velocities existing at the near and distant extents of l. The resultant formula for the time-mean stress

$$\tau = \rho l^2 \left(\frac{\partial u}{\partial y}\right)^2_{\pm} \qquad \ldots(6)$$

is well known. Here the subscript $\pm$ is a reminder that the positive and negative values of u' and v' do not necessarily occurr at the same instant so that $u'v'$ while apparently in the nature of a square of a velocity, may yet be of either sign. In the above, Prandtl proposed l as an empirical coefficient representing not only the effective physical size of the eddies, but also including such unknowns as the phase relation between u' and v' and any other imperfections of the model. For the known velocity distribution, he suggested $l = 0.4y$, y being the distance from the wall: this has proved to be a sufficiently close estimate for predicting the relation between velocity and

resistance. An extension of Reynolds' original approach to the problem of fluid friction via the mechanism of turbulence can be seen in the publications of L. Prandtl, G.I. Taylor and Von Karman, (1915 to 1932).

The various mixing length theories (Goldstein 1938, Schlichting 1955) have led to the formulation of the laws of velocity distribution in pipes and between parallel plates. The well known Prandtl's velocity distribution law for two dimensional turbulent flow can be written as:

$$\frac{\bar{u}}{V_{x_o}} = \frac{1}{\alpha} \log_e \frac{y}{y_1} \qquad \ldots(7)$$

where $\bar{u}$ is the local mean velocity at a distance y from the wall, V_{x_o} equals $\sqrt{\frac{\tau_o}{\rho}}$ (called the shear velocity), α, a characteristic of turbulence, is a universal constant, and y, is the distance from the effective hydraulic wall defined such that $\bar{u} = 0$ when $y = y_1$. The above equation is also written in the general form as

$$\frac{\bar{u}_{max} - \bar{u}}{V_{x_o}} = \frac{1}{\alpha} \log_e \frac{r}{y} \qquad \ldots(7a)$$

where $\bar{u} = \bar{u}_{max}$ at $y = r$, the radius of pipe. For flow between parallel plates, r is replaced by d, the half distance between the plates.

The "Shift" y_1 in Eq: (7) depends on the nature of the wall surface and is proportional to $\frac{\nu}{V_{x_o}}$ for smooth surface and to K, the size of roughness, for rough surfaces. Very comprehensive and systematic experiments by Nikuradse (1932) on smooth pipes yielded the values of constants in Eq: (7): $\alpha = 0.40$ and $y_1 = \frac{0.111\nu}{V_{x_o}}$. With these values Eq: (7) for smooth pipes can be written as

$$\frac{\bar{u}}{V_{x_o}} = 5.75 \log_{10} \frac{yV_{xo}}{\nu} + 5.5 \qquad \ldots(8)$$

Nikuradse's (1933) experiments on rough pipes with uniform sand roughness gave the value of $y_1 = \frac{k_s}{30}$, where k_s is the size of the sand particles. This value for y_1 is valid only for Nikuradse's uniform sand roughness but different values are obtained for other kinds of roughness. However, the above expression, $y_1 = \frac{k_s}{30}$, is generally used as the standard for the roughness and is termed the equivalent sand roughness. The formula for velocity distribution for fully rough turbulent flow then is

$$\frac{\bar{u}}{V_{x_o}} = 5.75 \log_{10} \frac{y}{k_s} + 8.5 \qquad \ldots(9)$$

From the above it is obvious that the wall will act as a smooth surface when $\frac{k_s}{30} < \frac{0.111\nu}{V_{x_o}}$ or $\frac{k_s V_{x_o}}{\nu} < 3.3$.

From Eqs: (8) and (9), the corresponding equations for average velocity of flow in pipes can be derived and written as

$$\frac{V}{V_{x_o}} = 5.75 \log_{10} \frac{YV_{xo}}{\nu} + 1.75 \quad \ldots \text{(Smooth)} \ldots (10)$$

and

$$\frac{V}{V_{x_o}} = 5.75 \log_{10} \frac{Y}{K_s} + 4.75 \left(\begin{matrix}\text{Completely} \\ \text{Rough}\end{matrix}\right) \ldots (11)$$

Equation (10) is in good agreement with experiments over a wide range of Reynolds number and certainly in the range $4 \times 10^3 \leq \frac{DV}{\nu} \leq 3.2 \times 10^6$. Nikuradse's experimental results from rough pipes also agreed with Eq: (10) provided that the pressure gradient was such that $\frac{K_s V_{xo}}{\nu} < 3.3$. Fully rough conditions occured only when $\frac{K_s V_{xo}}{\nu} > 60$. Between these values i.e. $3.3 < \frac{K_s V_{xo}}{\nu} < 60$, the flow was in a transitional state influenced both by the viscosity and the roughness.

Colebrook and White (1937), working on pipes of non-uniform surface roughnesses, made a particular study of the transitional zone. These experiments and also the results available on commercial pipes of cast iron, wrought iron and galvanised steel showed a gradual transition from smooth law at low velocities to rough law at high velocities in contrast to the abrupt transition in Nikuradse's experiments on artificial uniform sand roughness. They later (1939) established a transition law, by combining the smooth and rough pipe laws, which agrees

well with the experimental results obtained on commercial pipes. In the present notations, it can be written as

$$\frac{V}{Vxo} = -5.65^{*} \log_{10} \left(\frac{Ks}{3.7D} + \frac{1}{1.125 \frac{DVxo}{\nu}} \right) \quad \ldots(12)$$

In the case of non-circular pipes the question arises as to what values should be used for the constants in the above formulae, and also as to what parameter would best replace the diameter D. For laminar flows, it has been shown that the use of the hydraulic radius, with a corresponding change of the coefficient in the resistance formula, is adequate for all shapes of cross section. For turbulent flow, Schiller (1923) investigated this question for pipes of triangular, square, rectangular (aspect ratio 3.5:1) and star shaped cross sections. Using hydraulic diameter (equal to four times the hydraulic radius) as the linear dimension in the expression for Reynolds number, results obtained for the square and rectangular pipes agreed well with the Blasius formula; however, the Reynolds number in both the cases did not exceed 60,000. The results for the triangular section were in rather satisfactory agreement with the Blasius formula but those for the star shaped section fell around another line intersecting the Blasius' line. Experiments by Fromm (1923) and by Davies and White (1928) on smooth rectangular

---

* Value 5.65, with slight variations in other numerical values, better fits certain discharge measurements than 5.75.

pipes of large width-depth ratios indicated greater friction than circular pipes if the hydraulic diameter was used as the linear dimension in the expression for the Reynolds number. Fromm suggested a law similar to that of Blasius, but with different values of the constants. Huebscher (1947) made tests on three galvanised sheet metal pipes of circular, square and rectangular (aspect ratio 8:1) cross sections with the same hydraulic diameter. For equal values of the Reynolds number the friction coefficient was found to be the same for circular and square pipes but higher values were obtained for the rectangular pipe. Harnett, Koh and McComas (1962) conducted experiments on a square pipe and two rectangular pipes (aspect ratios 5:1 and 10:1) upto an approximate value of Reynolds number 2×10^5. Their results for square pipe agree very well with the Blasius law but for the rectangular sections the friction is slightly higher.

Although the use of hydraulic radius or diameter for the linear dimension in defining the Reynolds number has been questioned by some [Gunn and Darling (1963)], it can be seen from the results quoted above that the frictional characteristics of square pipes and rectangular pipes of small aspect ratio agree well with those of circular pipes. But the friction coefficient

of rectangular pipes of large aspect ratio is found to be higher. This can also be predicted by integration of Eq: (8) for an infinitely wide rectangular pipe which would result in

$$\frac{V}{V_{x_o}} = 5.75 \log_{10} \frac{dV_{x_o}}{\nu} + 3.0 \qquad \ldots(13)$$

with d equal to half the distance between the two long plates. For this case, d can be replaced by the hydraulic radius R and Eq: (14) can be written as

$$\frac{V}{V_{x_o}} = 5.75 \log_{10} \frac{RV_{x_o}}{\nu} + 3.0 \text{ (parellel plates-smooth)} \qquad \ldots(13a)$$

Similarly Eq: (10) for smooth circular pipes can be written in terms of the hydraulic radius as

$$\frac{V}{V_{x_o}} = 5.75 \log_{10} \frac{RV_{x_o}}{\nu} + 3.48 \text{ (Circular pipe smooth)} \qquad \ldots(10a)$$

In view of the previously quoted experiments, Eq: (10a) can be accepted to be valid for square pipes also.

Thus the results on smooth rectangular pipes of various aspect ratios may perhaps be predicted to lie within the two extremes defined by the lines given by Eq: (13a), for large aspect ratios and by Eq: (10a), for square pipes.

The corresponding formulae in terms of hydraulic radius for flow between parallel plates and circular pipes using Nikuradse's sand roughness can be written as

$$\frac{V}{V_{xo}} = 5.75 \log_{10} \frac{R}{K_s} + 6.0 \quad \text{(parallel plates rough)} \quad \ldots(14)$$

$$\frac{V}{V_{xo}} = 5.75 \log_{10} \frac{R}{K_s} + 6.48 \quad \text{(Circular pipes rough)} \quad \ldots(11a)$$

From these it is apparent that the laws governing the resistance to flow in circular pipes and rectangular pipes differ only slightly when hydraulic radius is used as a length parameter. Hence in Colebrook - White formula, the diameter of pipe D is generally replaced by 4R and is used as universal law for all types of conduits and flow conditions. Ackers (1958) has used this formula to prepare several useful charts for design purposes.

The application of the above laws to flow in open channels is discussed in the following section.

VI. 2. APPLICATION OF LOGARITHMIC LAWS TO FLOW IN OPEN CHANNELS

Despite many centuries of intense study of open channel flows, some of the main features of turbulent flow in them still remain obscure. Indeed progress in the study of pipe flows has been so much more informative that, today, some of the problems of open channels seem best resolved by partial analogy with pipes.

For example the universal velocity distribution formula Eq: (7), originally derived for a small region close to the wall has, in the case of pipes, been found valid even as far from the

wall as the centre of the pipe. In an open channel, however, while the structure of turbulence near the wall, is found to be the same as in the case of a pipe, there is one fundamental difference between the two flows. Since in the case of a pipe at its central plane there is transfer of fluid mass across the plane and the component v' may be great where as in an open channel a fluid mass can not come out of the free surface and v' must be zero there. It has been shown in Chapter IV that the effect of the free surface on suppressing the turbulent velocity component at right angles to the bed is noticeable as far as about 0.40 times the depth from the free surface. Although this great difference is inherent between the two cases yet the criterion that the time-mean product of the turbulent velocity components, $-\overline{u'v'}$, which represents the ratio of the shear stress to the mass density of the fluid is zero at the centre of a pipe, as also at the free surface of an open channel, allows comparison between the two cases. Since the variation of shear stress, from the wall to the free surface in an open channel and from the wall to the centre of a pipe is linear, the respective velocity distributions are usually described by similar laws. Experimental results also support this view.

Nevertheless, Ellison (1959) has attempted to derive another law for the velocity profile in a broad open channel.

Since the motion near the free surface differs from that in the constant stress region near the wall, he introduced a new empirical mixing constant for the free surface analogous to the universal turbulent constant for flow near a rigid wall. He obtained a number of different velocity profiles by assuming various values for his mixing constant and compared the results with logarithmic velocity profile but none of them agreed with it. One of his basic assumptions was that "the components of turbulence which contribute to the eddy viscosity near the surface are determined entirely by local quantities without any direct dependence on the total depth of flow". But this assumption seems contradicted by the present measurements, Chapter IV. Moreover his arguments led him to the results that the fluctuation in horizontal velocity must be zero at the free surface meaning thereby that it moves as a rigid sheet. Since this is not so, he modified his theory in such a way that it applied only to the eddy viscosity, and thus eliminated the horizontal component of turbulence.

The usual logarithmic velocity distribution has been found to agree well with the actual velocities measured on the centre line of the channel, where the motion may be expected to be two dimensional. The value of τ_o, the shear stress at the bed, in such a case is exactly equal to ϱgds and the value of V_{xo} is then precisely known. Measurements by Vanoni (1941) on the centre

line of a rectangular flume confirmed Eq: (7a). Subsequent measurments by Vanoni (1946) in a flume with clear water flows and also with sediment suspensions showed that the value of the universal constant, α, which is about 0.40 for clear water, decreases in suspended sediment flows. The presence of suspended sediment perhaps damps the turbulence, and changes its structure. Tracy and Lester (1961), investigating the friction coefficient in a rectangular steel flume with inner surfaces covered with synthetic enamel, also measured the velocity profiles. Their average results, for two dimensional conditions at the centre of the flume, when plotted as $\frac{\bar{u}}{V_{x_o}}$ against log $\frac{yV_{x_o}}{\nu}$ lay somewhat below the line given by Eq: (8), while individual values of V_{x_o} appeared to define straight lines parallel to it. The flume had some waviness which may account for such parallel lines.

Attempts have been made to derive the laws for friction coefficient in open channels based on logarithmic velocity distribution. Formulae (13) and (14), derived for flow between parallel plates, can be assumed to be applicable for flow in a rectangular channel of large width-depth ratio. But in narrow channels the problem is complicated by the non-uniform distribution of shear stress along the perimeter and also by the presence of secondary currents. No doubt these two factors are present also in pipes of non-circular cross section. But in open channels the existence of free surface seems to emphasize the effect and leads

to a curious depression of the location of maximum velocity. How this affects the friction is not really known but it is generally believed that the friction coefficient increases because of the secondary currents.

Keulegan (1938) attempted to apply logarithmic velocity distribution to predict the friction of open channels by introducing several coefficients to include the channel shape, free surface and non-uniform distribution of shear stress. His general formulae when simplified are the same as Eqs: (13) and (14) for flow in a rectangular channel of infinite width with the terms $\beta - \bar{\epsilon} \frac{V}{V_x}$ added on the righthand side. For smooth channel his equation may be written as:

$$\frac{V}{V_x} = 5.75 \log \frac{RV_x}{\nu} + 3.0 + \beta - \bar{\epsilon} \frac{V}{V_x} \qquad \ldots(15)$$

The coefficient β takes the channel shape into consideration. It is constant for 90° - triangular channel having value of 0.48. For rectangular section, it takes on the value given by $5.75 \log_{10} (\frac{d}{R}) - 2.5 \frac{d}{B}$, being zero for a channel of infinite width and 0.48 when depth equals half the channel width. Hence the equations for 90° - triangular channels and rectangular channels of width-depth ratio 2:1 become the same as for circular pipes but for the term $\bar{\epsilon} \frac{V}{V_x}$. The coefficient $\bar{\epsilon}$, the magnitude of which will depend on the cross sectional shape, was introduced to take the effect of free surface and non-uniform distribution of shear stress along the perimeter. Kaulegan, assuming these

corrective terms to be small, merged them into the wall constants, and computed the values of K_s for different wall materials in Bazin's data. Bazin's wooden channels appeared to behave as a smooth wavy surface at low values of the Reynold's number and tended to be rough at high values of the Reynold's number.

Further investigation on these lines was made by Powell (1946). He experimented on rectangular channel, with a smooth surface and also with artificial roughness of square steel strips extending up the side walls. Powell varied the slopes of the channels and included a particularly wide range of width-depth ratios from 10:1 to 2:1. The treatment of his data was based on Keulegan's theoretical considerations although he neglected the effect of the free surface and non-uniform distribution of shear stress along the perimeter. In effect, for smooth channel his method was to plot $\frac{V}{V_x} - \beta$ against the logarithm of the Reynold's number, based on hydraulic radius and shear velocity. For the larger depths and so for the larger Reynold's number, the measured velocities were generally higher than those given by formula (15). The slope of the line on the logarithmic plot therefore tended to become steeper. Similar results were obtained also for the rough channel. Powell attributed this to a smaller value of the

universal constant, about 0.33, in open channels. In the discussion, Keulegan reasoned that non-uniform distribution of shear stress could not be neglected if $\frac{d}{B}$ was large. With certain assumptions regarding the distribution of shear stress, the coefficient $\overline{\epsilon}$ (as in Eq: 15) was found to be negative and hence was expected to give higher velocities.

Kirschmer (1949) presented his own experimental results on a smooth concrete rectangular channel along with those of Raju on "theoretically smooth" rectangular channel and of Varwick on (i) smooth trapezoidal channel painted with tar, and (ii) trapezoidal and triangular channels roughened with three different Nikuradse's sands on the walls. On comparing the aforementioned results with those on pipes for the same values of $\frac{4RV}{\nu}$, or $\frac{R}{K}$, the friction in all the channels was found to be higher than in the pipes. Besides, for the same degree of roughness, the friction coefficient was found to depend on the shape of the cross section and to increase in the order: (1) trapezoidal, (2) triangular, (3) rectangular. This increase was attributed to the secondary currents which were said to be more pronounced in rectangular than in triangular or trapezoidal sections. An objection to this conclusion is that the same kind of effect would have been obtained, had the surfaces been not perfectly smooth. Also the rough channels are likely to have been rougher than

those of Nikuradse's rough pipes even though the same sand was used.

It can be said that the discharge of open channels of known roughness can be predicted reliably from pipe theory within ± 3 percent. Yet two of the main puzzles of open channels, the effect of the corners where sides and bed join and where sides and free surface join, and also the effect of the existance of the free surface itself, remain unresolved. Certainly square pipes results demonstrate that four corners do not increase the resistance coefficient, and we may guess the corners are compensated by the secondary currents they generate, though the details of such compensation or over compensation remain to be explored.

Regarding the free surface, here the puzzle is very difficult because it includes the strange behaviour of water just below the surface where often a considerable patch of unresisted water remains apparently unaccelerated while subject to the action of gravity and slope. At the surface itself, turbulence exists, yet it is of a pseudo two-dimensional kind in which its third component, but not its derivatives, is zero. Thus at this stress-free place the turbulence cannot be as three dimensional in an open channel as at the centre of a pipe.

Therefore experiments with 90° - triangular channels seem particularly interesting. Their cross section is half a square, like that of a 2:1 rectangular channel, though their free surface is 40 percent greater. Unfortunately the two shapes, the triangle and the rectangle are also very different, and the several actions seem almost impossible to disentangle.

However the discharge of smooth triangular channels has been measured by some investigators and their results are given in table below:

TABLE VI.1.

Investigator	Experimental details	Remarks
Owen (1953)	Flume length: 55ft. Slopes: 1 in 2000, 1 in 1000 & 1 in 500. Depths: Upto 10 inches.	The results lie on a line parallel to circular pipe law giving low values of friction coefficient.
Moeller-Hartman (1957)	Flume length: 150 ft. Slopes: 1 in 1000, 1 in 600 & 1 in 340.	Friction coefficient is slightly less for slope in 1000 and slightly higher for the other two slopes than circular pipe law.
Powell and Posey (1959)	Flume length: 400 ft. Slopes: 1 in 2000 to 1 in 500. Depths: Upto 2.5 ft.	Friction coefficient is about 7% less than that given by circular pipe law.

As described earlier, such low values of friction coefficient have also been obtained by Powell with a smooth rectangular channel of large depth-width ratios. Thus regarding a 90^{o} - triangular channel as equivalent to half of the square pipe, the only possible explanation for the reduced resistance is the presence of the free surface and non-uniform distribution of shear stress along the perimeter.

VI. 3. EXPERIMENTAL RESULTS ON SMOOTH RECTANGULAR CHANNEL

VI. 3.1. VELOCITY MEASUREMENTS

The mean values of the velocities, at various points along the depth in the central plane of the channel, were obtained from the local instantaneous values from the photographs as described earlier in (IV.3). These values and the various other quantities calculated for depths of flow 1.55 cm. and 2.58 cm. with slope of the channel 1 in 2000, and 2.555 c.m. and 5.095 c.m. with slope 1 in 1000 are given in Appendix (IIB), Tables (1-4).

The results plotted as $\frac{\bar{u}}{V_{xo}}$ against log $\frac{yV_{xo}}{\nu}$ are shown in Fig. (VI.1), where $\bar{u}$ represents the mean velocity at a distance y from the channel bed. The universal velocity distribution law for smooth surfaces given by Eq: (8) is also represented by line (2) on this diagram. Outside the wall region, for $\frac{yV_{xo}}{\nu} \gtrsim 40$, the measured velocities for all depths

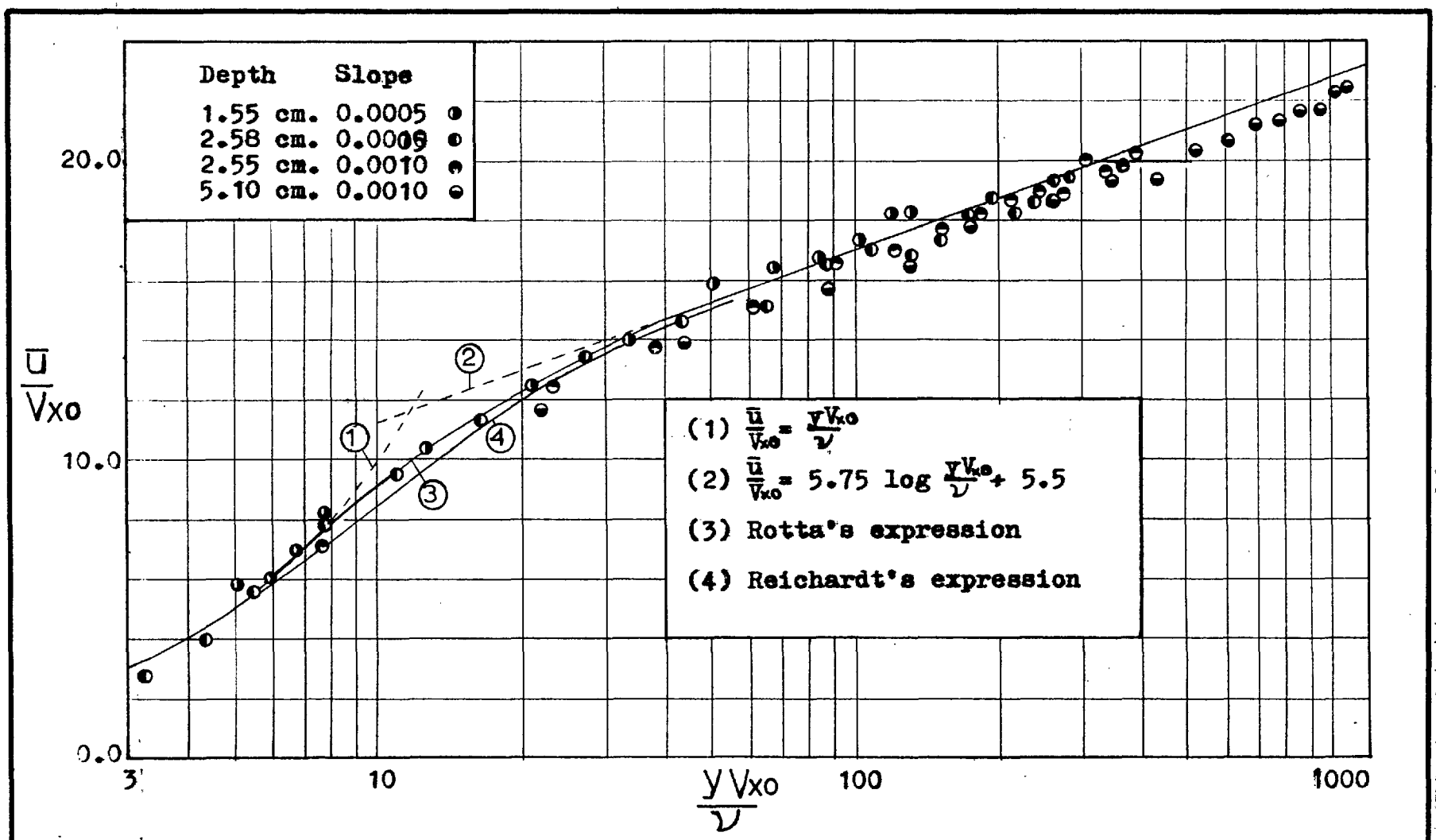


FIG.VI.1. VELOCITY DISTRIBUTION IN CENTRAL PLANE OF CHANNEL WITH SMOOTH BED.

agree well with Eq: (8), except when the depth of flow was 5.095 c.m. with slope 1 in 1000, for which the velocities were some what lower giving points slightly below the line. There is no obvious reason for this except that the joints in the glass plates on the bed or same surface waves or both might have slowed the motion.

Originally the universal velocity distribution (Eq: 7) was derived by assuming viscous stresses to be zero in the basic expression for the shear stress, $\tau = \mu \frac{d\bar{u}}{dy} - \rho \overline{u' v'}$. Hence Eq: (8) tends to be inacurate in the region very close to the wall where it over-estimates $\rho \overline{u' v'}$ and under-estimates $\mu \frac{d\bar{u}}{dy}$. This region of inapplicability extends from the wall upto the region where $\frac{y V_{xo}}{\nu}$ approximately equals 40, and Eq: (8) is valid only when $\frac{\bar{u}}{V_{xo}} > 14.0$. The region near the wall is difficult to explore because y is so very small (for example when V_{xo} = 1 cm/sec and ν = 0.01 c.m.^{2}/sec. then the whole region lies within 4.0 m.m. of the wall) that it is not possible to measure the velocity there with ordinary instruments such as a pitot tube. However, using hot-wire anemometers, Reichardt (1940) with a closed channel and Laufer (1951, 1954) with a closed channel and with a pipe, have successfully mapped out this region. They confirm that extremely close to the wall a region exists where viscous stresses appear completely to dominate the flow so that the

velocities follow the relation $\frac{\bar{u}}{V_{x_o}} = \frac{yV_{x_o}}{\nu}$, as shown by curve (1) on the diagram. With some uncertainty of measurements very close to the wall, the agreement with this relation is fairly good upto $\frac{\bar{u}}{V_{x_o}} \approx 6$ or $\frac{yV_{x_o}}{\nu} \approx 6$. Hinze (1959), on the basis of results obtained by Reichardt and Laufer, reports this value of $\frac{yV_{x_o}}{\nu}$ to be between 5.0 and 6.7.

In the transition zone, where turbulent stresses begin noticeably to retard the flow, various simplifying assumptions have been proposed to predict the velocity distribution. Hinze (1959) discusses fully the details of the various assumptions and compares the results with the experimental values actually obtained by Reichardt and Laufer. The curves for the several relations deviate some what from each other, and because of scatter of the experimental data in this transition region it is difficult to decide which relation satisfies the experimental results best. Reichardt's data generally lie below Laufer's data, perhaps due to the fact that Laufer (1954) applied additive correction upto + 10% to the measured values near the wall reasoning that the hot wire indicates low values near the wall. Hence if Laufer's data with his correction are accepted as more accurate than Reichardt's data, his results confirm the curves of Rotta (1950) and Reichardt (1951). These two relations are used to compare the results obtained in the present experiments

and are described below.

Rotta, considering that in the transition zone the total shear stress is determined both by viscous and turbulence effects, and putting y_o for the distance from the wall upto which the viscous stresses completely dominate the flow, assumed $\ell = \alpha\ (y - y_o)$ in Prandtl's expression $\tau = (\varrho \ell^2 \left/\frac{d\bar{u}}{dy}\right/ + \nu)\frac{d\bar{u}}{dy}$, and derived the relation,

$$\frac{\bar{u}}{V_{xo}} = \frac{1}{2\alpha \frac{\ell V_{xo}}{\nu}}\left[1 - \sqrt{\left(\frac{2\ell V_{xo}}{\nu}\right)^2 + 1}\right] + \frac{1}{\alpha}\log_e\left[\frac{2\ell V_{xo}}{\nu} + \sqrt{\left(\frac{2\ell V_{xo}}{\nu}\right)^2 + 1}\right] + \frac{y_o V_{xo}}{\nu}$$

For $y = y_o$, this formula reduces to $\frac{\bar{u}}{V_{xo}} = \frac{yV_{xo}}{\nu}$ and for large values it becomes:

$$\frac{\bar{u}}{V_{xo}} = \frac{1}{\alpha}\log_e \frac{yV_{xo}}{\nu} + \frac{1}{\alpha}(\log_e 4\alpha - 1) + \frac{y_o V_x}{\nu},$$

which is the same as formula (8), with $\frac{1}{\alpha}(\log_e 4\alpha - 1) + \frac{y_o V_{xo}}{\nu}$ equal to 5.5. This gives $\frac{y_o V_{xo}}{\nu} = 6.83$ for $\alpha = 0.40$. With these values the relation is shown by curve (3) on the diagram in Fig. (VI.1).

Reichardt, in the expression, $= (\mu + \epsilon)\frac{d\bar{u}}{dy}$ assumed $\frac{\epsilon}{\mu} = \left(\frac{yV_{xo}}{\nu} - \frac{y_o V_{xo}}{\nu}\right)\tanh \frac{\frac{yV_{xo}}{\nu}}{\frac{y_o' V_{xo}}{\nu}}$ and gave the relation

$$\frac{\bar{u}}{V_{xo}} = \frac{1}{\alpha}\log_e\left(1 + \alpha\frac{yV_{xo}}{\nu}\right) + C\left[1 - e^{-\left(\frac{yV_{xo}}{\nu} \Big/ \frac{y_o' V_{xo}}{\nu}\right)\frac{\frac{yV_{xo}}{\nu}}{\frac{y_o' V_{xo}}{\nu}}} e^{-b\frac{yV_{xo}}{\nu}}\right]$$

In the above, with α = 0.40, he assumed $\frac{y_o' V_{xo}}{2} \approx 11$ for $\frac{\epsilon}{\lambda\zeta} = 1$; and for the constants c and b he obtained values 7.80 and 0.33 respectively from the corresponding boundary conditions. With these values for the constants the relationship is shown by curve (4) on the diagram in Fig. (VI.1).

The deviation between the two curves (3) and (4), has a maximum value of about 10% of $\frac{\bar{u}}{V_{xo}}$ at $\frac{YV_{xo}}{\nu} \approx 10$. The present experimental results in this region seem more to support curve (3), obtained from Rotta's expression, than curve (4), from Reichardt's expression.

VI.3.2. FRICTION COEFFICIENT

The results for uniform flow, for each of four slopes 0.0005, 0.0010, 0.0015 and 0.0020, are given in Appendix (IIA), Tables (3-6). The maximum depth of flow was about 4.50 inches for the smaller slopes. But for the steeper slopes the maximum depth was less, since a discharge of about 0.65 cu.sec. was the maximum that could be run in the flume without undue disturbances or waves from upstream or generated locally.

In Fig. (VI.2), the results are plotted as $\frac{V}{V_x}$ against $\log \frac{RV_x}{\nu}$. Two lines, denoted by (1) and (2), are drawn on the diagram representing Eq: (13a) for flow between parallel plates and Eq: (10a) for smooth circular pipes(valid also for square pipes) respectively. With smaller depths, the points generally

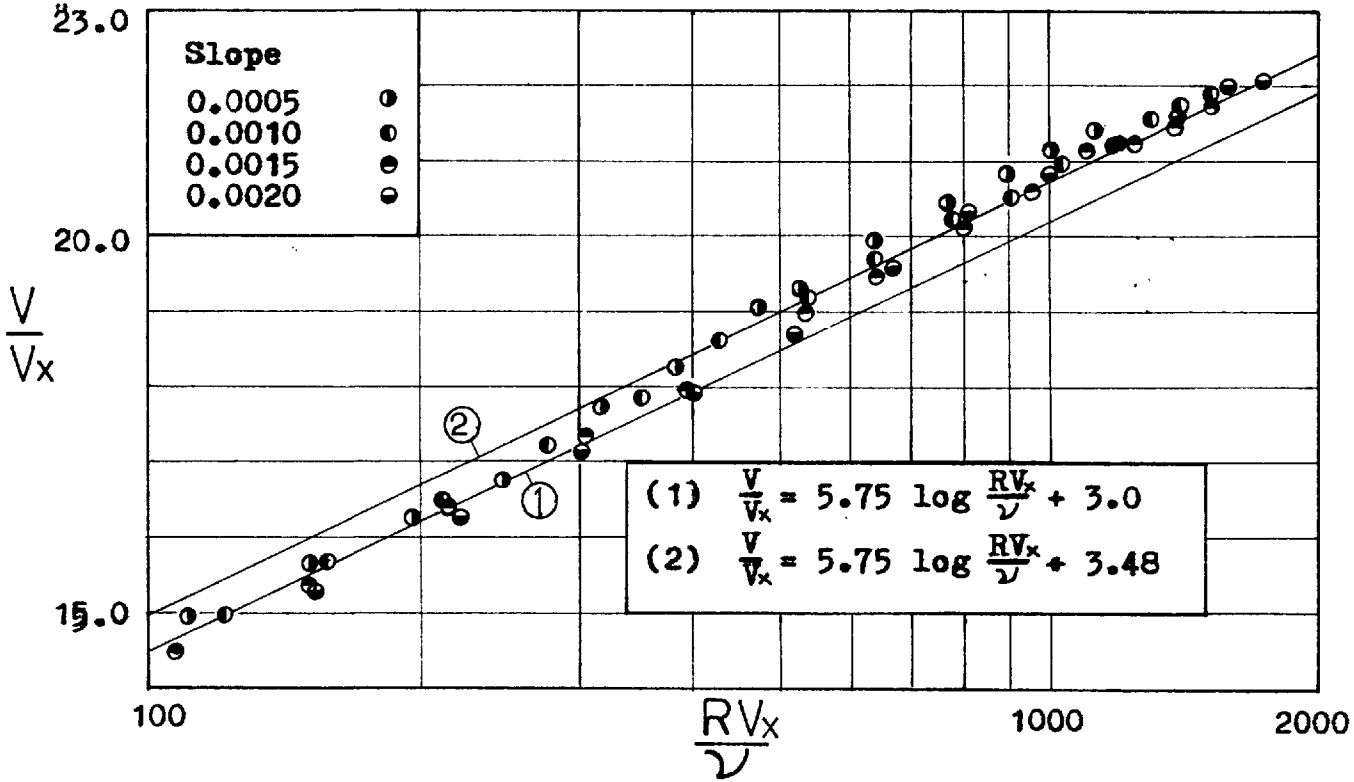


FIG.VI.2. FRICTION COEFFICIENT RESULTS WITH SMOOTH BED AND SIDE WALLS.

lie on the line (1), satisfying Eq: (13a). But as the depth and hence the depth-width ratio increases the points approach the line (2), given by Eq: (10a).

Although it would seem that the line (2) could be the upper limit for the points for a depth-width ratio of 1:2, which corresponds to half of a square pipe, some of the points lie above this line even as the maximum depth-width ratio attained was no more than 1:3. These results contradict the general concept that for large depth-width ratios the friction coefficient increases and the average velocity decreases becauses of the secondary currents. Such small friction coefficients or such high average velocities have also been reported by other investigators [Powell (1946) on rectangular channel and Owen (1953) and Powell and Posey (1959) on 90° - triangular channels]. Kennedy and Fulton (1961), working on smooth rectangular channels, also obtained higher velocities than given by the smooth pipe law and suggested that the secondary currents probably reducethe effect of boundary roughness and so slightly increase the channel capacity. It is difficult to ascertain how far this statement is correct; however the effect of the secondary currents and of the non-uniform shear stress distribution along the perimeter, together with the effect of the free surface inhibiting the vertical component of turbulence, may be the causes of reduced friction and higher average velocity.

Since the Reynolds number, $\frac{RV_x}{\nu}$, changes with depth of flow, the effects of the depth-width ratio and of the Reynolds number can only be separated by comparing results for different slopes, by selecting particular runs all having the same depth, or all having the same Reynolds number. As a matter of convenience such values are obtained by interpolation with good accuracy from the plot of depth - discharge curves. In the present experiments this effect was investigated and $\frac{V}{V_x}$ versus $\frac{RV_x}{\nu}$ is plotted in Fig. (VI.3), with different symbols for each of the six different depth-width ratios shown. For each depth the values of $\frac{RV_x}{\nu}$ varied over a two-fold range, as the slopes were varied from 0.0005 to .0020. Then the results for each depth can be represented by a straight line as shown in Fig. (VI.3). From values of $\frac{V}{V_x}$ read from these straight lines Fig. (VI.3a) has been prepared showing how $\frac{V}{V_x}$ varies when the shape-factor, $^{d}/_{B}$, is changed while $\frac{RV_x}{\nu}$ remains constant. Clearly this diagram, Fig.(VI.3a), shows a general tendency for the deeper and narrower channels to flow somewhat faster. The differences are small, no more than 2 or 3 percent variation in $\frac{V}{V_x}$ due to doubling the depth-width ratio, nevertheless this evidence is sufficient to confirm the previous interpretation of the points in Fig.(VI.2) where they are seen gradually drifting from line (1) to the line(2). Fig. (VI.3a) confirms that the drift of Fig. (VI.2)

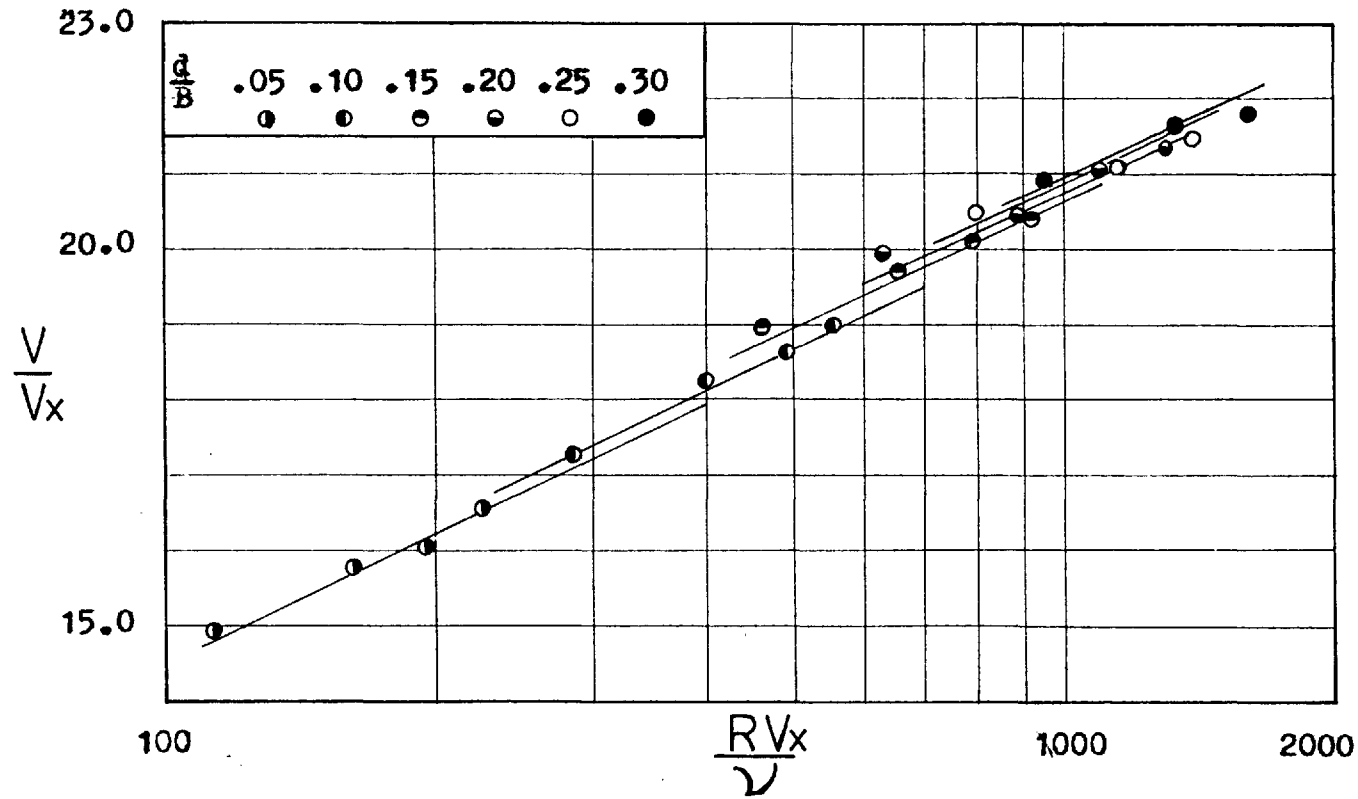


FIG.VI.3. INTERPOLATED RESULTS OF FRICTION COEFFICIENT FOR VARIOUS VALUES OF $\frac{RV_x}{\nu}$ AT CONSTANT $\frac{d}{B}$ RATIOS

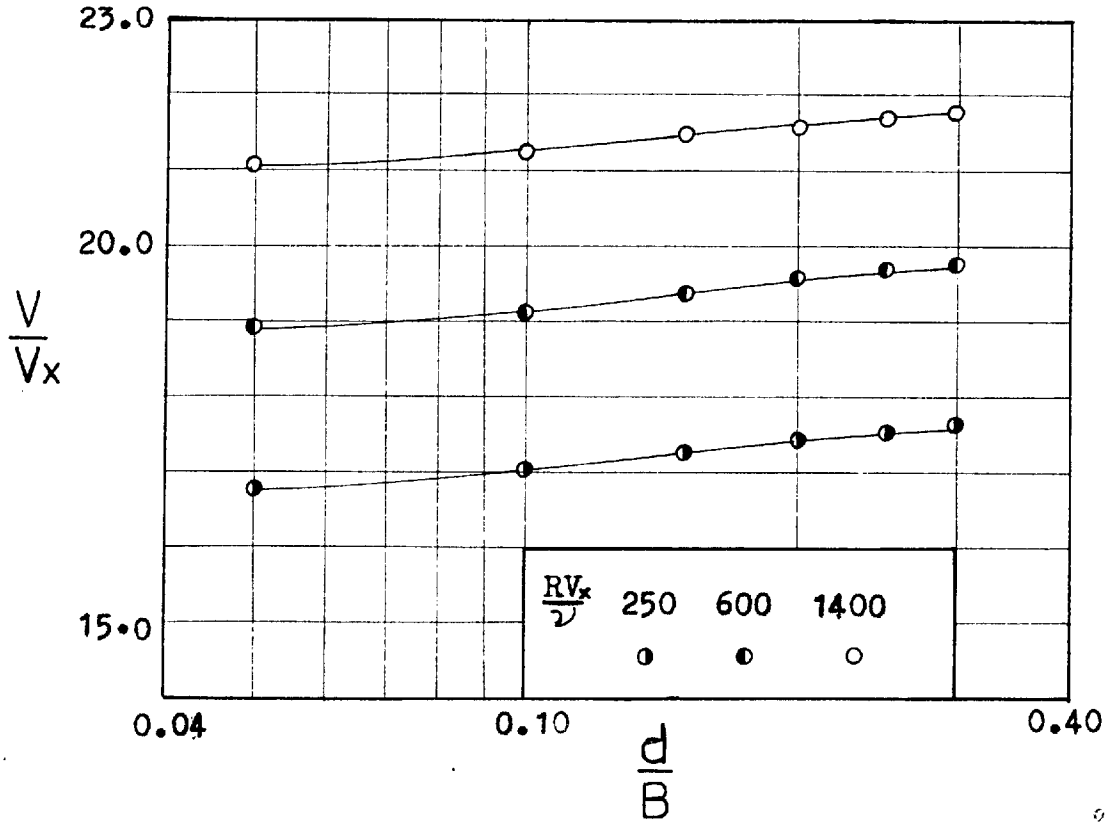


FIG.VI.3.a. INTERPOLATED RESULTS OF FRICTION CO-EFFICIENT FOR VARIOUS $\frac{d}{B}$ RATIOS AT CONSTANT VALUES OF $\frac{RV_x}{\nu}$.

is in fact wholly due to change in aspect ratio and therefore does not denote a change in the "universal constant".

VI.4. EXPERIMENTAL RESULTS ON RECTANGULAR CHANNEL WITH ROUGH BED AND SMOOTH SIDE WALLS

VI.4.1. DETERMINATION OF DATUM PLANE FOR MEASUREMENT OF DEPTH WHEN THE BED IS ROUGH

The datum plane is defined to represent the origin for vertical measurements and it lies somewhere between the crests and the troughs of the roughness and its precise position may depend on the shape and concentration of the particular roughness. Nikuradse (1933) determined the location of the wall of each of his rough pipes of uniform sand roughness by calculating the equivalent radius of a pipe, having the same volume as the volume of water contained in the rough pipe. Similarly, Schlichting (1936), working on closed rectangular channel with three fixed smooth walls and one interchangeable wall, fitted with various kinds and patterns of roughness elements of known dimensions, computed the volume of roughness elements and divided it by the area of the plate to find the zero level. Similar methods have also been used for an open channel by Reinus (1961) working with sand roughness and steel balls fixed on a smooth bottom.

This method of "equal volume" for determining the datum gives satisfactory results only when the size of the roughness is very small compared with the depths of flow.

In an open channel the datum plane may be said to be correctly chosen when the curves of velocity distribution and of discharge both extrapolate smoothly to the same zero point. It is also convenient that this should be on the same straight line as those points of the semi-logarithmic plot which are not far from the wall. Einstein and El-Samni (1949), from mean velocity variation over a bed on which were fixed hemi-spherical elements, found that the semi-logarithmic plot was a straight line when the theoretical bed was assumed to be at a distance $0.40r$ below a plane tangent to the top of the hemi-spheres of radius r.

Any difference in the position of the datum plane may appreciably change both constants in the semi-logarithmic plot, and the slope of the line may appear to differ from 5.75, and so may lead to wrong conclusions. Sayre and Albertson (1963), performing experiments on a rectangular flume with steel metal baffles fixed on the bed, measured the depths from the flume bed and reported a slope of 6.06 for the semi-logarithmic plot. Had the datum plane been taken slightly above the flume bed, a slope of 5.75 would have been the result.

In the present experiments on rough beds, one with stabilized sand rippled bed and the other two with gravel filled in, it was impracticable to use the "equal volume" method. Nonetheless recently Vanoni and Hwang (1967) have used a method based on "equal volume" by filling a known volume of dry sand in the hollows of the stabilized rippled bed and determined the mean elevation. This may not always give satisfactory results, particularly with small depths of flow, as seen from Einstein and El-Samni's experiments. Hence in the present work the position of the datum plane or theoretical bed level was found by trial, by plotting the mean velocity distributions with various positions of the origin, till a satisfactory straight line in the semi-logarithmic plot was obtained.

For the rippled bed the datum was found to be at $\frac{3}{8}$ of average ripple height below the mean crest level, the average ripple height being 0.32 inches or 8m.m. When the troughs of the rippled bed were filled with gravel upto crests, the mean crest level was found to be a satisfactory position of the datum plane. For the fully gravelled bed, the datum plane was taken at half median diameter of the gravel below the average top grain level, the median diameter being 3.6m.m. This gave a good straight line of the mean velocity distribution in semi-logarithmic plot. The top average grain

level was found by taking the readings with point gauge at various distances along the flume on top of a plate of known thickness and of a size, 10 inches x 10 inches, to cover perhaps 5000 grains. The maximum deviation from the average of such readings was about ± 0.015 inches. By subtracting the thickness of the plate from the average value, the mean top grain level was obtained.

VI.4.2. SURFACE ROUGHNESS MEASUREMENT

Nikuradse's experiments on rough pipes with uniform sand roughness gave y_1 in Eq: (7) equal to $\frac{Ks}{30}$ where Ks is the size of the sand particles. Later it has been demonstrated by Schlichting (1936) that, if K is taken as "projected height" or any other measure of the roughness elements, this value of y_1 is not a constant fraction of K, but varies with the shape of roughness and even for the same roughness shape it varies with different concentrations or spacing of the roughness elements. The general practice has been to define the surface roughness in terms of "Equivalent Sand Roughness". If, for a fully-rough two dimensional turbulent flow, $\frac{\bar{u}}{V_{xo}}$ is plotted against log y, a value of y_1 is obtained for that particular surface using Eq: (7) and then the value of K_s, the equivalent sand roughness, is obtained as 30 y_1. However, the value of K_s obtained from a particular velocity profile taken at a particular section will represent only some kind of average

of the roughness immediately upstream of the section. Since, by its very nature, roughness is irregular, it follows that velocity profiles taken at different places are likely to be somewhat different and to yield individual values of K_s varying from the channel as a whole. Also, false measurements may occur when instruments such as the pitot tube or the hot-wire are placed close against a roughness element. In the present work these particular difficulties were avoided by using a photographic technique in which the motion of particles was recorded in a field including a complete ripple length from which an ensemble mean of a number of local instantaneous values in a 4.m.m. deep strip was obtained to represent the local mean velocity at a particular height.

Another method of determining the mean value of the equivalent sand roughness for a particular surface is from the discharge and slope i.e. from the friction coefficient. When the flow is fully rough and the depths are very small compared to the width of the channel, the effect of smooth side walls can be neglected and Eq: (14) for flow between rough parallel plates can be adopted. For depths exceeding 0.1 B, the effect of side walls may be considerable and the results may deviate appreciably from Eq: (14).

To eliminate the effect of the side walls, the method known as "Einstein-Johnson Method" (Einstein 1942, Johnson 1942) is frequently used.

All of the three above methods were tried in the present experiments. The results and the resulting values of the equivalent sand roughness obtained for the various beds are discussed below.

VI.4.2.1. FROM VELOCITY MEASUREMENTS

Local values of the mean velocities at various points along the depth were obtained from photographs as described earlier. The velocities and the various quantities calculated for the three beds are given in Appendix (II.B), Tables (5 to 18).

To evaluate y_1 as later described the results are plotted as $\frac{\bar{u}}{Vxo}$ against log y for various depths and Reynolds numbers of flow, shown in Figs. (VI.4), (VI.5) and(VI.6) for rippled, gravel filled in troughs of ripples and fully gravelled beds respectively. The straight lines are drawn through the resulting points, to correspond with the selected datums giving a slope of 5.75. Although there is some scatter of the points because of the inevitable uncertainty of the mean of a turbulent velocity, there seems no systematic dependence on the Reynolds number. Hence all the flows can be taken to be in the

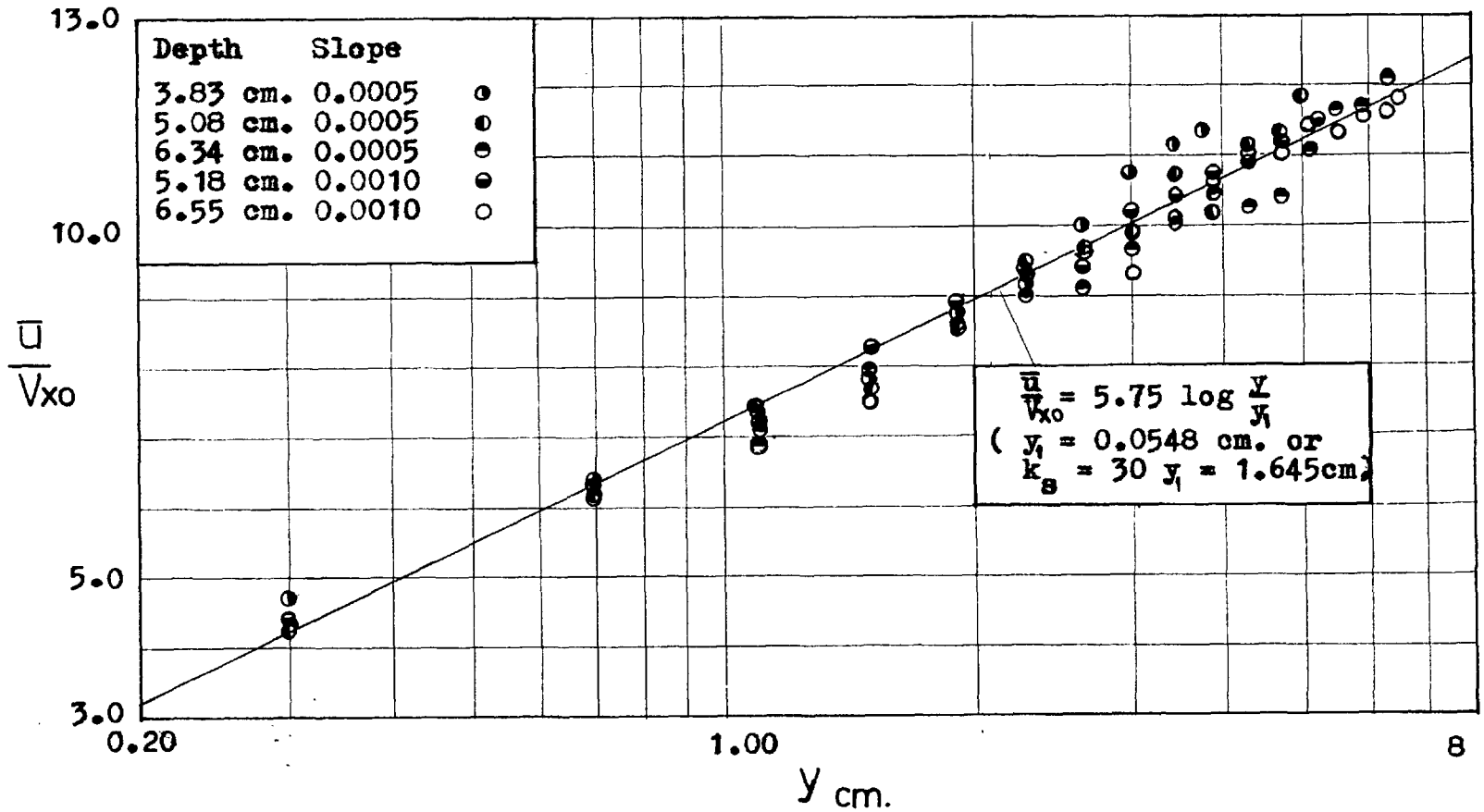


FIG.VI.4. VELOCITY DISTRIBUTION IN CENTRAL PLANE OF CHANNEL WITH RIPPLED BED .

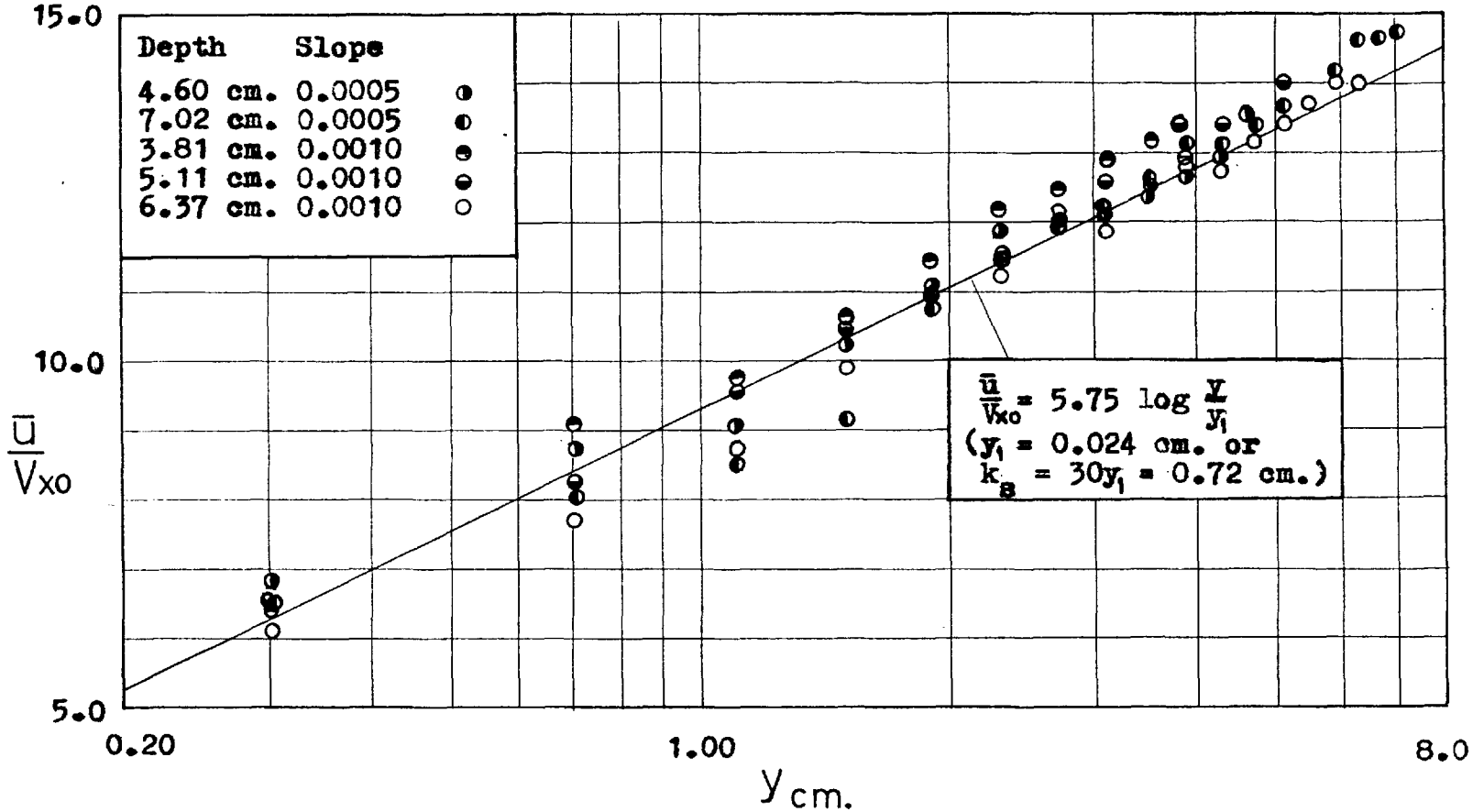


FIG.VI.5. VELOCITY DISTRIBUTION IN CENTRAL PLANE OF CHANNEL WITH GRAVEL IN TROUGHS OF RIPPLED BED .

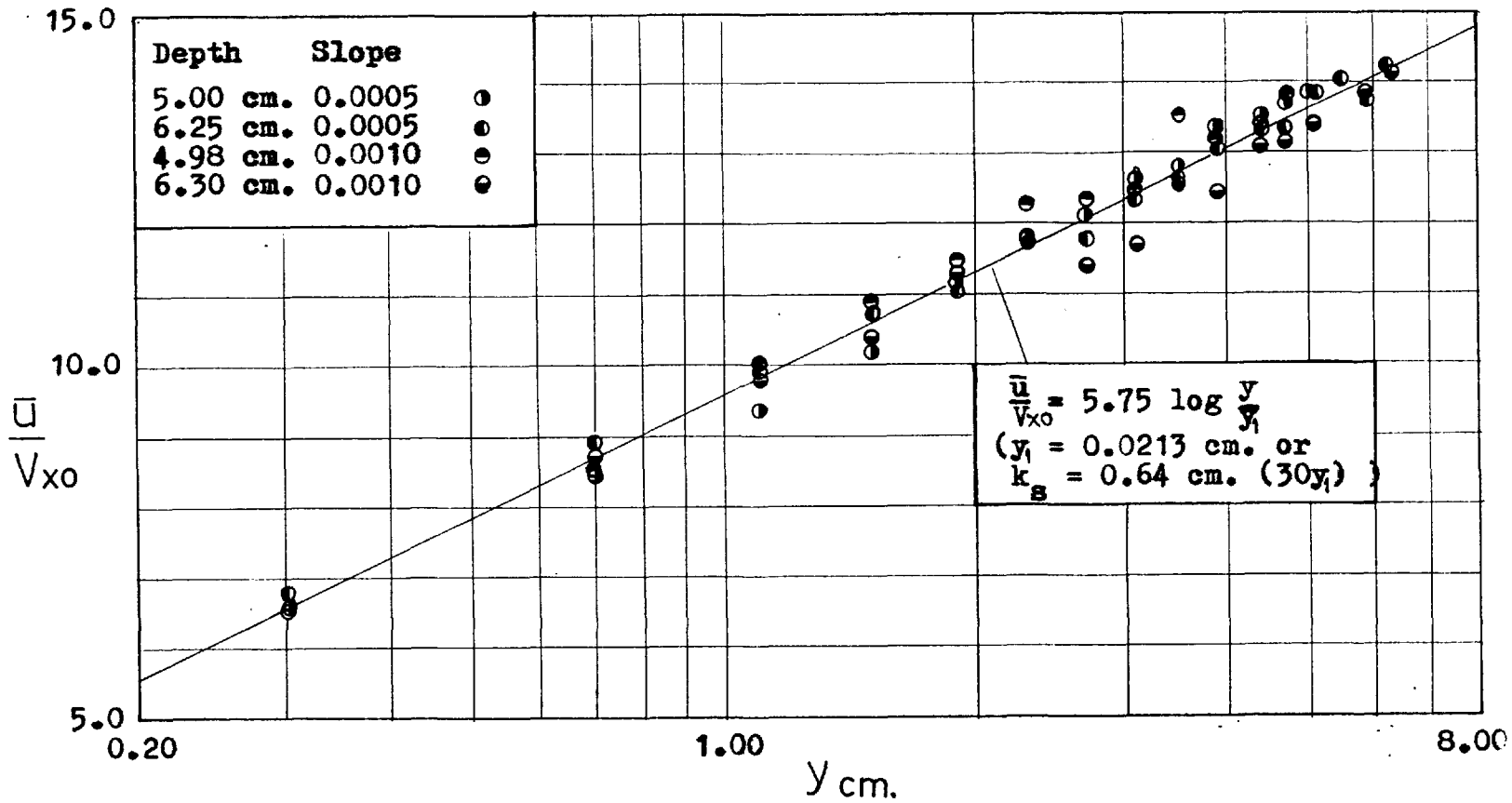


FIG.VI.6. VELOCITY DISTRIBUTION IN CENTRAL PLANE OF CHANNEL WITH FULLY GRAVELLED BED .

fully rough regime. Making use of the formula,

$$\frac{\bar{u}}{V_{xo}} = 5.75 \log_{10} \frac{y}{y_1},$$

the resulting values of y_1 and hence the equivalent sand roughness Ks (equal to 30 y_1) for each bed are as follows:

Table (VI.2.)

Bed	K_s c.m.
Stabilized sand rippled bed.	1.645
Rippled bed with gravel filled in troughs of the ripples.	0.72
Fully gravelled bed.	0.64

These give values for $\frac{K_s V_{xo}}{\nu}$ greater than 100, above which most walls usually act as if fully rough.

VI. 4.2.2. FROM FRICTION COEFFICIENT NEGLECTING SIDE WALL

The depths and discharges for various slopes of the channel were measured. The convenient least slope of the channel was 0.0005 and this was increased by equal steps of 0.0005 upto the maximum of 0.0030 for the rippled bed, 0.0015 for the gravel filled in troughs of the ripples and 0.0020 for the fully gravelled bed. These were the steepest slopes beyond which either it was difficult to determine the precise depth of flow due to surface waves generated by the rippled bed or the grains of the gravelled beds started moving. In all cases the velocities were much less than

$\sqrt{gd}$, the Froude number at most being 0.60. Flows at depths of about 4.50 inches and less were run for each slope on the rippled bed and of about 4.0 inches and less on gravelled beds. (Appendix II.A., Tables 7 to 19) The datum plane or the theoretical bed for measurements of the depths on each bed was taken to be the same as already determined from the velocity profiles [Figs. (VI.4) to (VI.6)].

When the friction coefficient is calculated for a channel with rough bed and smooth side walls, the mean value of the roughness appears to decrease with increase of depth of flow, so giving greater average velocities in a deep channel with smooth side walls than in one with rough side walls. This is very clearly seen in Figs. (VI.7), (VI.8) and (VI.9) where $\frac{V}{V_x}$ is plotted against log $\frac{d}{B}$, V_x is taken equal to $\sqrt{Rgs}$ and is thus the average for bed and sides. More over the diagrams show that for a particular depth of flow or value of $\frac{d}{B}$, there is no effect of slope or the Reynolds number on value of $\frac{V}{V_x}$, as the points for each bed lie on a single curve despite the several different slopes of the channel. There is some scatter of the points for the rippled bed because of some uncertainty in measuring the depths of ruffled water.

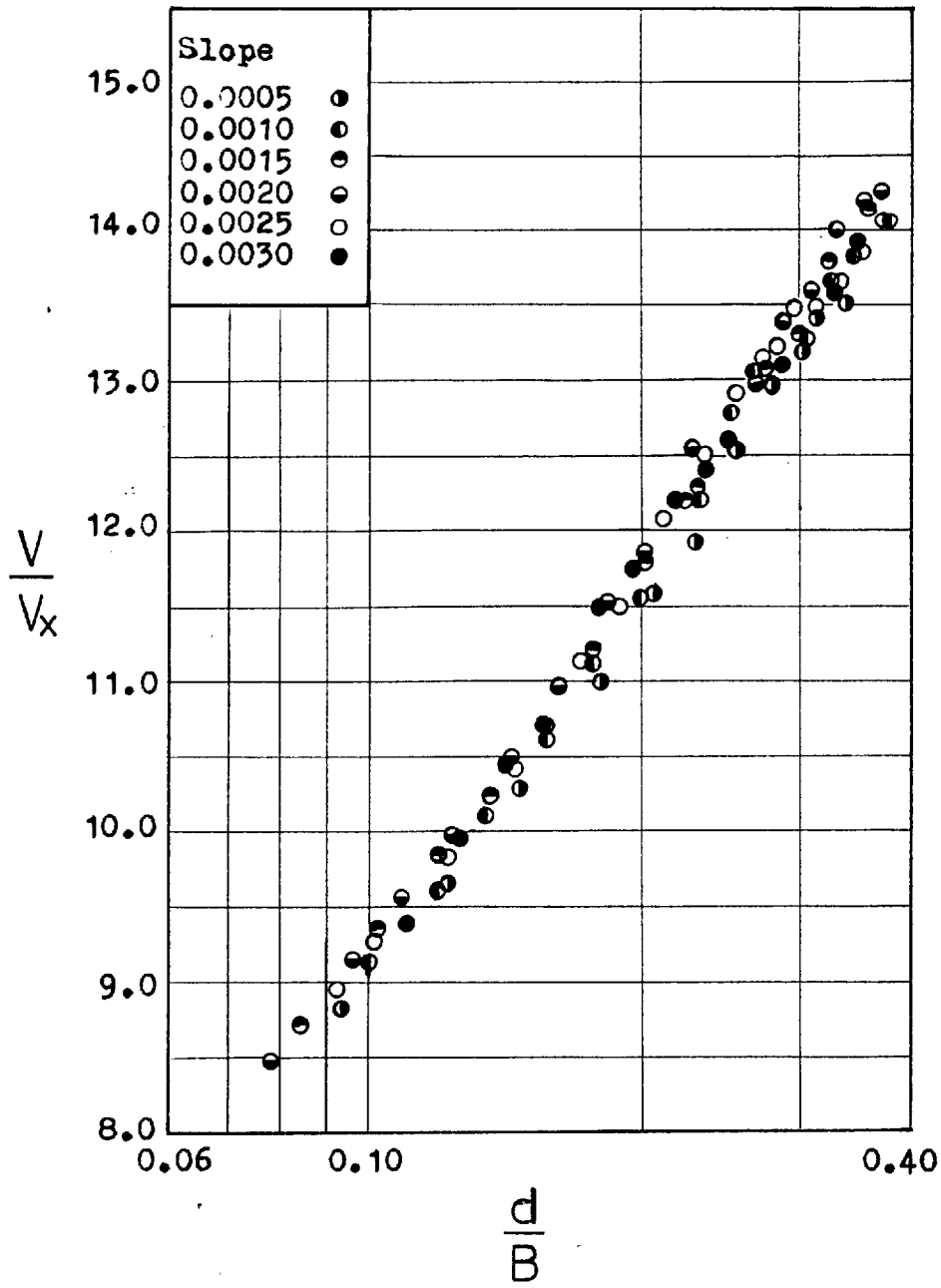


FIG.VI.7. FRICTION COEFFICIENT RESULTS FOR FULL PERIMETER OF CHANNEL WITH RIPPLED BED AND SMOOTH SIDE WALLS.

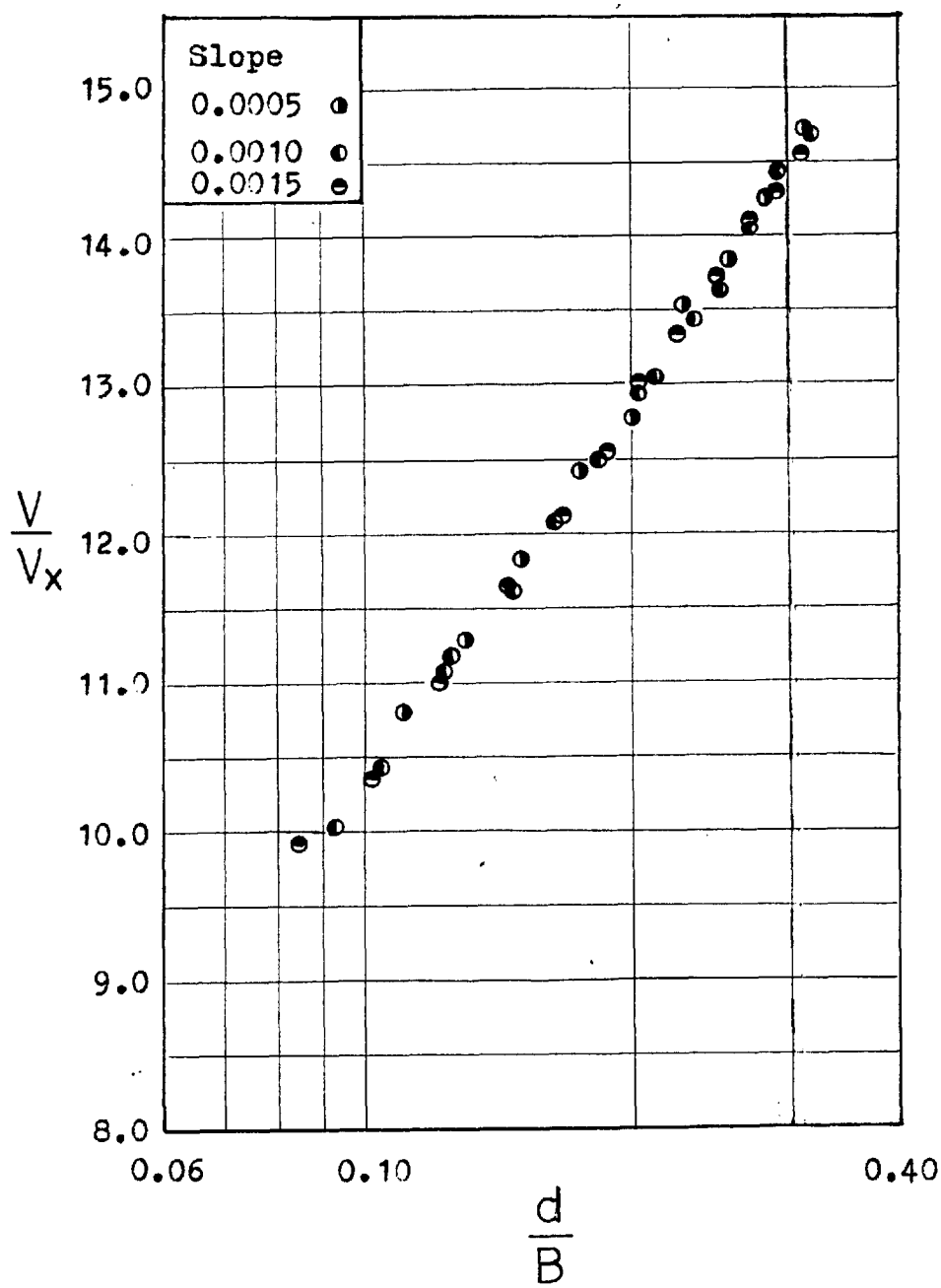


FIG.VI.8. FRICTION COEFFICIENT RESULTS FOR PERIMETER OF CHANNEL WITH GRAVEL FILLED IN TROUGHS OF RIPPLED BED AND SMOOTH SIDE WALLS .

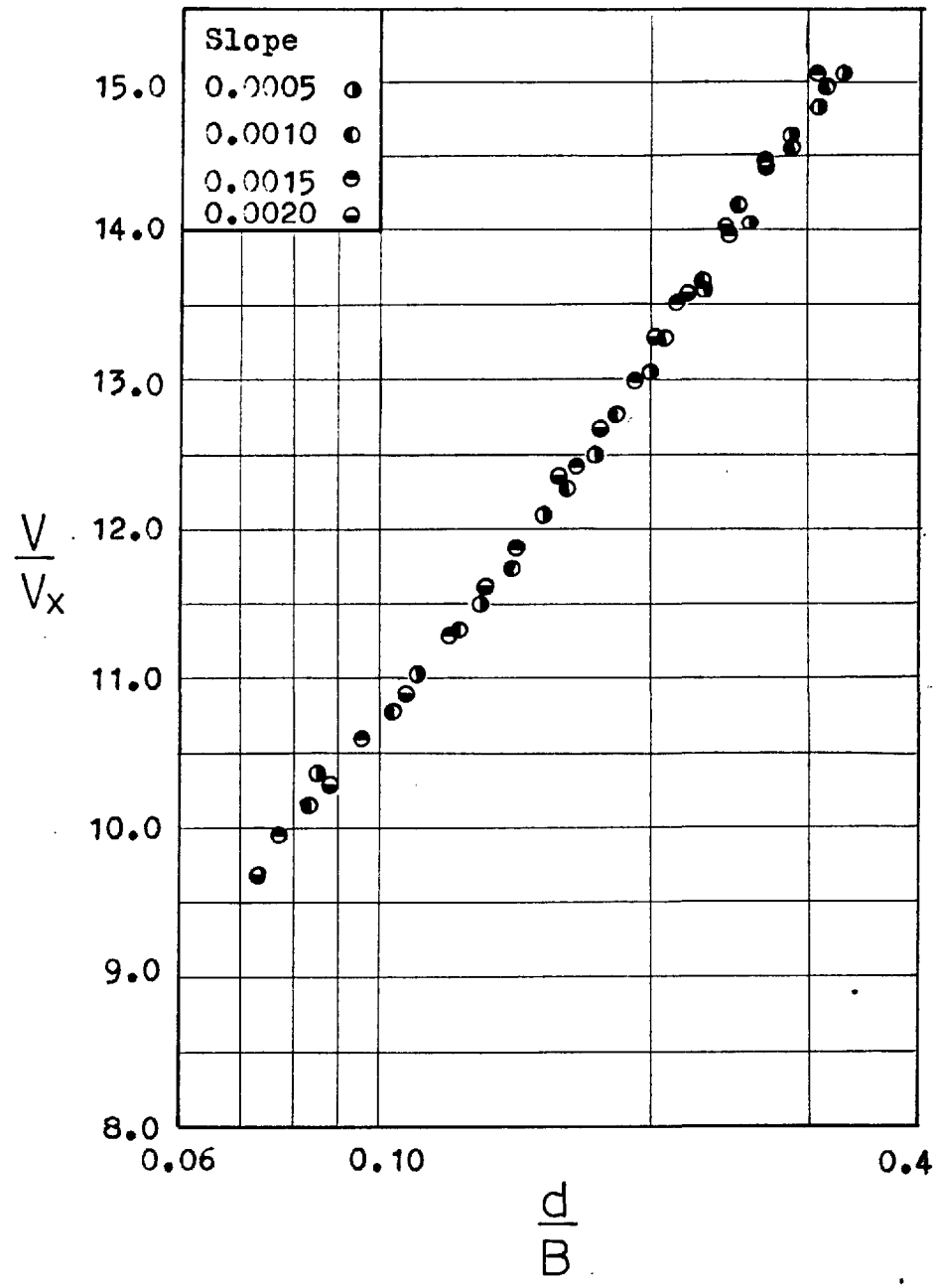


FIG.VI.9. FRICTION COEFFICIENT RESSULTS FOR FULL PERIMETER OF CHANNEL WITH FULLY GRAVELLED BED AND SMOOTH SIDE WALLS .

It is known that the shear stress distribution along the perimeter of a channel section is non-uniform even when the whole perimeter is uniformly roughened. When the bed is smooth and the walls are rough the phenomenon seems particularly complicated. For small depths of flow, the resistance offered by the smooth side walls may perhaps be very small compared to the resistance of the rough bed and the walls can then be neglected. The results so obtained are plotted as $\frac{V}{V_{xo}}$, where V_{xo} is equal to $\sqrt{dgs}$, against $\log \frac{d}{B}$ in Figs. (VI.10), (VI.11) and (VI.12) for the three beds; straight lines with slope of 5.75 are drawn through the points for small values of $\frac{d}{B}$ on each diagram. For larger values of $\frac{d}{B}$ more resistance is offered by the side walls and the points start deviating from the straight lines drawn on the diagrams giving lower values of $\frac{V}{V_{xo}}$. Applying Formula (14) valid for flow between rough parallel plates, the values of K_s corresponding to the straight lines for various beds are as follows:

Table (VI.3)

Bed	K_s c.m.
Stabilized sand rippled bed	1.125
Rippled bed with gravel filled in troughs of the ripples	0.72
Fully gravelled bed	0.64

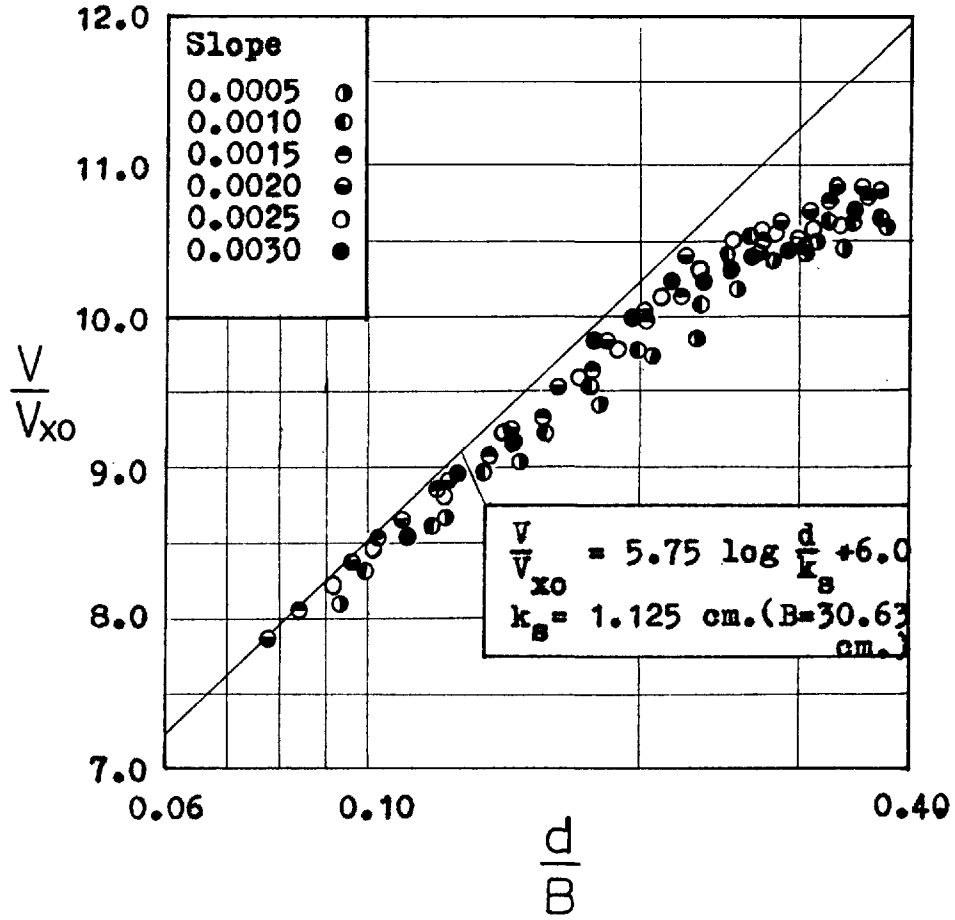


FIG.VI.10. FRICTION COEFFICIENT RESULTS FOR CHANNEL WITH RIPPLED BED NEGLECTING RESISTANCE OF SIDE WALLS .

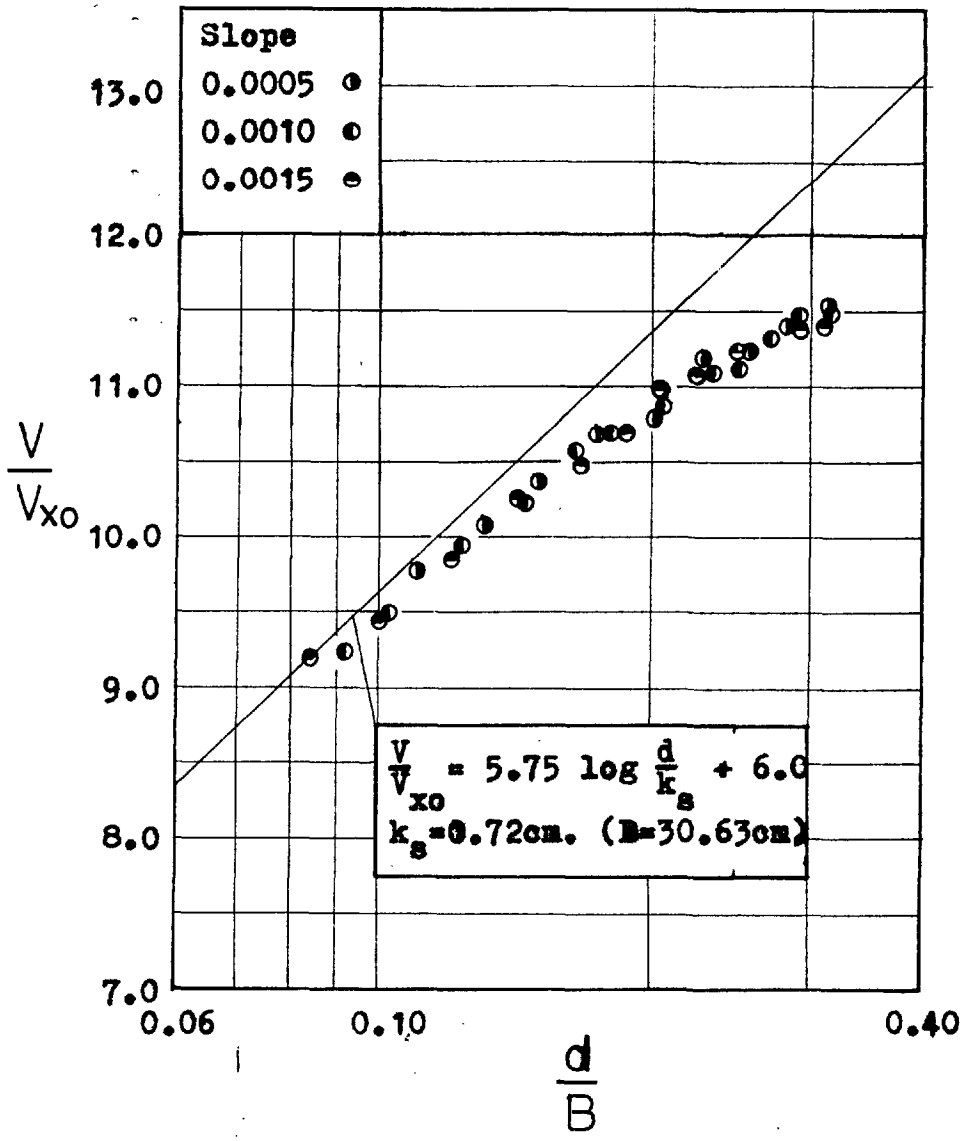


FIG.VI.11. FRICTION COEFFICIENT RESULTS FOR CHANNEL WITH GRAVEL FILLED IN TROUGHS OF RIPPLED BED NEGLECT-RESISTACE OF SIDE WALLS .

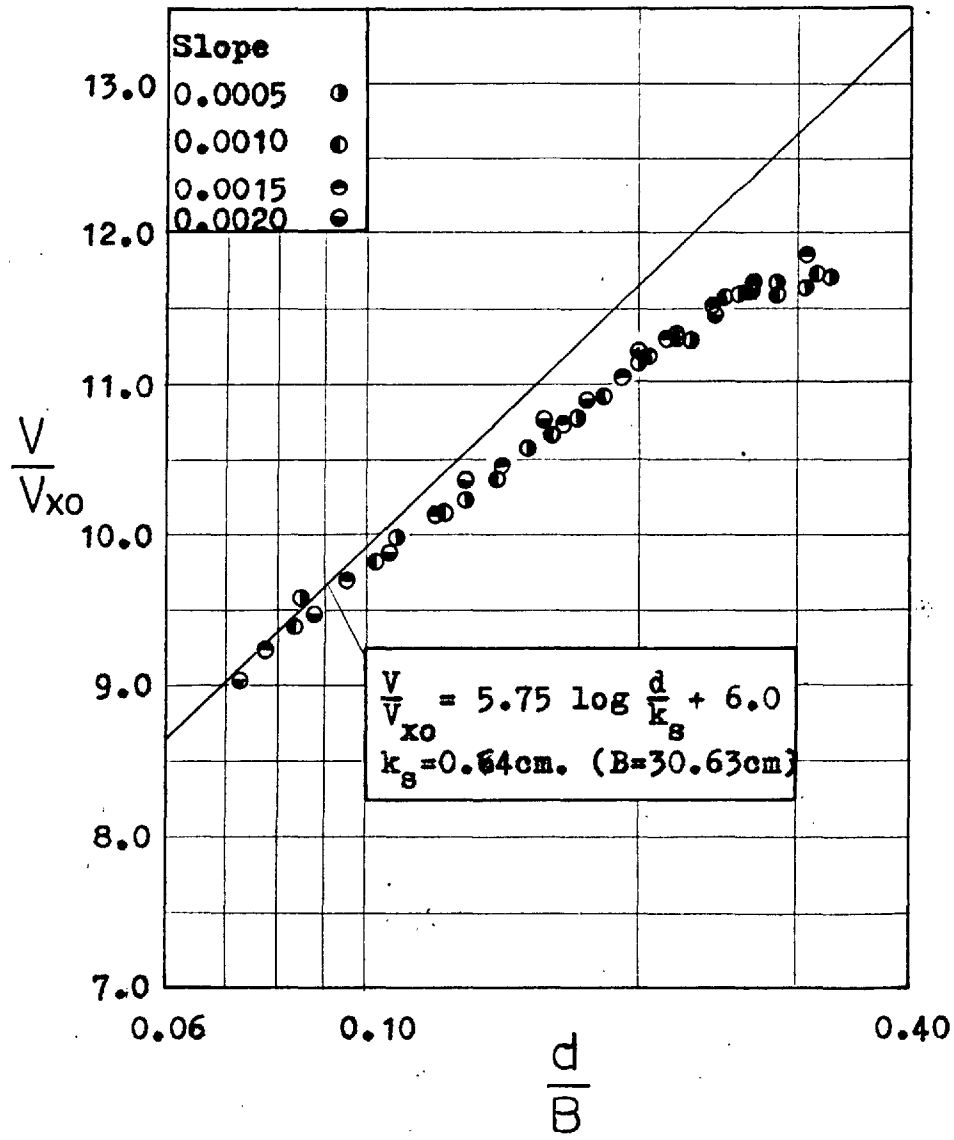


FIG.VI.12. FRICTION COEFFICIENT RESULTS FOR CHANNEL WITH FULLY GRAVELLED BED NEGLECTING RESISTANCE OF SIDE WALLS.

Two of the above values agree with those previously obtained from velocity measurements (Table VI.1) but K_s for the rippled bed is about 30% less than previously. The reason for this was ultimately traced to a systematic variation of ripple size, their height being 0.32" when averaged over the whole test length, whereas their height was 0.40" in the vicinity of the velocity traverses. Their shape and spacing were also different, so perhaps no further explanation could be sought and the value of the equivalent sand roughness for the whole of the rippled bed can be accepted as 1.125 c.m.

VI.II.2.3. APPLYING EINSTEIN-JOHNSON METHOD FOR SIDE WALL EFFECT

This method gives the expression:

$A = 2 A_w + A_b$ or $B d = 2 R_w d + R_b B$,

where the subscript "w" is for wall and "b" for bed. Generally, in Manning's formula, some value of n is either assumed or predetermined from the experiments for the side walls, and knowing the value of V and S, the value of R_w is obtained. Then from the above relation the value of R_b and then the friction coefficient for the bed are determined. In the present experiments, Blasius law, which can be taken to be true for smooth open channels within the accuracy of measurements, was used for the side walls to find R_w as given below,

$$R_w = \left[0.25 \left(\frac{0.0395}{gs} \right)^4 \nu^1 V^7 \right]^{1/5}$$

Knowing the value of R_w, value of R_b is calculated from the basic relation.

The values are given in Appendix (II.A), Tables (7 to 19), and are plotted as $\frac{V}{V_{xb}}$ against log $\frac{R_b}{B}$ in Figs. (VI.13), (VI.14) and (VI.15). On the diagrams straight lines representing Eq: (14) for the friction coefficient, with values of K_s for the beds as obtained earlier in Table (VI.2), are also shown. The results show that the points for $\frac{V}{V_{xb}}$ lie above the straight lines drawn and this deviation increases with the increase of depth of flow or value of R_b; and, as a result, the values of K_s obtained by this method may be considerably less than the true values and may decrease with increasing depth.

VI.4.3. DISCUSSION OF RESULTS

The foregoing measurements of surface roughness show that the constants obtained from velocity measurements and by the method of neglecting side walls agree except in the case of the rippled bed where the velocity measurements give the local value of equivalent sand roughness while the second method naturally gives the mean value for the whole bed. When the side wall effect was eliminated by the Einstein-Johnson method the bed roughness obtained was far less than its true value, and the error became more as the depth increased.

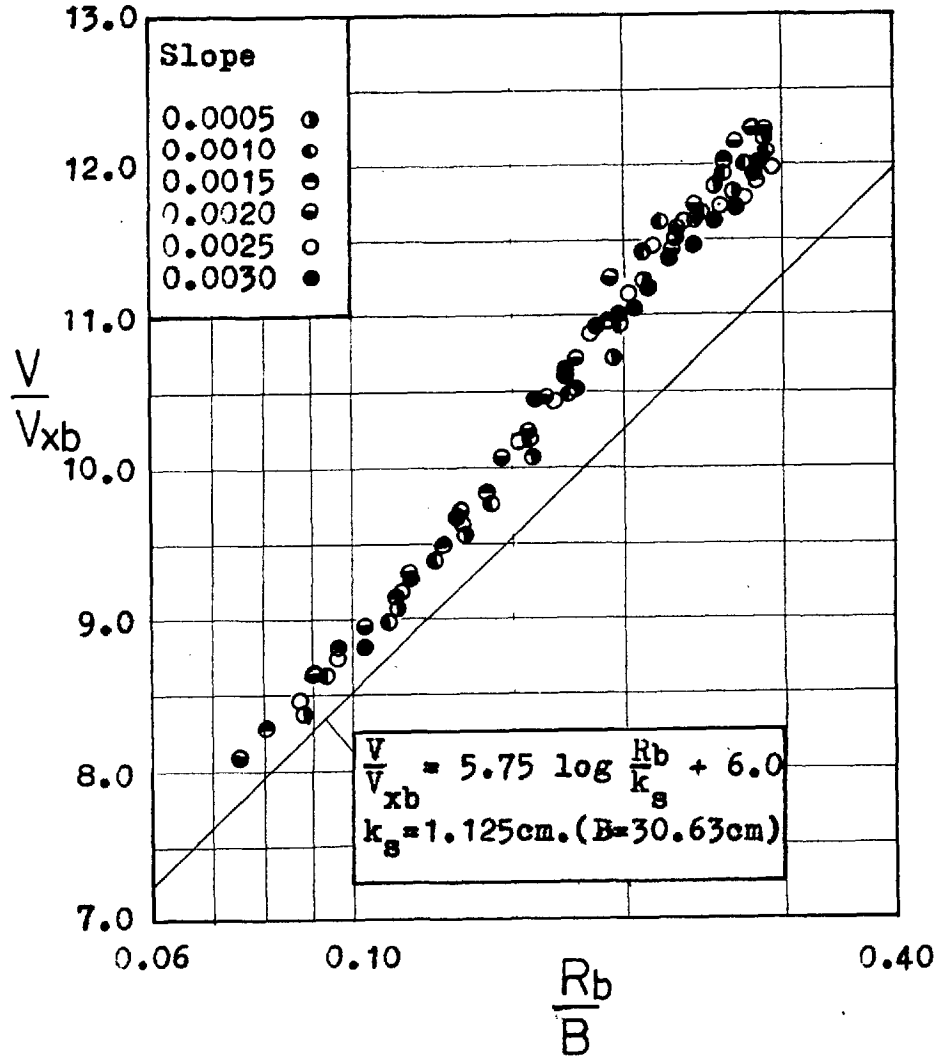


FIG.VI.13. FRICTION COEFFICIENT RESULTS FOR CHANNEL WITH RIPPLED BED ELIMINATING EFFECT OF SIDE WALLS BY EINSTEIN - JOHNSON'S METHOD .

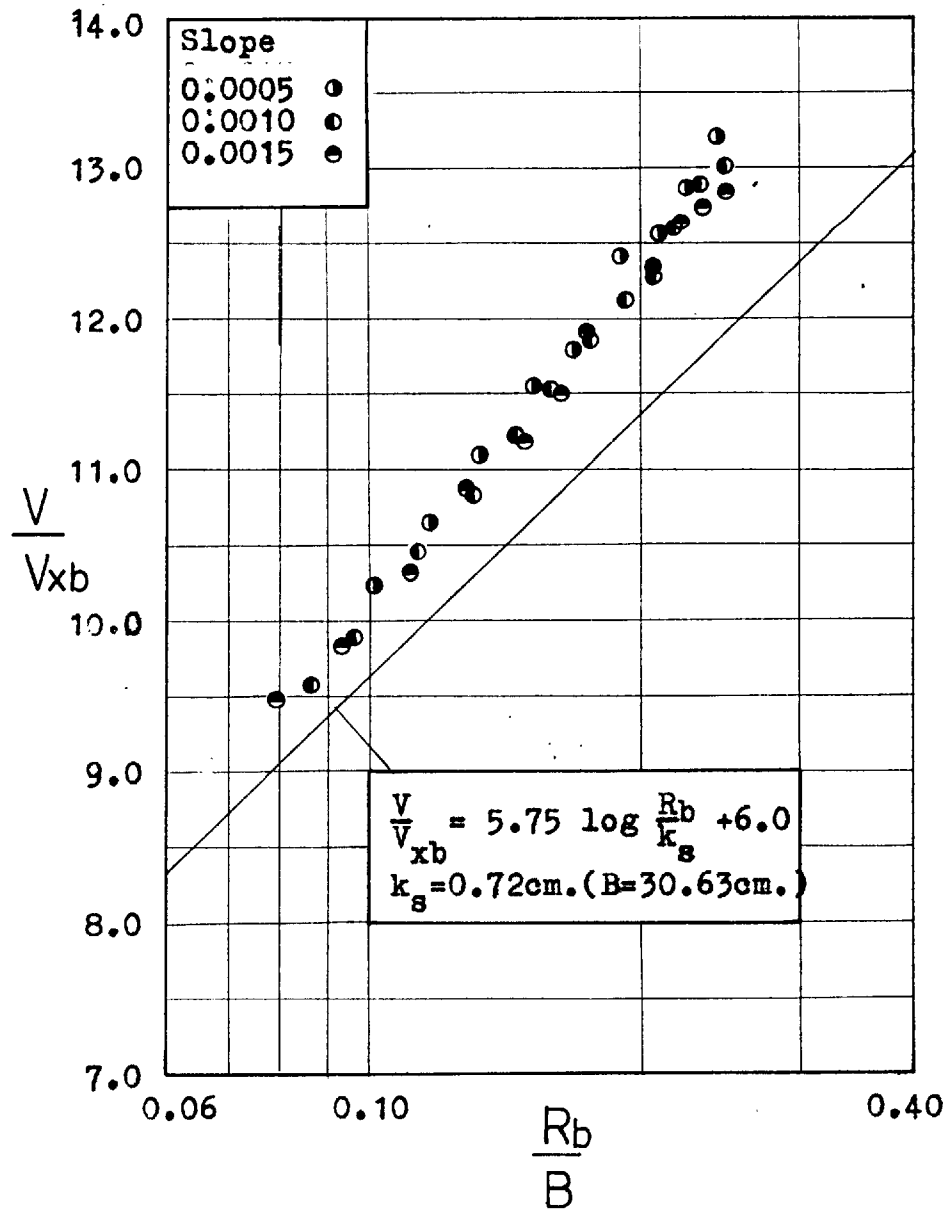


FIG.VI.14. FRICTION COEFFICIENT RESULTS FOR CHANNEL WITH GRAVEL IN TROUGHS OF RIPPLED BED ELIMINATING EFFECT OF SIDE WALLS BY EINSTEIN—JOHNSON'S METHOD .

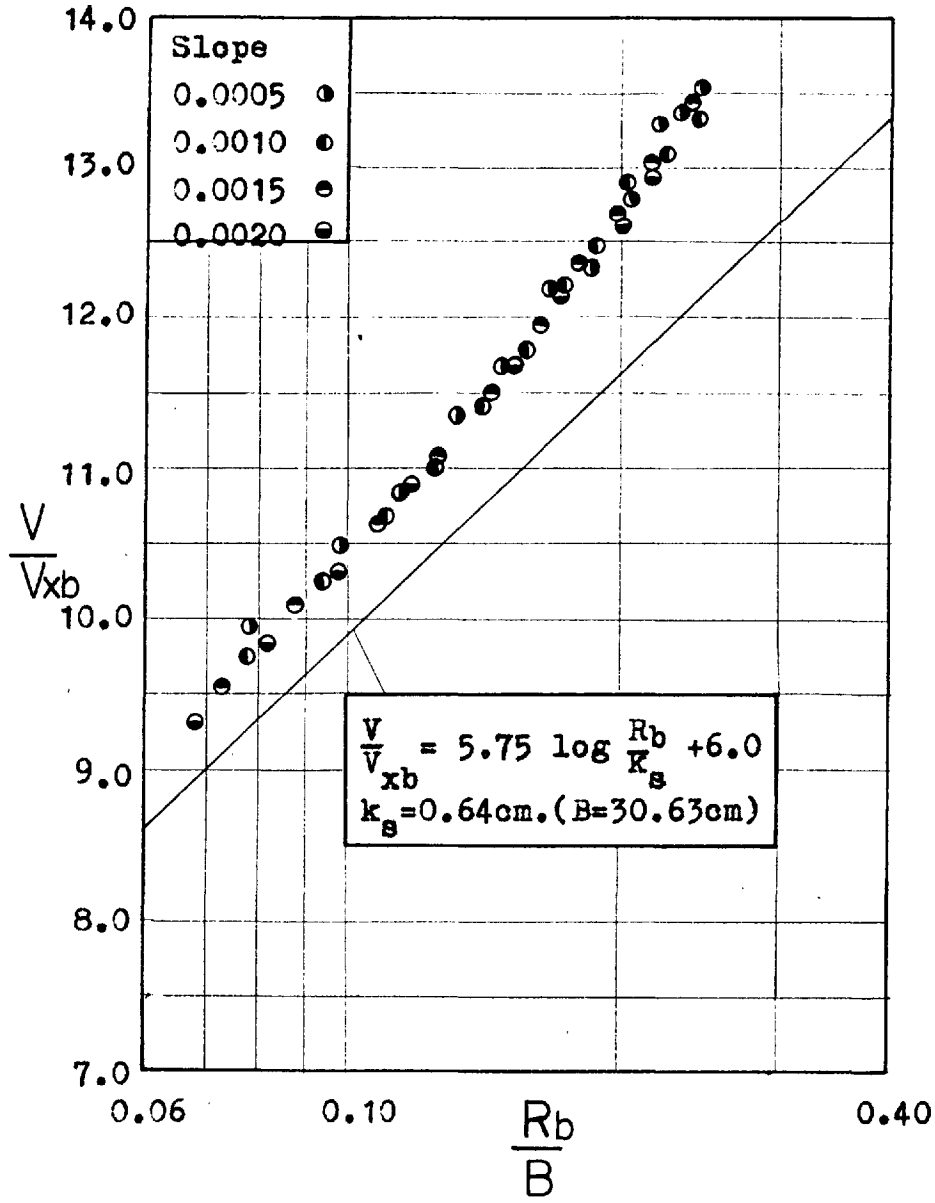


FIG.VI.15. FRICTION COEFFICIENT RESULTS FOR CHANNEL WITH FULLY GRAVELLED BED ELIMINATING EFFECT OF SIDE WALLS BY EINSTEIN - JOHNSON'S METHOD .

However, according to Yassin (1954) this method gives satisfactory results, despite certain deviations, when based on Manning-Strickler formula. Possibly the method may serve where much accuracy is not required, but in the laboratory, where inaccuracy may lead to wrong conclusions it would seem out of place.

Recently Vanoni and Hwang (1967) used the Einstein-Johnson method to determine the friction coefficient due to form drag of ripples. They performed the experiments on two types of stabilized rippled beds in a flume with smooth side walls. They argued that the friction coefficient is a function of $\frac{R_b}{e\overline{H}}$, where R_b is the bed hydraulic radius, e, the exposure parameter, is areal concentration of roughness elements and $\overline{H}$ is the average ripple height. In the above relation value of $e\overline{H}$ is constant for a particular rippled bed and so their results plotted as $\frac{V}{V_{xb}}$ against log R_b will not change the slope of the line, which according to them in the present notations is about 9.5. In the present work if the datum plane on each bed for determining the depths of flow was taken lower, the straight lines of approximately same slope could have been passed through the results plotted in Figs. (VI.13), (VI.14) and (VI.15). But there seems to be no reason why the slope of this semi-logarithmic plot should change so much from the value, 5.75, obtained from velocity distribution. Further, Vanoni and Hwang used Eq: (11a)

for rough pipes and from their results calculated the values of equivalent sand roughness for the two stabilized rippled beds for different depths of flow. From this they concluded "....that there is no equivalent sand roughness for rippled beds, and suggests that K_s values for surfaces that are very dissimilar from sand-covered surfaces may also vary with flow depth, thus making erroneous all calculations based on the assumption of a constant K_s". Indeed this kind of result did appear to emerge from the present experiments when the side wall effect was eliminated by this method, and did do so not only for the rippled bed but also for the gravelled beds. Hence actually it is not the rippled bed which gives a varying K_s but rather it is this particular method for eliminating the side wall effect which has given a misleading result.

In Figs. (VI.10), (VI.11) and (VI.12), where the side wall is not taken into consideration, the results with deeper flows are seen progressively to deviate more and more from the wide channel law as more resistance is contributed by the side walls. Robinson and Albertson (1952) working on a 9" wide and 14 ft. long rectangular channel, with artificial roughness elements fixed on the bed and with smooth side walls, experimented over a range of depths from 2" to 8.5". Neglecting the side walls, they tried to pass a straight line through the resulting points which were plotted

in a way similar to in Figs. (VI.10, VI.11, VI.12), and the slope of the line obtained was accordingly much less than 5.75. The objection to such a relation is that it is not universal since the slope of the straight line drawn will depend both upon the degree of roughness and also upon the particular range of depth-width ratio. As an alternative, it is perhaps simpler to tabulate the amount by which $\frac{V}{V_{xo}}$ decreases as $\frac{d}{B}$ increases. Table (VI.4) gives for certain values of $\frac{d}{B}$ the percentage deviation of $\frac{V}{V_{xo}}$ from Formula (14).

TABLE (VI.4)

$\frac{d}{B}$	deviations of $\frac{V}{V_{xo}}$ from formula (14)			
	Rippled bed	Gravell filled in troughs	Fully gravelled bed	Mean Value
0.10	-1.18	-1.04	-1.01	-1.08
0.15	-2.63	-2.82	-2.75	-2.73
0.20	-3.42	-3.96	-4.30	-3.90
0.25	-4.15	-5.85	-5.23	-5.10
0.30	-5.80	-6.90	-7.10	-6.60

From the above table it is seen that the percentage deviations for the three different beds for each $^{d}/_{B}$ are about the same within the accuracy of measurements. Hence the mean values in the last column can be used as corrections to the formula which then can be relied upon either for predicting $\frac{V}{V_{xo}}$ or conversely for determining K_s from an observed value of $\frac{V}{V_{xo}}$.

For the moment the values in Table (VI.4) are restricted to the range of the present experiments, namely to $0.1 < {}^{d}/_{B} < 0.3$, though, no doubt, when more experimental values become available the table can be extended to cover the whole range of practical interest.

1. When the water upstream was disturbed the lower crtical Reynolds number, $\frac{RV}{\nu}$, proved to be nearly 700 (P.35) as it is in closed rectangular ducts. Evidently the stability of laminar motion is not sensitive to the kind of restriction occuring at the air-water interface.

2. The distribution of $\frac{\sqrt{\overline{u'^2}}}{V_{xo}}$ in the open channel proved to be numerically the same as in a pipe or in a closed duct, where as the distribution of $\frac{\sqrt{\overline{v'^2}}}{V_{xo}}$ was characteristically different, and the effect of the free surface extended downward as far as 0.4 d below the free surface, (PP.55 & 63; Figs. IV.5b & IV.8b, PP.57 & 61).

3. Except close to the wall, the intensity of the turbulence was found to be determined by the position of the point concerned and by the magnitude of the drag at the wall, and solely by these two variables: it was independent of other variables, and of the nature of the wall. (P.92; Figs. IV.27 & 28, PP. 90 & 91).

4. The mid stream distribution of turbulent stress $\rho\overline{u'v'}$ agreed numerically with the straight line calculated from slope and depth, and did so for all bed conditions. So, on the centre line, the externally applied forces are carried wholly by turbulence: neither secondary currents nor viscosity contribute. (Figs. IV.9, IV.15, IV.20 & IV.25, PP.66, 74, 80 & 86).

5. In the present experiments, the coefficient of correlation, $\frac{\overline{u'v'}}{\sqrt{\overline{u'^2}}\ \sqrt{\overline{v'^2}}}$, had a constant value of approximately - 0.50, irrespective of the nature of the wall (P.93).

6. When the bed was plane (rough or smooth) the secondary currents formed a pattern satisfying Prandtl's hypothesis, flowing towards the corner and then away from it along side walls and bed, and accordingly at each side the motion divided into a pair of cells. However when the bed was rippled, the upper cell became dominant, and the stagnation point was displaced a considerable distance away from the corner, and flow was downwards towards the bed, thenalong the bed towards the corner, and upwards along the side. There were then four distinct cells in each half of the channel. (P.116; Fig. V.9, P.118).

7. For turbulent flow in smooth rectangular channels of shallow depth the friction coefficient, after allowing for the different constants of integration, is exactly as predicted from the empirical constants determined from circular pipes. Unfortunately, for finite depth-width ratios, the relevant constants of integration are not known, though certain investigations of square pipes and of 90° triangular channels disclose some what less resistance than circular pipes of equal hydraulic radius (Table VI.1, P.39). This tendency begins to be evident in the present experiments which extend to a depth-width ratio of 1:3. (P.147; Figs. VI.3 & VI.3.a., PP.149 & 150).

8. Einstein and Johnson have proposed a method for separating the drag of bed and sides of composite channels with rough beds and smooth sides. However in the present experiments their method was found to give a bed roughness far less than its true value, and the error increased when the depth was increased. Their method therefore is liable to give misleadingly small results. (PP. 170-174).

REFERENCES

Ackers, P. (1958) "Resistance to Fluids Flowing in Channels and Pipes". Hydrauls. Res. Pap., 1, H.M.S.O., London.

Allen, J. (1934) "Streamline and Turbulent Flow in Open Channels". Phil. Mag. (7), 17.

Allen, J. and Ullah, M.I. (1967) "The Flow of Water through Smooth Open Channels of Narrow Rectangular and T - Shaped Cross Sections". Proc. Instn Civ. Engrs , 36.

Bazin, H. (1865) "Recherches Hydrauliques". Mem. Pres. par divers savants, Paris.

Blasius, H. (1913) "Das Ahnlich keitsgesetz bei Reibungs vorgangen in Flussigkeiten". Forscharb. Geb. Ingwes., 131.

Brundrett, E. and Baines, W.D. (1964) "The Production and Diffusion of Vorticity in Duct Flow". J. Fluid Mech., 19.

Casey, H. (1935) "Uber Geschiebebewegung". Mitt. preuss. Versanst. Wasserb. Schiffb., 19.

Chuang, H. and Cermark, J.E. (1965) "Turbulence Measured by Electrokinetic Transducers". J. Hydraul. Div. Am. Soc. Civ. Engrs , HY6, 91.

Clayton, B.R. and Massey, B.S. (1966) "Flow Vizualization in Water: A Review of Techniques". J. Sci. Instrum., 44.

Colebrook, C.F. (1939) "Turbulent Flow in Pipes with Particular Reference to the Transition Region Between the Smooth and Rough Pipe Laws". J. Instn Civ. Engrs , 11.

Colebrook, C.F. and White, C.M. (1937) "Experiments with Fluid Friction in Roughened Pipes". Proc. R. Soc. (A), 161.

Cornish, R.J. (1928) "Flow in Pipe of Rectangular Cross Section". Proc. R. Soc. (A), 120.

Cunningham, A. (1882) "Recent Hydraulic Experiments". Minut. Proc. Instn Civ. Engrs., 71.

Davies, S.J. and White, C.M. (1928) "An Experimental Study of the Flow of Water in Pipes of Rectangular Section". Proc. R. Soc. (A), 119.

Einstein, H.A. (1942) "Formulas for the Transportation of Bed Load". Trans. Am. Soc. Civ. Engrs , 107.

Einstein, H.A. and El-Samni, E.S.A. (1949) "Hydrodynamic Forces on a Rough Wall". Rev. mod. Phys., 21.

Einstein, H.A. and Li, H. (1958) "Secondary Currents in Straight Channels". Trans. Am. geophys., 39.

Ellison, T.H. (1960) "A Note on Velocity Profile and Longitudinal Mixing in a Broad Open Channel". J. Fluid Mech., 8.

Fage, A. (1933) "Fluid Flow in Rough Pipes". Aeronaut. Res. Comm., R & M. 1585.

Fage, A. (1936) "Turbulent Flow in a Circular Pipe". Phil. Mag. (7), 21.

Fage, A. and Townend, H.C.H. (1932) "An Examination of Turbulent Flow with an Utramicroscope". Proc. R. Soc. (A), 135.

Francis, J.B. (1878) "On the Cause of the Maximum Velocity of Water Flowing in Open Channel being Below the Surface". Trans. Am. Soc. Civ. Engrs., 7.

Fromm, K. (1923) "Stromungswiderstand in rauhen Rohren". Z. angew. Math. Mech., 3.

Gessner, F.G. and Jones, J.B. (1965) "On Some Aspects of Fully Developed Turbulent Flow in Rectangular Channels". J. Fluid Mech., 23.

Gibson, H.A. (1909) "On the Depression of the Filament of Maximum Velocity in a Stream Flowing Through an Open Channel". Proc. R. Soc. (A), 82.

Goldstein, S. (1938) "Modern Developments in Fluid Dynamics". Clarendon Press, Oxford, II.

Grossman, L.M., Li, H. and Einstein, H.A. (1957) "Turbulence in Civil Engineering: Investigations in Liquid Shear Flow by Electro-magnetic Induction". J. Hydraul. Div. Am. Soc. Civ. Engrs , HY5, 83.

Gunn, D.J. and Darling, C.W.W. (1963) "Fluid Flow and Energy Loss in Non - Circular Conduits". Trans. I. Chem. Engrs , 41, 4.

Hall, A.A. (1938) "Measurement of the Intensity and Scale of Turbulence". Aeronaut. Res. Comm., R & M., 1842.

Hartnett, J.P., Koh, J.C.Y. and McComas, S.T. (1962) "A Comparison of Predicted and Measured Friction Factors for Turbulent Flow Through Rectangular Ducts". Trans. Am. Soc. Mech. Engrs , 82.

Hinze, J.O. (1959) "Turbulence: An Introduction to its Mechanism and Theory". McGraw-Hill Book Co., Inc., New York, N.Y.

Hopf, L. (1923) "Die Messung der hydraulischen Rauhigkeit". Z. Angew. Math. Mech., 3.

Horton, R.E., Leach, H.R. and Vanvliet, R. (1934) "Laminar Sheet Flow". Trans. Am. Geophys., 15.

Huebscher, P.S. (1947) "Friction in Round, Square and Rectangular Ducts". Heat. Pip. Air Condit., 19.

Ippen, A.T. and Raichlen, F. (1957) "Turbulence in Civil Engineering: Measurements in Free Surface Streams". J. Hydraul. Div. Am. Soc. Civ. Engrs , HY5, 83.

Johnson, J.W. (1942) " The Importance of Considering Side-Wall Friction in Bed-Load Investigations". Civ. Engng , Am. Soc. Civ. Engns , 12, 6.

Kalinske, A.A. (1940) "Relation of Statistical Theory of Turbulence to Hydraulics". Trans. Am. Soc. Civ. Engrs , 105.

Kennedy, R.J. and Fulton, J.F. (1961) "The Effect of Secondary Currents upon the Capacity of a Straight Open Channel". Trans. Engng Inst. Can., 5, 1.

Keulegan, G.H. (1938) "Laws of Turbulent Flow in Open Channels". J. Natn. Bur. Stand., 21.

Kirschmer, O. (1949) "Pertes de Charge dans les Condites forcees et les Canaux decouverts". Revue gen. Hydraul., 15.

Lamb, H. (1932) "Hydrodynamics". University Press, Cambridge.

Laufer, J. (1951) "Investigation of Turbulent Flow in a Two-Dimensional Channel". NACA Rep., 1053.

Laufer, J. (1954) "The Structure of Turbulence in Fully Developed Pipe Flow". NACA Rept., 1174.

Liggett, J.A., Chiu, C.L. and Miao, L.S. (1965) "Secondary Currents in a Corner". J. Hydraul. Div. Am. Soc. Civ. Engrs., HY6, 91.

Moeller - Hartman, W. (1957) "Ahfluss in offenen Driecksgerinnen". Mitt. hannover. Versanst. Grundb. Wassbau, P.16.

Möller, M. (1883) "Studen Uber die Bewegung des Wassers in Flussen mit Bezugnahme auf die Ausbildung des Flussprofiles". Z. Bauw., P. 201.

Neymenyi, P.F. (1946): Discussion of "Transportation of Suspended Sediment by Water" by Vanoni, V.A., Trans. Am. Soc. Civ. Engrs , 111.

Nikuradse, J. (1926) "Untersuchungen Uher die Geschwindig Keitsverteilung in turbulenten Stromungen". V D I Forschhft., 281.

Nikuradse, J. (1930) "Turbulente Stromung in nicht Kreis formigen Rohren". Ing. -Arch., 1.

Nikuradse, J. (1932) "Gesetzmabigkeit der turbulenten Stromung in glatten Rohren". ForschHft., 356.

Nikuradse, J. (1933) "Stromungsgesetze in rauhen Rohren". ForschHft., 361.

Owen, W.M. (1953) "Correlation Between Pipe Flow and Uniform Flow in Triangular Open Channels". Trans. Am. geophys., 18.

Owen, W.M. (1954) "Laminar to Turbulent Flow in a Wide Channel". Trans. Am. Soc. Civ. Engrs , 119.

Powell, R.W. (1946): Discussion of "Transportation of Suspended Sediment by Water" by Vanoni, V.A., Trans. Am. Soc. Civ. Engrs., 111.

Powell, R.W. (1946) "Flow in a Channel of Definite Roughness". Trans. Am. Soc. Civ. Engrs , 111.

Powell, R.W. and Posey, C.J. (1959) "Resistance Experiments in a Triangular Channel". J. Hydraul. Div. Am. Soc. Civ. Engrs , HY5, 85.

Prandtl, L. (1927) "Uber die ausgebildete Turbulenz". Proc. 2nd Int. Cong. App. Mech., Zurich.

Progress Report of Task Force (1963) "Friction Factors in Open Channels". J. Hydraul. Div. Am. Soc. Civ. Engrs , HY2, 89.

Raichlen, F. (1967) "Some Turbulence Measurements in Water". J. Engng. Mech. Div. Am. Soc. Civ. Engrs , EM2, 31.

Reichardt, H. (1938) "Messungen turbulenter Schwankungen". Naturwissenschaften, 26. Also Z. angew. Math. Mech., 18.

Reichardt, H. (1940) "Die Warmeubertragung in turbulenten Reibungsschichten". Z. angew. Math. Mech., 20.

Reichardt, H. (1951) "Vollstandige Darstellung der turbulenten Geschwindig Keitsverteilung in glatten Leitungen". Z. angew. Math. Mech., 31.

Reinus, E. (1961) "Steady Uniform Flow in Open Channels". K. tek. Hogsk. Handl., 179.

Replogle, J.A. and Chow, V.T. (1966) "Tractive Force Distribution in Open Channels". J. Hydraul. Div. Am. Soc. Civ. Engrs , HY2, 92.

Reynolds, O. (1883) "An Experimental Investigation of the Circumstances which determine whether the Motion of Water shall be Direct or Sinuous, and of the Law of Resistance in Parallel Channels". Phil. Trans. R. Soc., 174. Scientific Papers, 2.

Reynolds, O. (1894) "On the Dynamical Theory of Incompressible Viscous Fluids and the Determination of the Criterian". Phil. Trans. R. Soc., 186. Scientific Papers, 2.

Robinson, A.R. and Albertson, M.L. (1952) "Artificial Roughness Standard for Open Channels". Trans. Am. geophys., 33.

Rotta, J. (1950) "Das in Wandnahe gultige Geschwindig Keitsgesetz turbulenter Stromungen". Ing. - Arch., 18.

Sayre, W.W. and Albertson, M.L. (1963) "Roughness Spacing in Rigid Open Channels". Trans. Am. Soc. Civ. Engrs , 128.

Schiller, L. (1921) "Experimentelle Untersuchungen Zum Turbulenz Problem". Z angew. Math. Mech., 1.

Schiller, L. (1923) "Uber den Stromungswider Stand Von Rohren Verschiedenen Querschnitts Und Rauhigkeitsgrades". Z. angew. Math. Mech., 3.

Schlichting, H. (1936) "Experimentelle Untersuchungen zum Rauhigs Keits Problem". Ing. - Arch., 7. Also NACA, TM, 823.

Schlichting, H. (1955) "Boundary Layer Theory". McGraw - Hill Book Co., Inc., New York, N.Y.

Schuyf, J.P. (1966) "The Measurement of Turbulent Velocity Fluctuations with a Propellor - Type Current Meter". Jnl. hydraul. Res., 4, 2.

Sharp, B.B. (1966): Discussion of "Secondary Currents in a Corner" by Ligget, J.A., Chiu, C.L. and Miao, L.S., J. Hydraul. Div. Am. Soc. Civ. Engrs , HY5, 92.

Stanton, T.E. (1911) "The Mechanical Viscosity of Fluids". Proc. R. Soc. (A), 85.

Stanton, T.E. and Pannel, J.R. (1914) "Similarity of Motion in Relation of the Surface Friction of Fluids". Phil. Trans. R. Soc. (A), 214.

Stearns, F.B. (1883) "On the Current Meter, Together with a Reason why the Maximum Velocity of Water Flowing in Open Channels is Below the surface". Trans. Am. Soc. Civ. Engrs , 12.

Straub, L.G. (1939) "Studies of the Transition Region between Laminar and Turbulent Flow in Open Channels". Trans. Am. geophys., IV.

Straub, L.G., Silberman, E. and Nelson, H.C. (1958) "Some Observations on Open Channels Flow at Small Reynolds Numbers". Trans. Am. Soc. Civ. Engrs , 123.

Taylor, G.I. (1936) "Correlation Measurements in a Turbulent Flow through a Pipe". Proc. R. Soc. (A), 157.

Tracy, H.J. (1965) "Turbulent Flow in a Three Dimensional Channel". J. Hydraul. Div. Am. Soc. Civ. Engrs , HY6, 91.

Tracy, H.J. and Lester, C.M. (1961) "Resistance Coefficients and Velocity Distribution Smooth Rectangular Channels". Wat. - Supply Pap., Wash., 1592 - A.

Vanoni, V.A. (1941) "Velocity Distribution in Open Channels". Civ. Engng , Am. Soc. Civ. Engnrs , 11, 6.

Vanoni, V.A. (1946) "Transportation of Suspended Sediment by ater". Trans. Am. Soc. Civ. Engrs , 111.

Vanoni, V.A. and Hwang, L.S. (1967) "Relation between Bed Forms and Friction in Streams". J. Hydraul. Div. Am. Soc. Civ. Engrs., HY3, 93.

Wattendorf, F.L. and Kuethe, A.M. (1934) "Investigation of Turbulent Flow by means of the Hot-Wire Anemometer". Physics, 5.

Weatherburn, C.E. (1946) "A First Course in Mathematical Statistics". Cambridge University Press, London.

White, C.M. (1929) "Streamline Flow Through Curved Pipes". Proc. R. Soc. (A), 123.

Wood, D. (1879) "On the Flow of Water in Rivers". Trans. Am. Soc. Civ. Engrs , 8.

Yassin, A.M. (1953) "Mean Roughness Coefficient in Open Channels with Different Roughnesses of Bed and Side Walls". Mitt. Versanst. Wassbau Erdbau, Zurich, 27.

APPENDIX I

OPTICS OF PHOTOGRAPHIC ARRANGEMENT TO RECORD MOTION ACROSS MAIN FLOW.

I.A. DESIGN CALCULATIONS.

Distance from illuminated cross-section to the prism = 9'-6" (in water)

$= 9'\text{-}6'' \times \frac{3}{4} \simeq 7'\text{-}2''$ (in air).

Distance from prism to lens = 8" (in air).

Total distance from object to lens

$= 7'\text{-}2'' + 8'' = 7'\text{-}10'' \simeq 240$ cm.

The thin lens formula is

$$\frac{1}{f} = \frac{1}{u} + \frac{1}{v}$$

Where f is the focal length, u is the distance from object to lens and v is the distance from lens to image on the film.

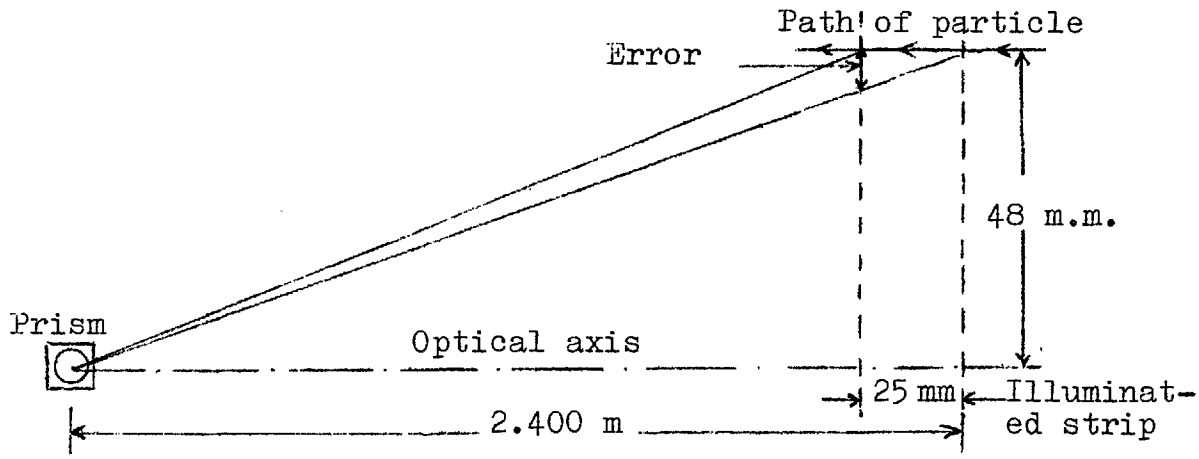
We have f = 50 cm. and u = 240 cm.

$\therefore$ From $\frac{1}{50} = \frac{1}{240} + \frac{1}{v}$

$v \simeq 63$ cm.

To obtain this image distance from the lens to the photographic film, the camera was mounted with bellows extensions, about 20 cm. in length, on a vertical aluminium tube 45 cm. long; and the lens was screwed to the bottom end of the tube.

I.B. APPARENT OUTWARD DRIFT DUE TO OPTICAL PARALLAX



For a particle passing the illuminated gap at 48m.m. from the optical axis, the angle of side ray = $\frac{48}{2400}$

$\therefore$ apparent outward drift = $\frac{48}{2400} \times 25 = \frac{1}{2}$ m.m.

Similarly for a particle,

at 36 m.m., the drift = $\frac{36}{2400} \times 25 = \frac{3}{8}$ m.m.

at 24 m.m., the drift = $\frac{24}{2400} \times 25 = \frac{1}{4}$ m.m.

and

at 12 m.m., the drift = $\frac{12}{2400} \times 25 = \frac{1}{8}$ m.m.

APPENDIX II

EXPERIMENTAL DATA .

APPENDIX II.A. FRICTION COEFFICIENT RESULTS

The various quantities in Tables 1 - 19 are as follows:

S = Slope of the flume

Q = Water discharge in cu.ft./sec.

d = Depth of flow in ft.

V = $\frac{Q}{Bd}$, the average velosity in ft./sec. where
B = the flume width (1.005 ft.)

R = $\frac{A}{P}$, the hydraulic radius in ft. where A is the area of cross section and P is the wetted perimeter

Rb = Bed hydraulic radius in ft. and is calculated as given in Chapter VI.

V_* = $\sqrt{RgS}$, the average shear velosity over the wetted perimeter in ft./sec.

V_{*o} = $\sqrt{dgS}$, the shear velosity at the bed on the central plane for two dimensional flow in ft./sec.

V_{*b} = $\sqrt{RbgS}$, the average bed shear velosity after eliminating the effect of side walls in ft./sec.

LAMINAR FLOW (Smooth bed)

Table 1. (Simple entrance)

Run No.	S	Q cu.ft./sec.	d ft.	Temp. °C	V ft./sec.	R ft.	V_* ft./sec.	$\frac{V}{V_*}$	$\frac{RV_*}{\nu}$
1.	0.0005	0.0022	0.0168	19.5	0.1210	0.0162	0.0162	8.050	23.90
2.	"	0.0032	0.0191	19.8	0.1665	0.0184	0.0172	9.680	29.00
3.	"	0.0064	0.0242	19.9	0.2619	0.0230	0.0193	13.600	40.80
4.	"	0.0094	0.0276	20.0	0.3398	0.0261	0.0205	16.569	49.50
5.	"	0.0132	0.0310	20.0	0.4225	0.0292	0.0217	19.490	58.40
6.	"	0.0145	0.0320	20.0	0.4503	0.0301	0.0220	20.470	61.00
7.	"	"	0.0358	20.0	0.4022	0.0334	0.0232	17.337	71.57
8.	"	0.0201	0.0497	19.6	0.4032	0.0452	0.0270	14.950	111.40
9.	0.0010	0.0041	0.0166	20.1	0.2485	0.0160	0.0227	10.950	33.70
10.	"	0.0068	0.0194	20.1	0.3499	0.0187	0.0245	14.258	42.45
11.	"	0.0017	0.0233	20.1	0.5004	0.0223	0.0268	18.680	55.20
12.	"	0.0147	0.0250	20.1	0.5863	0.0238	0.0277	21.173	60.99
13.	"	"	0.0300	20.1	0.4886	0.0283	0.0302	16.180	79.06
14.	"	0.0212	0.0407	20.1	0.5198	0.0376	0.0348	14.940	121.10

Table 2. (Obstructions in the entrance)

1.	0.0005	0.0072	0.0254	19.2	0.2853	0.0238	0.0196	14.570	42.20
2.	"	0.0087	0.0279	19.2	0.3115	0.0265	0.0206	15.100	49.40
3.	"	0.0105	0.0328	19.3	0.3197	0.0308	0.0223	14.366	62.00
4.	"	0.0142	0.0400	19.5	0.3522	0.0370	0.0244	14.424	82.48
5.	"	0.0199	0.0494	19.6	0.4010	0.0450	0.0269	14.903	110.60
6.	0.0010	0.0057	0.0184	18.7	0.3066	0.0178	0.0239	12.80	38.00
7.	"	0.0068	0.0196	19.1	0.3452	0.0188	0.0246	14.01	41.92
8.	"	0.0077	0.0203	19.4	0.3754	0.0195	0.0251	14.97	44.55
9.	"	0.0085	0.0215	19.5	0.3915	0.0206	0.0258	15.19	48.40
10.	"	0.0123	0.0288	19.6	0.4229	0.0273	0.0296	14.28	73.80
11.	"	0.0174	0.0363	19.6	0.4776	0.0338	0.0330	14.48	102.00
12.	"	0.0234	0.0431	19.7	0.5397	0.0397	0.0357	15.10	130.00

TURBULENT FLOW

Table 3. Smooth bed, Slope = 0.0005

Run No.	Q cu.ft./ sec.	d ft.	Temp. °C	V ft./sec.	R ft.	V_* ft./sec.	$\frac{V}{V_*}$	$\frac{RV_*}{\nu}$
1.	0.0201	0.0497	19.6	0.4032	0.0452	0.0270	14.95	111.4
2.	0.0289	0.0618	19.8	0.4652	0.0550	0.0298	15.64	150.2
3.	0.0397	0.0750	19.9	0.5267	0.0652	0.0324	16.25	194.8
4.	0.0520	0.0889	20.0	0.5819	0.0755	0.0349	16.69	243.0
5.	0.0739	0.1092	20.1	0.6737	0.0897	0.0380	17.73	315.2
6.	0.0948	0.1275	20.2	0.3794	0.1017	0.0405	18.25	381.7
7.	0.1257	0.1517	20.3	0.8245	0.1165	0.0433	19.04	468.9
8.	0.1506	0.1712	19.8	0.8758	0.1276	0.0453	19.31	530.0
9.	0.1954	0.2023	20.0	0.9610	0.1442	0.0482	19.94	641.3
10.	0.2532	0.2407	20.0	1.0470	0.1627	0.0512	20.45	768.3
11.	0.3176	0.2817	20.0	1.1219	0.1805	0.0539	20.81	897.5
12.	0.3857	0.3225	19.4	1.1900	0.1964	0.0562	21.16	1004.0
13.	0.4572	0.3646	19.5	1.2478	0.2113	0.0583	21.40	1123.2

Table 4. Smooth bed, slope = 0.0010

1.	0.0212	0.0407	20.1	0.5198	0.0376	0.0348	14.94	121.1
2.	0.0291	0.0490	20.4	0.5906	0.0446	0.0379	15.58	157.5
3.	0.0423	0.0610	19.9	0.6896	0.0544	0.0419	16.48	209.6
4.	0.0595	0.0750	20.0	0.7889	0.0653	0.0458	17.21	276.0
5.	0.0796	0.0898	20.1	0.8826	0.0762	0.0495	17.83	348.8
6.	0.1041	0.1053	20.2	0.9839	0.0870	0.0529	18.59	427.3
7.	0.1397	0.1270	20.4	1.0954	0.1013	0.0571	19.18	538.8
8.	0.1763	0.1471	20.4	1.1924	0.1138	0.0652	19.70	641.1
9.	0.2293	0.1750	20.0	1.3036	0.1298	0.0646	20.16	774.1
10.	0.2855	0.2033	19.5	1.3974	0.1448	0.0683	20.47	900.0
11.	0.3444	0.2296	19.8	1.4925	0.1576	0.0712	20.95	1030.7
12.	0.4104	0.2600	20.0	1.5705	0.1713	0.0943	21.15	1174.0
13.	0.4789	0.2879	20.0	1.6552	0.1830	0.0768	21.56	1296.3
14.	0.5448	0.3154	19.7	1.7187	0.1938	0.0790	21.76	1401.7
15.	0.6184	0.3462	19.7	1.7772	0.2050	0.0812	21.88	1525.0

Table 5. Smooth bed, slope = 0.0015

Run No.	Q cu.ft./sec.	d ft.	Temp. °C	V ft./sec.	R ft.	V_* ft./sec.	$\frac{V}{V_*}$	$\frac{RV_*}{\nu}$
1.	0.0180	0.0323	20.0	0.5540	0.0304	0.0383	14.47	107.3
2.	0.0275	0.0414	19.9	0.6595	0.0383	0.0430	15.34	151.5
3.	0.0434	0.0544	20.0	0.7935	0.0480	0.0484	16.40	214.4
4.	0.0649	0.0692	20.0	0.9390	0.0608	0.0542	17.33	303.8
5.	0.0892	0.0840	20.1	1.0569	0.0720	0.0590	17.92	392.5
6.	0.1340	0.1075	20.1	1.2403	0.0886	0.0654	18.96	535.7
7.	0.1688	0.1244	20.1	1.3502	0.0997	0.0694	19.45	640.2
8.	0.2280	0.1508	19.8	1.5042	0.1160	0.0749	20.10	797.3
9.	0.2883	0.1758	19.9	1.6318	0.1303	0.0793	20.57	951.3
10.	0.3522	0.1996	19.9	1.7560	0.1428	0.0831	21.14	1092.5
11.	0.4157	0.2250	20.0	1.8382	0.1554	0.0866	21.22	1242.1
12.	0.4835	0.2500	20.0	1.9245	0.1669	0.0898	21.43	1383.0
13.	0.5640	0.2779	19.5	2.0193	0.1790	0.0930	21.72	1516.5

Table 6. Smooth bed, slope = 0.0020

1.	0.0273	0.0375	19.9	0.7232	0.0349	0.0474	15.25	152.3
2.	0.0430	0.0491	20.0	0.8715	0.0447	0.0537	16.24	221.2
3.	0.0647	0.0628	19.2	1.0260	0.0558	0.0599	17.12	302.5
4.	0.0920	0.0777	19.3	1.1789	0.0673	0.0658	17.91	401.7
5.	0.1279	0.0948	19.4	1.3417	0.0798	0.0717	18.72	519.7
6.	0.1759	0.1152	19.5	1.5199	0.0937	0.0777	19.57	663.3
7.	0.2304	0.1358	19.5	1.6877	0.1069	0.0830	20.34	808.8
8.	0.2960	0.1600	20.2	1.8406	0.1214	0.0884	20.82	995.2
9.	0.3657	0.1842	20.8	1.9756	0.1348	0.0932	21.20	1181.1
10.	0.4519	0.2129	20.9	2.1120	0.1496	0.0981	21.52	1383.3
11.	0.5398	0.2392	21.1	2.2459	0.1620	0.1022	21.99	1567.5
12.	0.6184	0.2642	21.2	2.3294	0.1731	0.1056	22.10	1736.0

Table 7. Stabilized sand rippled bed, slope = 0.0005

Run No.	Q cu.ft./sec.	d ft.	Temp. OC	V ft./sec.	R ft.	V_* ft./sec.	$\frac{V}{V_*}$	V_{*o} ft./sec.	$\frac{V}{V_{*o}}$	Rb ft.	V_{*b} ft./sec.	$\frac{V}{V_{*b}}$
1.	0.0298	0.0941	18.6	0.3155	0.0793	0.0357	8.83	0.0389	8.10	0.0882	0.0377	8.37
2.	0.0475	0.1228	18.7	0.3847	0.0987	0.0398	9.65	0.0445	8.65	0.1126	0.0425	9.05
3.	0.0658	0.1483	18.8	0.4413	0.1145	0.0429	10.28	0.0489	9.03	0.1333	0.0463	9.53
4.	0.0928	0.1814	18.9	0.5090	0.1333	0.0463	10.99	0.0540	9.42	0.1591	0.0506	10.06
5.	0.1175	0.2077	18.7	0.5630	0.1469	0.0486	11.58	0.0578	9.74	0.1783	0.0536	10.50
6.	0.1397	0.2312	18.9	0.6014	0.1583	0.0505	11.91	0.0610	9.86	0.1953	0.0561	10.72
7.	0.1688	0.2565	19.0	0.6549	0.1698	0.0523	12.52	0.0643	10.18	0.2117	0.0584	11.21
8.	0.1985	0.2825	19.0	0.6991	0.1808	0.0540	12.96	0.0674	10.37	0.2285	0.0607	11.52
9.	0.2223	0.3049	19.0	0.7289	0.1898	0.0553	13.19	0.0701	10.40	0.2431	0.0626	11.64
10.	0.2367	0.3148	19.1	0.7482	0.1935	0.0558	13.40	0.0712	10.50	0.2484	0.0632	11.84
11.	0.2635	0.3399	18.8	0.7712	0.2028	0.0571	13.50	0.0740	10.42	0.2651	0.0654	11.79
12.	0.3178	0.3808	19.0	0.8303	0.2166	0.0590	14.06	0.0783	10.60	0.2882	0.0681	12.20

Table 8. Stabilized sand rippled bed, slope = 0.0010

1.	0.0479	0.1004	18.9	0.4744	0.0837	0.0519	9.14	0.0569	8.34	0.0940	0.0550	8.63
2.	0.0637	0.1188	19.2	0.5339	0.0960	0.0556	9.60	0.0618	8.63	0.1098	0.0594	8.99
3.	0.0805	0.1353	19.2	0.5918	0.1066	0.0586	10.10	0.0660	8.96	0.1236	0.0631	9.38
4.	0.1051	0.1584	19.3	0.6601	0.1205	0.0623	10.60	0.0714	9.24	0.1424	0.0676	9.76
5.	0.1290	0.1775	18.7	0.7230	0.1312	0.0650	11.12	0.0756	9.56	0.1570	0.0710	10.18
6.	0.1586	0.2008	18.9	0.7860	0.1434	0.0680	11.56	0.0804	9.77	0.1747	0.0750	10.48
7.	0.2060	0.2343	19.0	0.8751	0.1598	0.0717	12.20	0.0868	10.07	0.1990	0.0800	10.94
8.	0.2380	0.2522	19.3	0.9393	0.1679	0.0735	12.78	0.0901	10.42	0.2103	0.0822	11.43
9.	0.2635	0.2678	18.9	0.9787	0.1747	0.0750	13.05	0.0929	10.54	0.2207	0.0842	11.62
10.	0.3176	0.3050	19.2	1.0360	0.1898	0.0782	13.25	0.0991	10.45	0.2470	0.0891	11.63
11.	0.3561	0.3254	18.8	1.0887	0.1975	0.0798	13.65	0.1024	10.64	0.2589	0.0912	11.94
12.	0.3917	0.3469	19.0	1.1234	0.2052	0.0813	13.82	0.1057	10.63	0.2727	0.0937	11.99
13.	0.4386	0.3737	19.0	1.1679	0.2143	0.0831	14.06	0.1097	10.65	0.2894	0.0964	12.11

Table 9. Stabilized sand rippled bed, slope = 0.0015

Run No.	Q cu.ft./sec.	d ft.	Temp. OC	V ft./sec.	R ft.	V_* ft./sec.	$\frac{V}{V_*}$	V_{*o} ft./sec.	$\frac{V}{V_{*o}}$	Rb ft.	V_{*b} ft./sec.	$\frac{V}{V_{*b}}$
1.	0.0438	0.0845	19.1	0.5155	0.0723	0.0591	8.72	0.0639	8.07	0.0801	0.0622	8.29
2.	0.0622	0.1030	19.1	0.6013	0.0855	0.0643	9.36	0.0705	8.52	0.0964	0.0683	8.80
3.	0.0818	0.1205	19.1	0.6752	0.0972	0.0685	9.85	0.0763	8.85	0.1114	0.0734	9.20
4.	0.1019	0.1372	19.0	0.7393	0.1077	0.0721	10.25	0.0814	9.08	0.1254	0.0779	9.49
5.	0.1279	0.1565	19.1	0.8130	0.1193	0.0759	10.71	0.0869	9.35	0.1411	0.0826	9.84
6.	0.1587	0.1770	19.2	0.8920	0.1309	0.0795	11.22	0.0925	9.65	0.1572	0.0871	10.24
7.	0.2026	0.2039	19.2	0.9885	0.1450	0.0837	11.81	0.0992	9.96	0.1776	0.0927	10.66
8.	0.2379	0.2242	19.3	1.0558	0.1550	0.0865	12.20	0.1041	10.14	0.1922	0.0964	10.95
9.	0.2522	0.2329	18.5	1.0772	0.1592	0.0877	12.29	0.1061	10.15	0.1987	0.0981	10.98
10.	0.3364	0.2758	18.9	1.2136	0.1781	0.0928	13.09	0.1154	10.51	0.2283	0.1050	11.56
11.	0.3845	0.3014	19.3	1.2692	0.1864	0.0954	13.30	0.1207	10.52	0.2466	0.1091	11.63
12.	0.4357	0.3227	18.5	1.3436	0.1965	0.0974	13.79	0.1249	10.76	0.2585	0.1118	12.02
13.	0.5154	0.3600	18.5	1.4244	0.2097	0.1006	14.15	0.1319	10.80	0.2823	0.1189	11.98

Table 10. Stabilized sand rippled bed, slope = 0.0020

1.	0.0441	0.0783	18.7	0.5600	0.0678	0.0661	8.48	0.0710	7.88	0.0747	0.0694	8.07
2.	0.0637	0.0961	18.9	0.6595	0.0807	0.0721	9.15	0.0787	8.38	0.0905	0.0764	8.63
3.	0.0804	0.1098	19.0	0.7280	0.0901	0.0762	9.55	0.0841	8.65	0.1025	0.0813	8.95
4.	0.1006	0.1249	18.9	0.8013	0.1000	0.0803	9.98	0.0897	8.93	0.1153	0.0861	9.30
5.	0.1286	0.1437	19.1	0.8908	0.1117	0.0848	10.50	0.0962	9.26	0.1310	0.0919	9.69
6.	0.1592	0.1624	19.1	0.9754	0.1227	0.0889	10.97	0.1023	9.54	0.1461	0.0970	10.05
7.	0.1992	0.1845	19.2	1.0740	0.1350	0.0932	11.52	0.1090	9.85	0.1632	0.1025	10.48
8.	0.2328	0.2025	19.2	1.1440	0.1443	0.0964	11.87	0.1142	10.02	0.1770	0.1068	10.71
9.	0.2866	0.2266	19.1	1.2585	0.1562	0.1003	12.55	0.1208	10.42	0.1941	0.1118	11.25
10.	0.3781	0.2721	19.4	1.3827	0.1765	0.1066	12.97	0.1324	10.45	0.2276	0.1210	11.43
11.	0.4252	0.2905	17.9	1.4565	0.1841	0.1089	13.38	0.1368	10.65	0.2390	0.1241	11.74
12.	0.4751	0.3120	18.2	1.5151	0.1925	0.1113	13.61	0.1416	10.70	0.2536	0.1278	11.86
13.	0.5293	0.3317	18.4	1.5879	0.1998	0.1134	14.00	0.1462	10.86	0.2654	0.1306	12.16
14.	0.5842	0.3540	18.5	1.6420	0.2077	0.1157	14.20	0.1510	10.87	0.2799	0.1341	12.24
15.	0.6239	0.3710	18.7	1.6733	0.2134	0.1172	14.27	0.1546	10.82	0.2908	0.1369	12.22

Table 11. Stabilized sand rippled bed, slope = 0.0025

Rtn No.	Q cu.ft./sec.	d ft.	Temp. OC	V ft./sec.	R ft.	V_* ft./sec.	$\frac{V}{V_*}$	V_{*o} ft./sec.	$\frac{V}{V_{*o}}$	Rb ft.	V_{*b} ft./sec.	$\frac{V}{V_{*b}}$
1.	0.0660	0.0924	18.9	0.7111	0.0781	0.0793	8.97	0.0863	8.24	0.0874	0.0840	8.47
2.	0.0788	0.1020	18.9	0.7687	0.0848	0.0826	9.30	0.0906	8.48	0.0959	0.0879	8.75
3.	0.1067	0.1215	18.9	0.8740	0.0978	0.0888	9.85	0.0989	8.83	0.1127	0.0953	9.17
4.	0.1456	0.1458	18.8	0.9939	0.1130	0.0954	10.41	0.1084	9.16	0.1332	0.1033	9.62
5.	0.1952	0.1717	18.6	1.1313	0.1280	0.1015	11.15	0.1176	9.62	0.1538	0.1111	10.18
6.	0.2308	0.1896	18.6	1.2114	0.1377	0.1053	11.50	0.1236	9.80	0.1680	0.1161	10.43
7.	0.2823	0.2119	18.4	1.3254	0.1491	0.1096	12.10	0.1306	10.15	0.1844	0.1218	10.88
8.	0.3365	0.2355	18.2	1.4217	0.1604	0.1136	12.51	0.1377	10.32	0.2018	0.1274	11.16
9.	0.3868	0.2552	18.5	1.5082	0.1692	0.1167	12.92	0.1433	10.52	0.2155	0.1317	11.45
10.	0.4320	0.2738	18.3	1.5697	0.1773	0.1195	13.14	0.1485	10.57	0.2288	0.1357	11.57
11.	0.4566	0.2842	18.6	1.5988	0.1815	0.1209	13.23	0.1512	10.57	0.2363	0.1378	11.60
12.	0.5293	0.3133	18.4	1.6807	0.1930	0.1247	13.48	0.1588	10.58	0.2567	0.1435	11.71
13.	0.5831	0.3343	18.3	1.7359	0.2007	0.1271	13.65	0.1640	10.58	0.2710	0.1475	11.77
14.	0.6398	0.3550	18.6	1.7931	0.2080	0.1294	13.86	0.1690	10.60	0.2844	0.1511	11.87
15.	0.6893	0.3721	18.7	1.8432	0.2138	0.1312	14.05	0.1731	10.65	0.2956	0.1541	11.96

Table 12. Stabilized sand rippled bed, slope = 0.0030

1.	0.0980	0.1107	18.7	0.8811	0.0907	0.0937	9.40	0.1034	8.55	0.1037	0.1000	8.81
2.	0.1239	0.1254	19.2	0.9833	0.1004	0.0985	9.98	0.1100	8.94	0.1162	0.1060	9.28
3.	0.1554	0.1425	19.0	1.0853	0.1110	0.1036	10.48	0.1173	9.25	0.1305	0.1122	9.67
4.	0.2336	0.1790	18.7	1.2985	0.1320	0.1129	11.50	0.1315	9.87	0.1595	0.1241	10.46
5.	0.2704	0.1958	18.5	1.3740	0.1409	0.1167	11.78	0.1376	10.00	0.1728	0.1291	10.64
6.	0.3241	0.2178	18.6	1.4805	0.1520	0.1211	12.22	0.1450	10.20	0.1893	0.1351	10.96
7.	0.3672	0.2358	18.6	1.5492	0.1605	0.1245	12.44	0.1509	10.25	0.2030	0.1402	11.05
8.	0.4029	0.2498	19.0	1.6044	0.1669	0.1270	12.64	0.1554	10.34	0.2133	0.1434	11.19
9.	0.4502	0.2670	19.0	1.6778	0.1744	0.1298	12.93	0.1606	10.42	0.2255	0.1476	11.37
10.	0.5065	0.2883	19.0	1.7478	0.1844	0.1335	13.10	0.1669	10.45	0.2409	0.1525	11.46
11.	0.5631	0.3078	19.1	1.8200	0.1909	0.1358	13.40	0.1725	10.53	0.2542	0.1568	11.60
12.	0.6190	0.3273	19.2	1.8815	0.1982	0.1384	13.60	0.1779	10.59	0.2676	0.1608	11.70
13.	0.6792	0.3453	19.2	1.9569	0.2047	0.1406	13.92	0.1827	10.71	0.2788	0.1641	11.93

Table 13. Rippled bed with gravel in troughs, slope = 0.0005

Run No.	Q cu.ft./sec.	d ft.	Temp. OC	V ft./sec.	R ft.	V_* ft./sec.	$\frac{V}{V_*}$	V_{*o} ft./sec.	$\frac{V}{V_{*o}}$	Rb ft.	V_{*b} ft./sec.	$\frac{V}{V_{*b}}$
1.	0.0467	0.1114	20.7	0.4144	0.0912	0.0383	10.81	0.0424	9.78	0.1012	0.0404	10.25
2.	0.0608	0.1309	20.5	0.4623	0.1039	0.0409	11.30	0.0459	10.07	0.1170	0.0434	10.65
3.	0.0775	0.1508	20.9	0.5114	0.1160	0.0432	11.83	0.0493	10.38	0.1323	0.0462	11.08
4.	0.1009	0.1761	21.0	0.5700	0.1304	0.0458	12.44	0.0532	10.70	0.1509	0.0493	11.56
5.	0.1249	0.2021	20.9	0.6149	0.1441	0.0482	12.76	0.0570	10.78	0.1695	0.0522	11.78
6.	0.1579	0.2303	20.8	0.6825	0.1579	0.0504	13.54	0.0609	11.20	0.1880	0.0550	12.41
7.	0.1899	0.2601	20.8	0.7266	0.1714	0.0525	13.83	0.0647	11.23	0.2083	0.0579	12.55
8.	0.2211	0.2851	20.9	0.7716	0.1819	0.0541	14.26	0.0678	11.39	0.2230	0.0600	12.86
9.	0.2605	0.3154	20.6	0.8219	0.1938	0.0558	14.71	0.0713	11.53	0.2403	0.0622	13.21

Table 14. Rippled bed with gravel in troughs, slope = 0.0010

1.	0.0470	0.0928	20.8	0.5047	0.0783	0.0502	10.05	0.0547	9.23	0.0864	0.0528	9.56
2.	0.0578	0.1045	21.0	0.5504	0.0865	0.0528	10.43	0.0580	9.49	0.0964	0.0557	9.88
3.	0.0794	0.1251	20.8	0.6316	0.1002	0.0568	11.12	0.0635	9.95	0.1133	0.0604	10.46
4.	0.1035	0.1467	20.9	0.7023	0.1135	0.0605	11.61	0.0687	10.22	0.1306	0.0649	10.82
5.	0.1279	0.1659	21.0	0.7668	0.1247	0.0634	12.10	0.0731	10.50	0.1454	0.0684	11.21
6.	0.1514	0.1833	21.2	0.8222	0.1343	0.0658	12.50	0.0768	10.70	0.1582	0.0714	11.51
7.	0.1877	0.2090	21.1	0.8936	0.1476	0.0689	12.96	0.0820	10.89	0.1761	0.0754	11.85
8.	0.2241	0.2331	21.1	0.9565	0.1592	0.0716	13.36	0.0866	11.04	0.1937	0.0790	12.10
9.	0.2545	0.2527	21.2	1.0024	0.1681	0.0736	13.62	0.0902	11.11	0.2072	0.0818	12.25
10.	0.2900	0.2725	20.5	1.0589	0.1767	0.0754	14.04	0.0937	11.30	0.2193	0.0840	12.60
11.	0.3286	0.2933	20.6	1.1146	0.1852	0.0772	14.43	0.0972	11.47	0.2318	0.0865	12.88
12.	0.3756	0.3204	20.8	1.1665	0.1957	0.0794	14.70	0.1016	11.49	0.2489	0.0896	13.02

Table 15. Rippled bed with gravel in troughs, slope = 0.0015

Run No.	Q cu.ft./ sec.	d ft.	Temp. OC	V ft./sec.	R ft.	V_* ft./sec.	$\frac{V}{V_*}$	V_{*o} ft./sec.	$\frac{V}{V_{*o}}$	Rb ft.	V_{*b} ft./sec.	$\frac{V}{V_{*b}}$
1.	0.0497	0.0843	20.6	0.5864	0.0722	0.0591	9.93	0.0638	9.19	0.0792	0.0619	9.47
2.	0.0671	0.1011	20.7	0.6602	0.0842	0.0638	10.35	0.0699	9.45	0.0937	0.0672	9.82
3.	0.0925	0.1217	20.8	0.7560	0.0980	0.0689	10.99	0.0767	9.86	0.1110	0.0732	10.32
4.	0.1243	0.1443	21.0	0.8572	0.1121	0.0736	11.65	0.0835	10.26	0.1292	0.0790	10.85
5.	0.1597	0.1680	21.0	0.9456	0.1259	0.0780	12.12	0.0901	10.50	0.1487	0.0846	11.18
6.	0.1933	0.1883	21.0	1.0210	0.1370	0.0813	12.55	0.0954	10.70	0.1631	0.0888	11.50
7.	0.2238	0.2042	20.7	1.0908	0.1452	0.0837	13.03	0.0993	10.98	0.1742	0.0918	11.88
8.	0.2611	0.2250	20.9	1.1547	0.1554	0.0866	13.32	0.1043	11.08	0.1892	0.0956	12.08
9.	0.3095	0.2498	21.0	1.2332	0.1668	0.0898	13.74	0.1098	11.23	0.2062	0.0999	12.34
10.	0.3568	0.2725	21.0	1.3027	0.1767	0.0924	14.10	0.1147	11.35	0.2212	0.1033	12.61
11.	0.3956	0.2917	20.9	1.3496	0.1845	0.0944	14.29	0.1187	11.37	0.2336	0.1061	12.72
12.	0.4423	0.3138	21.0	1.4026	0.1932	0.0966	14.52	0.1231	11.39	0.2482	0.1093	12.83

Table 16. Fully gravelled bed, slope = 0.0005

Run No.	Q cu.ft./sec.	d ft.	Temp. OC	V ft./sec.	R ft.	V_* ft./sec.	$\frac{V}{V_*}$	V_{*o} ft./sec.	$\frac{V}{V_{*o}}$	Rb ft.	V_{*b} ft./sec.	$\frac{V}{V_{*b}}$
1.	0.0303	0.0850	18.5	0.3544	0.0727	0.0342	10.36	0.0370	9.58	0.0787	0.0356	9.95
2.	0.0458	0.1089	18.4	0.4180	0.0895	0.0380	11.01	0.0419	9.98	0.0987	0.0399	10.48
3.	0.0609	0.1296	18.6	0.4675	0.1029	0.0407	11.48	0.0457	10.23	0.1154	0.0431	10.84
4.	0.0800	0.1520	18.6	0.5240	0.1167	0.0434	12.09	0.0495	10.58	0.1325	0.0462	11.34
5.	0.0987	0.1727	18.7	0.5686	0.1285	0.0455	12.50	0.0527	10.78	0.1479	0.0488	11.65
6.	0.1276	0.2007	18.8	0.6326	0.1434	0.0485	13.04	0.0569	11.13	0.1672	0.0519	12.19
7.	0.1581	0.2296	18.8	0.6854	0.1576	0.0504	13.61	0.0607	11.28	0.1868	0.0548	12.50
8.	0.1918	0.2592	18.9	0.7363	0.1710	0.0525	14.03	0.0636	11.58	0.2058	0.0576	12.79
9.	0.2283	0.2867	18.9	0.7924	0.1825	0.0542	14.62	0.0679	11.66	0.2210	0.0597	13.28
10.	0.2557	0.3096	19.0	0.8219	0.1916	0.0555	14.80	0.0706	11.64	0.2352	0.0615	13.35
11.	0.2825	0.3297	19.0	0.8525	0.1991	0.0566	15.06	0.0729	11.70	0.2463	0.0630	13.54

Table 17. Fully gravelled bed, slope = 0.0010

1.	0.0409	0.0835	19.1	0.4875	0.0716	0.0480	10.15	0.0518	9.40	0.0780	0.0501	9.73
2.	0.0586	0.1031	19.1	0.5654	0.0855	0.0525	10.77	0.0576	9.81	0.0947	0.0552	10.24
3.	0.0785	0.1226	19.2	0.6376	0.0985	0.0563	11.32	0.0628	10.15	0.1107	0.0597	10.68
4.	0.0988	0.1408	19.3	0.6982	0.1100	0.0595	11.73	0.0673	10.37	0.1254	0.0635	10.99
5.	0.1255	0.1621	19.3	0.7706	0.1226	0.0628	12.27	0.0722	10.67	0.1417	0.0675	11.41
6.	0.1558	0.1844	19.3	0.8408	0.1349	0.0659	12.76	0.0770	10.91	0.1582	0.0714	11.78
7.	0.1895	0.2067	18.9	0.9125	0.1464	0.0687	13.29	0.0816	11.19	0.1737	0.0748	12.20
8.	0.2231	0.2283	18.9	0.9722	0.1570	0.0711	13.67	0.0858	11.34	0.1885	0.0779	12.48
9.	0.2622	0.2509	19.0	1.0400	0.1674	0.0734	14.17	0.0899	11.57	0.2028	0.0808	12.87
10.	0.3224	0.2873	19.1	1.1166	0.1828	0.0767	14.55	0.0962	11.61	0.2264	0.0854	13.08
11.	0.3785	0.3179	19.1	1.1848	0.1947	0.0792	14.96	0.1012	11.71	0.2448	0.0888	13.35

Table 18. Fully gravelled bed, slope = 0.0015

Run No.	Q cu.ft./sec.	d ft.	Temp. °C	V ft./sec.	R ft.	V_* ft./sec.	$\frac{V}{V_*}$	V_{*o} ft./sec.	$\frac{V}{V_{*o}}$	Rb ft.	V_{*b} ft./sec.	$\frac{V}{V_{*b}}$
1.	0.0441	0.0775	18.9	0.5662	0.0672	0.0570	9.94	0.0612	9.25	0.0729	0.0593	9.54
2.	0.0632	0.0953	19.0	0.6594	0.0801	0.0622	10.60	0.0679	9.71	0.0884	0.0653	10.09
3.	0.0936	0.1204	19.0	0.7730	0.0971	0.0685	11.28	0.0763	10.13	0.1094	0.0727	10.63
4.	0.1240	0.1422	19.0	0.8675	0.1108	0.0732	11.86	0.0829	10.47	0.1269	0.0783	11.08
5.	0.1605	0.1659	18.6	0.9626	0.1247	0.0776	12.40	0.0895	10.75	0.1453	0.0838	11.49
6.	0.2060	0.1925	18.8	1.0650	0.1392	0.0820	12.99	0.0964	11.04	0.1649	0.0892	11.93
7.	0.2497	0.2154	18.9	1.1535	0.1508	0.0853	13.52	0.1020	11.30	0.1809	0.0935	12.34
8.	0.3044	0.2431	18.9	1.2460	0.1638	0.0890	14.00	0.1083	11.50	0.1996	0.0982	12.69
9.	0.3626	0.2706	18.9	1.3336	0.1759	0.0922	14.47	0.1143	11.66	0.2174	0.1025	13.02
10.	0.4485	0.3083	18.9	1.4473	0.1911	0.0961	15.07	0.1220	11.86	0.2404	0.1078	13.43

Table 19. Fully gravelled bed, slope = 0.0020

1.	0.0453	0.0729	18.6	0.6186	0.0637	0.0640	9.66	0.0685	9.03	0.0690	0.0667	9.28
2.	0.0634	0.0883	18.7	0.7140	0.0751	0.0696	10.26	0.0754	9.47	0.0826	0.0729	9.79
3.	0.0855	0.1072	18.7	0.8209	0.0884	0.0755	10.88	0.0831	9.88	0.0988	0.0798	10.29
4.	0.1245	0.1304	18.8	0.9497	0.1035	0.0816	11.63	0.0916	10.36	0.1178	0.0871	10.90
5.	0.1718	0.1575	18.8	1.0852	0.1199	0.0879	12.35	0.1007	10.77	0.1391	0.0946	11.47
6.	0.2049	0.1758	18.5	1.1598	0.1302	0.0916	12.66	0.1064	10.90	0.1532	0.0993	11.68
7.	0.2596	0.2019	18.6	1.2791	0.1440	0.0963	13.28	0.1140	11.22	0.1722	0.1053	12.15
8.	0.3001	0.2212	18.3	1.3498	0.1536	0.0995	13.57	0.1194	11.30	0.1860	0.1095	12.33
9.	0.3526	0.2442	18.4	1.4366	0.1644	0.1029	13.96	0.1254	11.45	0.2018	0.1140	12.60
10.	0.4131	0.2688	18.5	1.5297	0.1751	0.1062	14.40	0.1316	11.63	0.2178	0.1184	12.92

APPENDIX II.B. VELOCITY DISTRIBUTION AND TURBULENCE RESULTS

The various quantities in Tables 1 - 18 are as follows:

y = Distance from wall in cm.

$\bar{u}$ = Local mean velosity in cm./sec.

$\sqrt{\overline{u'^2}}$ = Intensity of Turbulence velosity in X-axis in cm./Sec.

$\sqrt{\overline{v'^2}}$ = Intensity of Turbulence velosity in Y-axis in cm./sec.

$-\overline{u'v'}$ = Turbulence shear stress/mass density of fluid in cm.2/sec.2

$\Psi = \frac{\overline{u'v'}}{\sqrt{\overline{u'^2}}\sqrt{\overline{v'^2}}}$ the Coefficient of Correlation

Note: Values marked with crosses are omitted

Table 1. Smooth bed; d = 1.55 cm., S = 0.0005, Temp. = 19.4°c
$V_{*o} = \sqrt{\tau_o/\rho}$ = 0.872 cm./sec

y cm.	u cm./sec.	$\sqrt{\overline{u'^2}}$ cm./secs	$\sqrt{\overline{v'^2}}$ cm./sec.	$-\overline{u'v'}$ cm.2/sec.2	$\frac{u}{V_{*o}}$	$\frac{y V_{*o}}{\nu}$	$\frac{y}{d}$	$\frac{\sqrt{\overline{u'^2}}}{V_{*o}}$	$\frac{\sqrt{\overline{v'^2}}}{V_{*o}}$	$\frac{-\overline{u'v'}}{\tau_o/\rho}$	$-\Psi$
0.06	5.05	–	–	–	5.79	5.1	0.039	–	–	–	–
0.07	5.20	–	–	–	5.96	6.0	0.045	–	–	–	–
0.08	6.05	–	–	–	6.94	6.8	0.051	–	–	–	–
0.09	6.20	–	–	–	7.11	7.7	0.058	–	–	–	–
0.15	9.05	2.09	0.25	0.40	10.37	12.8	0.097	2.40	0.29	0.53	0.76
0.25	10.80	1.88	0.39	0.47	12.40	21.3	0.161	2.16	0.44	0.61	0.64
0.40	12.15	1.88	0.73	0.50	13.93	34.1	0.258	2.16	0.83	0.66	0.37
0.60	13.80	1.31	0.55	0.47	15.82	51.2	0.387	1.51	0.63	0.62	0.65
0.80	14.35	1.55	0.49	0.39	16.45	68.2	0.516	1.77	0.56	0.51	0.51
1.00	14.55	1.98	0.55	0.27	16.70	85.3	0.645	1.12	0.63	0.35	0.49
1.20	15.15	1.04	0.40	0.23	17.37	102.4	0.774	1.19	0.45	0.30	0.55
1.40	15.85	0.73	0.31	0.10	18.18	119.5	0.903	0.84	0.36	0.13	0.44
1.55	15.85	0.68	0.00	0.00	18.18	132.2	1.000	0.78	0.00	0.00	0.00

Table 2. Smooth bed; d = 2.58 cm., S = 0.0005, Temp. = 19.3°c
$V_{*o} = \sqrt{\tau_o/\rho}$ = 1.125 cm./sec.

0.03	3.05	–	–	–	2.71	3.3	0.012	–	–	–	–
0.04	4.35	–	–	–	3.87	4.4	0.015	–	–	–	–
0.05	6.15	–	–	–	5.47	5.5	0.019	–	–	–	–
0.07	8.80	–	–	–	7.82	7.7	0.027	–	–	–	–
0.10	10.65	–	–	–	9.46	11.0	0.039	–	–	–	–
0.15	12.70	2.60	0.67	0.65	11.29	16.5	0.058	2.31	0.60	0.51	0.37
0.25	15.15	2.15	1.02	1.09	13.46	27.4	0.097	1.91	0.90	0.86	0.50
0.40	16.40	1.53	0.94	0.65	14.60	43.9	0.155	1.36	0.84	0.51	0.45
0.60	17.00	1.60	1.00	1.04	15.10	65.8	0.233	1.42	0.89	0.82	0.65
0.80	18.50	1.35	0.84	0.52	16.44	87.8	0.310	1.20	0.75	0.41	0.46
1.00	19.10	1.30	0.95	0.71	17.00	109.7	0.388	1.16	0.84	0.56	0.58
1.20	18.90	1.40	0.75	0.68	16.80	131.6	0.465	1.25	0.67	0.54	0.64
1.40	19.40	1.66	0.96	0.56	17.25	153.5	0.543	1.48	0.85	0.44	0.35
1.60	20.45	1.21	0.66	0.40	18.17	175.5	0.620	1.08	0.59	0.32	0.50
1.80	21.10	0.93	0.52	0.35	18.75	197.4	0.700	0.82	0.46	0.28	0.73
2.00	20.50	1.08	0.47	0.35	18.22	219.3	0.775	0.96	0.42	0.27	0.69
2.20	20.90	0.99	0.80	0.22	18.57	241.3	0.853	0.88	0.70	0.17	0.28
2.40	21.65	0.97	0.22	0.11	19.24	263.2	0.930	0.86	0.20	0.09	0.50
2.58	21.80	0.92	0.00	0.00	19.36	283.0	1.000	0.82	0.00	0.00	0.00

Table 3. Smooth bed; d = 2.555 cm., S = 0.0010, Temp. = 19.2°c
$V_{*o} = \sqrt{\tau_o/\rho}$ = 1.583 cm./sec.

y cm.	$\bar{u}$ cm./sec.	$\sqrt{\overline{u'^2}}$ cm./sec.	$\sqrt{\overline{v'^2}}$ cm./sec.	$-\overline{u'v'}$ cm.2/sec.2	$\frac{\bar{u}}{V_{*o}}$	$\frac{y V_{*o}}{\nu}$	$\frac{y}{d}$	$\frac{\sqrt{\overline{u'^2}}}{V_{*o}}$	$\frac{\sqrt{\overline{v'^2}}}{V_{*o}}$	$\frac{-\overline{u'v'}}{\tau_o/\rho}$	$-\psi$
0.05	12.95	3.54	0.67	0.93	8.18	7.7	0.020	2.24	0.42	0.37	0.39
0.15	19.60	3.84	1.46	2.00	12.38	23.2	0.059	2.42	0.92	0.80	0.36
0.25	21.65	2.62	1.66	2.06	13.67	38.6	0.098	1.66	1.05	0.82	0.47
0.40	23.95	2.67	1.45	2.19	15.12	61.7	0.156	1.69	0.92	0.88	0.56
0.60	26.10	2.47	1.50	1.95	16.48	92.6	0.235	1.56	0.95	0.78	0.53
0.80	26.70	1.91	1.37	1.28	16.86	123.5	0.313	1.21	0.86	0.51	0.49
1.00	27.85	2.02	1.14	0.87	17.60	154.3	0.391	1.28	0.72	0.35	0.38
1.20	28.80	2.00	1.20	1.45	18.19	185.2	0.470	1.26	0.76	0.58	0.60
1.40	29.60	1.73	1.14	0.94	18.69	216.0	0.548	1.09	0.72	0.38	0.48
1.60	29.90	1.70	0.96	0.97	18.88	247.0	0.626	1.07	0.60	0.39	0.60
1.80	29.70	1.92	1.03	0.76	18.76	277.8	0.705	1.21	0.65	0.30	0.38
2.00	31.70	1.49	0.74	0.59	20.02	308.7	0.783	0.94	0.47	0.24	0.54
2.20	31.05	1.48	0.69	0.31	19.61	339.5	0.861	0.94	0.44	0.12	0.30
2.40	31.35	1.26	0.56	0.18	19.80	370.4	0.939	0.79	0.35	0.07	0.26
2.55	32.00	1.00	0.00	0.00	20.21	394.3	1.000	0.63	0.00	0.00	0.00

Table 4. Smooth bed; d = 5.095 cm., S = 0.0010, Temp. = 19.4°c
$V_{*o} = \sqrt{\tau_o/\rho}$ = 2.236 cm./sec.

0.10	26.20	4.69	0.92	1.80	11.72	21.9	0.020	2.10	0.41	0.36	0.42
0.20	31.00	4.42	1.89	3.62	13.86	43.7	0.039	1.98	0.85	0.72	0.43
0.40	35.10	3.76	1.92	4.16	15.70	87.5	0.078	1.68	0.86	0.83	0.58
0.60	36.80	4.08	2.01	4.76	16.46	131.3	0.118	1.82	0.90	0.95	0.58
0.80	40.00	3.92	2.04	4.55	17.89	175.0	0.157	1.75	0.91	0.91	0.57
1.20	41.65	2.85	1.82	2.90	18.63	262.5	0.235	1.28	0.82	0.58	0.56
1.60	43.20	2.64	1.86	2.00	19.32	350.0	0.314	1.18	0.83	0.40	0.41
2.00	43.10	3.08	1.95	3.45	19.27	437.6	0.392	1.38	0.87	0.69	0.58
2.40	45.45	2.69	1.77	2.53	20.33	525.1	0.470	1.20	0.79	0.51	0.53
2.80	46.00	3.08	1.70	2.95	20.57	612.6	0.549	1.38	0.76	0.59	0.56
3.20	47.40	2.65	1.22	1.14	21.20	700.0	0.627	1.18	0.55	0.23	0.35
3.60	47.30	2.04	1.34	0.50	21.15	787.7	0.706	0.91	0.60	0.10	0.18
4.00	48.25	1.78	1.37	1.01	21.58	875.2	0.784	0.79	0.61	0.20	0.42
4.40	48.25	2.18	1.39	0.86	21.58	962.7	0.863	0.97	0.62	0.17	0.28
4.80	49.65	1.93	0.52	0.25	22.20	1050.0	0.941	0.86	0.23	0.05	0.25
5.10	50.00	1.72	0.00	0.00	22.36	1115.0	1.000	0.77	0.00	0.00	0.00

Table 5. Rippled bed; d = 3.83 cm., S = 0.0005, Temp. = 17.8°c
$V_{*o} = \sqrt{\tau_o/\rho}$ = 1.37 cm./sec.

y cm.	u cm./sec.	$\sqrt{\overline{u'^2}}$ cm./sec.	$\sqrt{\overline{v'^2}}$ cm./sec.	$-\overline{u'v'}$ cm.2/sec.2	$\frac{\bar{u}}{V_{*o}}$	$\frac{y V_{*o}}{\nu}$	$\frac{y}{d}$	$\frac{\sqrt{\overline{u'^2}}}{V_{*o}}$	$\frac{\sqrt{\overline{v'^2}}}{V_{*o}}$	$\frac{-\overline{u'v'}}{\tau_o/\rho}$	$-\psi$
0.30	6.50	1.12	1.62	1.28	4.74	38.5	0.078	0.81	1.18	0.68	0.70
0.70	8.75	1.93	1.98	1.47	6.38	89.9	0.183	1.41	1.44	0.78	0.38
1.10	10.10	1.66	1.42	1.44	7.36	141.3	0.287	1.21	1.03	0.76	0.61
1.50	10.70	1.90	1.51	1.09	7.80	192.6	0.391	1.38	1.10	0.58	0.38
1.90	12.00	1.36	1.29	0.46	8.75	244.0	0.495	0.99	0.94	0.25	0.26
2.30	12.50	1.34	1.01	0.51	9.11	295.3	0.600	0.98	0.73	0.27	0.38
2.70	13.75	1.35	1.08	0.59	10.02	346.7	0.704	0.98	0.79	0.31	0.40
3.10	14.75	1.02	0.94	0.28	10.75	398.1	0.809	0.74	0.69	0.15	0.29
3.50	15.30	0.98	0.44	0.26	11.15	449.5	0.913	0.71	0.32	0.14	0.60
3.83	15.60	0.97	0.00	0.00	11.37	492.2	1.000	0.71	0.00	0.00	0.00

Table 6. Rippled bed; d = 5.08 cm., S = 0.0005, Temp. = 17.6°c
$V_{*o} = \sqrt{\tau_o/\rho}$ = 1.579 cm./sec.

0.30	6.70	1.82	2.15	1.60	4.25	44.5	0.059	1.15	1.36	0.64	0.41
0.70	9.70	2.14	2.28	2.11	6.15	104.0	0.138	1.35	1.44	0.85	0.43
1.10	11.70	1.81	2.00	1.94	7.41	163.4	0.217	1.15	1.27	0.78	0.53
1.50	12.20	2.29	1.95	1.66	7.73	222.8	0.295	1.45	1.24	0.67	0.37
1.90	13.50	2.37	2.33	2.50	8.55	282.2	0.374	1.50	1.48	1.00	0.45
2.30	15.00	1.35	1.67	1.64	9.50	341.6	0.453	0.86	1.06	0.66	0.72
2.70	15.20	2.16	1.41	1.44	9.63	401.0	0.532	1.37	0.90	0.58	0.47
3.10	15.60	1.68	1.42	0.87	9.88	460.4	0.610	1.07	0.90	0.35	0.37
3.50	17.00	1.87	1.35	0.74	10.77	520.0	0.689	1.18	0.86	0.30	0.29
3.90	16.05	2.10	0.88	0.56	10.17	579.3	0.768	1.33	0.56	0.22	0.30
4.30	17.60	1.85	1.13	1.24	11.15	638.7	0.847	1.17	0.72	0.50	0.59
4.70	17.90	1.72	0.54	0.57	11.34	698.1	0.926	1.09	0.35	0.22	0.61
5.08	18.70	1.69	0.00	0.00	11.85	754.2	1.000	1.07	0.00	0.00	0.00

Table 7. Rippled bed; d = 6.34 c.m., S = 0.0005, Temp. = 19.9°c
$V_{*o} = \sqrt{\tau_o/\rho}$ = 1.764 cm./sec.

y cm.	u cm./sec.	$\sqrt{\overline{u'^2}}$ cm./sec.	$\sqrt{\overline{v'^2}}$ cm./sec.	$-\overline{u'v'}$ cm.2/sec.2	$\frac{u}{V_{*o}}$	$\frac{y\,V_{*o}}{\nu}$	$\frac{y}{d}$	$\frac{\sqrt{\overline{u'^2}}}{V_{*o}}$	$\frac{\sqrt{\overline{v'^2}}}{V_{*o}}$	$\frac{-\overline{u'v'}}{\tau_o/\rho}$	$-\psi$
0.30	7.70	1.21	2.85	2.85	4.36	52.4	0.047	0.68	1.61	0.92	0.83
0.70	11.15	2.02	2.27	2.01	6.32	122.3	0.110	1.14	1.28	0.65	0.44
1.10	12.10	2.76	2.51	2.94	6.86	192.2	0.173	1.57	1.42	0.94	0.42
1.50	14.00	2.75	2.24	2.62	7.94	262.2	0.236	1.56	1.27	0.84	0.42
1.90	15.10	2.21	1.65	1.34	8.56	331.9	0.300	1.25	0.93	0.43	0.37
2.30	15.90	2.14	1.87	2.05	9.01	401.8	0.363	1.21	1.06	0.66	0.51
2.70	16.10	2.05	1.86	2.05	9.13	471.7	0.426	1.16	1.05	0.66	0.54
3.10	17.10	2.08	1.71	1.36	9.69	541.6	0.489	0.18	0.97	0.44	0.38
3.50	17.70	1.66	1.68	1.73	10.03	611.5	0.552	0.94	0.95	0.56	0.62
3.90	18.40	2.01	1.48	1.64	10.43	681.3	0.615	1.14	0.84	0.53	0.55
4.30	18.10	2.07	1.54	1.35	10.26	751.2	0.678	1.17	0.87	0.43	0.42
4.70	18.35	1.73	1.55	1.40	10.40	821.1	0.741	0.98	0.88	0.45	0.52
5.10	19.60	1.50	0.97	0.74	11.11	891.0	0.804	0.85	0.55	0.24	0.51
5.50	20.55	1.98	0.67	0.45	11.65	960.9	0.867	1.13	0.38	0.15	0.34
5.90	20.60	1.39	0.90	0.16	11.70	1030.7	0.930	0.79	0.51	0.05	0.13
6.34	21.30	1.48	0.00	0.00	12.07	1108.1	1.000	0.84	0.00	0.00	0.00

Table 8. Rippled bed; d = 5.18 cm., S = 0.0010, Temp. = 20.6°c
$V_{*o} = \sqrt{\tau_o/\rho}$ = 2.254 cm./sec.

0.30	9.90	2.24	2.88	4.62	4.39	68.1	0.058	0.99	1.28	0.91	0.72
0.70	13.80	3.55	3.07	5.06	6.12	159.0	0.135	1.57	1.36	1.00	0.47
1.10	15.95	2.79	2.98	4.72	7.08	250.0	0.212	1.24	1.32	0.93	0.57
1.50	18.70	2.62	2.62	3.61	8.30	340.7	0.290	1.16	1.16	0.71	0.53
1.90	20.00	2.55	1.79	1.45	8.87	431.6	0.367	1.13	0.79	0.29	0.32
2.30	21.20	1.84	2.02	1.75	9.40	522.5	0.444	0.82	0.90	0.34	0.47
2.70	21.20	1.83	1.98	2.27	9.40	613.3	0.522	0.81	0.88	0.45	0.63
3.10	23.00	2.50	2.09	2.30	10.20	704.2	0.599	1.11	0.93	0.45	0.44
3.50	23.50	2.40	1.43	0.90	10.43	795.0	0.676	1.06	0.64	0.18	0.26
3.90	24.20	2.17	1.49	0.55	10.74	885.9	0.753	0.96	0.66	0.11	0.17
4.30	24.60	1.97	1.59	1.17	10.91	976.8	0.831	0.88	0.70	0.23	0.37
4.70	25.40	1.84	1.05	0.50	11.27	1067.7	0.908	0.82	0.46	0.10	0.26
5.18	26.00	1.71	0.00	0.00	11.54	1175.8	1.000	0.76	0.00	0.00	0.00

Table 9. Rippled bed; d = 6.55 c.m., S = 0.0010, Temp. = 20.3°c
$V_{*o} = \sqrt{\tau_o/\rho}$ = 2.537 c.m./sec.

y cm.	$\bar{u}$ cm./sec.	$\sqrt{\overline{u'^2}}$ cm./sec.	$\sqrt{\overline{v'^2}}$ cm./sec.	$-\overline{u'v'}$ cm.2/sec.2	$\frac{\bar{u}}{V_{*o}}$	$\frac{y\,V_{*o}}{\nu}$	$\frac{y}{d}$	$\frac{\sqrt{\overline{u'^2}}}{V_{*o}}$	$\frac{\sqrt{\overline{v'^2}}}{V_{*o}}$	$\frac{-\overline{u'v'}}{\tau_o/\rho}$	$-\psi$
0.30	10.75	2.20	3.51	5.81	4.24	76.1	0.046	0.86	1.39	0.90	0.75
0.70	16.10	2.91	2.52	4.10	6.35	177.5	0.107	1.15	0.99	0.64	0.56
1.10	18.15	2.78	2.64	2.60	7.15	279.0	0.168	1.10	1.05	0.40	0.35
1.50	19.00	2.74	3.24	5.42	7.49	380.5	0.229	1.08	1.28	0.84	0.61
1.90	21.95	3.25	1.92	3.24	8.65	482.0	0.290	1.28	0.75	0.50	0.52
2.30	23.80	3.28	2.23	4.34	9.38	583.0	0.351	1.29	0.88	0.67	0.59
2.70	24.60	3.29	2.17	3.28	9.70	684.9	0.412	1.30	0.85	0.51	0.46
3.10	23.50	3.00	1.70	3.14	9.26	786.4	0.473	1.18	0.67	0.50	0.62
3.50	25.55	3.11	2.00	4.92	10.07	887.8	0.534	1.23	0.79	0.76	0.79
3.90	27.15	3.02	2.11	2.90	10.70	989.3	0.595	1.19	0.83	0.45	0.45
4.30	28.15	2.95	2.08	2.45	11.10	1090.8	0.656	1.16	0.82	0.38	0.40
4.70	28.05	3.93	2.21	2.53	11.06	1192.2	0.717	1.55	0.87	0.39	0.29
5.10	29.15	2.68	1.66	1.30	11.49	1293.7	0.778	1.06	0.66	0120	0.29
5.50	28.65	1.99	1.42	0.74	11.30	1395.2	0.939	0.78	0.56	0.12	0.26
5.90	29.35	2.18	1.38	0.70	11.57	1496.7	0.900	0.86	0.54	0.11	0.23
6.30	29.50	2.15	1.22	0.83	11.63	1598.1	0.961	0.85	0.48	0.13	0.32
6.55	30.10	2.69	0.00	0.00	11.87	1663.0	1.000	1.06	0.00	0.00	0.00

Table 10. Rippled bed with gravel in troughs;
d = 4.60 cm., S = 0.0005, Temp. = 20.9°c, ν°c.
$V_{*o} = \sqrt{\tau_o/\rho}$ = 1.503 cm./sec.

0.30	10.25	2.55	1.03	0.47	6.82	39.5	0.065	1.70	0.68	0.47	0.4(
0.70	13.15	2.47	1.56	0.65	8.75	92.1	0.152	1.64	1.04	0.65	0.38
1.10	13.60	1.83	1.30	0.60	9.05	144.7	0.239	1.22	0.87	0.60	0.57
1.50	15.35	2.07	1.14	0.66	10.22	197.4	0.326	1.38	0.76	0.66	0.64
1.90	16.70	1.80	1.09	0.44	11.11	250.0	0.413	1.20	0.73	0.44	0.51
2.30	17.85	2.30	0.83	0.46	11.88	302.6	0.500	1.53	0.55	0.46	0.55
2.70	18.20	1.60	0.93	0.39	12.11	355.2	0.587	1.06	0.62	0.39	0.59
3.10	18.20	1.79	0.93	0.30	12.11	408.0	0.674	1.19	0.62	0.30	0.41
3.50	18.60	1.30	0.83	0.33	12.38	460.5	0.760	0.87	0.55	0.33	0.69
3.90	19.00	1.48	1.13	0.24	12.65	513.1	0.848	0.98	0.75	0.24	0.32
4.30	19.50	1.10	0.51	0.06	12.98	565.8	0.935	0.73	0.34	0.06	0.25
4.60	20.40	1.35	0.00	0.00	13.58	605.2	1.000	0.90	0.00	0.00	0.00

Table 11. Rippled bed with gravel in troughs; d = 7.02 cm., S = 0.0005, Temp. = 20.8°c, $V_{*o} = \sqrt{\tau_o/\rho}$ = 1.856 cm./sec.

y cm.	$\bar{u}$ cm./sec.	$\sqrt{\bar{u}'^2}$ cm./sec.	$\sqrt{\bar{v}'^2}$ cm./sec.	$-\overline{u'v'}$ cm.^{2}/sec.^{2}	$\frac{\bar{u}}{V_{*o}}$	$\frac{y V_{*o}}{\nu}$	$\frac{y}{d}$	$\frac{\sqrt{\bar{u}'^2}}{V_{*o}}$	$\frac{\sqrt{\bar{v}'^2}}{V_{*o}}$	$\frac{-\overline{u'v'}}{\tau_o/\rho}$	$-\Psi$
0.30	12.10	2.84	1.41	2.04	6.52	48.7	0.043	1.53	0.76	0.59	0.51
0.70	15.00	2.44	1.52	2.43	8.08	113.5	0.100	1.32	0.82	0.71	0.65
1.10	15.80	2.20	1.90	2.55	8.51	178.5	0.157	1.18	1.02	0.74	0.67
1.50	17.00	1.65	1.75	2.29	9.16	243.4	0.214	0.89	0.94	0.66	0.79
1.90	20.00	3.16	1.15	1.75	10.75	308.2	0.270	1.70	0.62	0.51	0.48
2.30	21.25	2.81	1.70	2.10	11.45	373.1	0.328	1.52	0.92	0.61	0.44
2.70	22.05	2.55	1.75	2.27	11.88	438.0	0.385	1.38	0.94	0.66	0.51
3.10	22.60	2.31	2.02	2.26	12.18	503.0	0.442	1.25	1.09	0.65	0.48
3.50	23.50	2.14	1.78	2.03	12.66	568.0	0.500	1.15	0.96	0.59	0.53
3.90	24.50	1.83	1.42	1.54	13.20	632.7	0.556	0.99	0.77	0.45	0.59
4.30	24.15	1.91	1.67	1.78	13.01	697.6	0.613	1.03	0.90	0.52	0.56
4.70	24.90	1.74	1.20	0.97	13.42	762.5	0.670	0.94	0.65	0.28	0.46
5.10	25.40	1.95	1.16	1.16	13.68	827.4	0.726	1.05	0.62	0.34	0.51
5.50	25.55	2.21	1.00	1.18	13.77	892.3	0.783	1.19	0.54	0.34	0.53
5.90	26.40	2.30	0.92	0.92	14.22	957.2	0.840	1.24	0.50	0.27	0.43
6.30	27.25	1.90	0.71	0.74	14.68	1022.1	0.900	1.02	0.38	0.21	0.55
6.70	27.25	1.75	0.74	0.37	14.68	1087.0	0.954	0.95	0.40	0.10	0.29
7.02	27.40	1.51	0.00	0.00	14.76	1138.9	1.000	0.81	0.00	0.00	0.00

Table 12. Rippled with gravel in troughs; d = 3.81 cm., S = 0.0010, Temp. = 20.8°c, $V_{*o} = \sqrt{\tau_o/\rho}$ = 1.935 cm./sec.

0.30	12.55	3.12	2.28	3.42	6.49	50.7	0.078	1.61	1.18	0.91	0.48
0.76	17.60	2.49	1.91	2.52	9.10	118.4	0.184	1.29	0.99	0.67	0.53
1.10	18.90	2.56	1.80	2.75	9.77	186.0	0.288	1.32	0.93	0.74	0.60
1.50	20.60	3.08	1.70	2.56	10.65	253.7	0.393	1.59	0.88	0.68	0.49
1.90	22.20	2.61	1.76	2.04	11.47	321.3	0.498	1.35	0.91	0.55	0.41
2.30	23.60	1.84	1.60	0.78	12.20	389.0	0.603	0.95	0.83	0.21	0.27
2.70	24.15	1.94	1.34	1.22	12.48	456.6	0.708	1.00	0.69	0.33	0.47
3.10	25.10	1.79	0.86	0.27	12.97	524.2	0.813	0.93	0.45	0.07	0.18
3.50	25.55	1.60	0.70	0.70	13.20	591.9	0.918	0.83	0.36	0.19	0.62
3.81	26.00	1.54	0.00	0.00	13.44	645.0	1.000	0.80	0.00	0.00	0.00

Table 13. Rippled bed with gravel in troughs; d = 5.11 cm.
S = 0.0010, Temp. = 20.8°c, $V_{*o} = \sqrt{\tau_o/\rho}$ = 2.240 cm./sec.

y cm.	$\bar{u}$ cm./sec.	$\sqrt{\overline{u'^2}}$ cm./sec.	$\sqrt{\overline{v'^2}}$ cm./sec.	$-\overline{u'v'}$ cm.^{2}/sec.^{2}	$\frac{\bar{u}}{V_{*o}}$	$\frac{y V_{*o}}{\nu}$	$\frac{y}{d}$	$\frac{\sqrt{\overline{u'^2}}}{V_{*o}}$	$\frac{\sqrt{\overline{v'^2}}}{V_{*o}}$	$\frac{-\overline{u'v'}}{\tau_o/\rho}$	$-\Psi$
0.30	14.50	2.70	2.51	4.92	6.47	58.4	0.059	1.20	1.12	0.96	0.73
0.70	18.50	2.64	2.13	2.86	8.26	136.3	0.137	1.18	0.89	0.56	0.51
1.10	21.40	2.94	2.24	3.45	9.55	214.2	0.215	1.31	1.00	0.68	0.52
1.50	23.45	2.89	1.55	1.68	10.47	292.1	0.294	1.29	0.69	0.33	0.38
1.90	25.60	3.47	1.98	2.89	11.43	370.0	0.372	1.55	0.88	0.57	0.42
2.30	25.65	3.25	1.68	2.12	11.45	447.9	0.450	1.45	0.75	0.42	0.39
2.70	27.00	3.18	1.79	1.67	12.06	525.8	0.528	1.42	0.80	0.33	0.29
3.10	28.25	3.34	1.62	2.21	12.61	603.7	0.607	1.49	0.72	0.43	0.41
3.50	28.20	2.78	1.31	1.26	12.60	681.6	0.685	1.24	0.58	0.25	0.35
3.90	29.00	2.52	1.72	1.66	12.95	759.5	0.763	1.25	0.76	0.32	0.38
4.30	30.20	2.07	0.90	0.62	13.48	837.4	0.841	0.92	0.40	0.12	0.33
4.70	30.00	2.12	0.65	0.61	13.40	915.3	0.920	0.95	0.29	0.12	0.45
5.11	31.50	1.98	0.00	0.00	14.06	995.1	1.000	0.88	0.00	0.00	0.00

Table 14. Rippled bed with gravel in troughs; d = 6.37 cm. S = 0.0010,
Temp. = 21.1°c, $V_{*o} = \sqrt{\tau_o/\rho}$ = 2.500 cm./sec.

0.30	15.25	2.17	2.35	4.80	6.10	66.0	0.047	0.87	0.94	0.77	1.05
0.70	19.20	3.31	2.12	4.63	7.68	154.0	0.110	1.32	0.85	0.74	0.66
1.10	21.80	2.69	2.67	3.25	8.72	241.9	0.173	1.08	1.07	0.52	0.45
1.50	24.75	3.33	2.60	3.92	9.90	329.8	0.235	1.33	1.04	0.63	0.45
1.90	27.35	2.72	2.25	3.53	10.94	417.8	0.298	1.09	0.90	0.57	0.58
2.30	28.00	2.85	2.01	4.40	11.20	505.7	0.361	1.14	0.80	0.70	0.77
2.70	29.55	2.53	2.49	2.14	11.82	593.7	0.424	1.01	1.00	0.34	0.34
3.10	29.50	2.16	2.00	1.76	11.82	681.6	0.486	0.86	0.80	0.28	0.41
3.50	31.25	2.84	1.84	2.95	12.50	769.6	0.549	1.13	0.74	0.47	0.56
3.90	32.10	3.25	1.62	3.01	12.84	857.5	0.612	1.30	0.65	0.48	0.57
4.30	31.80	3.13	1.68	1.56	12.72	945.5	0.675	1.25	0.67	0.25	0.30
4.70	32.85	2.67	1.60	1.44	13.14	1033.4	0.738	1.07	0.64	0.23	0.34
5.10	33.45	2.72	1.40	1.15	13.38	1121.4	0.800	1.09	0.56	0.18	0.30
5.50	34.40	2.28	1.28	1.02	13.76	1209.3	0.863	0.91	0.51	0.16	0.35
5.90	35.00	2.12	0.80	0.44	14.00	1297.3	0.926	0.85	0.32	0.07	0.26
6.37	35.05	2.01	0.00	0.00	14.02	1401.1	1.000	0.80	0.00	0.00	0.00

Table 15. Fully gravelled bed; d = 5.00 cm., Slope = 0.0005, Temp. = 18.3°c, $V_{*o} = \sqrt{\tau_o/\rho}$ = 1.566 cm./sec.

y cm.	$\bar{u}$ cm./sec.	$\sqrt{\overline{u'^2}}$ cm./sec.	$\sqrt{\overline{v'^2}}$ cm./sec.	$-\overline{u'v'}$ cm.2/sec.2	$\frac{\bar{u}}{V_{*o}}$	$\frac{y V_{*o}}{\nu}$	$\frac{y}{d}$	$\frac{\sqrt{\overline{u'^2}}}{V_{*o}}$	$\frac{\sqrt{\overline{v'^2}}}{V_{*o}}$	$\frac{-\overline{u'v'}}{\tau_o/\rho}$	$-\psi$
0.30	10.35	2.94	1.89	2.41	6.60	44.8	0.060	1.88	1.20	0.98	0.43
0.70	13.20	2.27	1.40	1.70	8.43	104.4	0.140	1.45	0.90	0.69	0.53
1.10	14.60	2.05	1.65	2.16	9.32	164.1	0.220	1.31	1.05	0.92	0.64
1.50	15.95	2.16	1.43	1.85	10.18	223.8	0.300	1.38	0.92	0.75	0.60
1.90	17.40	2.52	1.57	1.95	11.11	283.5	0.380	1.61	1.00	0.79	0.49
2.30	18.45	2.30	1.56	2.25	11.78	343.1	0.460	1.47	1.00	0.92	0.63
2.70	19.00	1.99	1.28	1.22	12.13	402.8	0.540	1.27	0.82	0.50	0.48
3.10	19.80	1.96	1.16	0.86	12.64	462.5	0.620	1.25	0.74	0.35	0.38
3.50	20.00	1.78	1.15	0.98	12.77	522.2	0.700	1.13	0.74	0.40	0.48
3.90	20.95	1.46	1.02	0.81	13.37	581.9	0.780	0.93	0.65	0.33	0.55
4.30	21.20	1.11	0.69	0.29	13.53	641.5	0.860	0.71	0.44	0.12	0.38
4.70	21.45	0.96	0.36	0.13	13.70	701.2	0.940	0.61	0.23	0.05	0.37
5.00	21.70	0.86	0.00	0.00	13.85	746.0	1.000	0.55	0.00	0.00	0.00

Table 16. Fully gravelled bed; d = 6.25 cm., S = 0.0005, Temp. = 18.4
Temp. = 18.4°c, $V_{*o} = \sqrt{\tau_o/\rho}$ = 1.751 cm./sec.

0.30	11.95	2.70	2.22	2.37	6.82	50.2	0.048	1.54	1.27	0.77	0.40
0.70	15.60	2.39	2.23	2.88	8.91	117.1	0.112	1.36	1.27	0.94	0.54
1.10	17.35	2.43	1.79	2.66	9.91	184.0	0.176	1.39	1.03	0.86	0.6
1.50	18.85	2.15	1.80	1.42	10.76	251.0	0.240	1.23	1.03	0.46	0.37
1.90	19.35	2.23	1.38	1.60	11.05	317.9	0.304	1.27	0.79	0.52	0.52
2.30	20.60	2.26	1.45	1.57	11.76	384.8	0.368	1.29	0.83	0.51	0.48
2.70	20.60	2.35	1.30	1.00	11.76	451.7	0.432	1.35	0.74	0.33	0.33
3.10	21.65	1.93	1.40	1.61	12.36	518.6	0.496	1.10	0.80	0.53	0.60
3.50	22.20	2.08	1.40	1.49	12.68	585.6	0.560	1.19	0.80	0.49	0.51
3.90	22.85	1.76	1.19	1.07	13.05	652.5	0.624	1.00	0.68	0.35	0.51
4.30	23.30	1.45	1.39	1.13	13.30	719.4	0.688	0.83	0.80	0.37	0.56
4.70	23.40	1.45	1.36	0.60	13.36	786.3	0.752	0.83	0.78	0.20	0.30
5.10	24.30	1.71	0.78	0.44	13.88	853.2	0.816	0.98	0.45	0.14	0.33
5.50	24.60	1.36	0.76	0.45	14.05	920.1	0.880	0.78	0.44	0.15	0.43
5.90	24.10	1.17	0.50	0.21	13.76	987.0	0.944	0.67	0.28	0.07	0.36
6.25	24.95	1.26	0.00	0.00	14.25	1045.0	1.000	0.72	0.00	0.00	0.00

Table 17. Fully gravelled bed; d = 4.98 cm., S = 0.0010,
Temp. = 18.5°c, $V_{*o} = \sqrt{\tau_o/\rho}$ = 2.211 cm./sec.

y cm.	$\bar{u}$ cm./sec.	$\sqrt{\overline{u'^2}}$ cm./sec.	$\sqrt{\overline{v'^2}}$ cm./sec.	$-\overline{u'v'}$ cm.2/sec.2	$\frac{\bar{u}}{V_{*o}}$	$\frac{y\,V_{*o}}{\nu}$	$\frac{y}{d}$	$\frac{\sqrt{\overline{u'^2}}}{V_{*o}}$	$\frac{\sqrt{\overline{v'^2}}}{V_{*o}}$	$\frac{-\overline{u'v'}}{\tau_o/\rho}$	$-\Psi$
0.30	14.5	3.58	2.72	4.98	6.55	63.5	0.060	1.62	1.23	1.02	0.51
0.70	18.65	3.14	2.37	4.58	8.45	148.2	0.140	1.42	1.07	0.94	0.62
1.10	22.15	3.36	2.48	4.25	10.02	233.0	0.221	1.52	1.12	0.87	0.51
1.50	24.10	3.62	2.16	3.85	10.90	317.6	0.301	1.64	0.98	0.79	0.49
1.90	25.40	2.97	2.14	3.19	11.49	402.3	0.381	1.34	0.97	0.65	0.50
2.30	27.20	2.61	1.46	1.82	12.30	487.0	0.462	1.18	0.66	0.37	0.48
2.70	27.30	2.45	1.55	2.33	12.35	571.8	0.542	1.11	0.70	0.48	0.61
3.10	27.50	2.60	1.40	1.93	12.44	656.5	0.623	1.18	0.63	0.39	0.53
3.50	30.00	1.76	1.47	1.29	13.57	741.2	0.703	0.80	0.66	0.26	0.50
3.90	29.00	1.76	1.30	0.74	13.11	825.9	0.783	0.80	0.59	0.15	0.33
4.30	29.75	1.78	0.98	0.73	13.45	910.5	0.863	0.81	0.44	0.15	0.42
4.70	30.45	1.48	0.56	0.22	13.77	995.3	0.944	0.67	0.26	0.05	0.26
4.98	30.60	1.15	0.00	0.00	13.84	1054.5	1.000	0.52	0.00	0.00	0.00

Table 18. Fully gravelled bed; d = 6.30 cm., S = 0.0010,
Temp. = 18.5°c, $V_{*o} = \sqrt{\tau_o/\rho}$ = 2.487 cm./sec.

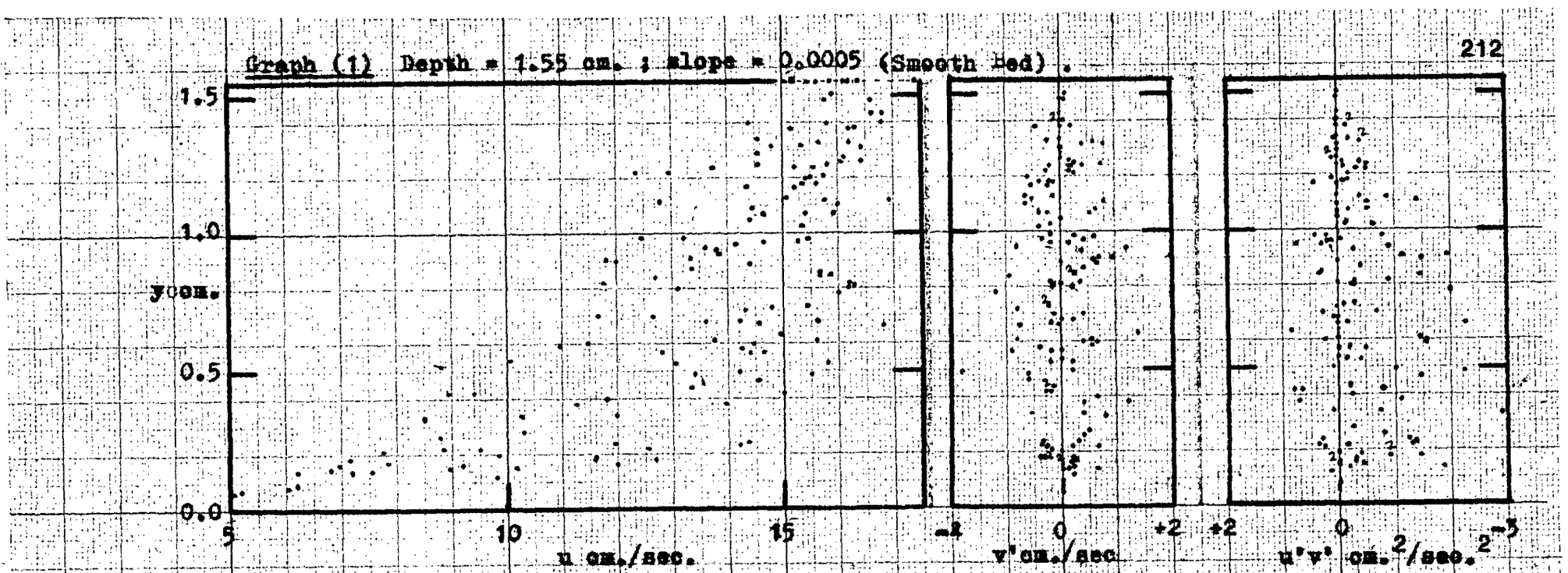
0.30	16.70	4.07	2.71	3.68	6.72	71.5	0.048	1.64	1.09	0.60	0.33
1.70	21.65	3.42	1.98	4.44	8.70	180.7	0.111	1.37	0.79	0.72	0.66
1.10	24.55	3.69	2.43	5.11	9.87	262.0	0.175	1.48	0.98	0.83	0.[illegible]
1.50	25.80	3.45	2.10	2.90	10.38	357.3	0.238	1.39	0.84	0.47	0.[illegible]
1.90	28.15	3.36	2.36	4.50	11.32	452.6	0.302	1.35	0.95	0.73	0.57
2.30	29.35	3.12	2.10	2.65	11.80	547.9	0.365	1.26	0.84	0.43	0.40
2.70	28.30	2.99	1.61	2.93	11.38	643.1	0.429	1.20	0.65	0.47	0.61
3.10	29.05	3.31	1.60	2.07	11.68	738.4	0.492	1.33	0.64	0.34	0.39
3.50	31.35	3.14	1.55	2.00	12.61	833.7	0.555	1.26	0.62	0.32	0.41
3.90	30.95	2.80	1.47	1.82	12.45	929.0	0.619	1.12	0.59	0.27	0.44
4.30	32.60	2.66	1.25	1.93	13.11	1024.3	0.683	1.07	0.50	0.31	0.58
4.70	32.70	2.65	1.31	1.29	13.15	1120.0	0.746	1.07	0.52	0.21	0.37
5.10	33.40	2.28	1.56	1.13	13.43	1214.8	0.810	0.92	0.63	0.18	0.32
5.90	34.50	2.13	0.91	0.54	13.87	1405.4	0.936	0.85	0.37	0.09	0.28
6.30	35.30	1.93	0.00	0.00	14.20	1500.7	1.000	0.78	0.00	0.00	0.00

APPENDIX III .

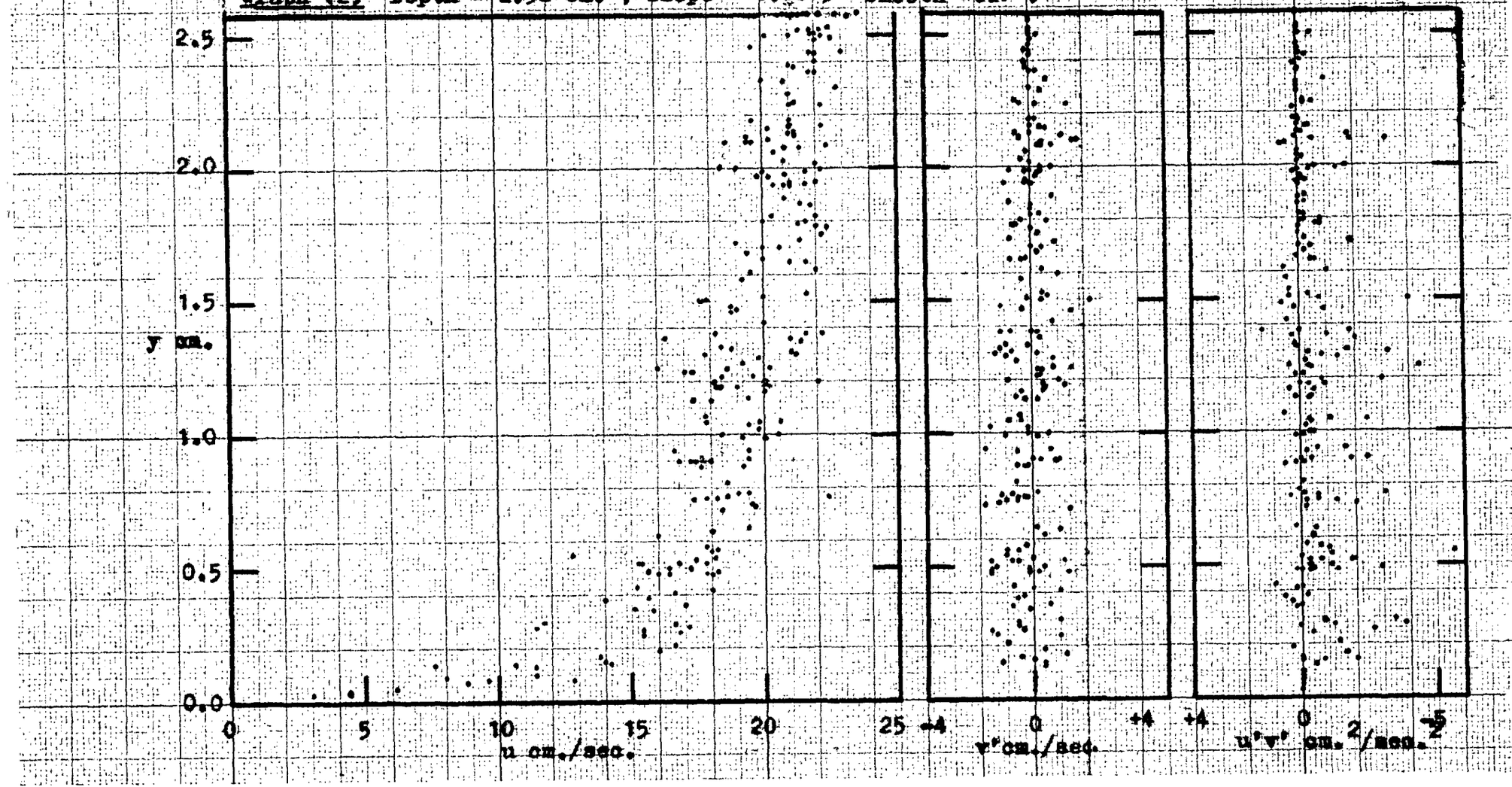
DATA OF u , v' AND u'v' OBTAINED FROM PHOTOGRAPHS .

Note : Vertical distances in case of smooth bed are measured from the bed and are denoted by y ; but in case of rough beds such distances are measured from free surface and are denoted by y'.

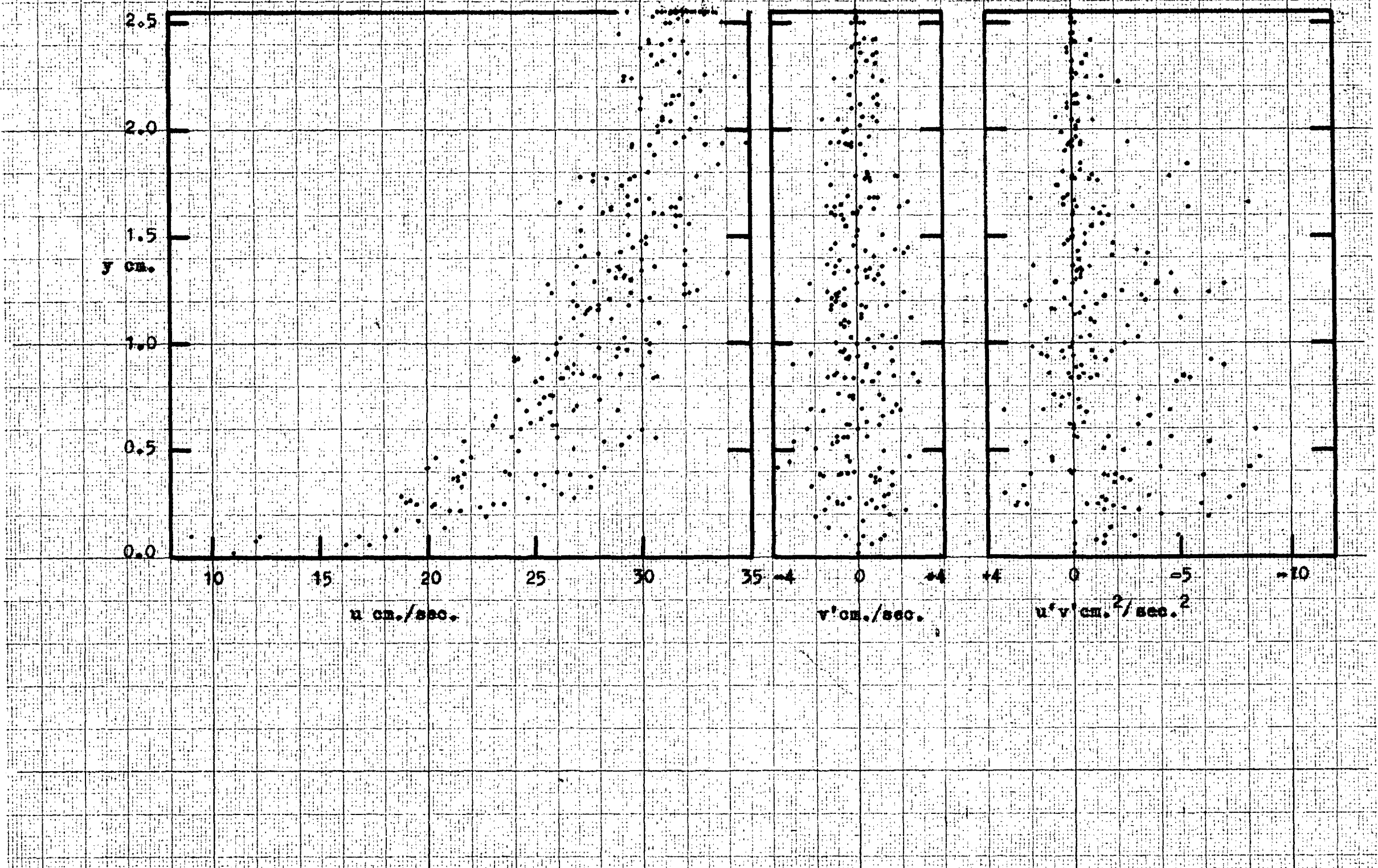
Graph (1) Depth = 1.55 cm. ; slope = 0.0005 (Smooth Bed).



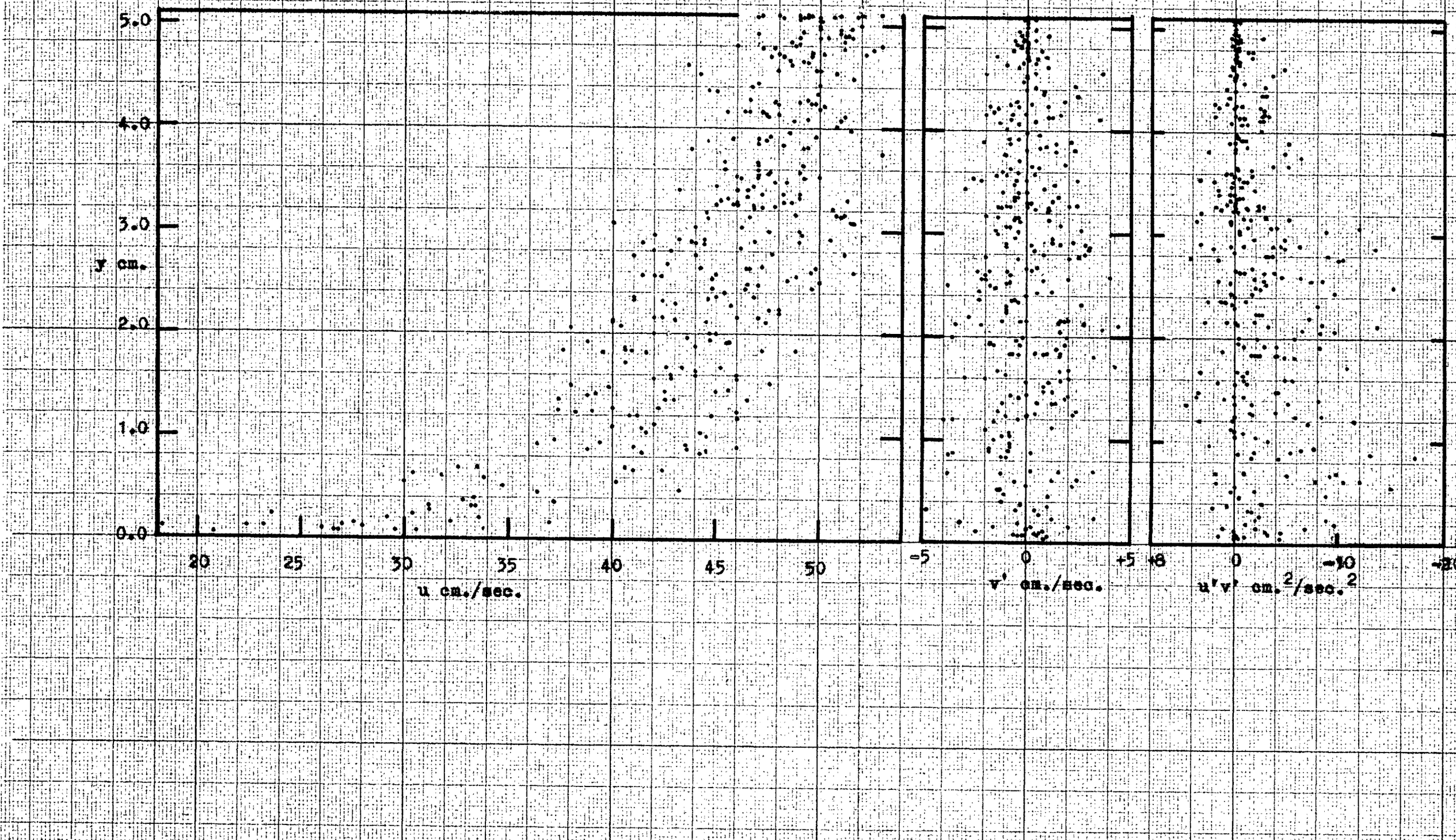
Graph (2) Depth = 2.58 cm. ; slope = 0.0005 (Smooth Bed).



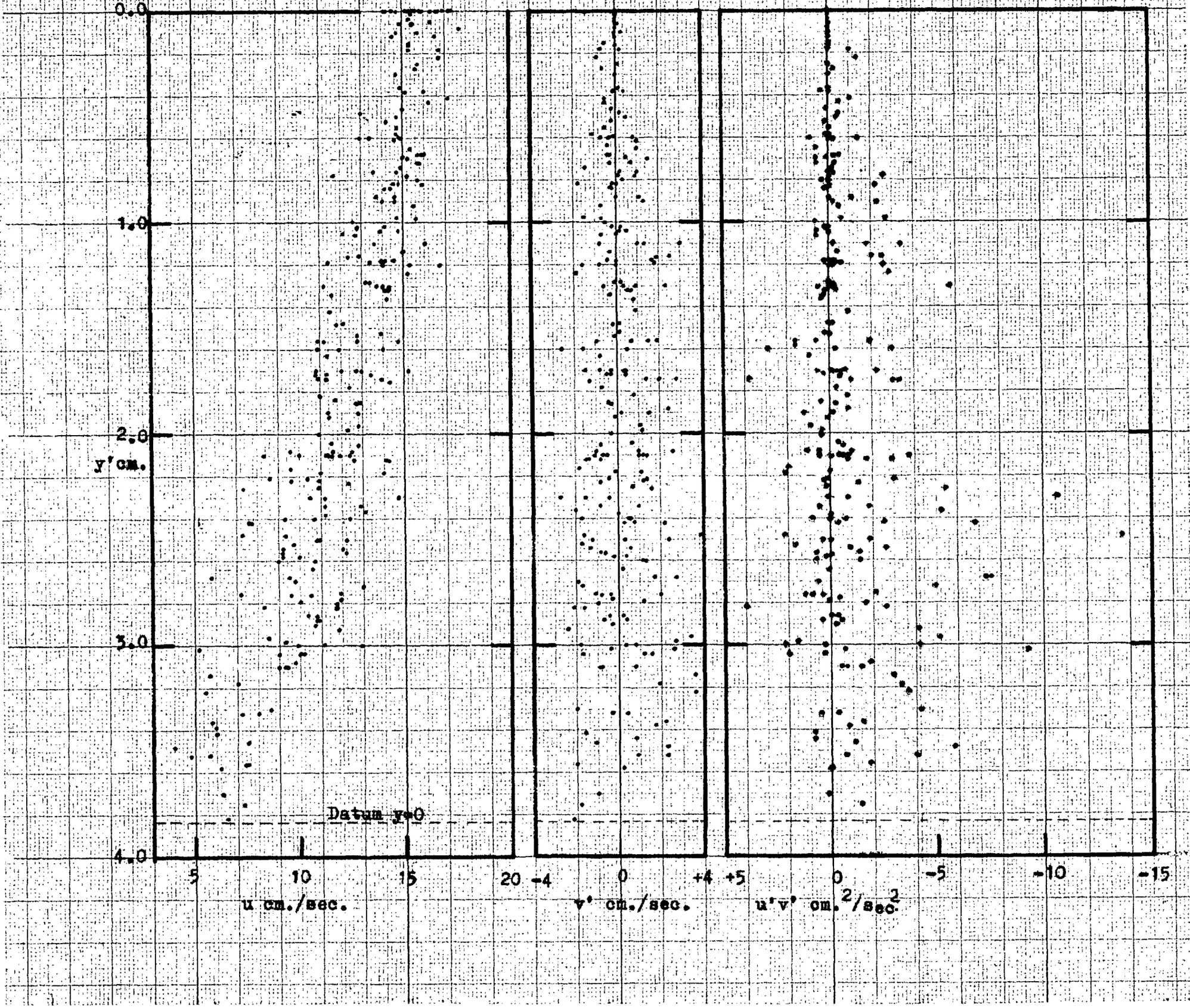
Graph (3) Depth = 2.555 cm. ; slope = 0.0010 ($S_{mooth\ Bed}$).



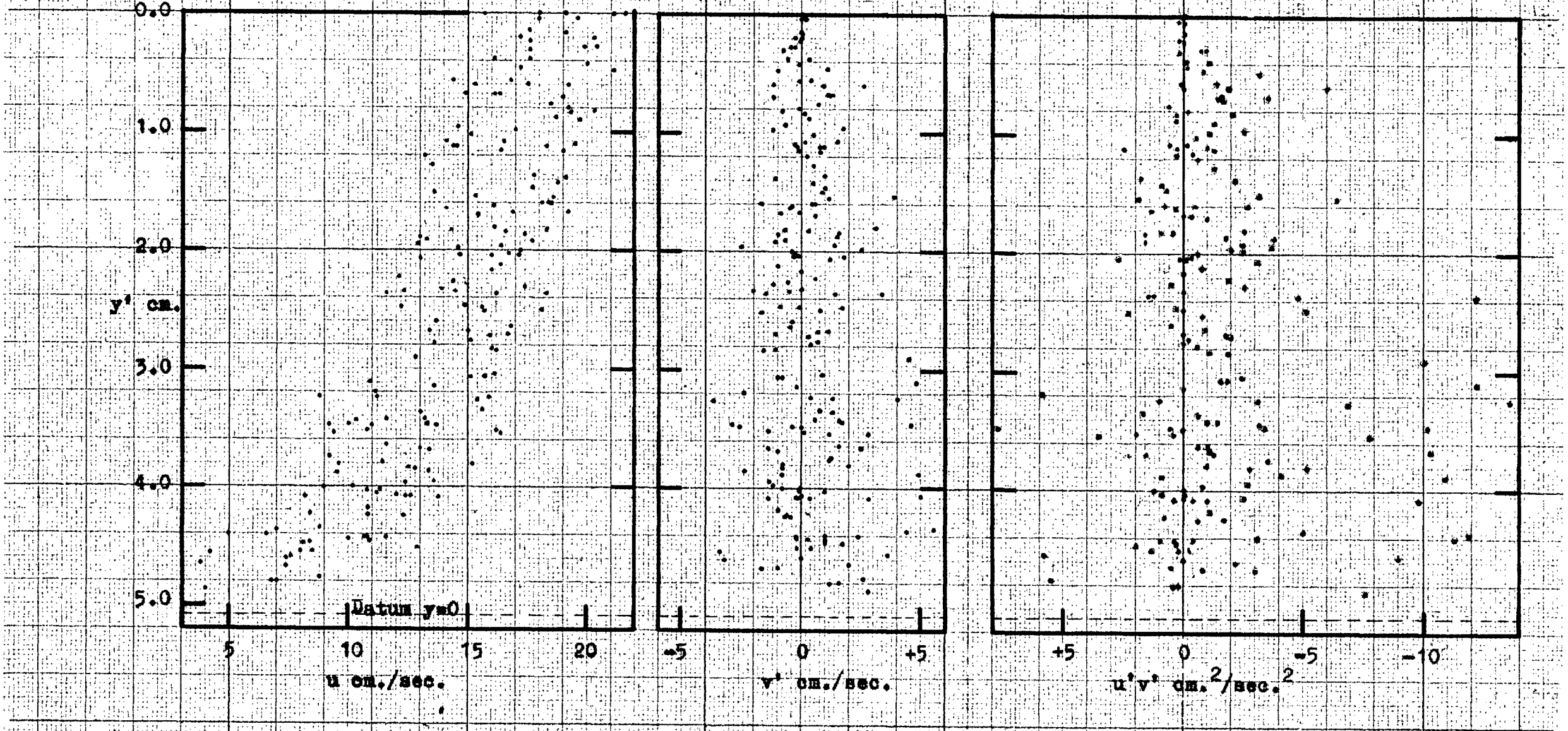
Graph (4) Depth = 5.095 cm. ; slope = 0.0010 (Smooth Bed).



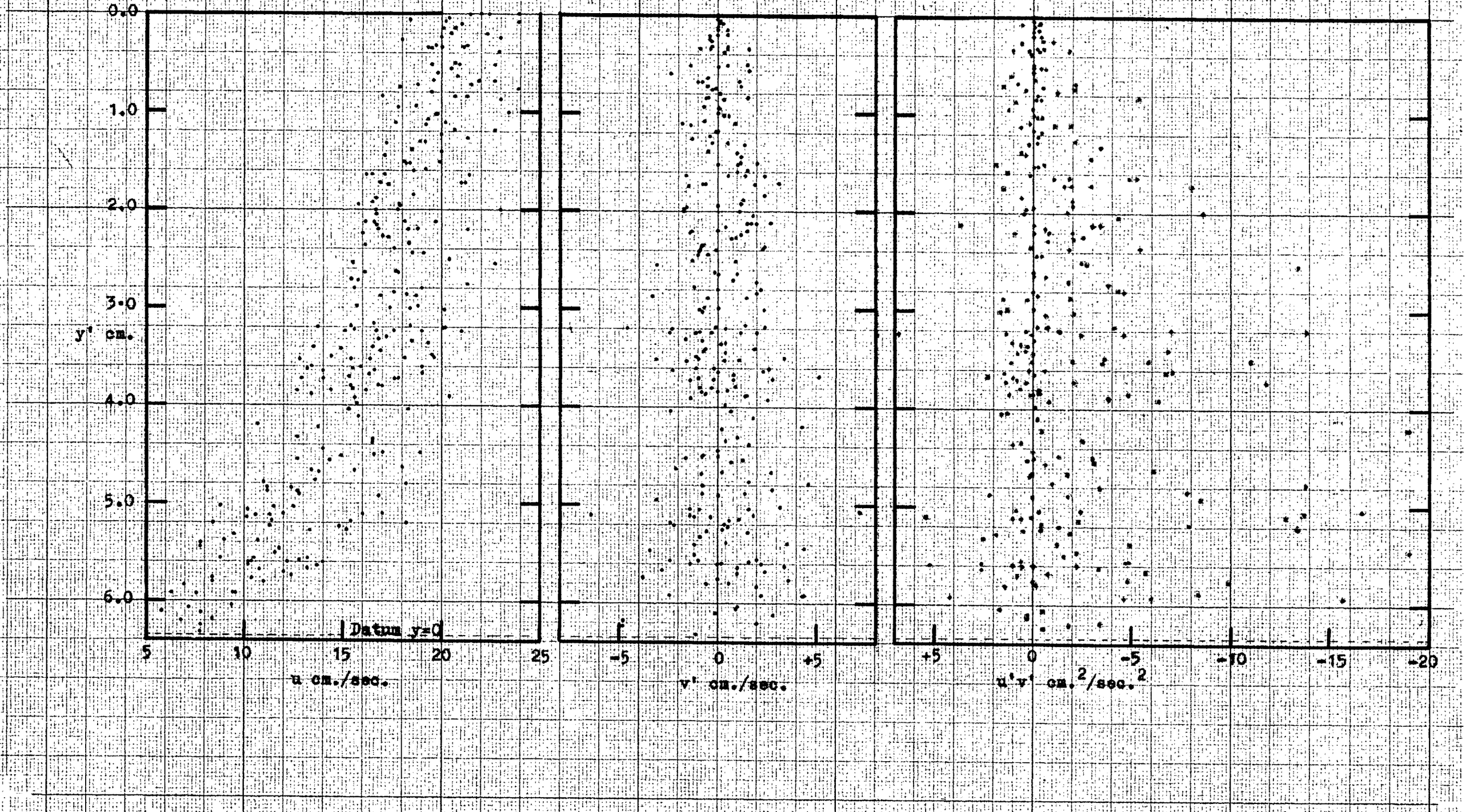
Graph (5) Rippled Bed : Depth = 3.83 cm. ; Slope = 0.0005 .



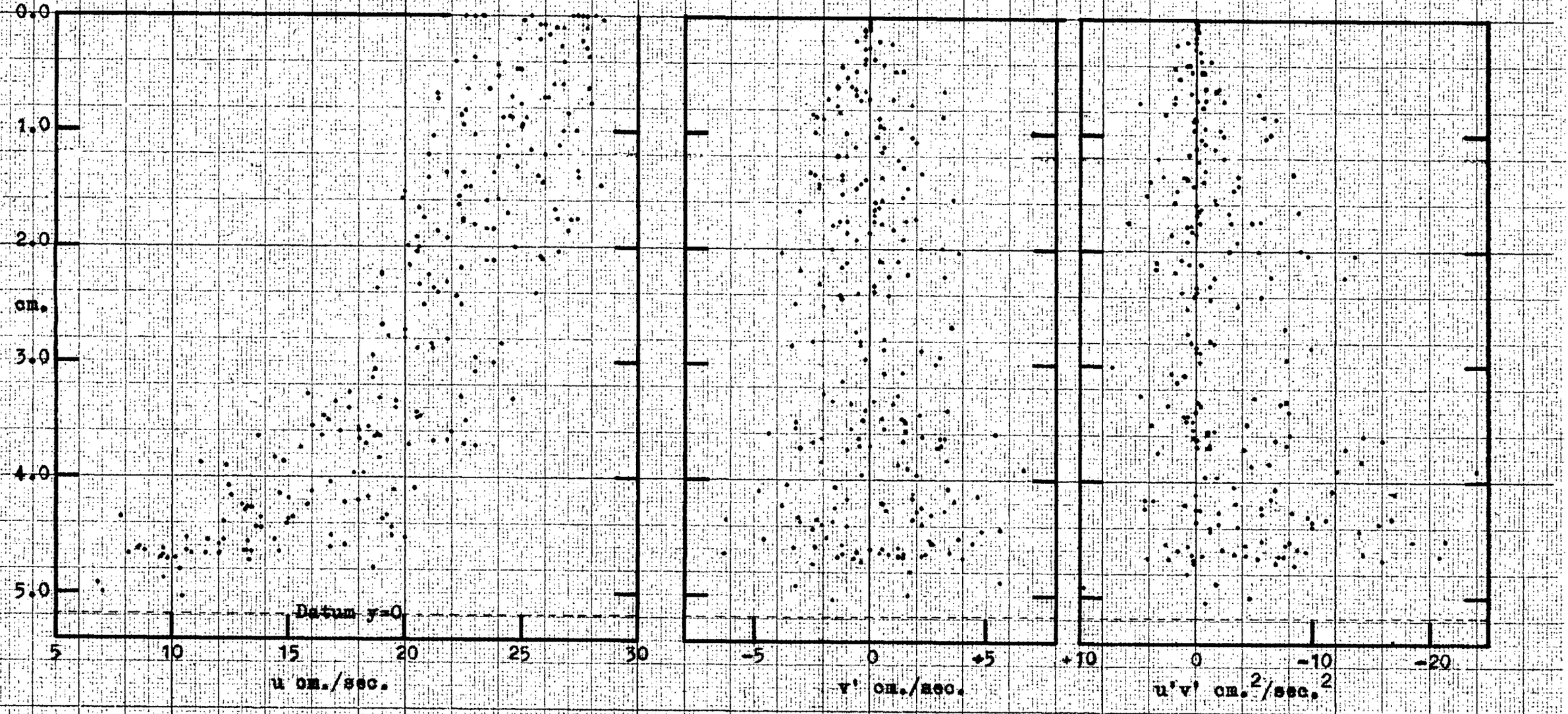
Graph (6) Rippled Bed : Depth = 5.08 cm. ; Slope = 0.0005 .



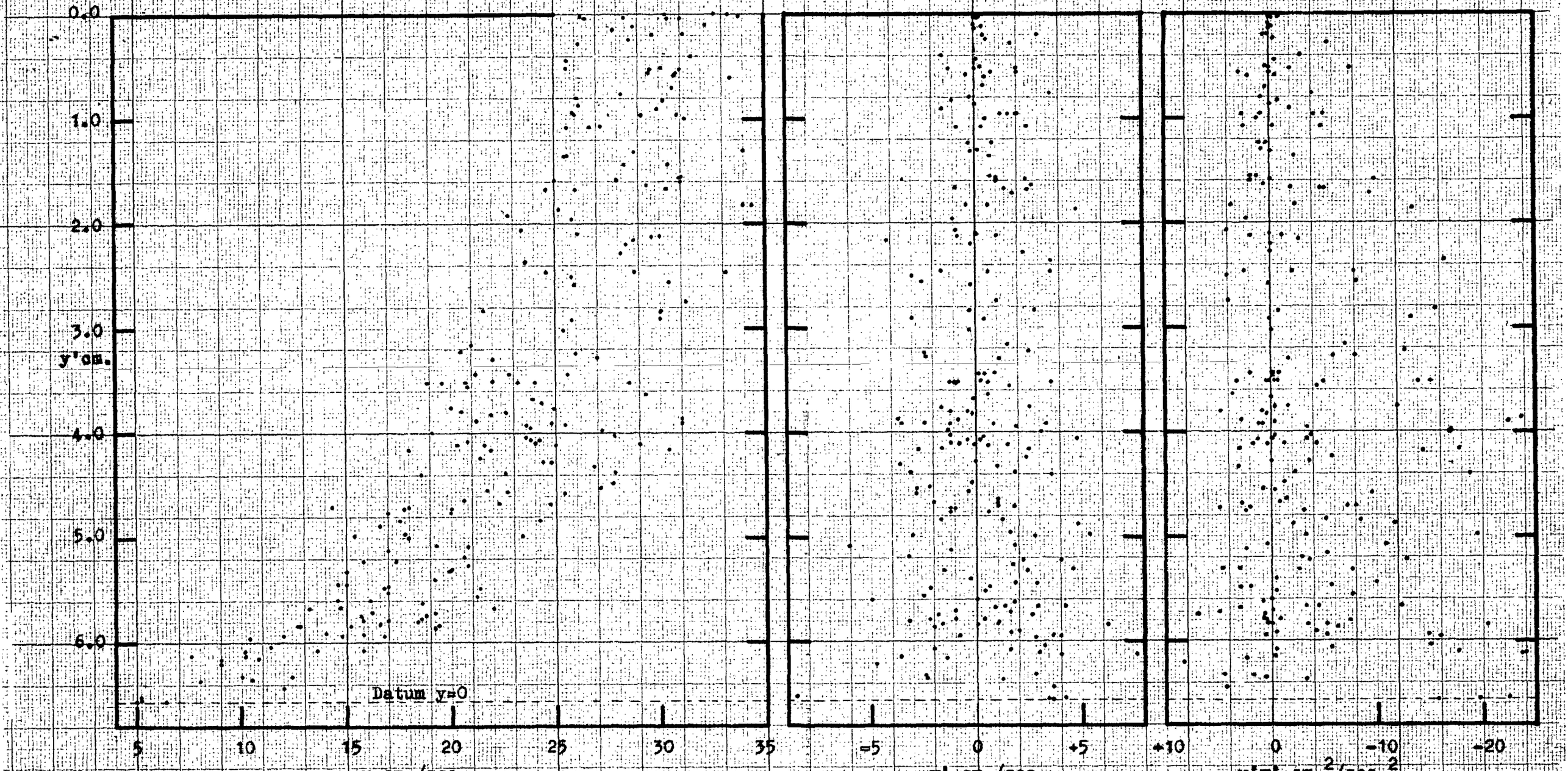
Graph (7) Rippled Bed : Depth = 6.34 cm. ; Slope = 0.0005 .

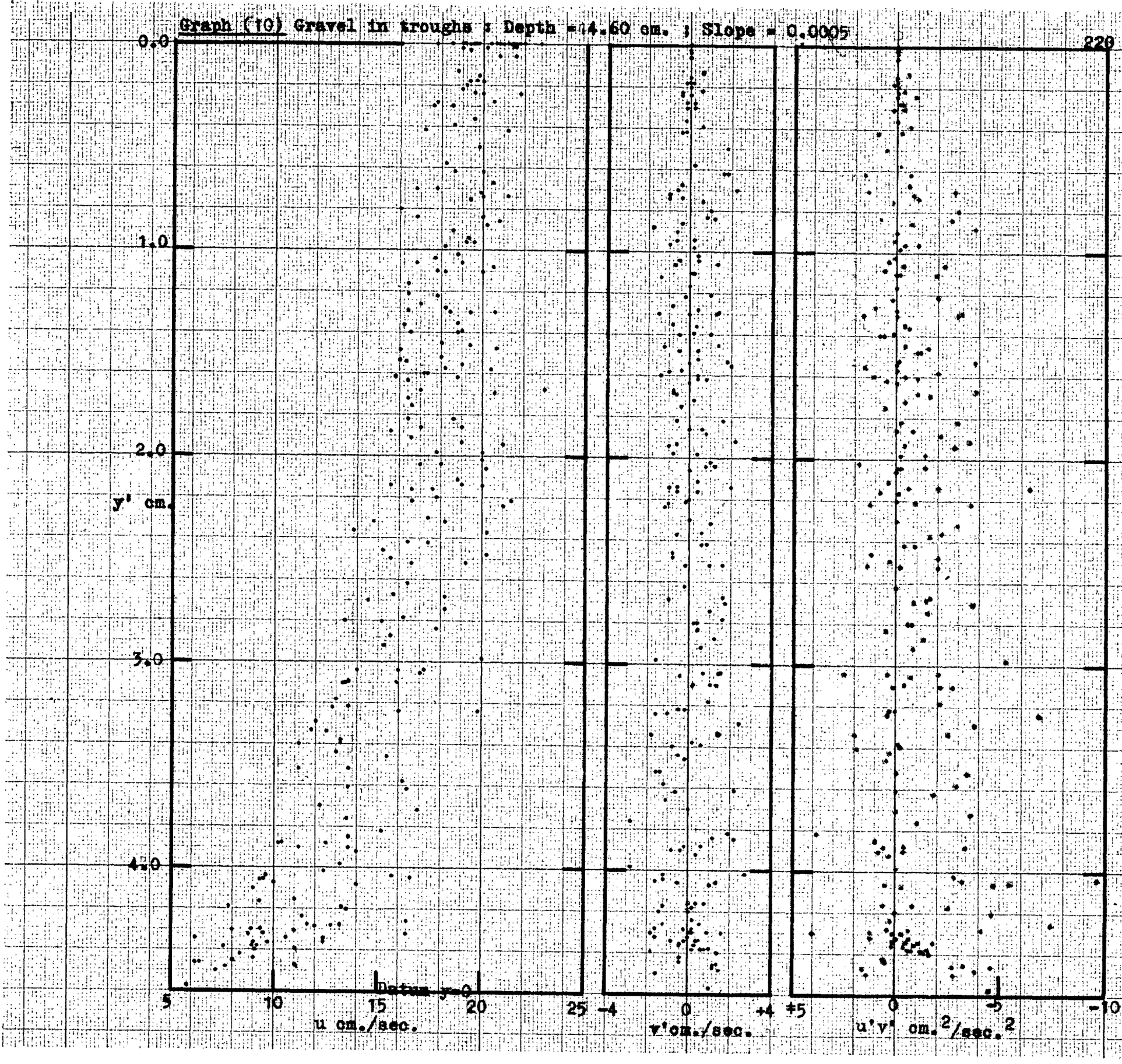


Graph (8) Rippled Bed : Depth = 5.18 cm. ; Slope = 0.0010 .

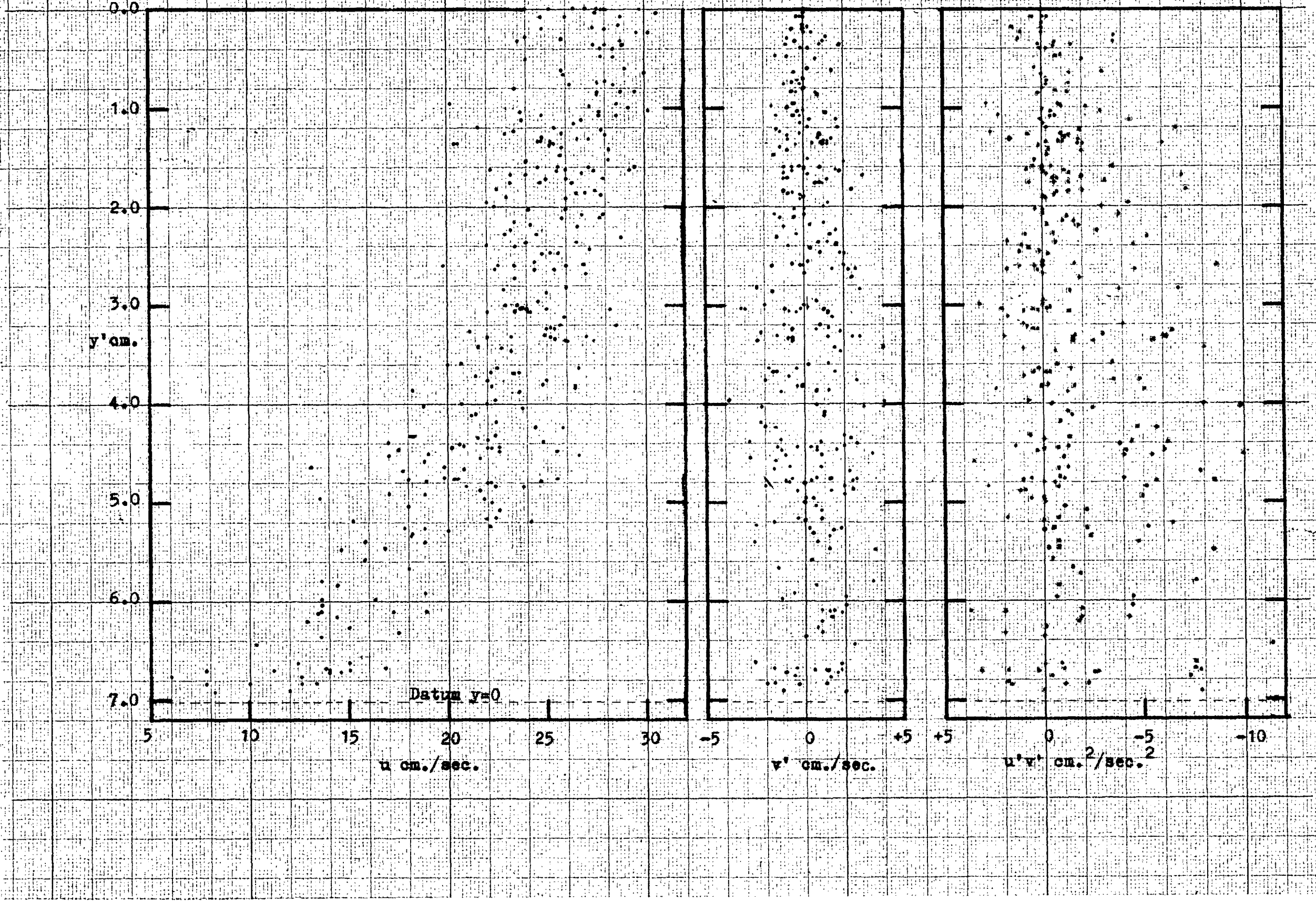


Graph (9) Rippled Bed : Depth = 6.55 cm. ; Slope = 0.0010 .

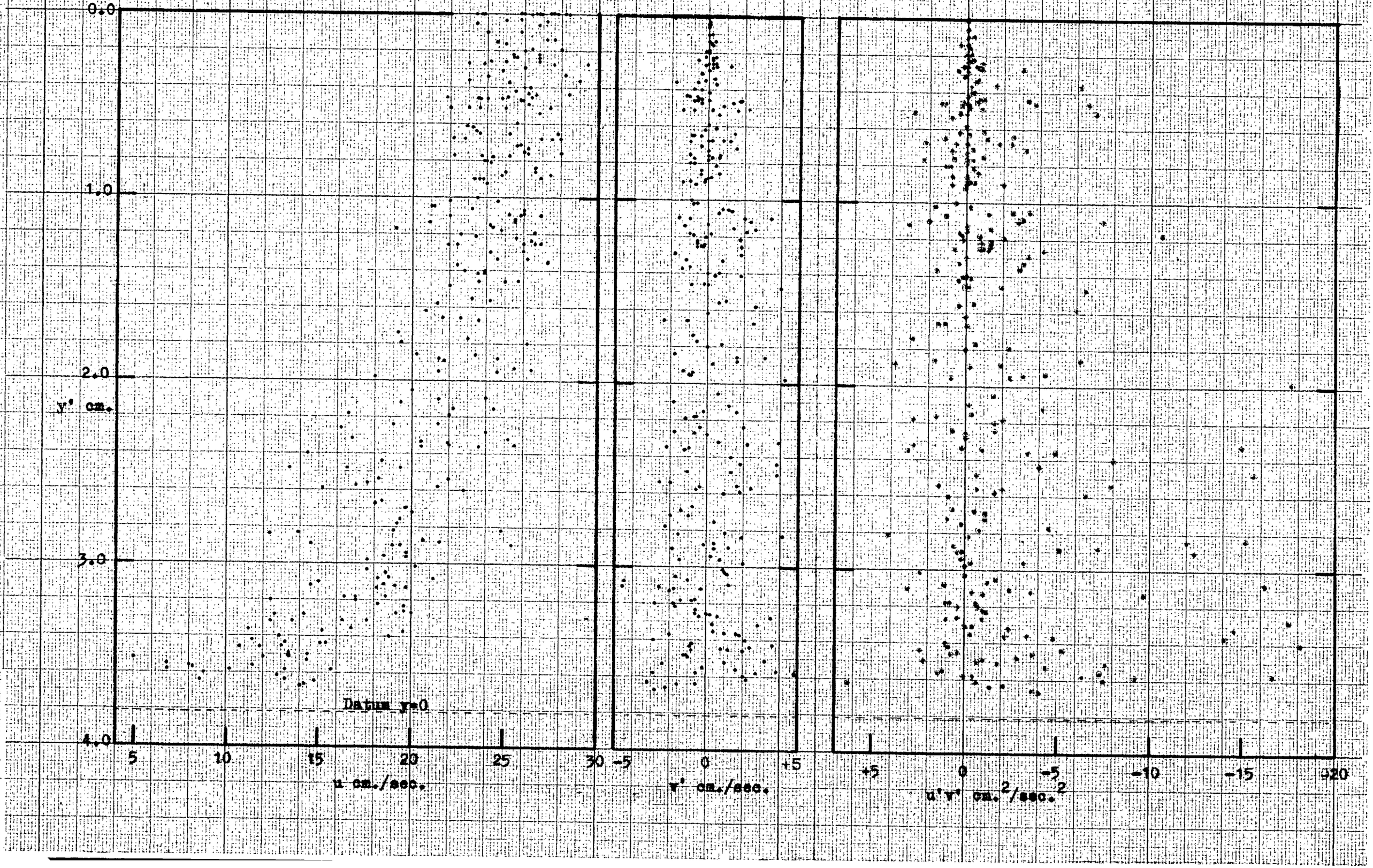



Graph (10) Gravel in troughs ; Depth = 4.60 cm. ; Slope = 0.0005
220
0.0
1.0
2.0
3.0
4.0
y' cm.
Datum y=0
5
10
15
20
25
u cm./sec.
-4
0
+4
v' cm./sec.
+5
0
-5
-10
u'v' cm.²/sec.²

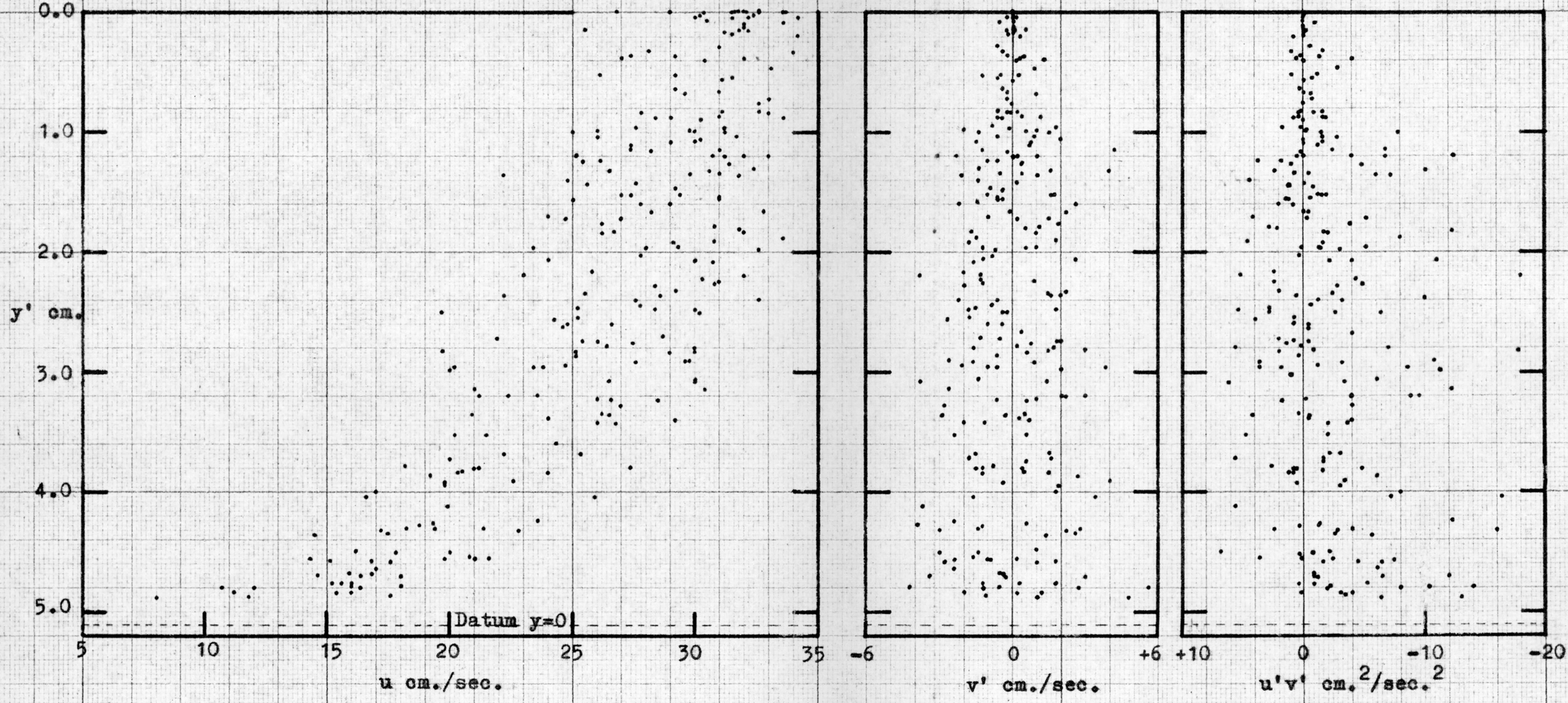
Graph (11) Gravel in troughs : Depth = 7.02 cm. ; Slope = 0.0005 .



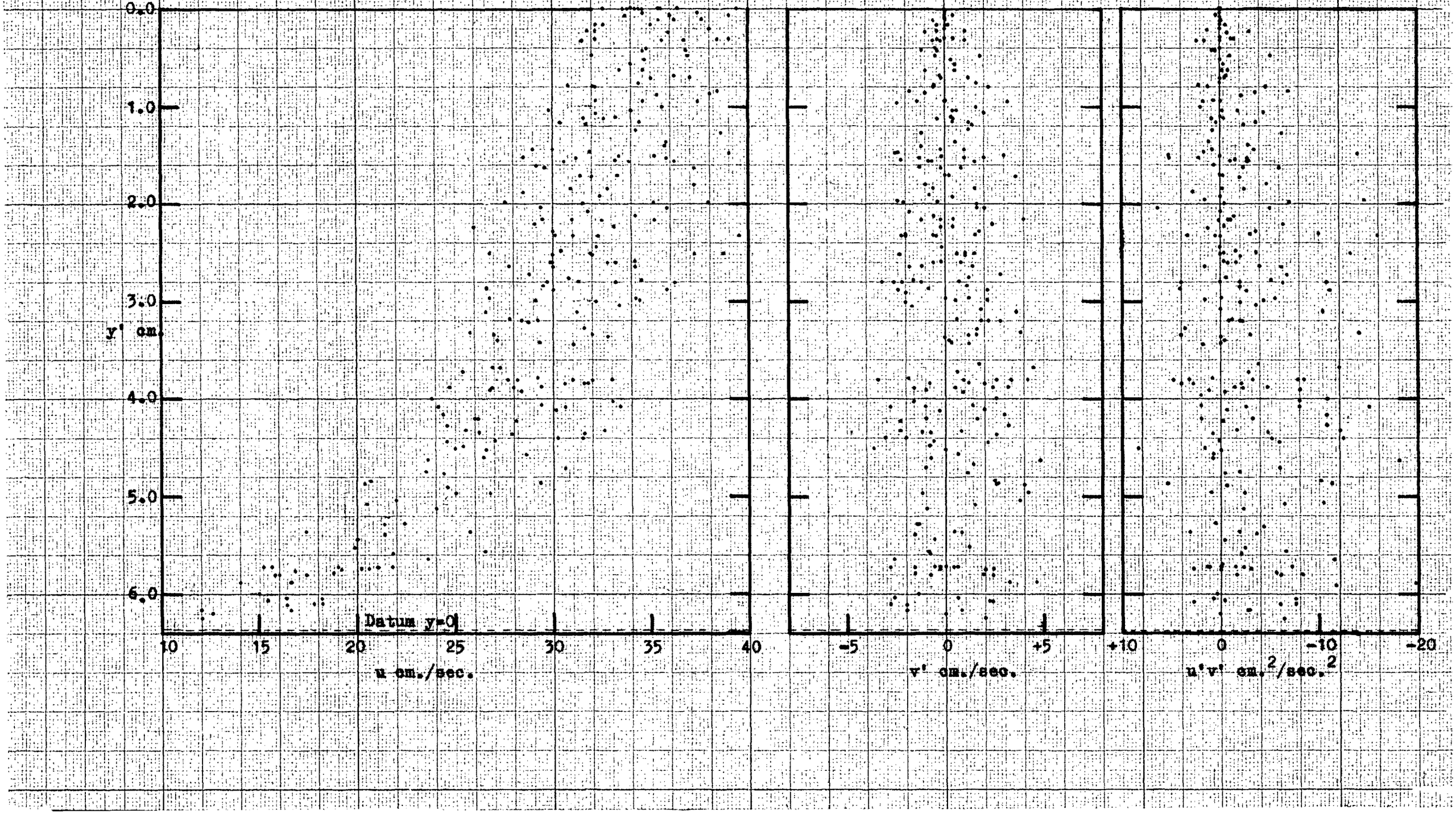
Graph (12) Gravel in troughs : Depth = 3.81 cm. ; Slope = 0.0010 .



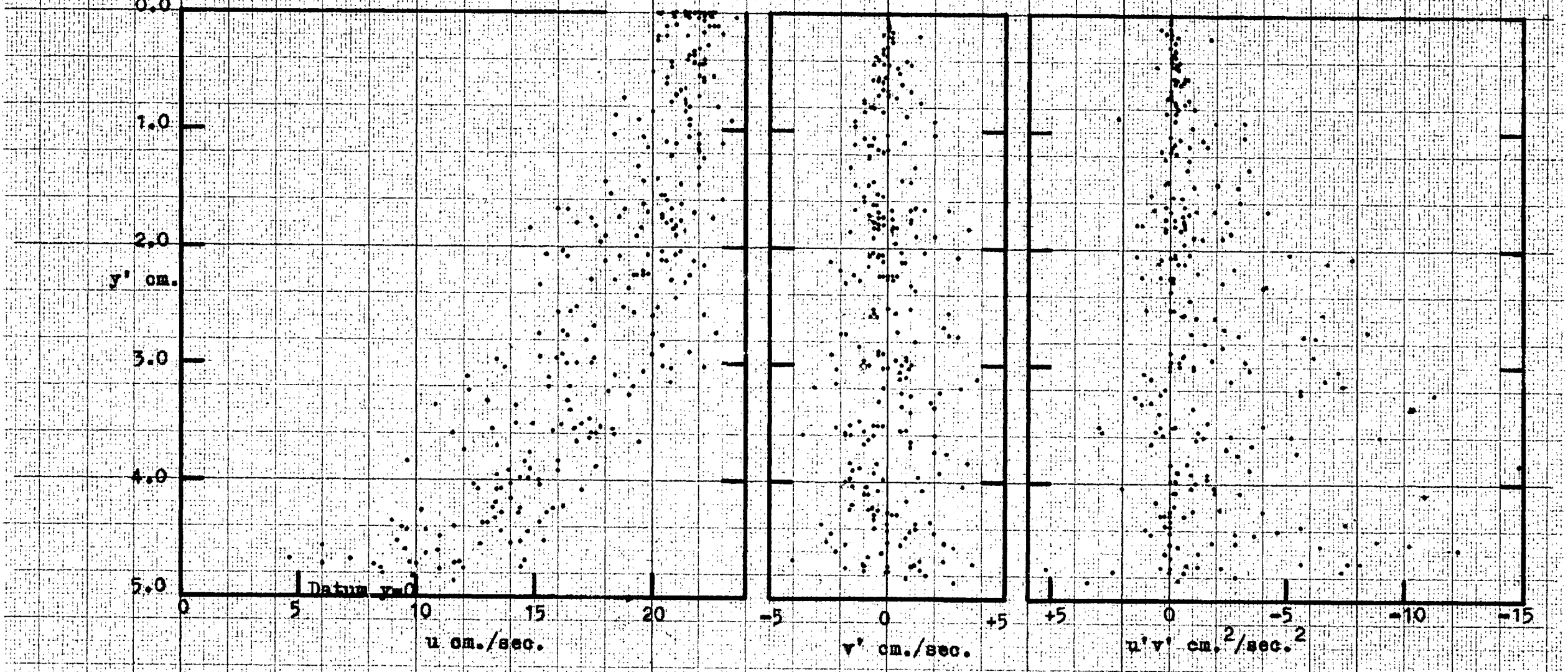
Graph (13) Gravel in troughs : Depth = 5.11 cm. ; Slope = 0.0010 .



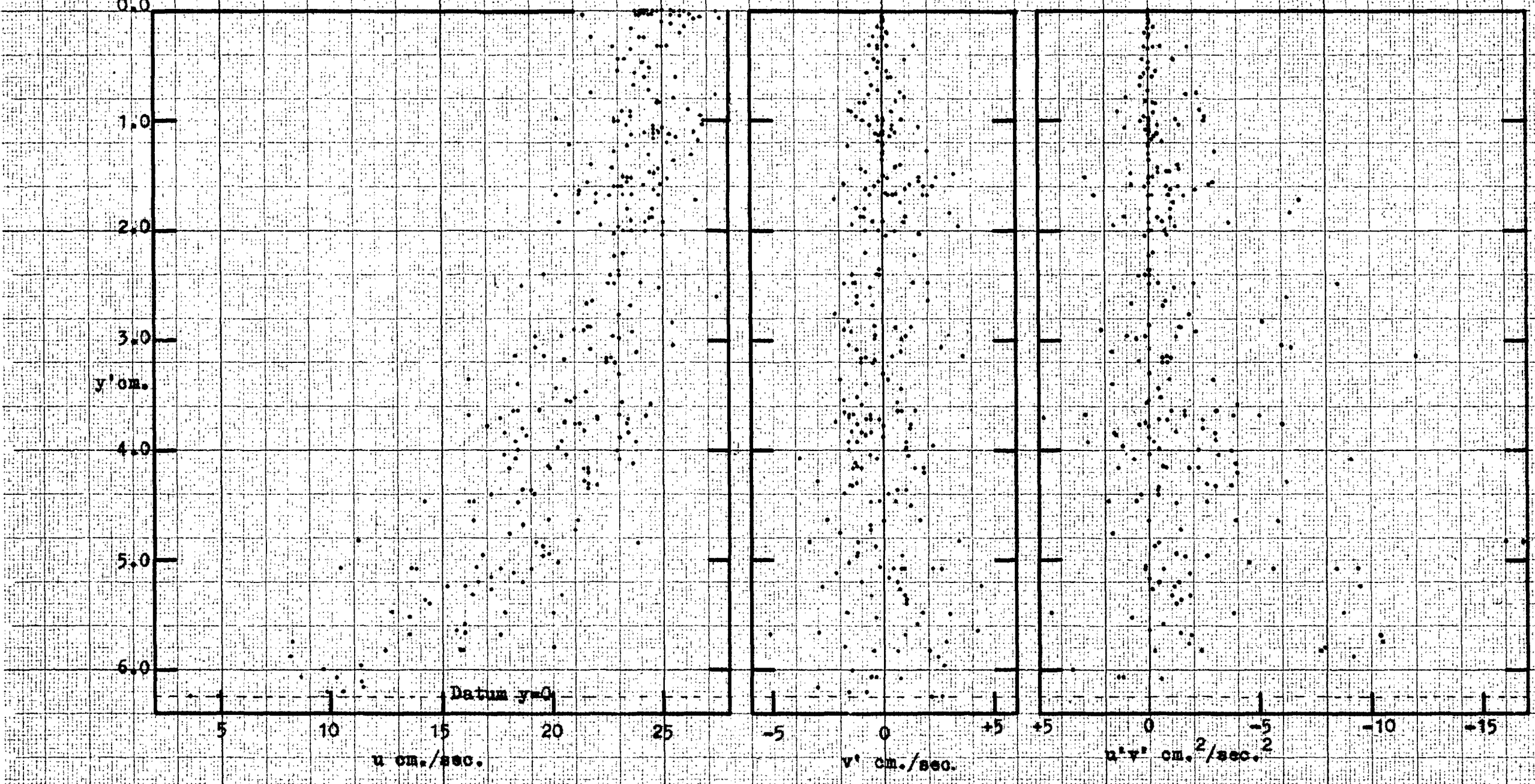
Graph (14) Gravel in troughs : Depth = 6.37 cm. ; Slope = 0.0010 .



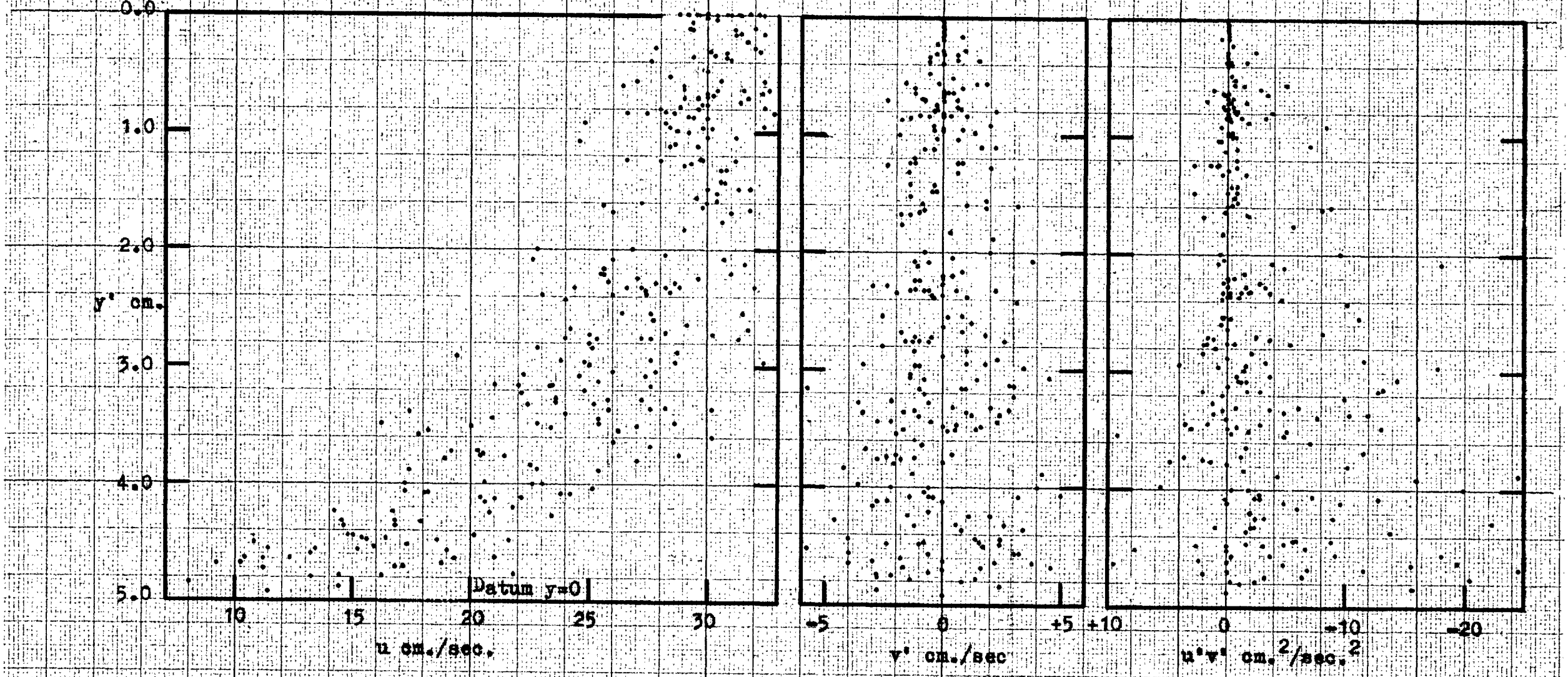
Graph (15) Fully gravelled bed ; Depth = 5.00 cm. ; Slope = 0.0005 .



Graph (16) Fully gravelled bed : Depth = 6.25 cm. ; Slope = 0.0005 .



Graph (17) Fully gravelled bed : Depth = 4.98 cm. ; Slope = 0.0010 .



Graph (18) Fully gravelled bed : Depth = 6.30 cm. ; Slope = 0.0010 .

